Bright, compact and biocompatible quantum dot/rod - bioconjugates for Förster resonance energy transfer based ratiometric biosensing and cellular imaging

Weili Wang

Submitted in accordance with the requirements for the degree of Doctor of Philosophy

The University of Leeds

School of Chemistry

September, 2016

The candidate confirms that the work submitted is his/her own, except where work which has formed part of jointly authored publications has been included. The contribution of the candidate and the other authors to this work has been explicitly indicated below. The candidate confirms that appropriate credit has been given within the thesis where reference has been made to the work of others.

The work in Chapter 2 and 3 of the thesis has appeared in publication as follows:

Weili Wang, Yuan Guo, Christian Tiede, Siyuan Chen, Michal Kopytynski, Yifei Kong, Alexander Kulak, Darren Tomlinson, Rongjun Chen, Michael McPherson and Dejian Zhou. “An Ultra-efficient Cap-Exchange Protocol to Compact Biofunctional Quantum Dots for Sensitive Ratiometric Biosensing and Cell Imaging” *ACS Applied Materials and Interfaces* 2017 (review)

Author contributions:

Weili Wang (the candidate): performed all experiments (expect those outlined below), including QD surface modification, optimize ligand exchange, data analysis and draft the paper.

Dejian Zhou and Yuan Guo: supervised the whole experiments and revised the manuscript.

Christian Tiede, Darren Tomlinson and Michael McPherson: provide Yeast SUMO Affimer and Yeast SUMO target protein.

Siyuan Chen, Michal Kopytynski and Rongjun Chen: performed cell imaging experiments.

Alexander Kulak: performed AA (atom absorbance) measurement.

Yifei Kong: performed HPLC purified TA-ZW ligand.

Acknowledgements

First and foremost, the sincerest thanks go to my primary supervisor Dr Dejian Zhou and co-supervisor Dr Yuan Guo for continuous support of my PhD study. I greatly appreciate their patience, motivation and academic guidance throughout my research and writing of scientific papers and this thesis. I thank them for their generous contributions of time, knowledge and experience. I could not imagine having a better supervisor for my four-year PhD venture.

Besides Dr Zhou and Dr Guo, I would like to express my sincere gratitude to my internal assessor Dr Terence Kee and Dr Patrick McGowan, and external assessor Dr Liming Ying for their insight and suggestions on my reports, study progression and career planning. My special thanks are due to Dr Rongjun Chen, Dr Siyuan Chen and Dr Kopytynski Michal for helping me to do cell based studies at Imperial Collage London and sharing related experimental details. I also want to thank Dr Michael Ward for offering training and help in transmission electronic microscopy.

I am indebted to past and present members of the Zhou's group: Dr Yuan Guo, Dr Yifer Kong, Dr Haiyan Zhang, and Mr Lorico Lapitan. They not only provided me incredible research atmosphere in working hours, but also enjoyable activities on leisure time, both of which are really precious to me.

Table of Contents

List of Abbreviations

FRET	Fluorescent resonance energy transfer
aq	aqueous
QD	quantum dot
InP	indium phosphide
GaAs	gallium arsenide
CdSe	cadmium selenide
ZnS	zinc sulfide
PEG	polyethylene glycol
CdS	cadmium sulfide
HgTe	mercury telluride
TOP	trioctyl phosphine
TOPO	trioctyl phosphine oxide
QR	quantum rod
TDPA	tetradecylphosphonic
HPA	ethylphosphonic
ODE	octadecene
$(TMS)_2S$	bis(trimethylsilyl)sulfide
TGA	thioglycolic acid
GSH	glutathione
QY	quantum yield

MPA 3-mercaptopropionic acid

MBP maltose binding protein

DNA deoxyribonucleic acid

D_h hydrodynamic size

Vivo within the living

m/z mass / charge number of ions

UCEP ultra-efficient ligand-exchange protocol

LA lipoic acid

FRET Förster resonance energy transfer

TECP tris(2-carboxylethyl phosphine

TEM Transmission electron microscopy

QY quantum yield

DDA laurylamine

HPA ethylphosphonic acid

TDPA etradecylphosphonic acid

GSH glutathione

dTFIL dithiol-functionalized ionic liquid

EGF epidermal growth factor

List of Figures

Abstract

Cancer, a generic group of diseases, can affect distant sites of the human body to cause sever health consequences. According to the World Health Organization, 9.8 million people died from cancer in 2015 worldwide, about 1600 people per day. More seriously, the number of new cases is expected to increase 70% by 2030 to cause 12 million deaths globally. Early detection, accurate diagnosis and effective treatment are crucial in increasing cancer survival rates and reducing patients' suffering. In particular, precise cancer positioning that can guide surgery, chemotherapy and radiotherapy has important clinical significance in successful treatment. The nanotechnology-based diagnosis (*e.g.* QD/QR-bioconjugate probes) and/or treatment of different cancers have received great attention, which is growing to be a promising field in medical research. Over the past 20 years, not only have QD based probes been widely used in developing immunoassays, cellular labeling, cellular imaging, tissue imaging and *in vivo* imaging, but also being extended to researches such as the drug target and drug delivery system. And this thesis is composed of two parts:

Part I

An ultra-efficient ligand-exchange protocol (UCEP) to render commercial hydrophobic QDs completely water-soluble using >50-fold less of the air-stable lipoic acid (LA) based functional ligands with a rapid *in situ* reduction by tris(2-carboxylethyl phosphine, TECP) has been developed. The resulting water-soluble QDs are compact (D_h <10 nm), bright (retaining >90% of original fluorescence), resisting nonspecific adsorption and displaying good stabilities in biological buffers even with high salt contents (*e.g.* 2 M NaCl), making them well-suited for cell imaging and ratiometric biosensing. A DHLA-zwitterion capped QD prepared by the UCEP is readily biofunctionalized with hexa-histidine (His_8)-tagged small antibody mimetic proteins (also known as Affimers), allowing for rapid, ratiometric detection of its target protein down to 5 pM *via* the QD-sensitized Förster resonance energy transfer (FRET) readout signal. Moreover, compact biotin functionalized QDs are prepared by a facile, one-step cap-exchange process for ratiometric quantitation detection of 5 pM protein such as NeutrAvidin as well as for fluorescence imaging of target model cancer cells.

Part II

A stable, water-soluble rod-shaped fluorescence semiconductor nanocrystal (CdSe/CdS core/shell quantum rod, QR) was made by an efficient cap exchange protocol as described in Part I. However, in most cases the

fluorescence of the cap-exchanged QR was almost quenched, hindering their biomedical applications. Herein I have solved this problem by discovering a simple method that allows for efficient recovery of the QR quantum yield, making them suitable for biological applications. The resulting water-soluble QRs are compact (D_h < 20 nm), bright (recovering to >67% of original fluorescence), resisting nonspecific adsorption and displaying good stabilities in biological buffers, making them well-suited for ratiometric biosensing. After tris(2-carboxylethyl phosphine, (TECP) reduction, a dihydrolipoic acid-zwitterion ligand (DHLA-ZW) capped QR was self-assembled with (His_8)-tagged anti-yeast SUMO non-antibody binding proteins (nABPs), allowing for ratiometric detection of its target protein down to 5 pM by the QR-sensitized Förster resonance energy transfer (FRET) signal. Furthermore, compact biotin functionalized QRs are prepared by a facile, one-step cap-exchange process for ratiometric quantitation of labelled neutravidin down to 5 pM. Such sensitivity is among the very best for QR-FRET based biosensors.

Chapter 1 General introduction

1.1 Abstract

Fluorescent semiconductor nanocrystals, also known as quantum dots (QDs) or quantum rods (QRs), are a new type of fluorescent nanomaterials which have a number of advantageous properties compared to other fluorescent materials such as fluorescent proteins and organic dyes. These include excellent optical and chemical stability, high fluorescent quantum yield, broad absorption and size-tunable, narrow symmetric emission [1-5]. QDs are mostly composed of group IIB/VIA (*e.g.* CdSe) or IIIA /VA (*e.g.* InP, GaAs) elements, and are commonly have sizes of 1-10 nm, which are comparable to or smaller than the typical exciton (electron-hole pair) Bohr radius of the corresponding materials, leading to strong quantum confinement [6, 7]. QRs are rod shape semiconductor nanocrystals with diameters ranging from 2 to 10 nm and with lengths ranging from 5 to 100 nm[8]. Compared to the spherical QDs, QRs have several attractive properties that make them potentially better probes for some biomedical application than QDs. For example, QRs have larger absorption cross section,[9] faster radiative decay rate[10] and a bigger stokes shift[11] and can be functionalized with more binding moieties. Furthermore, QRs have higher extinction coefficient and hence have higher brightness for individual particle. These unique properties make QRs highly desirable for certain biological applications and bring in new possibilities for biological imaging.

Most high quality QDs are prepared by using organometallic precursors in high-boiling point coordinating solvents under high temperatures. They are naturally capped with hydrophobic ligands, such as trioctylphosphine (TOP), trioctylphosphine oxide (TOPO) and/or long chain fatty amines, making them insoluble in aqueous solutions and are therefore biologically incompatible. In 1998, the Nie and Alivisatos' research groups first addressed the biocompatibility problem independently by using ligand exchange and silica shell encapsulation, respectively, to make the QDs water-soluble and subsequently conjugated with specific bio-molecules as novel bioimaging probes[2, 3]. Nie's group used a thioglycolic acid (TGA) capped water-soluble CdSe/ZnS QD further conjugated with the protein transferrin for specific cell labelling. The transferrin conjugated QD could be recognized by cell surface transferring receptors and entered into cells effectively *via* receptor mediated endocytosis. This work demonstrated that QDs could be used to probe the specific ligand-receptor bindings inside living cells[2, 3]. Similar to QDs, high quality QRs are also synthesized to be only soluble in organic solvents[12]. In 2007, the Alivisatos' research groups design a method to transfer QRs into aqueous medium and make them bio-functional by surface silanization[8].

However, for most biological and analytical applications, the QDs should be carefully chosen and designed. Through specific modification of the surface capping ligands by approaches such as ligand exchange, silica encapsulation and amphiphilic polymer or lipid micelle encapsulation, the QDs can be made

stable, water-soluble and biocompatible[2, 3, 13]. QD-based fluorescent probes which have strong fluorescence with excellent photo-stability are therefore extremely well-placed for these studies. Over the past 20 years, not only have QD based probes been widely used in developing immunoassays, cellular labeling, cellular imaging, tissue imaging and *in vivo* imaging, but also being extended to researches such as the drug target and drug delivery system[14].

Despite such great developments, there are still significant challenges, especially for biomedical and clinical applications. For instance, the so called "blinking" which is a well-known phenomenon that limits the stability of quantum dot-based devices such as solar cells and light-emitting diodes. that can make tracking and trafficking studies unreliable. Moreover, most high qualities QDs contain heavy metal (e.g. Cd, Hg) and hence toxicity and cytotoxicity arising from the leaked heavy metals at physiological environment can limit their *in vivo* applications. Therefore significant further researches are still needed.

In this chapter, the quantum confinement effect and optical properties of QDs/QRs in comparison with organic dyes will be discussed first. Then several strategies for preparation, surface modification and bioconjugation of QDs/QRs will be introduced. After that, the principle and applications of FRET based QDs will be illustrated. And finally the background aims of my project will be introduced.

1.2 Distinct properties of semiconductor of QDs/QRs as fluorophores

1.2.1 Quantum confinement effect of QDs

As we all know, crystalline inorganic solids are divided into three classes: metal, semiconductors and insulators. The overlap of atomic orbitals forms continuous electronic energy levels called band structures, where electron-filled and empty bands are called valence and conduction bands, respectively. For metals, there is no band-gap separating the valence and conduction bands, electrons can move freely; whereas in semiconductors the valency/conduction bands are separated by a small band gap, while for insulators, the electron distributions are the same as semiconductors, but the band gap is much larger. All bulk semiconductor materials have defined valence and conduction bands, and the band-gap is specific for each semiconductor material. The QD fluorescence emission occurs when an electron excited to the conduction band and rapidly relaxed to the lowest energy level of the conduction band, returns to and recombines with a positively charged hole in the valence band. This gives the emission photon with energy exactly matching that of the band-gap. However, for QDs, the band-gap is not only dependent on the material but also on the size of the particles. This is because as the size of the QD decreases, there are fewer atoms (hence orbitals) in the dot to form the conduction and valence bands, leading to a greater band-gap (see Figure. 1-1). As a result, the biggest QD

has lowest band-gap (hence lowest energy, longest wavelength, red fluorescence), the middle QD has median band-gap (green) fluorescence and the smallest one has highest energy blue (hence highest energy, shortest wavelength, blue fluorescence) emission[15, 16]. Therefore different sized QDs produce their specific, distinct coloured emissions. Moreover, electrons at any valence band levels can be excited to any levels in the conduction band upon absorption of a photon, giving a rather broad absorption. These unique absorption and emission characteristics allow a single excitation wavelength to excite different coloured QDs at same time (see Figure 1-3), yet each still producing its specific distinct coloured emissions, making QDs extremely well-suited for multiplexed assays and imaging/tracking studies[16].

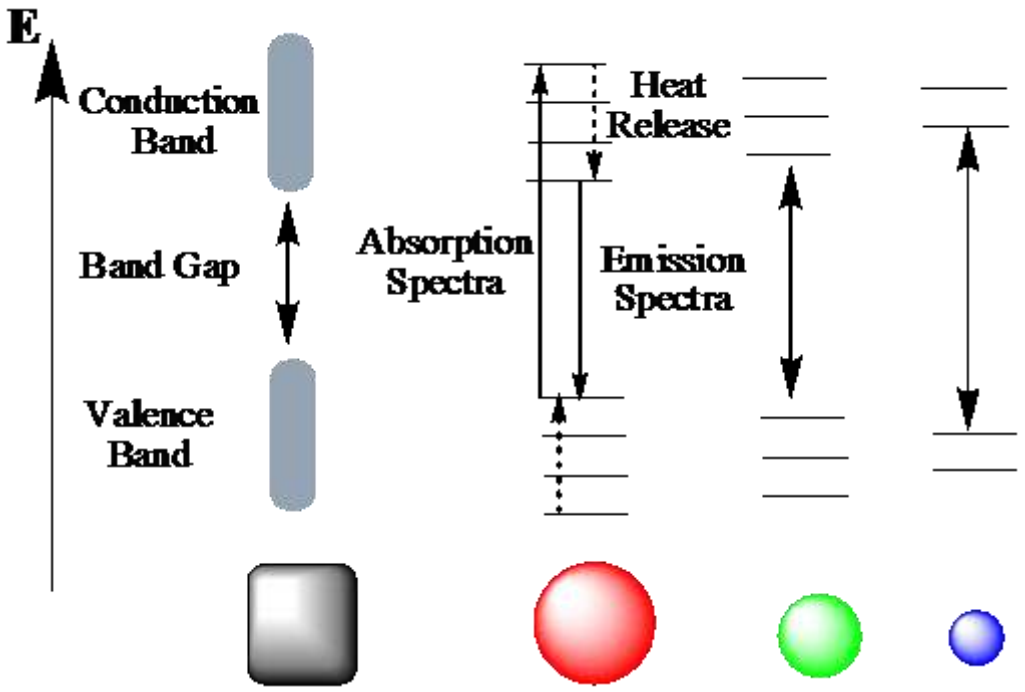

Figure 1-1: Schematic representation of the band gaps of a semiconductor bulk material (left) and three different sized QDs. For QDs, the wavelength of emitted light is strongly dependent on the particle size[16].

1.2.2 Optical properties of QDs and QRs

Another unique optical property of QDs is that their absorption and emission spectra are strongly dependent on the QD sizes, which can be finely controlled by changing the reaction time and temperature during synthesis[17, 18]. As the reaction time increase, the QDs will grow bigger and bigger. Hence different coloured QDs can be easily prepared by simply changing the QD growth time. For example, a 1.8 nm size CdSe QD emits a blue light, but a 7 nm CdSe QD emits a red light. Therefore, by using a range of different sized CdSe QDs, it is possible to cover all the colours of visible range of spectrum (see Figure. 1-2). Moreover, different sized QDs can be simultaneously used

to detect and track several different molecules simultaneously by conjugating each specific ligand to a specific coloured QD[19].

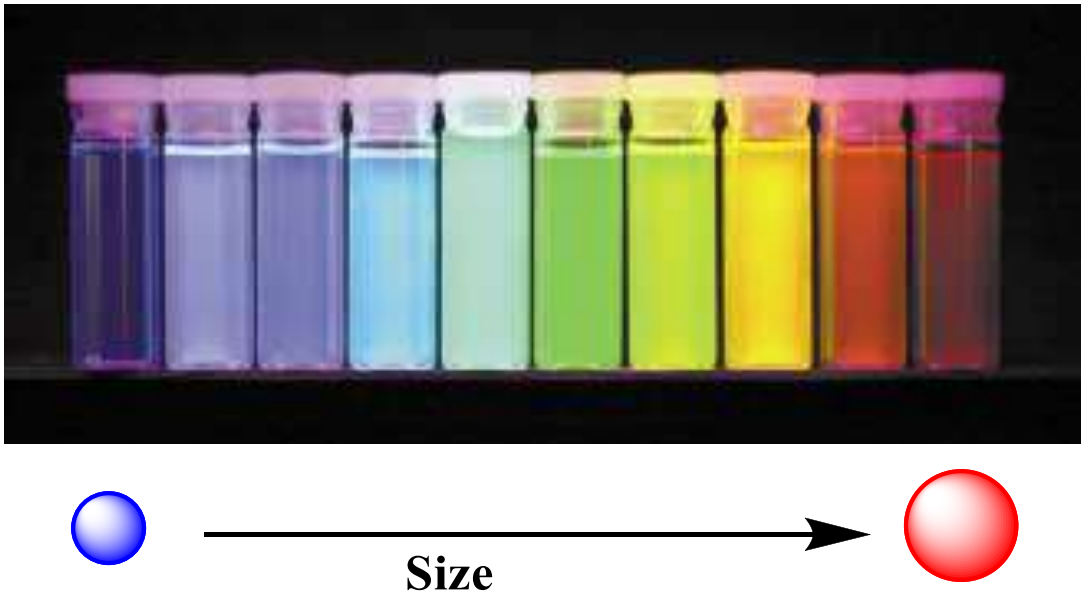

Figure 1-2: Ten distinguishable emission colours of CdSe/ZnS core/shell QDs excited with a near-UV lamp. From left to right (blue to red), the emission maxima are located at 443, 473, 481, 500, 518, 543, 565, 587, 610, and 655 nm respectively[19].

And Figure 1-3 shows the typical absorption and emission spectra of different sized CdSe/ZnS core/shell QDs, which all have broad absorption, different coloured QDs can be excited by a single excitation UV wavelength.

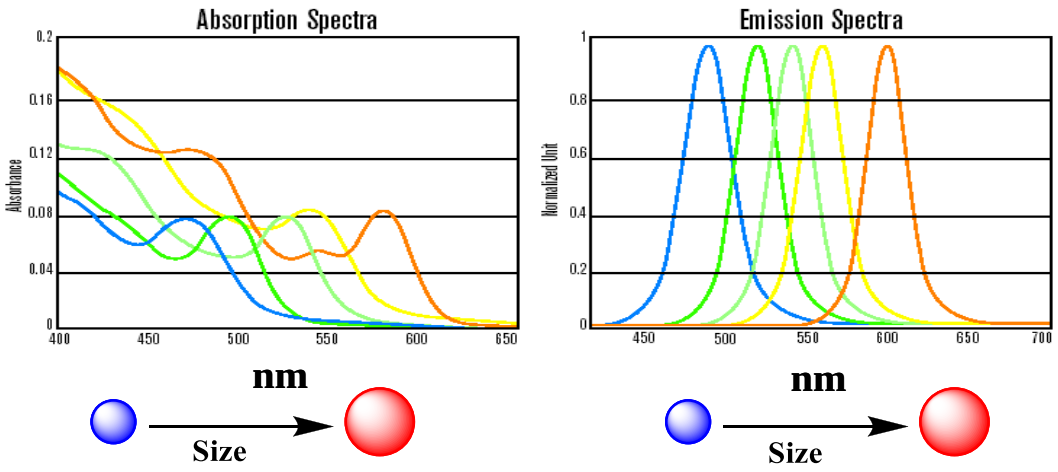

Figure 1-3: Typical absorption spectra (left) and emission spectra (right) of CdSe/ZnS core/shell QDs. The Figure is taken from Evident technologies: http://www.evidenttech.com

Besides spherical QDs, the rod-shaped QRs made of CdSe with different aspect ratios (length to diameter ratio) have also been prepared (Figure 1-4). Interestingly, by tuning the aspect ratio, the QR fluorescence can also be systematically tuned (Figure 1-5)[20].

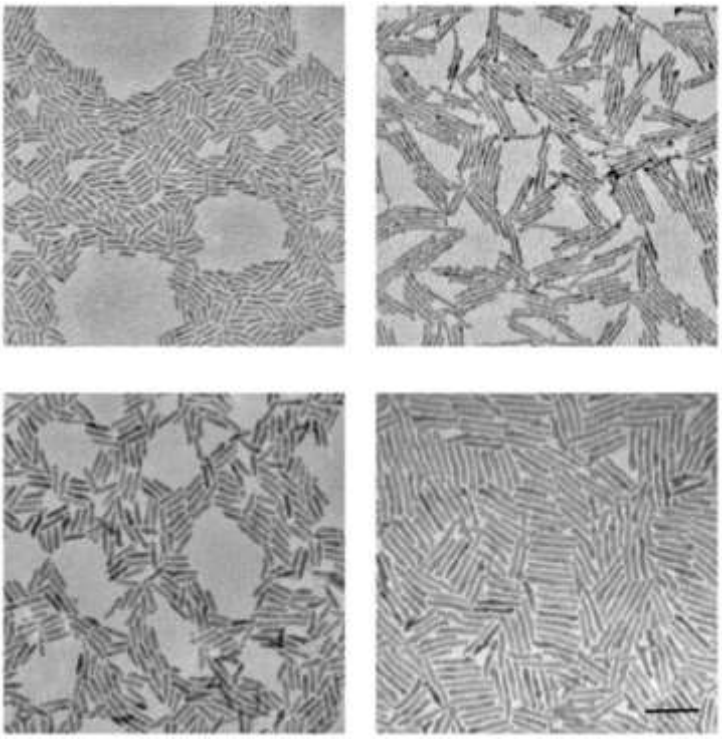

Figure 1-4: TEM images of four CdSe rod samples[20].

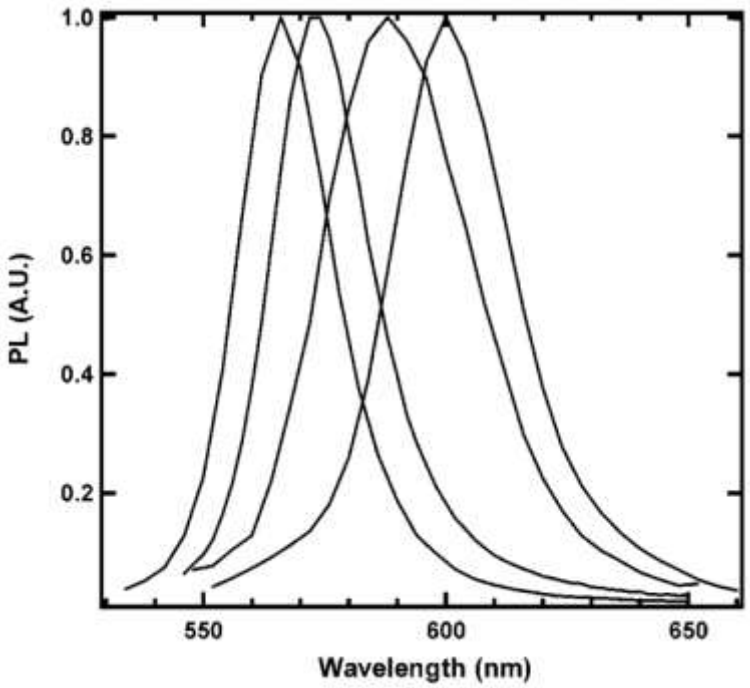

Figure 1-5: Photoluminescence spectra of 3.7 (±0.2) nm wide CdSe quantum rods with lengths of 9.2, 11.5, 28.0, and 37.2 nm, respectively (from left to right), excited at 450 nm[20].

In comparison, traditional organic fluorescent dyes tend to have relatively narrow absorptions and board asymmetric emissions. As a result, they can only be efficiently excited by a narrow range of specific lights, and therefore different coloured traditional fluorophores normally cannot be excited by a single light source. Moreover, the excitation light can also lead to irreversible oxidation of organic fluorescence dye, resulting in quick disappearance of fluorescence (or photobleaching), thus organic dyes tend to fade over time. Such drawbacks can seriously limit their applications in cell tracking/trafficking studies that require long term observations[21].

In contrast, QDs are made of solid inorganic nanocrystals which are much more robust against photo-oxidation (especially for those coated with a thick inorganic shell, e.g. core/shell QD). Moreover, the extremely high quantum yield (QY) (up to 100%) and large extinction coefficient make QDs up to 100 times as bright as organic dyes with 1000 times higher photo-stability over organic dyes. These properties are very important for detecting and marking bio-molecule long-term interaction in living cells[22], because the large molar extinction coefficients (e.g. 10^5-10^7 $M^{-1}cm^{-1}$), resisting photobleaching and chemical degradation, and two-photo absorption cross sections (10^3-10^4 GM) are much larger than fluorescent dyes[23].

In addition, the combination of using different materials and different particle sizes allows the preparation of various QDs with emission covering the whole

visible to near infrared region of spectrum (ca. 0.4-2.0 μm). This enables the use of different QD spectral signature at the same time, making specific detection of bio-molecules or cells easily recognizable. These advantages have enabled the QD being one of the most powerful fluorescent probes with very broad biomedical applications[2].

1.3 Synthesis, surface modification and bioconjugation of QDs and QRs

1.3.1 QD synthesis methods

A basic structure of a QD is comprised of a semiconductor core of hundred to thousand atoms, and coated with organic molecules (ligands) to promote solubility and prevent aggregation. The core where fluorescence comes from is typically composed of semiconductor material, such as CdSe. The core only QDs are directly capped with organic ligands and usually have low quantum yield and limited resistance to photo bleaching and chemical oxidation. Murray et al.[17] used $Cd(CH_3)_2$ and $(TMS)_2Se$ as the reaction precursors, which were added into TOPO ligand solvent at 350 °C with stirring. By controlling the growth temperature, they prepared CdSe core QDs with sizes ranging from 2.4 to 13 nm. The fluorescence quantum efficiency of the QDs was typically ~10%. Following on from this work, Peng et al.[18] obtained rod shape CdSe QDs (also named as quantum rod, QR) by changing the concentration of

precursors and the proportion of ligand. The quantum yield for luminescence in as grown rods is approximately 1% at room temperature, and is increased by a factor of 5 when a shell of a larger-bandgap material (CdS or ZnS) is grown on the core, as has been done with the QDs. Such quantum yields could be sufficient for biological labelling experiments, but are well below the maximum of 80% they have observed in dots. When thicker shells are grown on the QRs, the quantum yields are further decreased, which is likely due to cracking or strain at the core-shell interface. Besides, since Te^{2-} is more easily oxidized than Se^{2-}, it is generally harder to make CdTe QDs as compared to CdSe or CdS. Dmitri et al.[24] used laurylamine (DDA) to replace TOPO as reacting solvent and obtained highly luminescent CdTe QDs with an impressive fluorescence quantum efficiency of up to 65%. Its emission spectrum can cover from red to green range of the visible spectra range. Sanser et al.[25] used a mixed solvent of DDA and TOP and prepared different size CdTe QDs under different temperatures. They found that at higher reaction temperature, the faster the QD growth rate and the longer the fluorescence life time. Peng et al.[26] has improved the QD synthesis method by using CdO to replace $Cd(CH_3)_2$ as the precursor, and ethylphosphonic acid (HPA) and tetradecylphosphonic acid (TDPA) as the ligands. They have prepared high quality CdTe, CdSe, and CdS QDs in technical grade (90% purity) TOPO solvent. This synthetic method did not use organometallic cadmium in the reaction, and therefore greatly reducing the possibility of

environment pollution caused by the organometallic compounds. Qu et al.[27] also used the CdO precursor to prepare high quality CdSe QDs which displayed rather impressive fluorescence quantum efficiency (up to 85%) with narrow emission half-width of only 23 nm. On the basis of the above studies, they have optimised the alternative routes toward high quality CdSe QDs by using different scale of ligand, precursor and solvent[28]. As the QD synthesise methods improved, some reagents (oleic acid and ODE) which were cheaper and more environmentally friendly have been successfully used to replace the expensive and toxic organic reagents (TOPO and TOP)[29, 30]. Over the past few years, a few greener routes to synthesise high quality QDs have been reported. These include the use of liquid paraffin wax as well as olive oil to replace the TOPO and ODE solvent, presumably because liquid paraffin wax and olive oil are much cheaper. For example, Sapra et al.[31] used olive oil as solvent and ligand and successfully synthesised highly mono-disperse CdSe QDs, while Dai et al.[32] used liquid paraffin wax as solvent and ligand to prepare high quality ZnSe QDs.

1.3.1.1 QD synthesis in organic phase

Normally, several different methods have been developed to synthesis QDs: (1) high temperature organometallic approach using organometallic precursors and nonpolar organic solvents under inert atmosphere, (2) low

temperature aqueous approach by using convenient air-stable precursors. The most often used one is the organometallic approach. This is often done in high boiling point organic solvents at 250-300 ^{0}C by adding organometallic precursors in a coordinating solvent, under which the precursor pyrolyse quickly to form tiny crystal nucleus. The crystal nucleus gradually grows into QDs with time at the growing temperature. As the QD grows into a certain size, the surface curvature is reduced; allowing the coordination ligands to bind strongly onto the QD surface to block further growth as temperature is lowered, making them stable and well-dispersed in solvent. The precursors used here are typically metal alkyl compounds such as dimethyl cadmium. The ligands are typically trioctylphosphine (TOP), trioctylphosphine oxide (TOPO), and long chain amines (e.g. lauryl amine, DDA). This method can produce QDs with high fluorescence quantum yield, well-controlled and uniform sizes and core/shell structure. This is the most widely used approach to produce high quality QDs. It has been successfully used to synthesise group 12-16 (e.g. CdSe, CdS and CdSe/ZnS) QDs. Figure 1-6 shows the schematic procedures of the high temperature route to synthesise CdSe/ZnS core/shelled QDs[33].

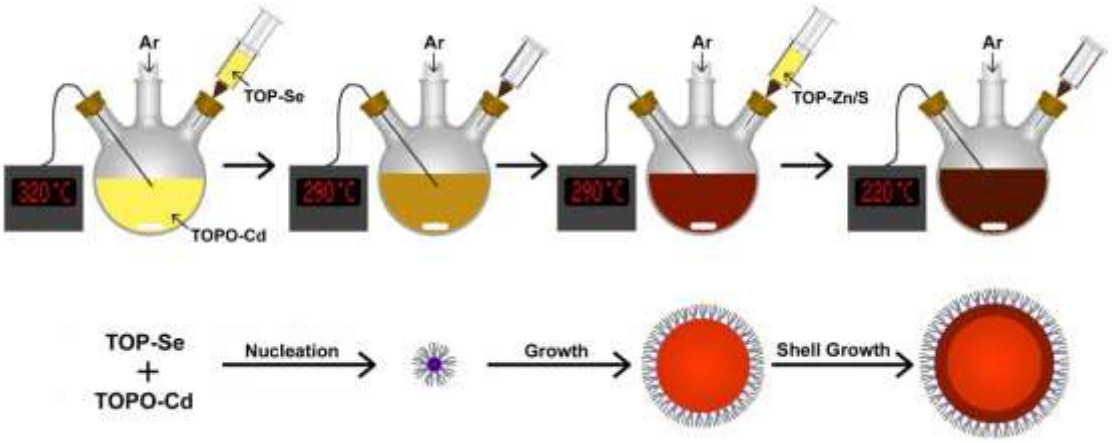

Figure 1-6: High-temperature coordinating solvent synthesis of colloidal CdSe quantum dots. For a typical reaction, a three-necked flask is placed in a heating mantle and equipped with a thermocouple and temperature controller. A cadmium precursor (e.g. cadmium oxide or cadmium acetate) is dissolved in the tri-n-octylphosphine oxide (TOPO) coordinating solvent in an inert atmosphere (argon or nitrogen flow). Under continuous stirring at high temperature (~320 °C), a selenium precursor dissolved in tri-n-octylphospine (TOP) is swiftly injected into the flask, initiating rapid nucleation of CdSe nanoparticles. Nucleation ceases quickly, partially due to the quick decrease in temperature (to ~290 °C) caused by the injection of the room-temperature solution, and particle growth ensues. When the desired size has been obtained, the solution may then be cooled (~220 °C) to prevent further particle growth. A passivating layer of ZnS may then be grown epitaxially by injection of zinc and sulfur precursors dissolved in TOP. Upon cooling to room temperature, these core-shell QDs may be isolated via precipitation[33].

The advantages of this method are that the QDs synthesized can be made of different layers of semiconductor materials (*i.e.* with core/shell structures) and coated with hydrophobic ligands to provide colloidal stability and surface passivity. Besides, a wide size range of QDs can be readily prepared by controlling the reaction time with each size nearly mono-disperse and the resulting QDs are highly crystalline with high quantum yields (e.g. > 80%). Its disadvantages include the use of toxic reagents, high costs, and low safety of operating procedures[33].

1.3.1.2 QD synthesis in the aqueous phase

Another approach is based on the aqueous synthetic route. Rajh et al.[34] first reported the preparation of CdTe core QDs coated by hydrosulfide group. Since then, the use of hydrosulfide based small molecule protective agents to make water soluble QDs has been improved gradually. The aqueous phase preparation methods usually use Zn^{2+}, Cd^{2+} or Hg^{2+} as the metal precursor, and Se^{2-} or Te^{2-} as anion precursor and functional thiol containing small molecules as the protective ligands, for instance, 2-mercaptoethanol, thioglycolic acid (TGA), mercaptoethylamine, glutathione (GSH), cysteine etc. Through reflux heating, the precursors first nucleate and then gradually grow into QDs which are capped with the thiol-containing ligands.

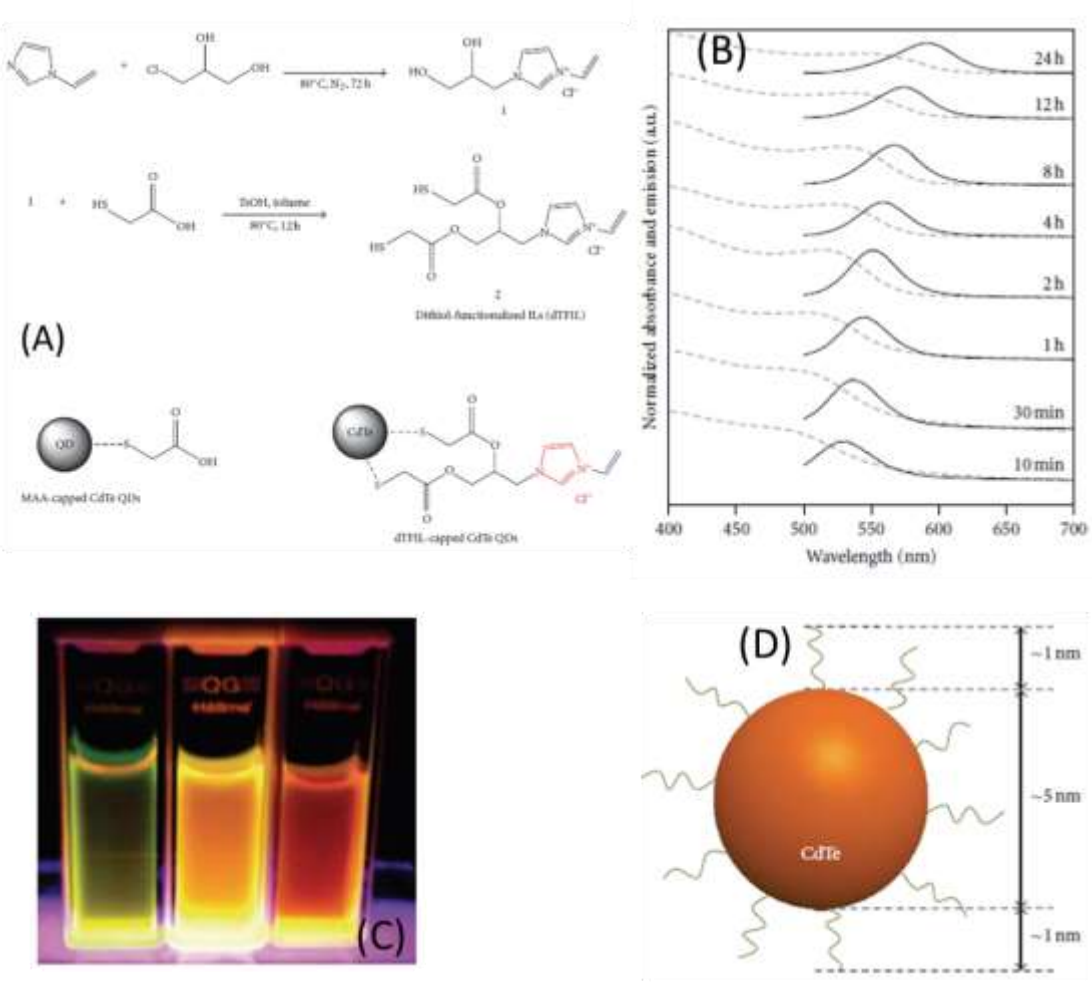

Figure 1-7: (A) CdTe QDs were synthesized via aqueous synthetic route in which Cd^{2+} ions and NaHTe were reacted in the presence of dithiol-functionalized ionic liquid (dTFIL). The control experiment with the use of mercaptoacetic acid (MAA) as a capping ligand was also conducted for comparison. (B) Absorption and photoluminescence spectra of IL-capped CdTe QDs with respect to the reaction time. PL spectra were recorded with an excitation at 470 nm. (C) Fluorescence images of dTFIL-capped CdTe QDs at different reaction times. All solutions were excited with a hand-held UV lamp. (D) Illustration of dTFIL-capped CdTe QD with estimated dimensions[35].

Figure 1-7 shows an effective method for aqueous synthesis of highly luminescent and stable CdTe QD by using thiol-functionalized ionic liquid as capping ligand molecules. The photoluminescence quantum yield of dithiol-functionalized ionic liquid (dTFIL) capped CdTe nanocrystals reached up to ~40%. The luminescent property was maintained for 8 weeks without obvious change of physical appearance, making it an attractive method to make functional QDs directly from the water phase[35].

QDs prepared by the aqueous synthetic method possess several merits: (1) the use of water as solvent; (2) use of inorganic salt as the reaction precursor; (3) the synthetic procedure is simple; (4) the QDs are readily water-soluble and can be applied to bio-system directly; (5) the QDs are capped with functional ligands, allowing for easy functionalisation and bioconjugation[35]. However, most of these QDs (except for CdTe and HgTe) tend to have relatively low quantum yield and relatively large particle size poly-diversity and low crystallinity. Moreover, since the core is directly exposed to the outside environment (this approach is not suitable for making high quality core/shell QDs)[35], their fluorescence is often sensitive to environmental changes, which can significantly restrict their applications.

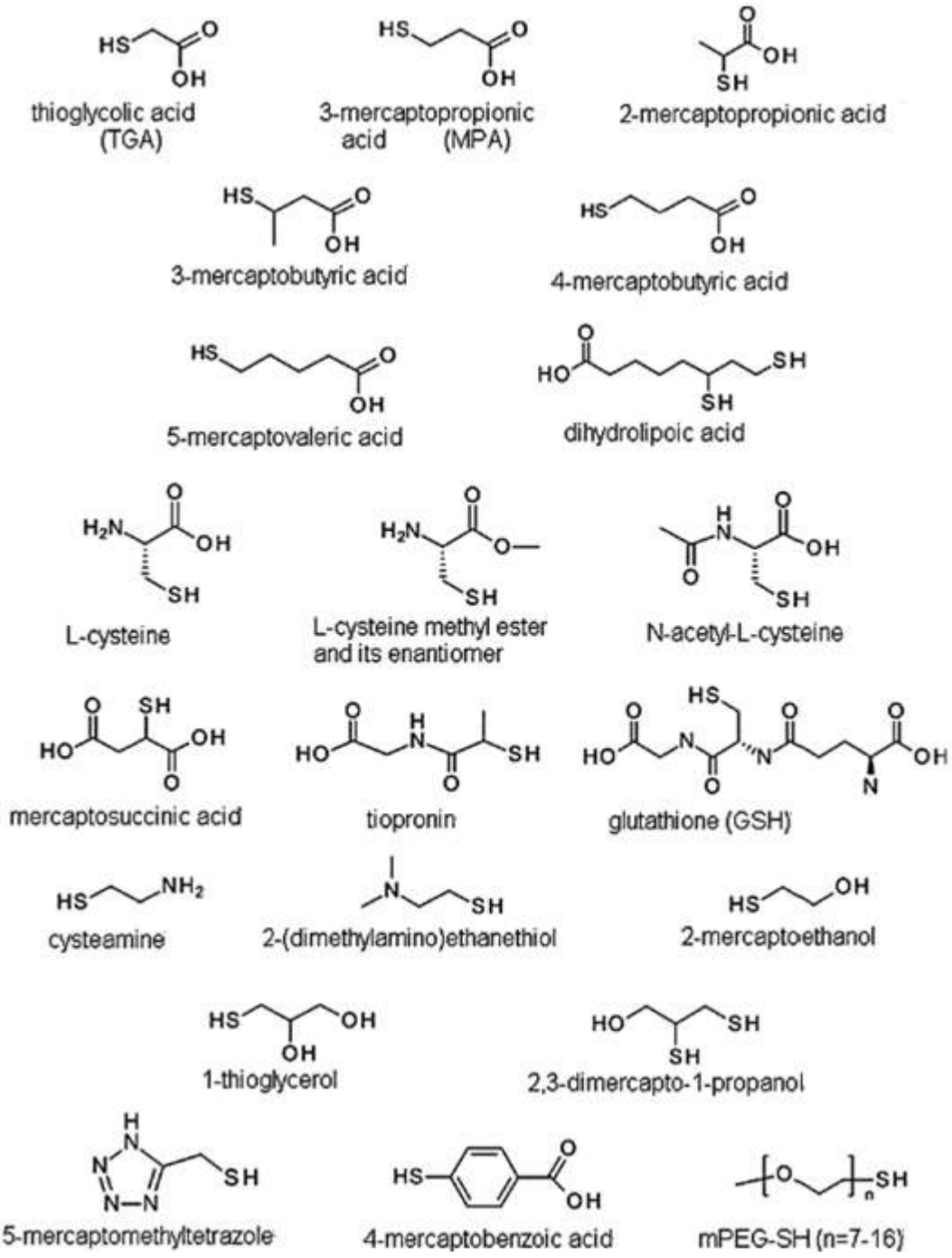

Figure 1-8: Chemical structures of thiol capping ligands that have been used in the synthesis of QDs in the aqueous phase[36].

Figure 1-8 shows a wide range of thiol containing compounds that have been successfully used as the capping ligands in the aqueous QD synthetic approach[36].

To increase the quantum yield and solve the problems outlined above, Guo et al.[37] changed the formulation of cadmium precursor and optimized the ratios between the protective agent and Cd^{2+}, and prepared a TGA coated CdTe QD with a QY as high as 50%. Using similar method, Rogach et al.[38] further improved the QY of the CdTe QD to 60%. While Li et al.[39] carefully investigated how the reaction conditions affected the preparation of mercaptopropanoic acid (MPA) coated CdTe QDs. They found that the pH and concentration of cadmium precursor solution strongly affected the QY of the resulting QD, with pH = 8.00 and 1.25 mM cadmium precursor concentration being optimum for the QD synthesis, under which the resulting CdTe QD exhibited a high QY of 67%. Their results indicated that the MPA ligand on the QD surface not only decreased the surface defects but also prevented the continuous growth of the QD. Zhao et al.[40] studied how the Cd/Te ratio affected the luminescence property of QDs. They found that the higher the Cd/Te ratio, the better passivation of the QD surface. In addition, Chen et al.[41] made a mercaptamine coated CdTe QD where they have used the amino functional group of the mercaptamine to conjugate the DNA molecules directly. After DNA conjugation, the fluorescence intensity and photo-stability were found to have improved dramatically, allowing it to be

used in imaging of living organism. Jiang et al.[42] prepared a CdS QD using glutathione (GSH) as protective agent. They found that increasing the reaction temperature decreased the reaction time dramatically while increased the QY up to 36%. In addition, Yang et al.[43] used a mixed glutathione (GSH) and cysteine (molar ratio = 1:3) as the protecting agents for QD synthesis. Since GSH and cysteine both contain amino- and carboxylic acid- groups which are charged and therefore offering good water solubility. The resulting CdTe QD displayed a highly impressive QY of as high as 70%, which is so far the highest for the CdTe QDs prepared by the aqueous synthetic route. Liu et al.[44] developed a one-step method to make ZnSxCd1-xSe mixed QDs using cysteine as the protecting agent in an aqueous solution. They found that after exposure to the ultra-violet light, cysteine decomposed to give S which subsequently bound to the QD surface, leading to a QD surface reconstruction and significantly increased QY to 26.5%. Last but not the least, Deng et al.[45] chose three different kinds of protecting agents (MPA, TGA, GSH) to make ZnSe and ZnxCd1-xSe QDs in the water phase. They found that the protective agents had significant impact on the growth speed and final size of the QDs.

In addition to the approaches mentioned above, a number of other aqueous based synthetic methods, such as the hydrothermal growth,[46] microwave assisted reaction and so on, have also been developed to make water-soluble QDs[47].

Despite a number of different synthesis methods have been developed to prepare QDs to be directly soluble in water or in organic phase, some further developments are still needed; 1) the elements used to synthesis the QDs are mostly toxic, which can limit their use in living organisms; 2) the route to synthesise the QDs in organic phase often needs high temperature, oxygen-free environment and organic solvent which can cause environmental pollution; 3) some synthesis procedure can be dangerous when using organometallic precursors; 4) the hydrophobic QDs should be surface modified before biological application; 5) the route to synthesise QDs in the water phase often produces low QY with limited stability under biological conditions, which can limit their use in biosensing and biomedical applications.

1.3.2 Structure of core/shell QDs

To date, most experiments often use core/shell QDs capped with hydrophobic TOPO surface ligands, which have high QY and can be made biocompatible after surface modification. Figure 1-9 shows typical structures of CdSe/ZnS core/shelled QDs coating with TOPO ligands.

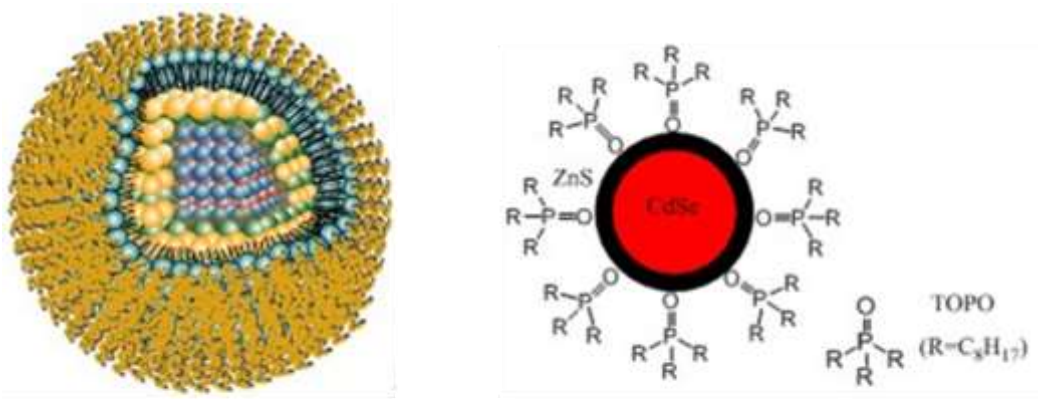

A B

Figure 1-9: (A) an illustration of the structure of a core-shell QD. The core is coated with an inorganic shell, which is further coated by a layer of organic ligands. The Figure is taken from Evident technologies: http://www.evidenttech.com. (B) Schematic structure of a CdSe/ZnS core/shell QD. High-quality QDs are normally stabilized by a layer of coordinative organic ligands, such as TOP (trioctylphosphine) or TOPO (trioctylphosphine oxide), which make them strongly hydrophobic and only soluble in nonpolar organic solvents.

The photo physical properties of QDs are strongly dependent on their surface properties; the presence of defects can seriously affect their fluorescence quantum efficiency. Core-only QDs usually have relatively low fluorescence quantum yield and limited resistance to photo-bleaching and chemical oxidation. If the defects only exist on the surface, then the QDs need to be capped by organic ligands to passivate the surface. However, organic ligands

can only passivate anionic but not cationic defects. Meanwhile the use of inorganic material shell can not only eliminate both anionic and cationic surface defects but also allow the formation a new type of core/shell QD[48]. Coating the QD core with another layer of lattice matching higher band-gap inorganic material shell can significantly improve the stability of the QDs. In this case, the exciton carriers are restricted within the core only upon photo-excitation, and thereby significantly improving fluorescence quantum yields[12, 49-51], resistance against photo-oxidation[52, 53], and chemical and thermal stability[54]. For example, Hines et al,[55] and Bawendi et al[6], have used $Zn(CH_3)_2$, $ZnEt_2$ and $(TMS)_2S$ as precursors to prepare CdSe/ZnS core/shell QDs, where the capping a ZnS shell not only can eliminate dangling bond(s) on the QD surface, but also confine the exciton carriers to the fluorescence core only, leading to significantly improved fluorescence quantum efficiency to around 40-50%. After that, Reissue et al[49], first used CdO as metal precursor added in a specifically scale HDA/TOPO coordinating solvent to prepare the CdSe core QD, and then used zinc stearate to coat the core QD with a ZnSe shell, yielding a CdSe/ZnSe core/shell QD with impressive fluorescence quantum efficiencies of 60-85%. Thereafter, Mekis et al[56], used $Cd(Ac)_2$ as metal precursor in HDA-TOPO-TDPA mixed solvent to prepare the CdSe core QD first, and then added H_2S gas into CdSe QD solution to obtain high luminescent CdSe/CdS core/shell QDs with adjustable fluorescence spectrum from green to red. Pron's group further made new core/shell/shell

CdSe/ZnSe/ZnS and CdSe/CdS/ZnS QDs[57-59] which can offer higher stability against photo-oxidation and higher QYs than the normal core/shell QDs.

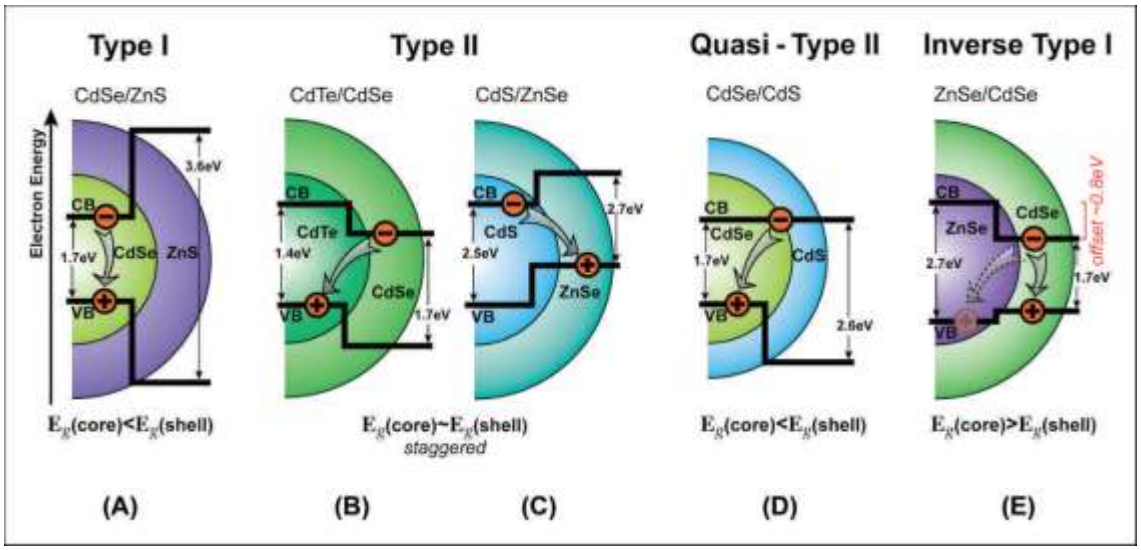

Figure 1-10: Schematic representation of energy-level alignment by selection core and shell materials, leading to the formation of different QD types. (A) Type I QD where both electron and hole are confined in the core; (B) Type II QD with localization the electron in the shell; (C) Type II QD with localization of the hole in the shell. (D) Quasi-Type II QD with localization of the electron in both and the core and shell. (E) Inverse-Type I QD with localization of both carriers in the shell[23].

So far, many types of core/shell QDs or core/shell/shell QDs made of II-VI, IV-VI, and III-V semiconductors have been prepared with different relative core and shell band energy and band gaps. As Figure 1-10 shows, there are four types of energy level alignments in core/shell QDs. For the Type I QDs (a

typical example CdSe/ZnS, where the shell valency and conduction bands are lower and higher than the corresponding core material), the core band gap is located within the shell band gap, therefore, the exciton carriers are fully confined within the core, the recombination probability of electron- hole pair is significantly increased, while the non-radiative decay is greatly suppressed. As a result, the QY is greatly increased. Any changes to the shell do not affect its fluorescence too much. For example, Hines and Guyot et al,[55] prepared the CdSe/ZnS QD first by coating with a 3 nm thick ZnS shell on the core (QY up to 50%). Type I configuration is most used in biological application because it offers the best confinement of exciton. For other three types, (Type II and inverse Type I) the electron and/or hole are located either in the core or in the shell. The exciton recombines across the core/shell interface; the energy of emission is less than the band gap of either the core or shell. It will offer lower absorption coefficients and increase photoluminescence (PL) decay times. Because of different semiconductor materials (ZnSe, CdS, or ZnS) have different energy gap, and have different absorption coefficients. The absorption coefficient determines how far into a material light of a particular wavelength can penetrate before it is absorbed. Furthermore, surface modifications like ligand exchange will form new surface traps. With the excited electrons being spread out of the core/shell structure, the fluorescence properties of such QDs are strongly dependent on surface properties, because surface traps can greatly reduce the QD fluorescence.

1.3.3 Surface modification of QDs and QRs

1.3.3.1 Surface modification of QDs

All QDs prepared are coated with a layer of hydrophobic or hydrophilic ligands which control the QDs' solvent dispersibility, effective volume, surface charge and function. The ligands control the QD's solubility, aggregation and/or precipitation in solution. It has been reported that multiple precipitation and centrifugation cycles often cause the QDs to aggregate and precipitate from solution, presumably due to the loss of some surface ligands[60]. Since most high-quality QDs are prepared by the high temperature organometallic route, these QDs are usually capped with hydrophobic ligands (such as TOPO) making them insoluble in aqueous system. However, for biological applications, water-solubility is essential and thus such hydrophobic QDs need to be surface modified to make them soluble in water. In this regard, a numbers of different approaches have been reported, which can be classified into three main methods: surface ligand exchange, silica encapsulation, and amphiphilic polymer or lipid micelle encapsulation, as shown in Fig. 1-11 [16, 61].

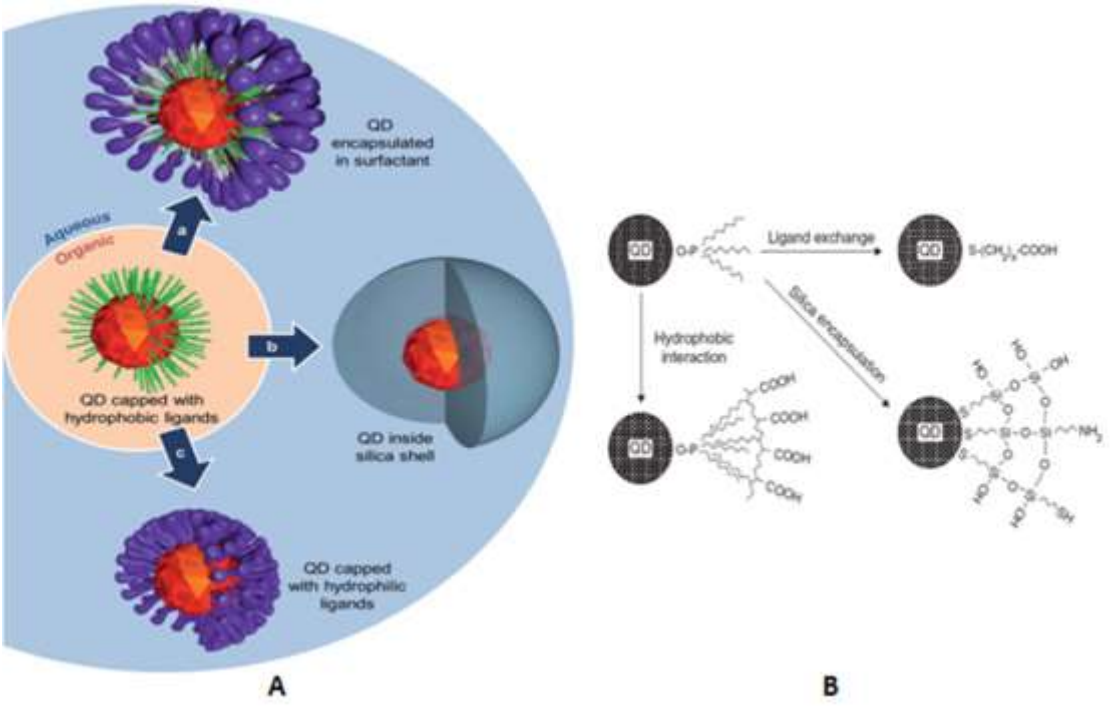

Figure 1-11: (A) schematic representation of different possible route to transfer QDs from organic to aqueous medium. (B) Three general surface chemistries used to convert QDs from hydrophobic to hydrophilic[16, 61].

Ligand exchange is a useful method which uses small molecules or polymers, such as mercapto- caboxylic acids [HS-(CH_2)n-COOH], dithiothreitol, dihydrolipoc acid, oligomeric, cross-linked dendrons and poly(ethylene glycol) (PEG), to replace the original ligands of QDs [3, 5, 62, 63]. These ligands all have terminal functional groups to anchor to QD surface, while hydrophilic functional groups are pointing outwards to provide water solubility and other functional groups for further conjugation to specific biomolecules, such as DNA, non-antibody binding proteins (nABP) or Biotin. This method only

adds/displaces a thin layer of ligands on QD surface, producing little influence on the hydrodynamic diameter (HD) of the QDs, and thus very useful for further making QD-FRET based sensors which require compact QD structures. However, there are also obvious drawbacks of this method; the stability of the new ligand is often affected by the surround environment such as temperature, pH value or salt concentration. It has been reported that dithiol-based molecules can provide better stability over mono-thiol based molecules, and tridentate thiol ligand can provide even better stability over dithiol-based molecules, because of the stronger multi-dentate binding[61, 64].

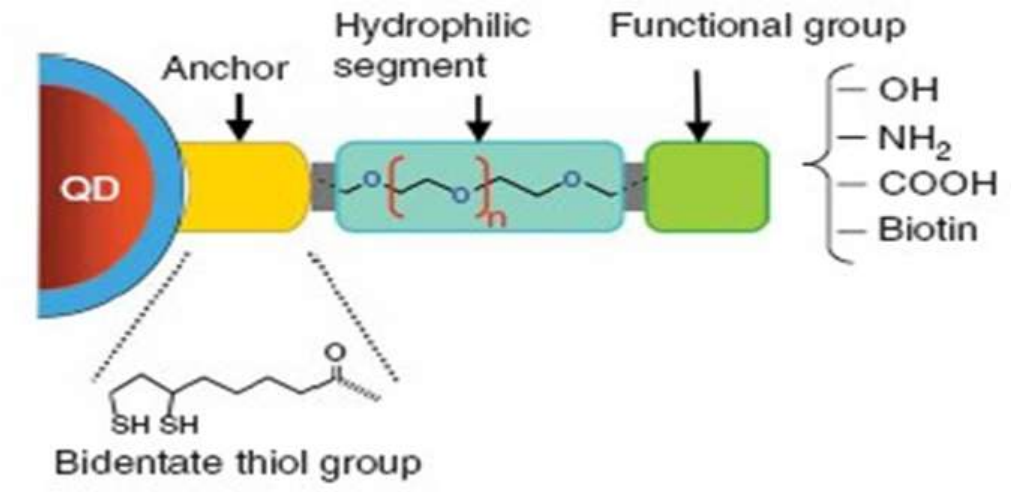

Figure 1-12: Modular design of hydrophilic ligands with terminal functional groups used in this study[64].

The Mattoussi group has designed a series of dihydroloic acid (DHLA) based ligands coupled with a poly(ethylene glycol) (PEG) linker and a terminal functional group. (Figure 1-12) Each ligand contains three main parts, anchor group (bidentate thiol group), hydrophilic segment (PEG chain) and terminal functional groups (biotin, carboxylic acid, or amine). Surface binding assays, cellular internalization and imaging experiments show that QDs capped with these ligands are stable over a broad pH range (*e.g.* 4~10) and accessible to simple bio-conjugation techniques such as protein conjugation of QDs driven by histidine coordination[65]. However, these ligands are directly bound to QDs' surface metal ions, and a large excess of expensive ligands are used (ligand:QD molar ratio of *ca.* 10^5 :1) which often lead to a significant decrease of the QY of the QD[64, 66]. Another method recently developed by the Mattoussi is the photo-ligation method (Figure 1-13) where they found that irradiation of the thiolic acid (TA) based ligands by UV light prior to mixing with hydrophobic QDs was sufficient to promote ligand exchange. More recently they found that the photo ligation of the TA based ligands with the QDs can also be carried out simply by using sunlight. They have further probed the nature of the photochemical transformation of the TA-ligands and found that irradiation (using either a UV photo reactor or sunlight) altered the nature of the disulfide groups in the TA, yielding a different product mixture from the chemically reduced ligands. Irradiation of the ligand in solution generates a mixture of monomeric and oligomeric compounds. Ligation onto the QDs selectively

favors oligomers, presumably due to their higher coordination affinity onto the metal-rich QD surfaces. This optically controlled ligation of QDs combined with the availability of a variety of multidentate multifunctional TA-modified ligands opened up new opportunities for developing fluorescent platforms with great promises for use in imaging and sensor design.[67]

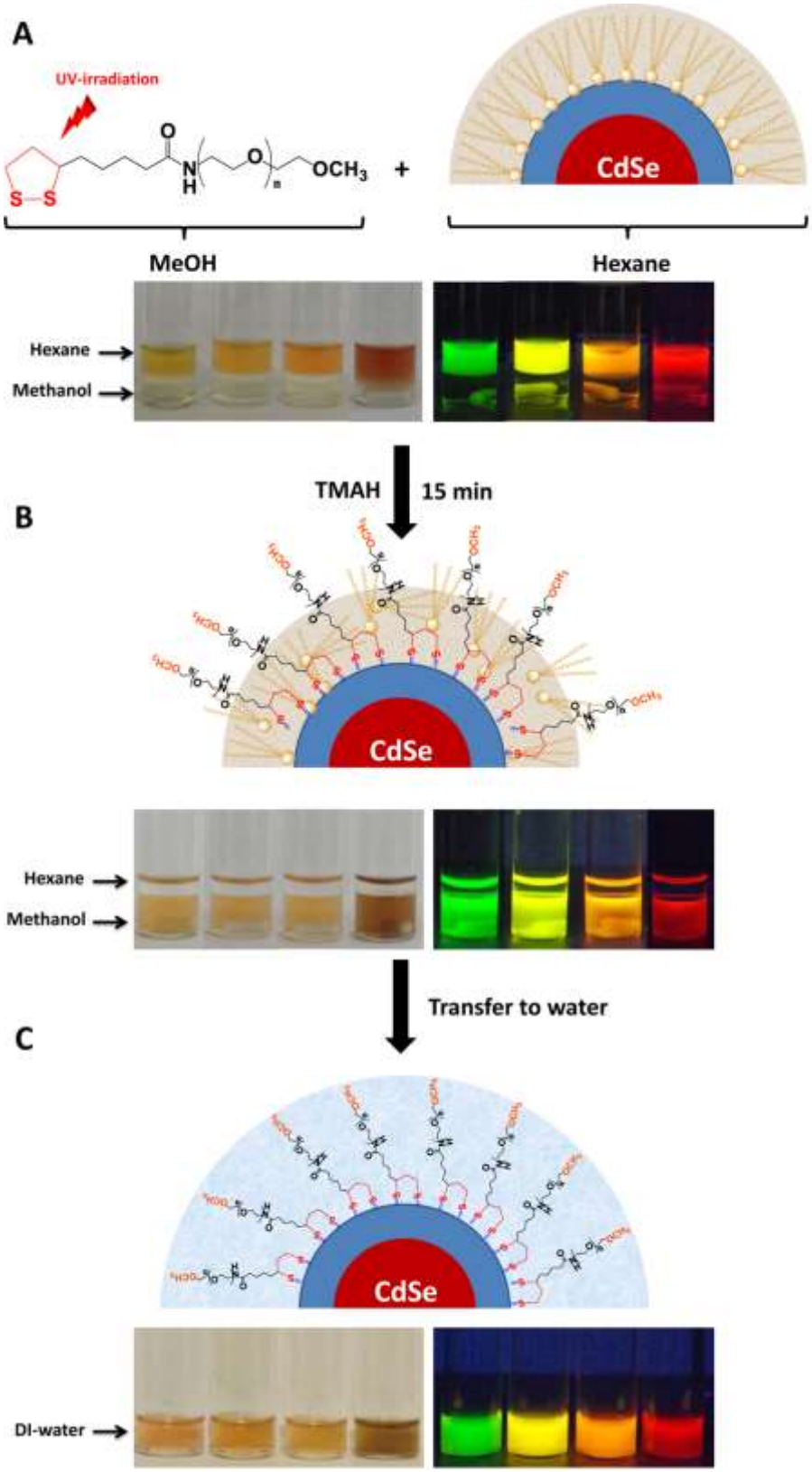

Figure 1-13: Schematic representation showing the cap exchange using preirradiated ligands. (A) Representation of the starting QDs and ligands

along with white light and fluorescence images of a two-phase mixture of TOP/TOPO-QDs in hexane and preirradiated TA-PEG750-OMe in methanol, immediately following mixing; four samples of distinct color QDs are shown. (B) Schematic representation of the QD ligation combined with white light and fluorescence images of the above two-phase solutions following phase transfer. (C) Schematics of the final hydrophilic PEG-capped QDs together with fluorescent images of these QDs in water. The dispersions were excited using hand-held UV lamp, with λex = 365 nm. The QD samples shown emit at 540 nm (green), 570 nm (yellow), 590 nm (orange), and 630 nm (red).[67]

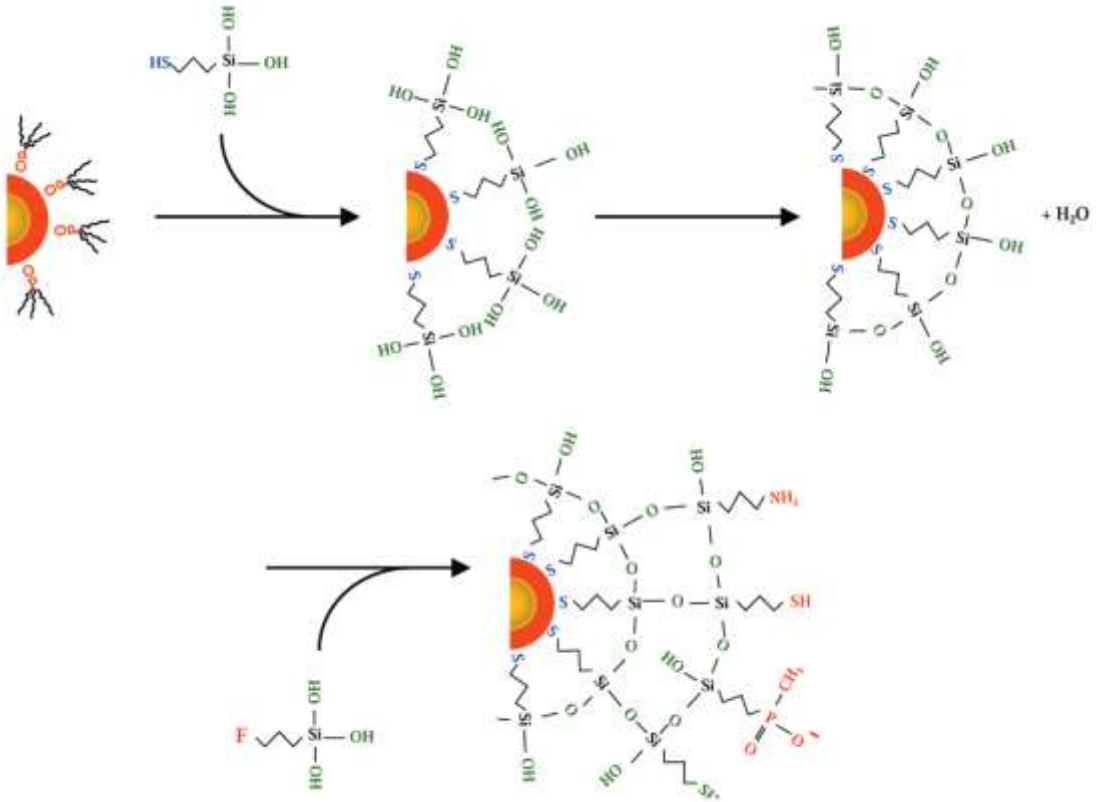

Figure 1-14: Sketch of the silanization method. The TOPO-capped CdSe/ZnS core/shell particles are dissolved in pure MPS, drawn in its hydrolyzed form for convenience in the figure. After basification, the MPS replaces the TOPO molecules on the surface. The methoxysilane groups (Si-OCH_3) hydrolyze into silanol groups (Si-OH), and form a primary polymerization layer. Heat strengthens the silanol-silanol bridges by converting them into siloxane bonds and releasing water molecules. Then, fresh silane precursors containing a functional group (F = -SH, -NH_2; -PO-(O^-)CH_3) are incorporated into the shell and may tailor the nanocrystal surface functionality. In a last step (not shown) the remaining hydroxyl groups are converted in methyl groups; this last step blocks further silica growth[68].

Another strategy shown in Figure 1-14, silica encapsulation, is to coat the QD surface with layers of silica which can also make the QDs soluble in water [69]. This method is quite similar to the ligand exchange strategy, where hydrophilic silica replaces the original ligands of QDs, and functional groups such as COOH, NH_2 and SH can be further introduced to conjugate functional biomolecules. However, QDs modified by this way normally have relatively big sizes which can limit their use in biology in situations that require compact sizes, e.g. FRET based biosensing.

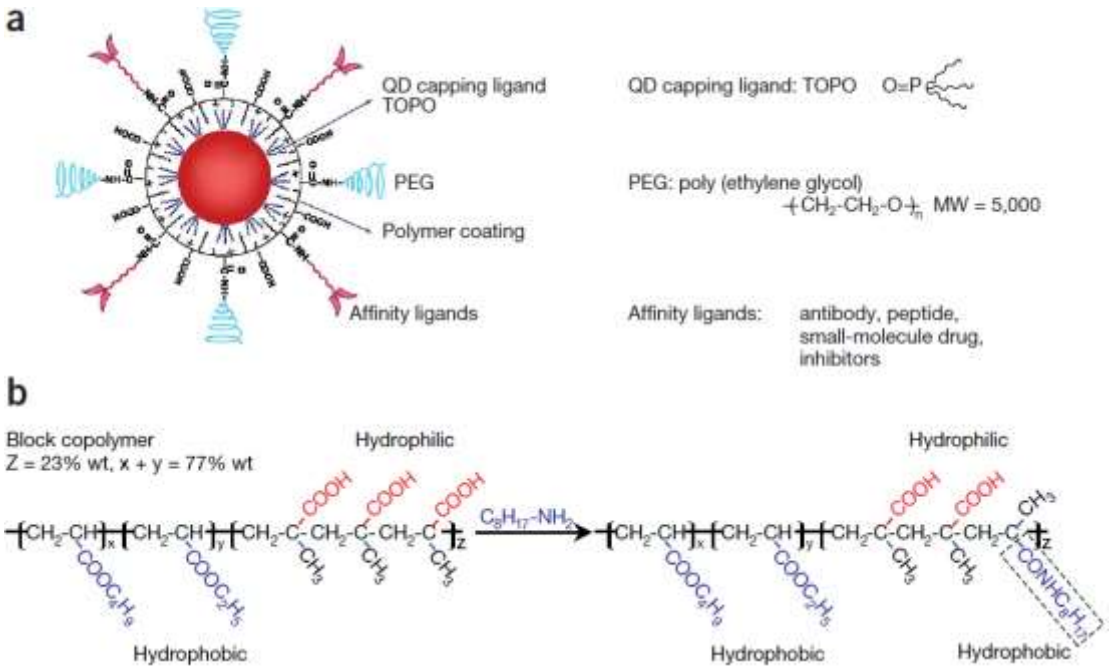

Figure 1-15: (a) Structure of a multifunctional QD probe, showing the capping ligand TOPO, an encapsulating copolymer layer, tumor-targeting ligands (such as peptides, antibodies or small molecule inhibitors) and polyethylene glycol (PEG). (b) Chemical modification of a triblock copolymer with an 8-carbon side chain. This hydrophobic side chain is directly attached

to the hydrophilic acrylic acid segment and interacts strongly with the hydrophobic tails of TOPO[70].

Amphiphilic polymer encapsulation is to wrap a hydrophobic QD particle with amphiphilic polymers to make it water-soluble[70, 71] (Figure 1-15). The amphiphilic polymer contains both hydrophobic and hydrophilic side groups. The hydrophobic side groups can interact with the hydrophobic ligands on the QD surface through van der Waals interactions and the exposed hydrophilic side groups provide water solubility [72, 73]. In this case, these polymers just interact with hydrophobic ligands on the QD surface; they do not directly interact with the QD surface atoms (no change of the QD surface coordination environment). Therefore the resulting water-soluble QDs can often maintain their native high QYs. However, QDs modified by this way often have large sizes with hydrodynamic diameters typically greater than 25 nm[22, 74], which could limit their applications in situations that require small sizes.

1.3.3.2 Surface modification of QRs

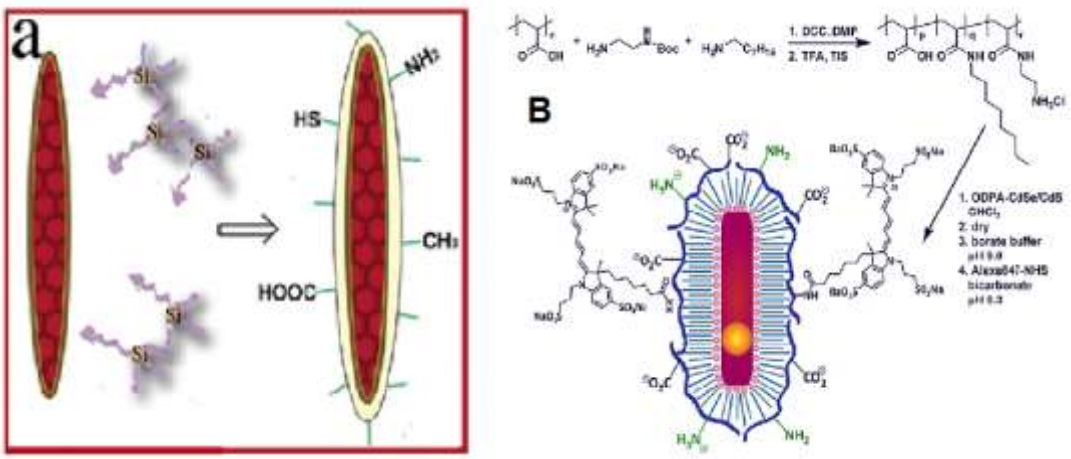

Figure 1-16: (a) A cartoon illustrating silanization of quantum rods. Cross-linked silanes are priming molecules for the surface coating. (b) Chemical synthesis of Dual-Emitting Hybrid Nano thermometers. QRs were transferred into water using a poly(acrylic acid)-based amphiphilic random copolymer displaying an optimized ratio of hydrophobic alkyl chains, carboxylic acids and alkyl amines[8, 75].

Similar to QDs, high-quality QRs are also prepared to be only soluble in the organic solvents. It is necessary to design a surface modification to make them soluble in water and render them biofunctional. In this regard, a numbers of different approaches have been reported. However, conventional surface ligand exchange method is generally not suitable for Quasi-Type II QRs[23] (e.g. CdSe/CdS) because cap-exchange with strongly coordinating hydrophilic ligands (e.g. thiol-containing ligands) lead to significantly quenched QR fluorescence. Therefore, two main methods have been used to

deal with QRs: silica encapsulation, and amphiphilic polymer or lipid micelle encapsulation as shown in Figure 1-16. QRs after silanization or encapsulation with an amphiphilic polymer shell are stable in aqueous buffer and biocompatible [8, 75].

1.3.4 Bioconjugation of QDs

QDs can be conjugated with specific biomolecules by several approaches as shown in Figure 1-17. After coating QDs with amphiphilic polymers, biomolecules can be linked to the QD surface *via* functional groups (i.e. –COOH, -OH, $-NH_2$, maleimide) by covalent bonding[76]. Alternatively biomolecules can also be directly linked to the QD surface by poly-Histidine-tags if the QD surface is accessible to direct binding. This is a simple, rapid and straightforward method for QD-bioconjugation, producing QD-bioconjugates with small hydrodynamic sizes. However, this method is not suitable for QD coated with dense surface capping ligands whose surface is not accessible. Furthermore, the biotin-avidin interaction is also a commonly used QD-bioconjugation approach, but the use of avidin or biotin-fuctionalized QDs will increase the size of QD-bioconjugate probe which will limit use in FRET analysis and cellular assays. Figure 1-17 illustrates an overview of the different bioconjugation methods between QDs and biomolecules.

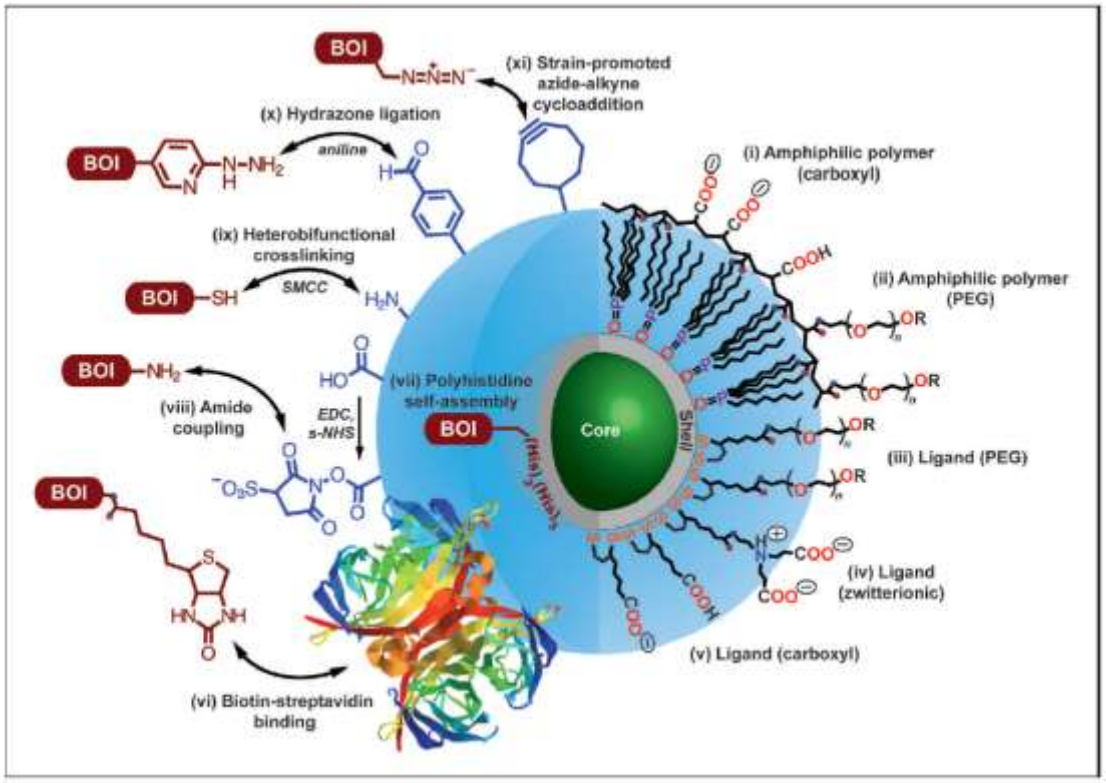

Figure 1-17: Illustrative overview of the chemistry of core-shell QDs. Coatings for aqueous solubility are as follows: (i) amphiphilic polymer coating with carboxyl(ate) groups; (ii) amphiphilic polymer coating with PEG oligomers; (iii) dithiol ligand with a distal PEG oligomer; (iv) dithiol ligand with a distal zwitterionic functionality; and (v) dithiol ligand with a distal carboxyl(ate) group. Common R groups include carboxyl, amine, and methoxy, although many others can be introduced (e.g., see vi, x, xi). Methods for conjugating biomolecules of interest (BOI) are as follows: (vi) biotin-streptavidin binding; (vii) polyhistidine self-assembly to the inorganic shell of the QD; (viii) amide coupling using EDC/s-NHS activation; (ix) heterobifunctional crosslinking using succinimidyl-4-(N-maleimidomethyl)cyclohexane-1-carboxylate (SMCC; structure not shown); (x) aniline-catalyzed hydrazone ligation; and (xi) strain-

promoted azide–alkyne cycloaddition. The double arrows are intended to represent conjugation between the functional groups and, in principle, their interchangeability (not reaction mechanisms or reversibility)[76].

1.3.5 QD and QR in cell marking and labelling

QDs have been successfully applied to label in vivo and in vitro systems, as well as in marking the structure of cells and proteins. The rationale here is that after conjugation of a specific antibody or small molecular ligand to the QD, it can specifically target/mark different intracellular organelles and/or skeletal systems, allowing for easy fluorescence detection via the specific coloured emission of the QD.

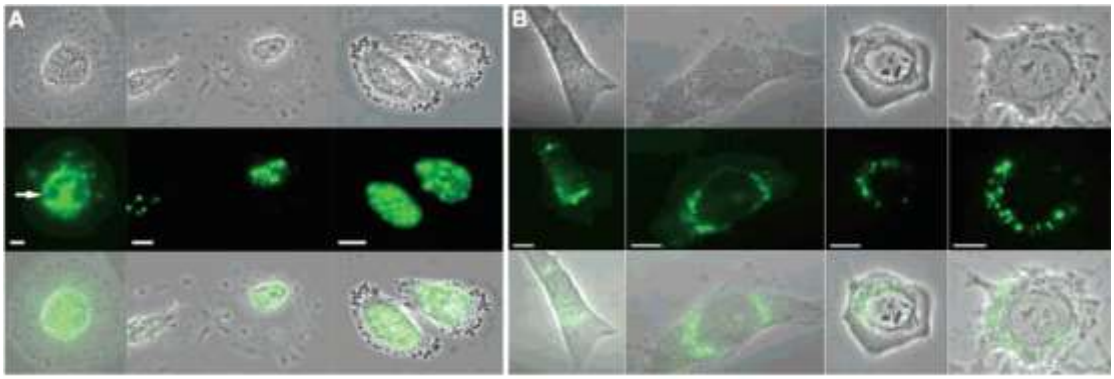

Figure 1-18: Localization of NLS-qdots in the nucleus (A) or in the perinuclear region (B). In both panels, the top row represents the phase contrast image, while the central row represents the fluorescence image. The bottom row is an overlay of the top and central rows. In certain cases, such as the cell at the far left of panel A, NLS-qdots localized inside the nucleus reveal finer

structures such as nucleoli within the nucleus, one of which is indicated with the arrow. Scale bars: 10 μm[77].

Through transfection, Chen et al.[77] managed to deliver a specific QD-marker molecule conjugate into the cell nucleus. In this experiment, they prepared a QD-peptide conjugate carrying the SV40 large T antigen nuclear localization signal (NLS) and transfected live cells with this conjugate. The movements of the QD-NLS conjugate from cytoplasm to the cell nucleus as well as its accumulation at the nucleus were monitored by fluorescence imaging shown in Figure 1-18. Besides live cell imaging, QD has been further applied to study the transportation pathway of endogenous proteins, cuticle proteins, cell matrixes and inside and outside of the cells.

Silanized QRs conjugated with various biomolecules through surface amino, mercapto, or carboxyl functional groups have also been prepared. Since antibody-antigen affinity is one of the most specific biological interactions and widely used for fluorescence imaging, Fu et al.[8] tested the conjugation of silanized particles with mercapto surface groups to anti-Her2 antibodies through a cross linker sulfo-SMCC as schematized in Figure 1-19. After incubating with the cells, the QR surface anti-Her2 antibody binds to the external domain of cancer cell surface over-expressed Her2, allowing for

specific targeting and fluorescence imaging of cancer marker Her2 on the cell surface in this case.

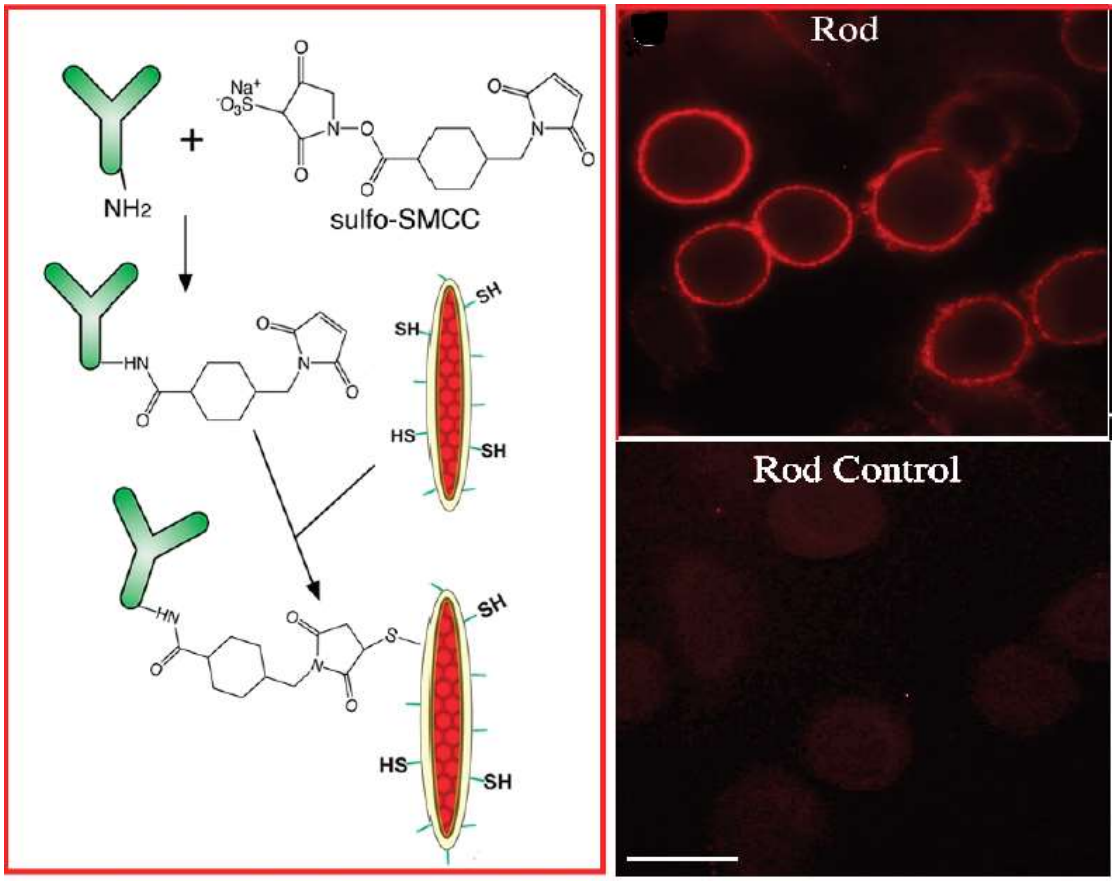

Figure 1-19: Schemes for antibody bioconjugation of quantum rods and Immuno-fluorescence labelling of breast cancer cell marker Her2 on breast cancer cells SK-BR-3. The Her2 marker was labelled with mouse anti-Her2 antibody and goat anti-mouse IgG F(ab')2 conjugated quantum rods/dots. The right bottom images show that there is minimum binding of free nanocrystals to the anti-Her2 antibody treated cells. Scale bar is 20 μm[8].

1.3.6 QDs in vivo imaging

Because of the high complexity of bio-systems, an effective fluorescence probe should satisfy a number of requirements. For instance, they should possess a good photo-stability against photobleaching, cause minimum disturbance to the intrinsic function of the organism, and have a high fluorescent quantum yield, etc. As discussed above, QDs can satisfy most of such requirements and therefore, the development of effective QD based in vivo imaging probes have attracted a great deal of research interest [78]. Dubertret et al.[22] increased the stability and biocompatibility of the QD by coating it with polyethylene glycol (PEG)-functionalised ligands and successfully used it to track and observe the development stages of African frog embryo. Kim et al.[79] injected the QD probes into the groin subcutaneous tissue of swine, and observed that the QDs could spread to the pre-lymph nodes for lymph nodes imaging. Gao et al.[71] investigated the specific imaging with the QD probes in mice as shown in Figure 1-20. They conjugated the QD with an antibody that can specifically recognize prostate specific membrane antigen (PSMA), a biomarker that is over-expressed in prostate cancer tumours. Through the subcutaneous injection, the size and position of planted prostate cancer tumour could be observed clearly in mice from the QD fluorescence. The structural design involves encapsulating luminescent QDs with an ABC triblock copolymer and linking this amphiphilic polymer to tumour-targeting ligands and drug-delivery functionalities. What they found

was that there was no non-specific adsorption in the kidney and brain tissues slices, but some QD markers were swallowed into cells after adsorbed on the histocyte surface. The high specificity and effective endocytosis ability of the QD revealed here will undoubtedly provide a new approach in studying drug target *in vivo*. This work therefore laid the foundation for the QD to be applied *in vivo* studies.

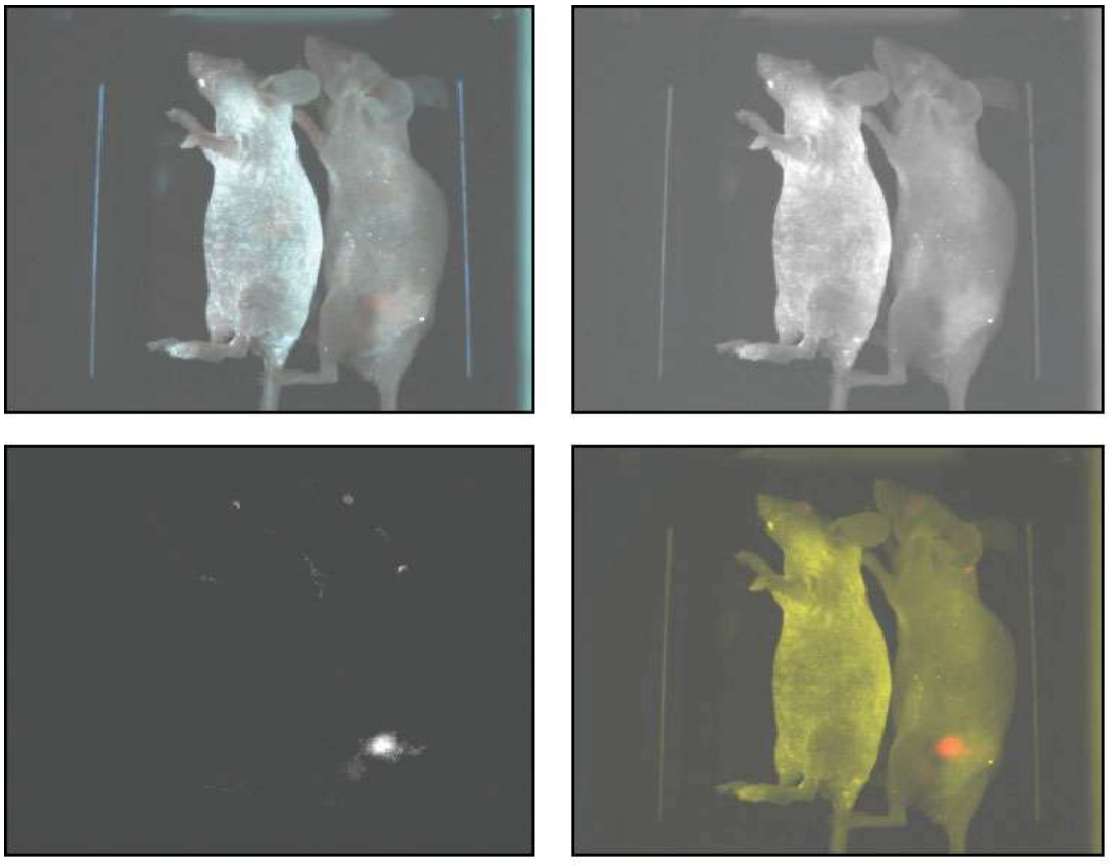

Figure 1-20: Spectral imaging of QD-PSMA Ab conjugates in live animals harboring C4-2 tumour xenografts. Orange-red fluorescence signals indicate a prostate tumour growing in a live mouse (right). Control studies using a healthy mouse (no tumour) and the same amount of QD injection showed no

localized fluorescence signals (left). (a) Original image; (b) unmixed auto fluorescence image; (c) unmixed QD image; and (d) super-imposed image[71].

After *in vivo* imaging, histological and immunocytochemical examinations confirmed that the QD fluorescence signals came from an underlying tumour. Note that QDs in deep organs such as liver and spleen were not detected because of the limited penetration depth of visible light[71].

In addition, QD can also be used for long term tissue optical imaging. Its biocompatibility can be enhanced via specific surface coating and engineering, making prolonged optical imaging of inside tissues possible. This is a property that the majority of fluorescent dye molecules cannot match. Morgan et al.[80] injected a near-infrared emitting CdMnTe/Hg QDs into a mice body, and confirmed it could be used for deep optical imaging of living organisms. However, the accumulation at the reticuloendothelial system and the influence of kidney filtration must be carefully considered before applying the QD in living body.

1.3.7 QD based Multiplexed assay/labelling

The fact that different coloured QDs can be excited by a single-colour light source yet each producing its specific, distinct colour emission make QDs excellent for developing multiplexed assays and labelling agents which can play a pivotal role in screening nucleic acid and protein. Jaiswal et al.[81] used

different coloured QDs conjugated with antigens against nucleus and cytoplasmic microtubules respectively for specific intracellular imaging. Using a single laser excitation, they found that the two different coloured QDs stained different regions of the same cell, and could be distinguished clearly. Kaul et al.[82] successfully labelled the WI-38 normal cells and U2OS cancer cells via their mortalin protein identity using QDs conjugated two different antibodies against such specific markers, allowing them to distinguish these two different cells using fluorescence microscopy.

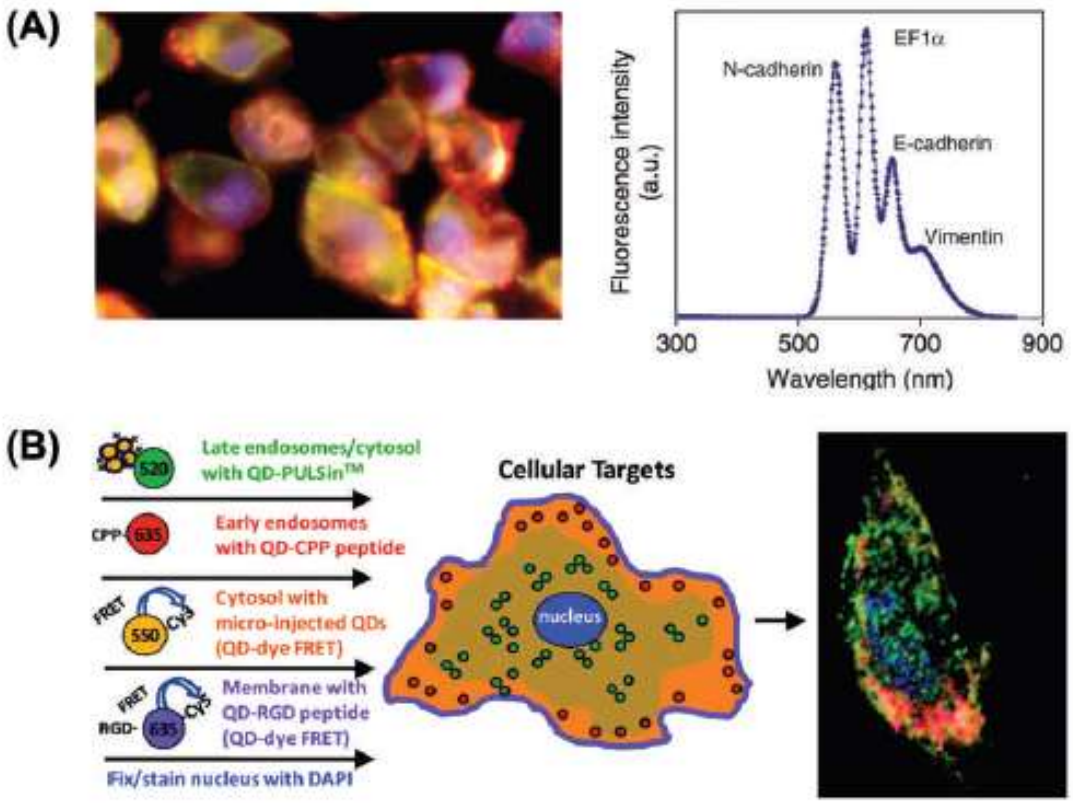

Figure 1-21: (A) the four markers, all associated with EMT, are N-cadherin, EF (elongation factor)-1α, E-cadherin and vimentin, and their corresponding QD colors are 565, 605, 655 and 705 nm. The cell nuclei were counterstained

blue by DAPI, and the QD data were captured under blue excitation. (**A left**) Color fluorescence image of highly metastatic prostate cancer cells (clone ARCaPm); (**A right**) single-cell QD data obtained from image **left**.[83] (**B**) Multicolour spatiotemporal strategy for labelling various subcellular compartments and structures with QDs and an example of a corresponding epifluorescence image.[84]

Xing et al.,[83] who used one colour of QD as an internal standard to target a housekeeping gene product that was expressed at a constant level. Four biomarkers—vimentin, N-cadherin, receptor activator of nuclear factor κB ligand, and E-cadherin—were labelled with secondary antibody conjugates of QD565, QD605, and QD655, respectively. An internal standard, elongation factor-1a, was labelled with QD705 (Figure 1-21A). They have achieved simultaneous staining of four different biomarkers with expression profiles consistent with western blot data. Moreover, QD staining provides spatial localization information (both inter- and intracellular), which is not possible with western blot or molecular biology techniques. Here, epifluorescence was used in combination with spectral imaging (vide infra). In general, more insight can be obtained from the detection of more biomarkers in parallel, suggesting a key role for the multiplexing advantages of QDs in diagnostic pathology. A report by Delehanty et al.[84] demonstrated spatiotemporal multicolour labelling

of live A594 cells (human alveolar adenocarcinoma) by using mixed delivery techniques over several days (Fig. 1-21B). When combined with four narrow bandpass filters, these QD probes provided four distinct spectral windows for imaging each of the aforementioned cellular components with a single excitation at 457 nm.

1.3.8 QD in drug target research.

There is overwhelming evidence that the discovery and verification of new drug targets is a key source for developing new drugs. Uncovering the drug target based on interactions between bio-molecules is one of the most important approaches. Chan et al.[85] noticed that the extremely high fluorescence stability of QD is an outstanding feature as compared to other organic dyes. Hence, it can be used to conduct long-term (from several minutes to hours) monitoring and tracking the interactions between bio-molecules. Another advantage of QD is that it can observe many target molecules in or on the surfaces of the living cells simultaneously by using different coloured QDs. In this case, how they can implement the biological functions inside the cells and their correlations can be studied. Over the past decade, an increasing number of new types of quantum dots have been reported. What is more, the size, shape and internal structure of these QDs can be controlled precisely.[86] These have provided a new path for the study of

receptor diffusion dynamics, ligand-receptor interactions, enzyme kinetics and so forth down to the single molecular level.[5, 70, 87, 88] For example, Sandra et al.[89] conjugated the 5-hydroxytryptamine to the quantum dots and used it to locate the receptor on the surface of cells successfully. At the same time, they examined the process how translocator proteins first drove the transmission of neurotransmitter when signal got through the intercellular space between adjacent nerve cells and then returned back to the cells. Recently, Lidke et al.[87] marked the epidermal growth factor (EGF) with quantum dots, use the specific ones to combine with EGF receptor and activate the signal transduction of erbB/EG Mediator.

Generally, to achieve the desired effect, one potent drug frequently needs to bind to its specific target molecules, while avoid binding to other non-target sites to avoid side effects. Combining different QDs with different drug target molecules is a superior way to detect the target sites simultaneously. Wood, K.V. et al.[90] had managed to mark three different intracellular organelles with three different coloured QDs in a single cell, the microtubule by a green, the Golgi apparatus by orange-yellow and the nucleus by red fluorescence QDs. After excitation by a single wavelength laser, the three colours are appeared simultaneously. Besides, using effective single molecule active compounds as the probe is another essential way to look for drug target spots. The active molecule-QD conjugates can then bind to the target spots on the surface of cells, allowing for easy identification of drug targets *via* the specific QD

fluorescence signals. This can improve the susceptibility and specificity in searching for the drug target spots.

The QD acting as an exceptionally promising fluorescent marker in organisms has been witnessed an increasing demand in the clinical drug applications. There is an pressing need to find out effective ways to enable drugs to enter and function in every target sites in the body, achieving the maximum therapeutic efficacy at the minimum dose range and without causing obvious toxic and side effects[91]. In this regards, the inorganic nanostructures (such as QDs) linked with bio-systems have attracted extensive interests because they combine the unique, size-dependent properties of nanomaterials and target specificity of biomolecules. Despite a relatively large size, the bio-connected QD was found to behave similarly to fluorescent protein probe in imaging of living cells. No apparent steric hindrance and dynamic problems were observed [77].

1.4. Fluorescence resonance energy transfer (FRET)

1.4.1 FRET principle

Fluorescence resonance energy transfer (FRET) is an energy transfer process which involves the non-radiative transfer of energy from a photo-excited donor molecule to ground state acceptor molecule in close proximity (*i.e*. typically <10 nm), leading to lower energy emission by the acceptor not directly excited. This efficiency of the energy transfer process is strongly dependent on the distance between donor and acceptor, and hence is widely used in a wide range of biological applications, e.g. biosensing, probing specific biorecognication and conformational changes of biomolecules. To achieve highly efficient FRET interactions, the following key criteria are required: (i) the emission spectrum of the donor fluorophore must significantly overlap the absorption spectrum of the accepter fluorophore; (ii) the orientation of the two dipoles affects their coupling efficiency, donor and acceptor must be aligned as linear so that an acceptor dipole can be induced by the donor; (iii) the donor/acceptor separation distance should be small, typically no greater than 10 nm; (iv) the donor has a high quantum yield[92, 93] (Figure 1-22).

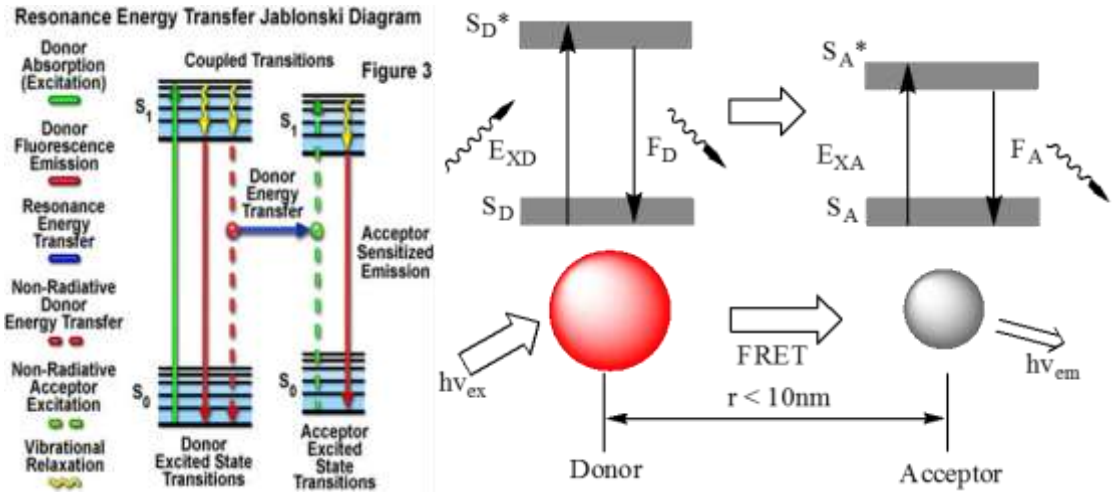

Figure 1-22: A schematic presentation of the FRET process. [92, 93]

The rate of energy transfer, k, for a single donor-acceptor pair separated by a distance *r* can be expressed by using the Förster formula[94].

$$k_{D-A} = \frac{B \times Q_D I}{\tau_D r^6} = \left(\frac{1}{\tau_D}\right) \times \left(\frac{R_0}{r}\right)^6 \qquad (1)$$

Where *I* is the integral of the spectral overlap function, and Q_D designates the quantum yield of the donor, R_0 is the Förster distance, is excitation radiative lifetime of donor. B is given in the following equation:

$$B = \frac{[9000 \times (ln\,10)]{k_p}^2}{128\pi^5 {n_D}^4 N_A} \qquad (2)$$

B is a constant that is related to the refractive index of the medium, (Avogadro's constant), and (the dipole orientation parameter). The value of the orientation factor, varies between 0 (for perpendicular alignment of the D-

A dipoles) and 4 (for parallel dipoles); and for random oriented diploes, k_p^2 = 2/3.

The FRET efficiency *E* is defined as:

$$E = \frac{k_{D-A}}{k_{D-A} + {\tau_D}^{-1}} = \frac{{R_0}^6}{{R_0}^6 + r^6} \qquad (3)$$

It is clear from the equation (3) that *E* is strongly dependent on the donor-acceptor distance *r*. Specifically, *E* represents the fraction of excited photo energy that is transferred from the donor to the acceptor.

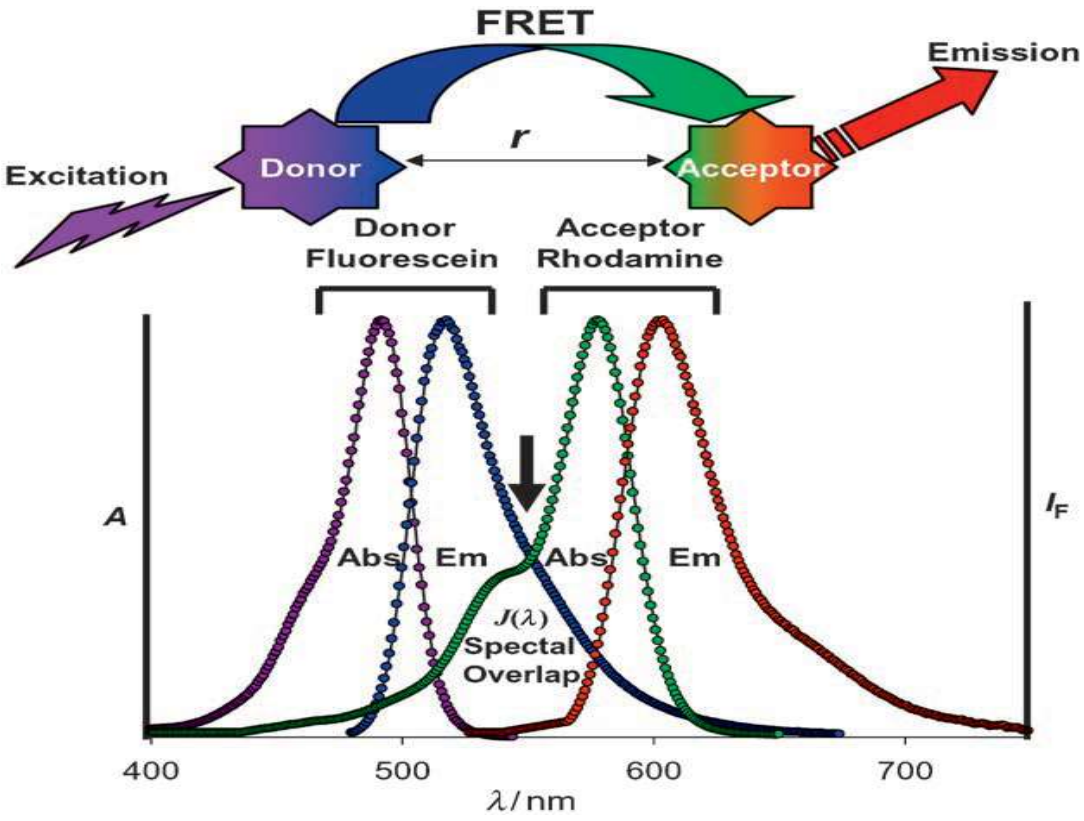

Figure 1-23: the absorption spectra and emission spectra of donor and acceptor [94]

FRET has long been an indispensable tool for probing molecular interactions. Method of FRET technology involves a single probe where two dyes (the quencher and the reporter) are in close proximity, *e.g.* < 10 nm. This technology can be used for bio-conjugate test to make sure the labeled protein or fluorescence protein has connected to the donor (QD). This is because a compact QD structure gives a small *r* value while the high QD fluorescence yields a large R_0 value, both factors are strongly beneficial to improve *E* and hence FRET based sensitivity as $E = 1/[1 + (r/R_0)^6]$. Since *r* is not only determined by the QD but also the associated bio-recognition molecule (binder) size, the use of small binders is also critical to improve FRET sensitivity[95, 96]. In order to make a good probe, the absorption spectrum of donor should have minimum overlap with that of the acceptor at the exciting wavelength (avoiding direct acceptor excitation, hence high background), and their emission spectra should have minimum overlap (ensuring easy separation of the donor and acceptor emissions), however, the donor emission should have strong overlap with the acceptor absorption spectrum for high FRET to happen [94]. (Figure. 1-23)

1.4.2 QD for FRET investigation

One example of such kinds of QD-bioconjugate probes are shown in Figure 1-24. A luminescent QD can act as efficient energy donor and FRET to labelled DNA, protein and protease assembled on the QD surface. The bridging DNA chain is rigid and so it can control the distance between QD and acceptor (dye) precisely. This construct has been successfully used to investigate the distance dependent FRET in the QD-bioconjugate system, confirming that the QD-FRET system still obeys the Förster equation despite a relatively large size of the QD donor.[97]

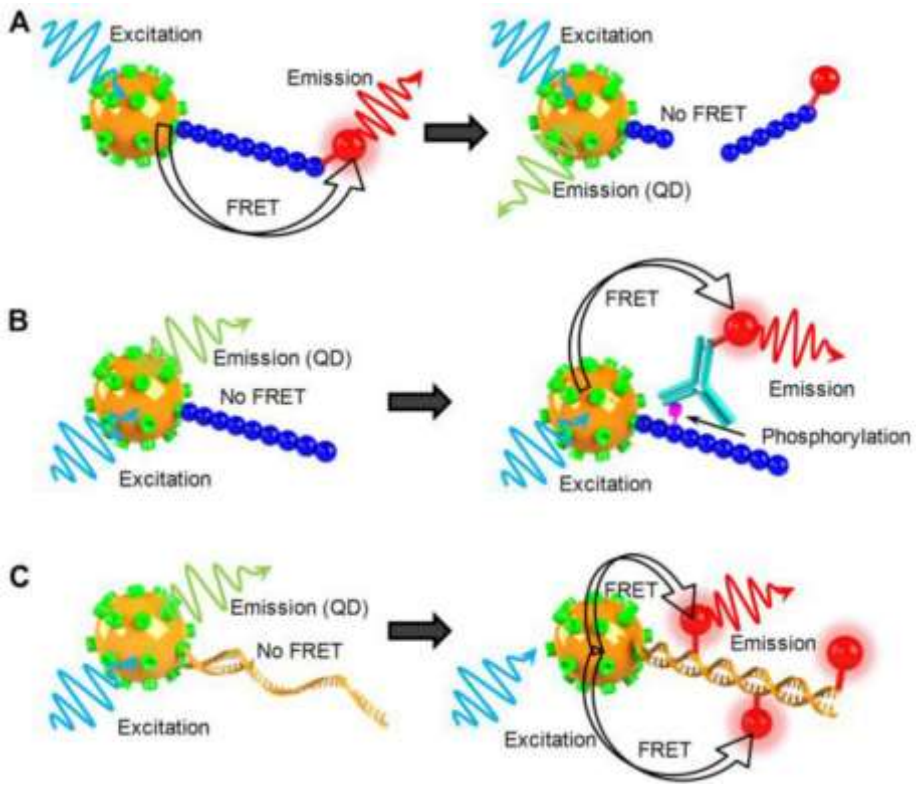

Figure 1-24: Schematic illustration of QD-FRET nanosensor for analysis of enzyme activity. a) QD-FRET sensor for the study of protease. b) QD-FRET

sensor for the study of protein kinase. c) QD-FRET sensor for the study of DNA polymerase. [97]

In this respect, Zhou, et al.[98] found that functional thiols are very useful in QD-bio-conjugation; where thiolated DNAs can directly self-assemble on to the mercapto-propionic acid (MPA) capped QD surface. Furthermore, it is possible to control the labelling position in the double-stranded DNA structure to conveniently control the separation distance between QD donor and dye acceptor to well within the R_0 of the FRET pair, leading to high FRET efficiency at low Acceptor/Donor ratios. However, the above self-assembled QD-DNA system was not suitable for specific DNA detection due to strong non-specific adsorption. Later on, Zhou, et al.[1] introduced a tri(ethylene glycol) linker in the QD surface coating ligands that eliminated the DNA non-specific adsorption, and the resulting QD-DNA conjugate was useful for both label and label free detection of DNA at low DNA probe/QD copy numbers. The schematics of the QD-FRET based sensing configurations are shown in Figure 1-25.

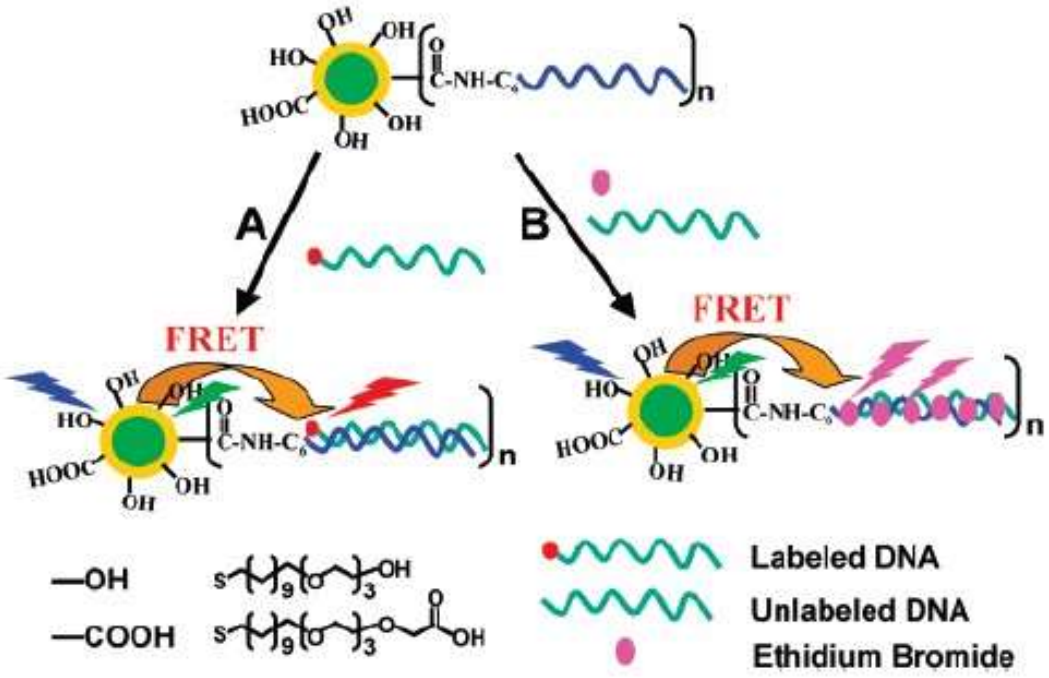

Figure 1-25: Schematic representation of the principles of the approaches for hybridization and label-free detection of DNA probes with a covalently coupled QD-DNA-T conjugate *via* a QD sensitized FRET signal[1].

In Figure 1-25(A), FRET from the QD to the labeled dye on DNA chain was used for detection of labeled DNA, while in (B) the specific intercalation of DNA intercalation dyes (ethidium bromide) within the formed dsDNA was used as acceptors for readout signal for label-free DNA detection. This design also allows the control of the separation distance between the QD donor and dye acceptor as well as the number of acceptors.

Zhan, et al[65] introduced a two thioctic acid (TA) groups chemically link to a zwitterion moiety as surface coating ligands on QDs and further bio-conjugated the QD to histidine-tagged proteins (mCherry). Moreover, the QD (donor) emission was quenched owing to FRET interactions with histidine-tagged mCherry (Figure 1-26). The absorption data shown in Figure 1-26 (b) indicate that there is an increasing contribution to the measured spectra at 586 nm, commensurate with the amount of added protein to the dispersion, which is attributed to the contribution of mCherry absorption. The composite photoluminescence spectra in Figure 1-26 (c) show that when the dispersions are excited at 400 nm (which coincides with the absorption valley of the protein) there is a progressive decrease in the QD emission concomitant with an increase in the contribution from mCherry when the molar concentration of the protein is increased. The absorption and fluorescence data confirm that conjugate formation has taken place.

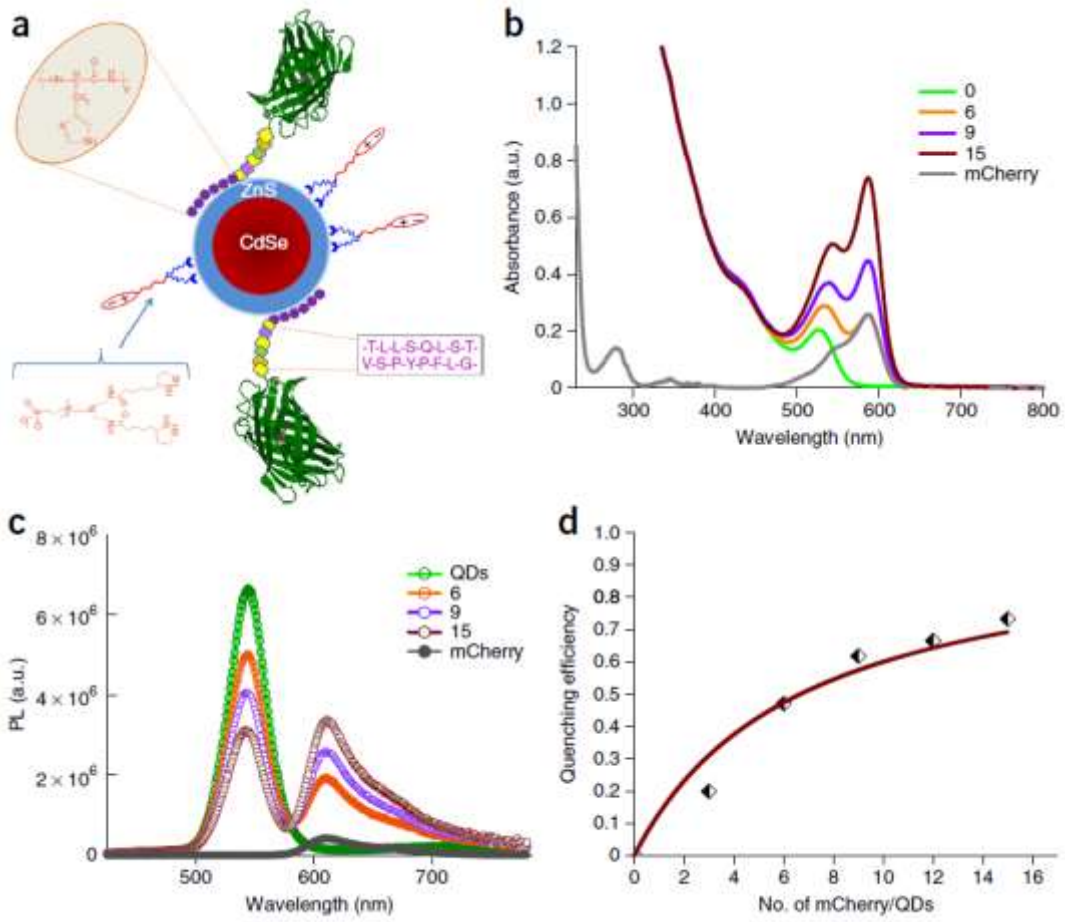

Figure 1-26: Protein conjugation of QDs driven by histidine coordination. (**a**) Schematic representation of a self-assembled QD-mCherry conjugate detailing the structure of the different components; a CdSe-ZnS QD photo ligated with bis(TA)-ZW ligands is shown. (**b, c**) absorption and photoluminescence (PL) spectra collected from dispersions of QDs self-assembled with mCherry at different molar ratios of 1:6, 1:9 and 1:15, along with the control samples of QDs and mCherry. The absorption spectra of the conjugates were normalized with respect to the value at 350 nm. The mCherry control spectrum was collected from a solution with the equivalent

mCherry concentration of 1:6 above. (**d**) Plot of FRET efficiency versus number of mCherry per QD conjugate.[65]

Besides basic photo physical and biosensing studies, QD-FRET based systems have been shown to be useful in a wide range of other biorelated applications. The advantages of this technology are that, (i) it allows for *in vivo* studies of molecular interactions such as monitor physiological responses, live cell imaging and localization of FRET organelles; (ii) it can be easily linked to other instrumentation, *e.g.* being miniaturized for high-throughput assays of combinatorial products; (iii) it is relatively cheap to implement; (iv) measurement can be carried out very rapidly often done in a convenient separation-free format; (v) it can offer accurate measure of small changes in distance. A few disadvantages of FRET based methods include; (i) it can only work at relatively short donor-acceptor separation distances (*e.g.* < 10 nm), hence pose a strict limitation of on the size of the probes; (iii) it only gives information on the donor-acceptor distance; (iv) large excess of free fluorophores can also interfere with the energy transfer[99-101]. To be compatible with different QD-FRET sensing mechanisms, the QDs (donor) and labelled biomolecules (acceptor) need close enough, and the size of the biomolecules should fit for the QDs (e.g. small-molecule, peptide, protein, polymer, and DNA,).

1.5. Conclusion and aim of this project

Quantum dots (QDs) and quantum rods (QRs) are a new type of fluorescent nanomaterial having unique size-dependent optical and electronic properties that are excellently suited for biomedical applications. These include size-tunable, bright, narrow symmetric fluorescence emission, excellent optical and chemical stability, and large absorption cross sections, and excellent resistance against photo-degradation. By controlling the size and/or composition, it is possible to produce QDs with emissions covering from the UV to the near infrared range. They have a number of advantageous properties over the traditional organic dyes or fluorescent proteins in biomedical applications. They have been used to develop bioconjugate probes and showed promising applications in cell marking, bio-imaging, bio-sensing, drug target and drug delivery research at the cellular and in vivo levels. A major limitation here is the potential toxicity and cytotoxicity of heavy metals contained in the QDs, and therefore the development of non-toxic QDs is imperative.

Several different methods have been developed to synthesise the QDs. These can be roughly divided into two main classes: the organic phase and the aqueous phase synthesis. The advantages of the organic phase synthesis are that the resulting QDs have high fluorescence QY, excellent crystallinity with good size mono-dispersity and stability. However, it often suffers from drawbacks such as requiring toxic reagents, high costs, and hazardous

operating procedure. Moreover, the QDs are capped by hydrophobic ligands and water-insoluble, which have to be made water-soluble before being used in biological systems. In contrast, the aqueous phase QD synthesis does not require any toxic solvent, it is cheaper and easier to operate, and moreover, the resulting QDs are readily water-soluble so can be directly used in bio-systems. However, most of these QDs have relatively low fluorescence QY, with limited chemical and photo stability.

QDs and QRs are excellently suited for FRET based application because of their broad absorption and narrow symmetric emission, allowing wide choices of excitation wavelengths to minimise the direct excitation of the acceptor, leading to low background. Most QD-FRET systems use QD as the FRET donor and organic dyes as the acceptor. The FRET efficiency can be finely controlled by tuning the distance between the QD and dyes as well as the number of acceptor dyes attached to each QD. The QD can be conjugated to a wide range of functional molecules, e.g. small-molecule, peptide, protein, polymer, and DNA, and the resulting QD-conjugates can act as novel FRET based sensing and imaging probes with broad ranges of biomedical applications.

As discussed above, compact, water-soluble core/shelled QDs can be prepared easily *via* the ligand exchange method, which can be conveniently bio-conjugated with biomolecules for biosensing *via* a highly efficient self-

assembly process with multi-Histidine-tagged biomolecules. However, there are still several challenges remained for the QD-FRET sensors 1) it can only work at relatively short donor-acceptor separation distances (*e.g.* < 10 nm); therefore, ligand exchange is better suited to make the required QDs than silica coating or amphiphilic polymer encapsulation. 2) Most current ligand exchange methods often produce significantly quenched QD, reducing the sensitivity of the resulting QD-FRET sensor.

This project aims to address the following fundamental questions:

1) to investigate why the cap-exchanged QDs often lose their fluorescence QYs;

2) to investigate whether it is possible to develop an efficient cap-exchange method to allow post-exchanged QDs to retain their native QYs and high stability under biologically relevant conditions through improving and optimizing the ligand exchange procedures; ;

3) to develop robust, sensitive ratiometric QD-FRET sensors for target proteins by combining such compact, bright QDs/QRs with small antibody mimetic proteins also known as non-antibody binding proteins (Affimers). The Affimers are a new class of antibody mimetic proteins recently developed in our collaborator's lab at the Faculty of Biological Sciences, University of Leeds. They have several advantageous properties over antibodies as target binders, including wide target choices; high binding affinity (low nM Kds),

rapid, cheap isolation, animal-free in vitro production (via bacteria expression) and excellent thermal-stability (Tm $\geqslant 80^{o}C$)[102]. More importantly, their much smaller molecular sizes (~1/10 of whole antibodies) are extremely well-suited for QD-FRET applications, allowing for significantly reduced donor-acceptor distance and hence improving sensitivity.

4) In the long term, to develop robust QD-Affimer fluorescence probes for clinical diagnostics and cancer tissue imaging. In fact, robust, sensitive, specific detection of cancer markers in fixed cancer tissues has great value in clinical cancer diagnostics, but this is still challenging as there are no commercial diagnostic reagents available (including many antibody based reagents,) that can always provide unambiguous, reliable identification under current clinical setting.

1.6 Reference

1. D. Zhou, L. Ying, X. Hong, E. A. Hall, C. Abell and D. Klenerman, *Langmuir*, 2008, **24**, 1659-1664.
2. M. Bruchez, M. Moronne, P. Gin, S. Weiss and A. P. Alivisatos, *Science*, 1998, **281**, 2013-2016.
3. W. C. Chan and S. Nie, *Science*, 1998, **281**, 2016-2018.
4. I. L. Medintz, A. R. Clapp, H. Mattoussi, E. R. Goldman, B. Fisher and J. M. Mauro, *Nature Materials*, 2003, **2**, 630-638.
5. X. Michalet, F. Pinaud, L. Bentolila, J. Tsay, S. Doose, J. Li, G. Sundaresan, A. Wu, S. Gambhir and S. Weiss, *Science*, 2005, **307**, 538-544.
6. B. O. Dabbousi, J. Rodriguez-Viejo, F. V. Mikulec, J. R. Heine, H. Mattoussi, R. Ober, K. F. Jensen and M. G. Bawendi, *The Journal of Physical Chemistry B*, 1997, **101**, 9463-9475.
7. C. A. Leatherdale, W.-K. Woo, F. V. Mikulec and M. G. Bawendi, *The Journal of Physical Chemistry B*, 2002, **106**, 7619-7622.
8. A. Fu, W. Gu, B. Boussert, K. Koski, D. Gerion, L. Manna, M. Le Gros, C. A. Larabell and A. P. Alivisatos, *Nano letters*, 2007, **7**, 179-182.
9. H. Htoon, J. Hollingworth, A. Malko, R. Dickerson and V. I. Klimov, *Applied physics letters*, 2003, **82**, 4776-4778.
10. A. Shabaev and A. L. Efros, *Nano letters*, 2004, **4**, 1821-1825.

11. J. Hu, L. Li, W. Yang, L. Manna, L. Wang and A. P. Alivisatos, *Science*, 2001, **292**, 2060-2063.

12. L. Manna, E. C. Scher, L.-S. Li and A. P. Alivisatos, *Journal of the American Chemical Society*, 2002, **124**, 7136-7145.

13. H. Zhang, P. G. Stockley and D. Zhou, *Faraday Discussions*, 2011, **149**, 319-332.

14. J. R. Lakowicz, *Principles of fluorescence spectroscopy*, Springer Science & Business Media, 2013.

15. S. J. Rosenthal, *Nature biotechnology*, 2001, **19**, 621-622.

16. A. Van Driel, G. Allan, C. Delerue, P. Lodahl, W. Vos and D. Vanmaekelbergh, *Physical Review Letters*, 2005, **95**, 236804.

17. C. Murray, D. J. Norris and M. G. Bawendi, *Journal of the American Chemical Society*, 1993, **115**, 8706-8715.

18. X. Peng, L. Manna, W. Yang, J. Wickham, E. Scher, A. Kadavanich and A. P. Alivisatos, *Nature*, 2000, **404**, 59-61.

19. M. Han, X. Gao, J. Z. Su and S. Nie, *Nature Biotechnology*, 2001, **19**, 631-635.

20. L.-s. Li, J. Hu, W. Yang and A. P. Alivisatos, *Nano Letters*, 2001, **1**, 349-351.

21. A. P. Alivisatos, W. Gu and C. Larabell, *Annu. Rev. Biomed. Eng.*, 2005, **7**, 55-76.

22. B. Dubertret, P. Skourides, D. J. Norris, V. Noireaux, A. H. Brivanlou and A. Libchaber, *Science*, 2002, **298**, 1759-1762.

23. E. Petryayeva, W. R. Algar and I. L. Medintz, *Applied Spectroscopy*, 2013, **67**, 215-252.

24. D. V. Talapin, S. Haubold, A. L. Rogach, A. Kornowski, M. Haase and H. Weller, *The Journal of Physical Chemistry B*, 2001, **105**, 2260-2263.

25. S. F. Wuister, F. van Driel and A. Meijerink, *Physical Chemistry Chemical Physics*, 2003, **5**, 1253-1258.

26. Z. A. Peng and X. Peng, *Journal of the American Chemical Society*, 2001, **123**, 183-184.

27. L. Qu and X. Peng, *Journal of the American Chemical Society*, 2002, **124**, 2049-2055.

28. L. Qu, Z. A. Peng and X. Peng, *Nano Letters*, 2001, **1**, 333-337.

29. W. W. Yu and X. Peng, *Angewandte Chemie International Edition*, 2002, **41**, 2368-2371.

30. L. S. Li, N. Pradhan, Y. Wang and X. Peng, *Nano Letters*, 2004, **4**, 2261-2264.

31. S. Sapra, A. L. Rogach and J. Feldmann, *Journal of Materials Chemistry*, 2006, **16**, 3391-3395.

32. Q. Dai, N. Xiao, J. Ning, C. Li, D. Li, B. Zou, W. W. Yu, S. Kan, H. Chen and B. Liu, *The Journal of Physical Chemistry C*, 2008, **112**, 7567-7571.

33. R. E. Bailey, A. M. Smith and S. Nie, *Physica E: Low-dimensional Systems and Nanostructures*, 2004, **25**, 1-12.

34. T. Rajh, O. I. Micic and A. J. Nozik, *The Journal of Physical Chemistry*, 1993, **97**, 11999-12003.

35. S. Y. Choi, J. P. Shim, D. S. Kim, T. Kim and K. S. Suh, *Journal of Nanomaterials*, 2012, **2012**, 10.

36. V. Lesnyak, N. Gaponik and A. Eychmüller, *Chemical Society Reviews*, 2013, **42**, 2905-2929.

37. J. Guo, W. Yang and C. Wang, *The Journal of Physical Chemistry B*, 2005, **109**, 17467-17473.

38. A. L. Rogach, T. Franzl, T. A. Klar, J. Feldmann, N. Gaponik, V. Lesnyak, A. Shavel, A. Eychmüller, Y. P. Rakovich and J. F. Donegan, *The Journal of Physical Chemistry C*, 2007, **111**, 14628-14637.

39. L. Li, H. Qian, N. Fang and J. Ren, *Journal of Luminescence*, 2006, **116**, 59-66.

40. K. Zhao, J. Li, H. Wang, J. Zhuang and W. Yang, *The Journal of Physical Chemistry C*, 2007, **111**, 5618-5621.

41. Q.-F. Chen, W.-X. Wang, Y.-X. Ge, M.-Y. Li, S.-K. Xu and X.-J. Zhang, *Chinese Journal of Analytical Chemistry*, 2007, **35**, 135-138.

42. C. Jiang, S. Xu, D. Yang, F. Zhang and W. Wang, *Luminescence*, 2007, **22**, 430-437.

43. Y. Yan, M. Ying, G. Feng, L. Zhang, L. Zhu, X. Ling, Y. Rui and Q. JIN, *Chemical Research in Chinese Universities*, 2008, **24**, 8-14.

44. F. C. Liu, T. L. Cheng, C. C. Shen, W. L. Tseng and M. Y. Chiang, *Langmuir*, 2008, **24**, 2162-2167.

45. Z. Deng, F. L. Lie, S. Shen, I. Ghosh, M. Mansuripur and A. J. Muscat, *Langmuir*, 2008, **25**, 434-442.

46. H. Zhang, L.-p. Wang, H. Xiong, L. Hu, B. Yang and W. Li, *Advanced Materials*, 2003, **15**, 1712-1715.

47. H. Qian, X. Qiu, L. Li and J. Ren, *The Journal of Physical Chemistry B*, 2006, **110**, 9034-9040.

48. X. Peng, M. C. Schlamp, A. V. Kadavanich and A. P. Alivisatos, *Journal of the American Chemical Society*, 1997, **119**, 7019-7029.

49. P. Reiss, J. Bleuse and A. Pron, *Nano Letters*, 2002, **2**, 781-784.

50. M. A. Malik, P. O'Brien and N. Revaprasadu, *Chemistry of Materials*, 2002, **14**, 2004-2010.

51. M. Danek, K. F. Jensen, C. B. Murray and M. G. Bawendi, *Chemistry of Materials*, 1996, **8**, 173-180.

52. M. Schlamp, X. Peng and A. Alivisatos, *Journal of Applied Physics*, 1997, **82**, 5837-5842.

53. N. Tessler, V. Medvedev, M. Kazes, S. Kan and U. Banin, *Science*, 2002, **295**, 1506-1508.

54. W. Guo, J. J. Li, Y. A. Wang and X. Peng, *Journal of the American Chemical Society*, 2003, **125**, 3901-3909.

55. M. A. Hines and P. Guyot-Sionnest, *The Journal of Physical Chemistry*, 1996, **100**, 468-471.

56. I. Mekis, D. V. Talapin, A. Kornowski, M. Haase and H. Weller, *The Journal of Physical Chemistry B*, 2003, **107**, 7454-7462.

57. J. Bleuse, S. Carayon and P. Reiss, *Physica E: Low-dimensional Systems and Nanostructures*, 2004, **21**, 331-335.

58. P. Reiss, S. Carayon, J. Bleuse and A. Pron, *Synthetic Metals*, 2003, **139**, 649-652.

59. D. V. Talapin, I. Mekis, S. Götzinger, A. Kornowski, O. Benson and H. Weller, *The Journal of Physical Chemistry B*, 2004, **108**, 18826-18831.

60. J. T. Kopping and T. E. Patten, *Journal of the American Chemical Society*, 2008, **130**, 5689-5698.

61. E. Gravel, C. Tanguy, E. Cassette, T. Pons, F. Knittel, N. Bernards, A. Garofalakis, F. Ducongé, B. Dubertret and E. Doris, *Chemical Science*, 2013, **4**, 411-417.

62. I. L. Medintz, H. T. Uyeda, E. R. Goldman and H. Mattoussi, *Nature Materials*, 2005, **4**, 435-446.

63. J. Aldana, Y. A. Wang and X. Peng, *Journal of the American Chemical Society*, 2001, **123**, 8844-8850.

64. H. T. Uyeda, I. L. Medintz, J. K. Jaiswal, S. M. Simon and H. Mattoussi, *Journal of the American Chemical Society*, 2005, **127**, 3870-3878.

65. N. Zhan, G. Palui and H. Mattoussi, *Nature Protocols*, 2015, **10**, 859-874.

66. K. Susumu, B. C. Mei and H. Mattoussi, *Nature Protocols*, 2009, **4**, 424-436.

67. F. Aldeek, D. Hawkins, V. Palomo, M. Safi, G. Palui, P. E. Dawson, I. Alabugin and H. Mattoussi, *Journal of the American Chemical Society*, 2015, **137**, 2704-2714.

68. D. Gerion, F. Pinaud, S. C. Williams, W. J. Parak, D. Zanchet, S. Weiss and A. P. Alivisatos, *The Journal of Physical Chemistry B*, 2001, **105**, 8861-8871.

69. D. Gerion, F. Pinaud, S. C. Williams, W. J. Parak, D. Zanchet, S. Weiss and A. P. Alivisatos, *Journal of Physical Chemistry B*, 2001, **105**, 8861-8871.

70. X. Wu, H. Liu, J. Liu, K. N. Haley, J. A. Treadway, J. P. Larson, N. Ge, F. Peale and M. P. Bruchez, *Nature Biotechnology*, 2003, **21**, 41-46.

71. X. Gao, Y. Cui, R. M. Levenson, L. W. Chung and S. Nie, *Nature Biotechnology*, 2004, **22**, 969-976.

72. B. Dubertret, Skourides, P., ect,, *Science*, 2002, **298**, 1759-1762.

73. H. Fan, Leve, E.W., ect,, *Nano Letters*, 2005, **5**, 645-648.

74. H. Fan, E. W. Leve, C. Scullin, J. Gabaldon, D. Tallant, S. Bunge, T. Boyle, M. C. Wilson and C. J. Brinker, *Nano Letters*, 2005, **5**, 645-648.

75. A. E. Albers, E. M. Chan, P. M. McBride, C. M. Ajo-Franklin, B. E. Cohen and B. A. Helms, *Journal of the American Chemical Society*, 2012, **134**, 9565-9568.

76. R. Freeman, T. Finder and I. Willner, *Angewandte Chemie International Edition*, 2009, **48**, 7818-7821.

77. F. Chen and D. Gerion, *Nano Letters*, 2004, **4**, 1827-1832.

78. M. E. Åkerman, W. C. Chan, P. Laakkonen, S. N. Bhatia and E. Ruoslahti, *Proceedings of the National Academy of Sciences*, 2002, **99**, 12617-12621.

79. S. Kim, Y. T. Lim, E. G. Soltesz, A. M. De Grand, J. Lee, A. Nakayama, J. A. Parker, T. Mihaljevic, R. G. Laurence and D. M. Dor, *Nature Biotechnology*, 2004, **22**, 93-97.

80. N. Y. Morgan, S. English, W. Chen, V. Chernomordik, A. Russo, P. D. Smith and A. Gandjbakhche, *Academic Radiology*, 2005, **12**, 313-323.

81. J. K. Jaiswal, H. Mattoussi, J. M. Mauro and S. M. Simon, *Nature Biotechnology*, 2003, **21**, 47-51.

82. K. Zeenia, T. Yaguchi, C. K. Sunil, T. Hirano, R. Wadhwa and K. Taira, *Cell Research*, 2003, **13**, 503-507.

83. Y. Xing, Q. Chaudry, C. Shen, K. Y. Kong, H. E. Zhau, L. W. Chung, J. A. Petros, R. M. O'Regan, M. V. Yezhelyev and J. W. Simons, *Nature Protocols*, 2007, **2**, 1152-1165.

84. J. B. Delehanty, C. E. Bradburne, K. Susumu, K. Boeneman, B. C. Mei, D. Farrell, J. B. Blanco-Canosa, P. E. Dawson, H. Mattoussi and I. L. Medintz, *Journal of the American Chemical Society*, 2011, **133**, 10482-10489.

85. W. C. Chan, D. J. Maxwell, X. Gao, R. E. Bailey, M. Han and S. Nie, *Current Opinion in Biotechnology*, 2002, **13**, 40-46.

86. K. A. Dick, K. Deppert, M. W. Larsson, T. Mårtensson, W. Seifert, L. R. Wallenberg and L. Samuelson, *Nature Materials*, 2004, **3**, 380-384.

87. D. S. Lidke, P. Nagy, R. Heintzmann, D. J. Arndt-Jovin, J. N. Post, H. E. Grecco, E. A. Jares-Erijman and T. M. Jovin, *Nature Biotechnology*, 2004, **22**, 198-203.

88. M. Dahan, S. Levi, C. Luccardini, P. Rostaing, B. Riveau and A. Triller, *Science*, 2003, **302**, 442-445.

89. S. J. Rosenthal, I. Tomlinson, E. M. Adkins, S. Schroeter, S. Adams, L. Swafford, J. McBride, Y. Wang, L. J. DeFelice and R. D. Blakely, *Journal of the American Chemical Society*, 2002, **124**, 4586-4594.

90. K. V. Wood and D. H. Klaubert, *Current Opinion in Biotechnology*, 2005, **16**, 1-2.

91. U. Pison, T. Welte, M. Giersig and D. A. Groneberg, *European Journal of Pharmacology*, 2006, **533**, 341-350.

92. I. L. Medintz and H. Mattoussi, *Physical Chemistry Chemical Physics*, 2009, **11**, 17-45.

93. A. Hawe, M. Sutter and W. Jiskoot, *Pharmaceutical Research*, 2008, **25**, 1487-1499.

94. R. P. Haugland, J. Yguerabide and L. Stryer, *Proceedings of the National Academy of Sciences*, 1969, **63**, 23-30.

95. A. R. Clapp, I. L. Medintz and H. Mattoussi, *ChemPhysChem*, 2006, **7**, 47-57.

96. K. E. Sapsford, L. Berti and I. L. Medintz, *Angewandte Chemie International Edition*, 2006, **45**, 4562-4589.

97. Y. Zhang and T.-H. Wang, *Theranostics*, 2012, **2**, 631-654.

98. D. Zhou, J. D. Piper, C. Abell, D. Klenerman, D.-J. Kang and L. Ying, *Chemical Communications*, 2005, 4807-4809.

99. M. Elangovan, R. Day and A. Periasamy, *Journal of Microscopy*, 2002, **205**, 3-14.

100. A. Lacoste and N. Mizrahi, Google Patents, 2012.

101. M. G. Erickson, B. A. Alseikhan, B. Z. Peterson and D. T. Yue, *Neuron*, 2001, **31**, 973-985.

102. T. Hey, E. Fiedler, R. Rudolph and M. Fiedler, *Trends in Biotechnology*, 2005, **23**, 514-522.

Chapter 2 Synthesis of ligands

In this Chapter, the synthesis of the surface capping ligands to be used in the preparation of robust, compact, biocompatible QDs/QRs probes in the following chapters are described. These compounds include several thioctic acid (TA) based ligands (TA-PEG750-OMe, TA-PEG2000-OMe, TA-Zwitterion, TA-PEG600-Biotin). The chemical structures of these ligands are shown in Figure 2-1.

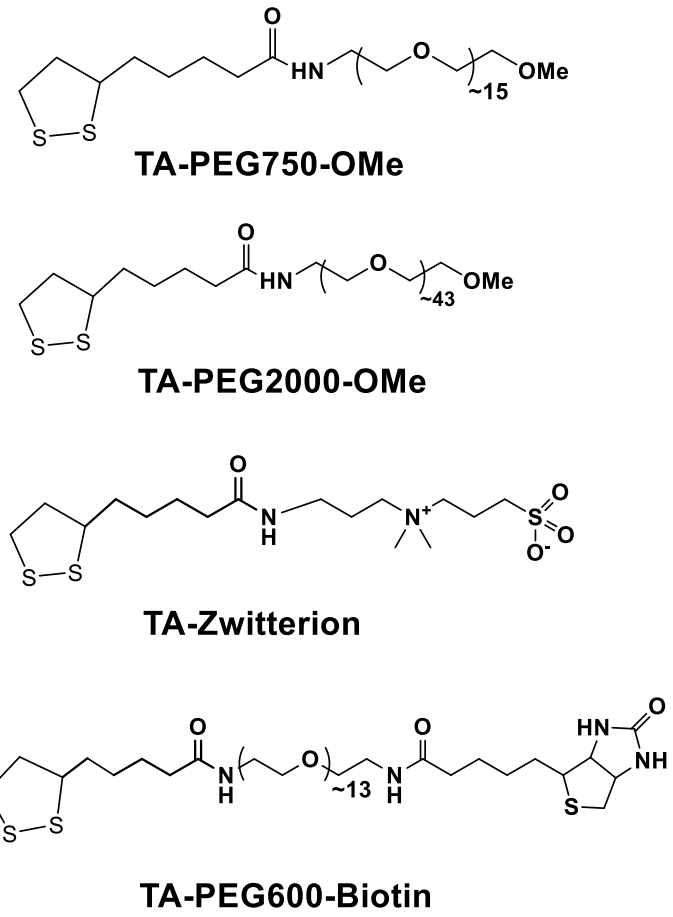

Figure 2-1: Chemical structures of TA-PEG750-OMe, TA-PEG2000-OMe, TA-Zwitterion, and TA-PEG600-Biotin.

2.1 Materials and Methods

2.1.1 Materials

Poly(ethylene glycol methyl ether) (average MW: 750; containing an average of ~15 PEG units, denoted as $PEG_{\sim 15}$ Acros organics); Poly(ethylene glycol methyl ether) (Average MW: 2000; containing an average of ~43 PEG units, denoted as $PEG_{\sim 43,}$ Acros organics); Polyethylene glycol (PEG) with an average molecular weight of 600 (containing an average of ~13 PEG units, denoted as $PEG_{\sim 13}$); 11-Azido-3,6,9-trioxaundecan-1-amine (> 90% monomer purity), N,N-dimethyl-1,3-propanediamine (>99%), 1,3-propane-sultone (> 99%), Triphenylphosphine (>98.5%), Dicyclohexylcarbodiimide (DCC, >99%), Dimethylaminopyridine (DMAP, >99%), Tris(2-carboxyethyl)phosphine hydrochloride (TCEP.HCl, >98%), Triethylamine (>99%), Chloroform (> 99.8%), Magnesium sulfate (>99%), Methanol (>99.9%), Potassium hydroxide, Methylene chloride (>98%), Sodium bicarbonate (>99.5%), Methanesulfonyl chloride (>99.7%), Sodium azide (>99.5%), Tri-phenylphosphine (>98.5%), Thioctic acid (TA, >99%), Ethyl acetate (>99.0%), and all other chemicals and reagents were all purchased from Sigma-Aldrich (Dorset, UK). These chemicals are purchased commercially from Sigma-Aldrich (Dorset, UK) and used without further purification unless stated otherwise. Solvents were obtained from Fisher Scientific (Loughborough, UK) and used as received.

2.1.2 Instrument and Methods[1-3]

All moisture-sensitive reactions are performed under nitrogen atmosphere using oven-dried glassware. All dry solvents are dried by innovative technology prior to use, or are taken from sealed-bottles under nitrogen atmosphere. Evaporations are performed under reduced pressure on a rotary evaporator. Reactions are monitored by TLC on silica gel 60 F254 plates on aluminium and stained by iodine. Flash column chromatography was performed on silica gel 60 A (Merck grade 9385). ^{1}H and ^{13}C NMR spectra of the samples are recorded on Brucker DPX300 (500 MHz for 1H, 125 MHz for ^{13}C) in $CDCl_3$. All chemical shifts are reported here in parts per million (ppm) and the coupling constants are reported in Hertz. Ultra-pure water (resistance >18.2 MΩ.cm) purified by an ELGA Purelab classic UVF system, was used for all experiments and making buffers. High resolution mass spectra (HR-MS) were obtained on a Bruker Daltonics MicroTOF mass spectrometer. Infra-red spectra were recorded on a PerkinElmer FT-IR spectrometer. UV-vis absorption spectra were recorded on a Varian Cary 50 bio UV-Visible Spectrophotometer over 200-800 nm using 1 mL quartz cuvette with an optical path of 1 cm or on a Nanodrop 2000 spectrophotometer (Thermo scientific) over the range of 200-800 nm using 1 drop of the solution with an optical path length of 1 mm. All centrifugations were carried out on a Thermo Scientific Heraeus Fresco 21 microcentrifuge

using 1.5 mL microcentrifuge tubes at room temperature (unless stated otherwise).

2.2 Ligand synthesis[1-8]

2.2.1 Synthesis of TA-PEG750-OMe and TA-PEG2000-OMe[1]

The synthetic routes for TA-PEG750-OMe and TA-PEG2000-OMe were shown in **Figure 2-2**

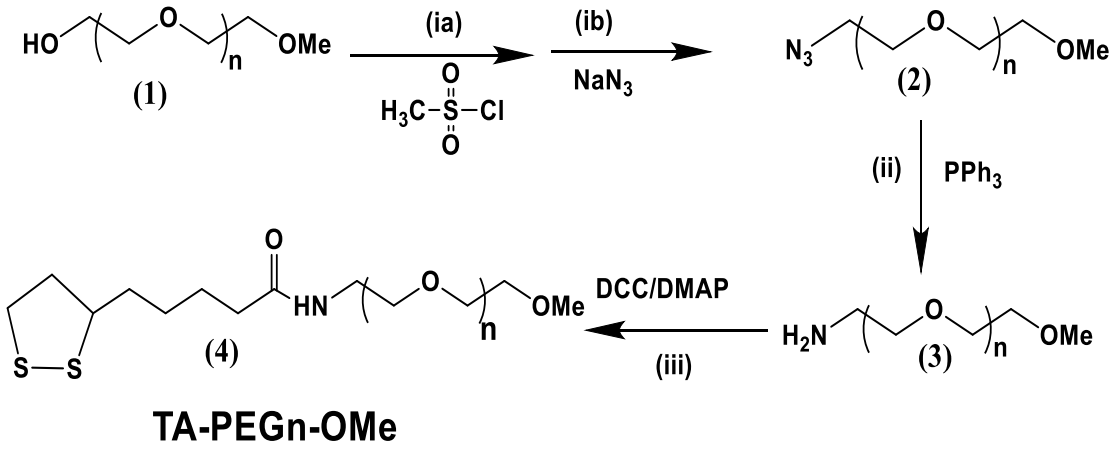

Figure 2-2: The synthetic route to TA-PEG750-OMe (n ≈ 15) and TA-PEG2000-OMe (n ≈ 43). The reaction conditions are: (ia) MsCl, Et_3N, THF; (ib) NaN_3, $NaHCO_3$, H_2O; (ii) PPh_3, EtOAc and 1 M HCl; (iii) thioctic acid, DCC/DMAP, CH_2Cl_2;

Step 1: Synthesis of MeO-PEG750-N_3 (compound 2)

Monomethoxypolyetheylene glycol with an average molecular weight of 750 (MeO-PEG750) (37.5 g, 50 mmol), THF (150 mL) and methanesulfonyl chloride (11.45 g, 100 mmol) were added in a 500 mL two-necked round-

bottomed flask equipped with an addition funnel, septa and a magnetic stirring bar. Triethylamine (Et_3N, 15 mL, 111 mmol) was loaded to the addition funnel. The reaction mixture was then purged with nitrogen and cooled to 0 °C in an ice bath. Triethylamine was then added dropwisely to the reaction mixture through the addition funnel (total addition time ~30 min). After that, the reaction mixture was allowed to warm up gradually to room temperature (~20 °C) and then stirred overnight. The product was checked by TLC on silica gel plate with $CHCl_3$:MeOH = 10:1 (vol/vol) as elution solvent, $R_{f\ (MsO–PEG750–OMe)}$ = 0.65, $R_{f\ (HO\text{-}PEG750–OMe)}$ = 0.35. After reaction was complete, the mixture was diluted with H_2O (50 ml) and $NaHCO_3$ (3.125 g, 37 mmol) was added. The resulting mixture was transferred to a separator funnel and extracted with $CHCl_3$ (60 mL × 3). The combined organic phase was evaporated by dryness on a rotary evaporator, yielding slightly yellowish oil, 40 g (48.3 mmol), 96.6% yields.

The product from above reaction(40 g), sodium azide (7.75 g, 120 mmol), THF (50 mL), H_2O (50 mL) and $NaHCO_3$ (3.125 g, 37 mmol) were then added to 500 ml two-necked round-bottomed flask equipped with a distilling head using a round-bottomed flask as a solvent trap. The solvent trap was cooled with an ice-bath. The biphasic reaction mixture was heated under N_2 to distil off the THF. The reaction mixture was then refluxed for overnight. After the reaction mixture was cooled to room temperature, it was transferred to a separator funnel. The product was extracted with $CHCl_3$ (100 mL × 5). The

product was checked with TCL using $CHCl_3$: MeOH =10:1 (vol/vol) as elution solvent, $R_{f\ (N3\text{-}PEG750\text{-}OMe)}$ = 0.75. The combined organic layers were dried over Mg_2SO_4 (~20 g, ~30 min) with stirring. The Mg_2SO_4 was filtered off and the dried organic layer was evaporated to dryness on a rotary evaporator. A pale brown oil (24.93g, yield: 66.7%) was obtained. ^{1}H NMR (500 MHz, $CDCl_3$): δ_H (ppm), 3.35 (m, 5H, -OC*H*$_3$ and N_3-C*H*$_2$-); 3.6-3.9 (m, 70H, C*H*$_2$ in repeated PEG groups), 7.33 (s, 1H, impurity residue $CHCl_3$).

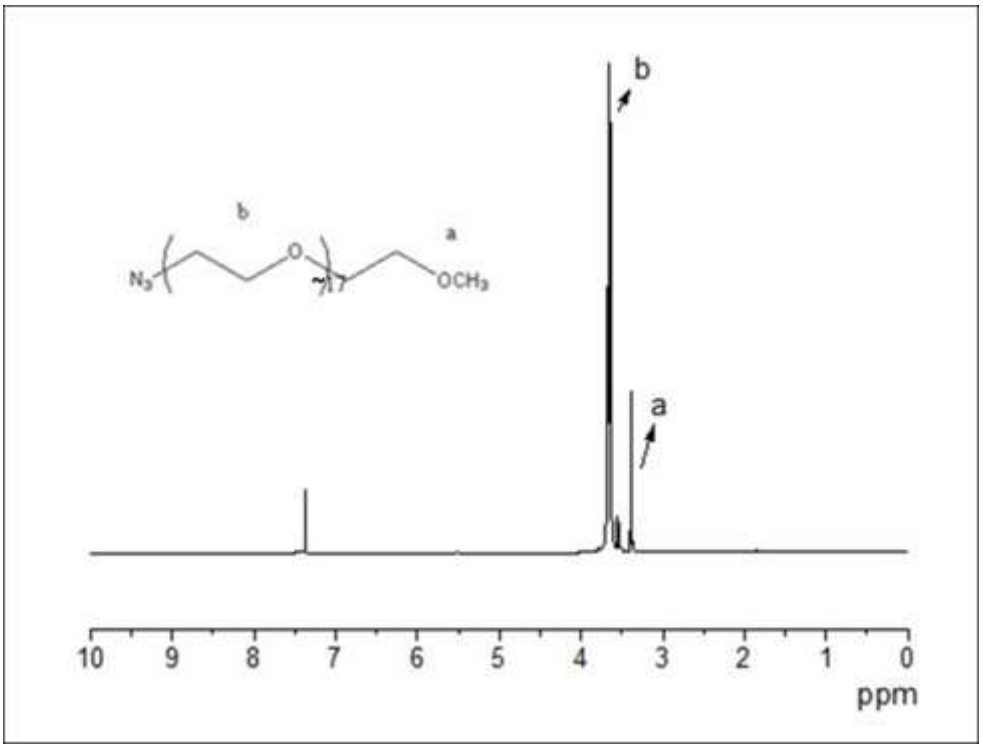

Figure 2-3: ^{1}H NMR spectrum in $CDCl_3$ of prepared MeO-PEG750-N_3.

Synthesis of MeO-PEG2000-N_3 (compound 2)

Poly(ethylene glycol methyl ether) with an average molecular weight of 2000 (MeO-PEG750) (30.0 g, 15 mmol), THF (150 mL) and methanesulfonyl chloride (3.82 g, 30 mmol) were added in a 500 ml two-necked round-bottomed flask equipped with an addition funnel, septa and a magnetic stirring bar. Triethylamine (Et_3N, 5 mL, 37 mmol) was loaded to the addition funnel. The reaction mixture was then purged with nitrogen and cooled to 0 °C in an ice bath. Triethylamine was then added dropwisely to the reaction mixture through the addition funnel (total addition time ~30 min). After that, the reaction mixture was allowed to warm up gradually to room temperature (~20 °C) and then stirred overnight. The mixture was then diluted with H_2O (50 ml) and $NaHCO_3$ (1.0 g, 10 mmol) was added. Sodium azide (2.60 g, 40 mmol) was then added to 500 ml two-necked round-bottomed flask equipped with a distilling head with a round-bottomed flask as a solvent trap. The solvent trap was cooled with an ice-bath. The biphasic reaction mixture was heated under N_2 to distil off the THF. The reaction mixture was then refluxed for ~8 hrs (or overnight). After the reaction mixture was cooled to room temperature, it was transferred to a separator funnel. The product was

extracted with $CHCl_3$ (100 mL × 5). The product was checked with TCL using $CHCl_3$: MeOH =5:1 (vol/vol) as elution solvent, $R_{f\ (N3\text{-}PEG2000\text{-}OMe)}$ = ~0.5. $R_{f\ (HO\text{–}PEG2000\text{–}OMe)}$ = 0.3. The combined organic layers were dried over Mg_2SO_4 (~20 g, ~30 min) with stirring. The Mg_2SO_4 was filtered off and the dried organic layer was evaporated to dryness on a rotary evaporator. A pale brown oil (27.8 g, yield: 85.2%) was obtained ^{1}H NMR (500 MHz, $CDCl_3$): δ_H (ppm), 3.35 (m, 5H, -OC*H*$_3$ and N_3-C*H*$_2$-); 3.6-3.9 (m, 205H, C*H*$_2$ in repeated PEG groups).

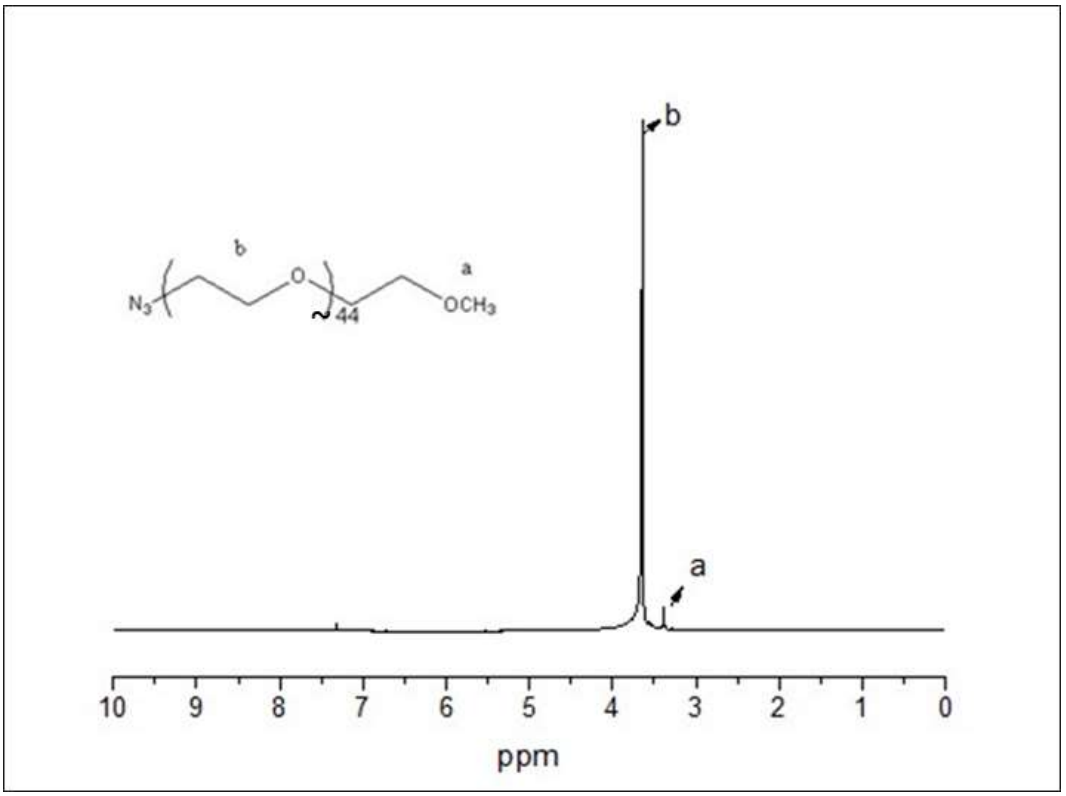

Figure 2-4: ^{1}H NMR spectrum in $CDCl_3$ of prepared MeO-PEG750-N_3

Step 2: Synthesis of OMe-PEG750-NH_2 (compound 3)

N_3–PEG750–OMe (8.0 g, ~10 mmol), EtOAc (150 mL) and 1 M HCl (25 ml, 25 mmol) were added into a 500 mL two-necked round-bottomed flask equipped with an addition funnel, septa and a magnetic stirring bar. Triphenyl-phosphine (2.8 g, ~10 mmol) dissolved in 100 ml EtOAc was transferred to the addition funnel. The reaction vessel was purged with N_2 and cooled to 0 °C in an ice-bath while stirring. The triphenyl-phosphine solution was then added dropwisely under N_2. The temperature was maintained to below 5 °C with an ice bath during the addition. Once the addition was complete, the reaction mixture was gradually warmed up to room temperature and stirred overnight under N_2. The reaction mixture was then transferred to a separation funnel and the biphasic solution was separated. The aqueous layer was collected and washed with EtOAc (100 mL × 2). The aqueous layer was transferred to a round-bottomed flask and cooled in an ice bath. KOH (13.5 g) was then added slowly to the aqueous solution under magnetic stirring until the KOH was dissolved (pH > 10). The aqueous solution was transferred into a separation funnel and extracted repeatedly with $CHCl_3$ (60 mL × 5). The

combined organic layer was dried over $MgSO_4$ for 20 mins. After filting off $MgSO_4$, the solvent was evaporated to dryness on a rotary evaporator, yielding a lightly yellow oil, 4.58 g, yield: 59.2%. R_fs ($CHCl_3$:MeOH = 10:1, vol/vol) for $R_{f\ (N3\text{-}PEG750\text{-}OMe)}$ = 0.75, $R_{f\ (NH2\text{-}PEG750\text{-}OMe)}$ = 0.25. ^{1}H NMR (500 MHz, $CDCl_3$), δ_H (ppm), 2.87 (2H, -N*H*$_2$), 3.35 (s, 3H, -OC*H*$_3$), 3.6-3.9 (70H, m, C*H*$_2$ in repeated PEG unit), 7.33 (s, 1H, impurity residue $CHCl_3$).

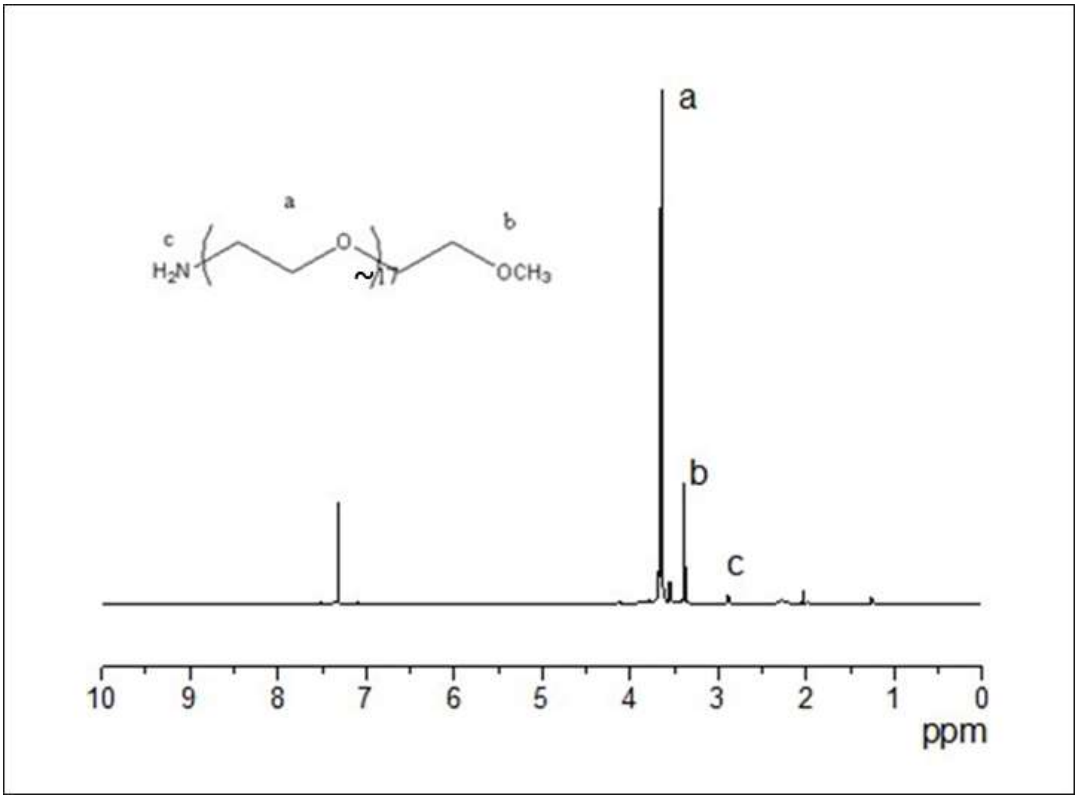

Figure 2-5: ^{1}H NMR spectrum of prepared MeO-PEG750-NH_2.

Synthesis of OMe-PEG2000-NH_2 (compound 3)

N_3–PEG2000–OMe (10.0 g, ~5 mmol), EtOAc (150 mL) and 1 M HCl (37.5 ml, 37.5 mmol) were added into a 500 mL two-necked round-bottomed flask equipped with an addition funnel, septa and a magnetic stirring bar. Triphenyl-phosphine (2.8 g, ~10 mmol) dissolved in 100 ml EtOAc was transferred to the addition funnel. The reaction vessel was purged with N_2 and cooled to 0 °C in an ice-bath while stirring. The triphenyl-phosphine solution was then added dropwisely under N_2. The temperature was maintained to below 5 °C with an ice bath during the addition. Once the addition was complete, the reaction mixture was gradually warmed up to room temperature and stirred overnight under N_2. The reaction mixture was then transferred to a separation funnel and the biphasic solution was separated. The aqueous layer was collected and washed with EtOAc (100 mL × 2). The aqueous layer was transferred to a round-bottomed flask and cooled in an ice bath. KOH (13.5 g) was then added slowly to the aqueous solution under magnetic stirring until the KOH was dissolved (pH > 10). The aqueous solution was transferred into a separation funnel and extracted repeatedly with $CHCl_3$ (60 mL × 5). The combined organic layer was dried over $MgSO_4$ for 20 mins. After filting off $MgSO_4$, the solvent was evaporated to dryness on a rotary evaporator, yielding a lightly yellow oil, 5.12 g, yield: ~51.2%. R_fs ($CHCl_3$:MeOH = 5:1, vol/vol) for $R_{f\ (N3\text{-}PEG2000\text{-}OMe)}$ = 0.5, $R_{f\ (NH2\text{-}PEG2000\text{-}OMe)}$ = 0.25. ^{1}H NMR (500 MHz, $CDCl_3$), δ_H (ppm), 2.87 (2H, -N*H*$_2$), 3.52 (s, 3H, -OC*H*$_3$), 3.6-3.9 (205H, m, C*H*$_2$ in repeated PEG unit), 7.33 (s, 1H, impurity residue $CHCl_3$).

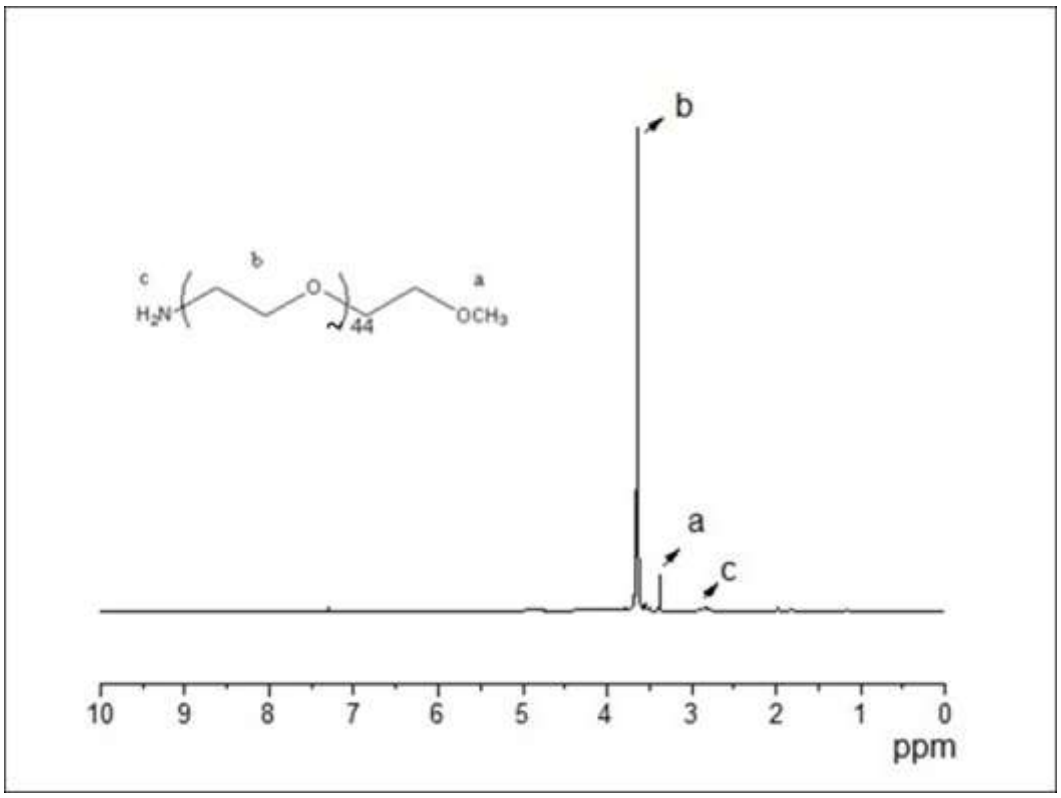

Figure 2-6*:* ^{1}H NMR spectrum of prepared MeO-PEG2000-NH_2.

Step 3: Preparation of TA-PEG750-OMe (Compound 4)

NH_2-PEG750-OMe (3.75 g, ~5.0 mmol), 4-(N,N-dimethylamino)pyridine (0.12 g, ~1.0 mmol), N,N'-dicyclo-hexylcarbodiimide (1.06 g, ~5.0 mmol) and

CH_2Cl_2 (80 mL) were added into a 250 mL round-bottomed flask equipped with a magnetic stirring bar and an addition funnel. The mixture was kept at 0 °C in an ice bath. Thioctic acid (1.03 g, ~5.0 mmol) dissolved in 30 mL of CH_2Cl_2 was transferred to the addition funnel. Thioctic acid solution was added dropwisely over 30 min under N_2 while stirring. After the addition was complete, the reaction mixture was allowed to warm up to room temperature gradually, and the mixture was stirred overnight. The mixture was then filtered off through celite and the celite plug was rinsed with $CHCl_3$. The solvent was then evaporated on a rotary evaporator, and the residue was added with saturated $NaHCO_3$. The aqueous mixture was extracted with ether (100 mL x 2). The aqueous layer was transferred to a separate funnel, and extracted with CH_2Cl_2 (100 mL x 2). The combined organic layer was dried over $MgSO_4$, after filtration, the solvent was evaporated to yield the desired product as a yellow solid, weight 2.30 g, yield = 48.4%. TLC analysis ($CHCl_3$: MeOH=10: 1 (vol/vol) as elution) results, $R_{f\ (TA\text{-}PEG750\text{-}OMe)}$ = ~0.6, whereas $R_{f\ (NH2\text{-}PEG750\text{-}OMe)}$ = 0.25. ^{1}H NMR (500 MHz, CDCl3), δ_H (ppm): 1.45 (2H, m), 1.60 (m, 4H), 2.10 (t, 2H); 2.50 (m, 2H), 3.08-3.30 (m, 3H), 3.40 (m, 5H, -OC*H*$_3$ + (CO)-NH-C*H*$_2$-), 3.6-3.9 (m, 70H, C*H*$_2$ in repeated PEG unit). 5.3 (s, 2H, CH_2Cl_2 residue solvent)

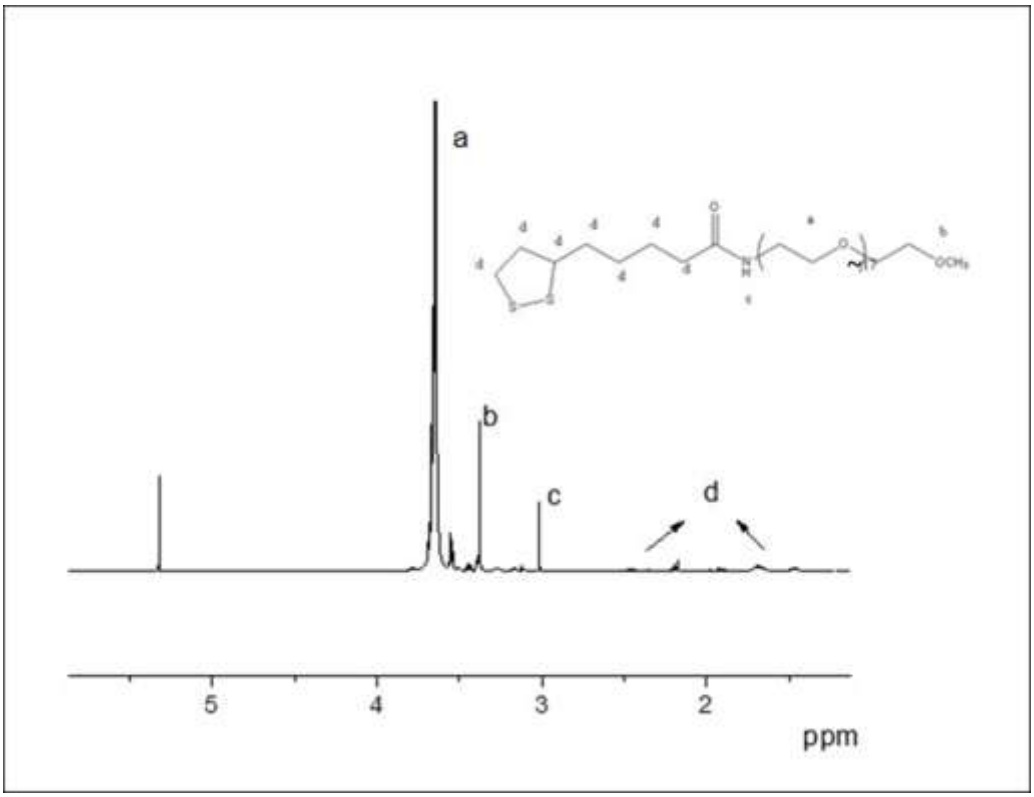

Figure 2-7*:* ^{1}H NMR spectrum of prepared MeO-PEG750-TA.

The TA-EG-OMe is m/z = 307.13 calculated by chemdraw software. For TA-PEG750-OMe, its LC-MS analysis revealed a single UV absorption band with a retention time of ~31.9 seconds. The corresponding MS spectrum displayed

a series of species with m/z ratios separated by multiple numbers of 44 (the molecular weight of the EG unit):659.13, 703.13, 747.13, 791.13, 835.13 and 879.13. The corresponding expected $[M+1H]^{1+}$ peaks with PEG repeat number of 8, 9, 10, 11, 12, 13 were 660.13, 704.37, 748.46, 792.50, 836.61 and 880.70., respectively Figure 2-8.

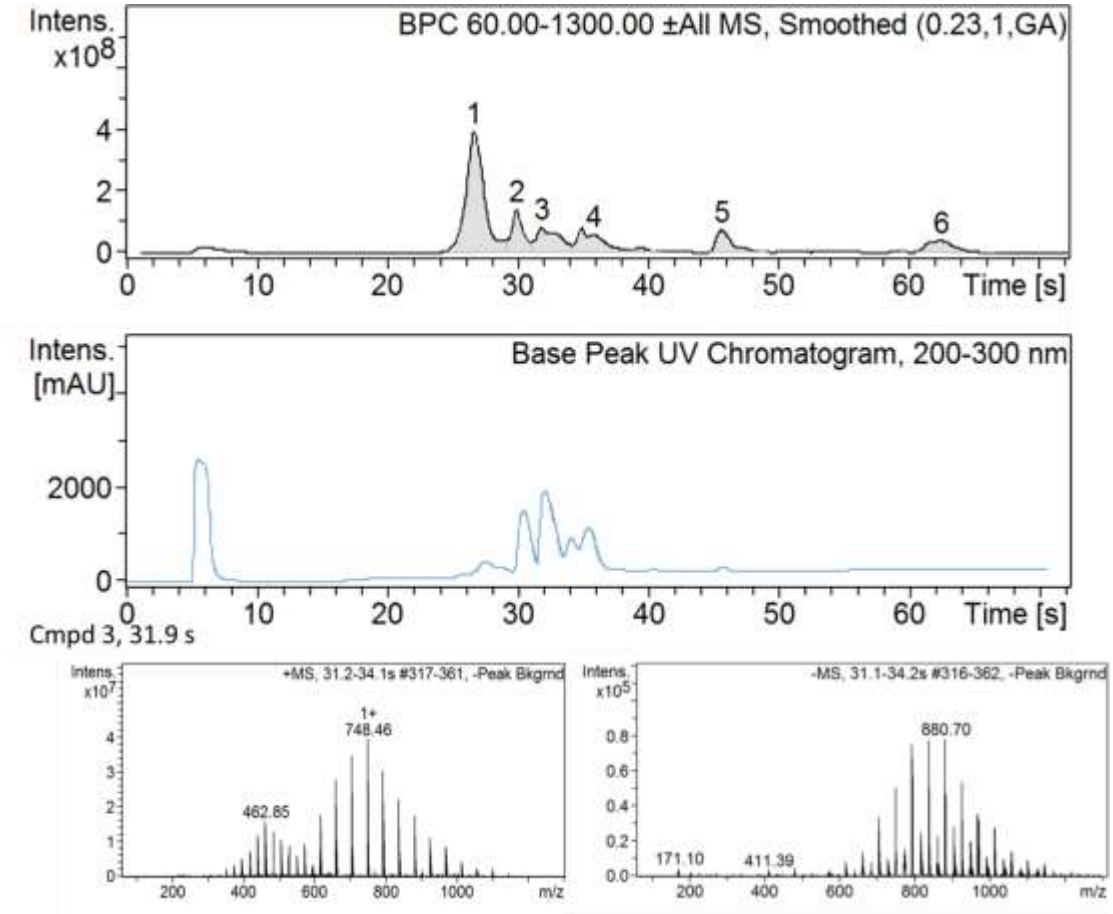

Figure 2-8: HPLC-MS: found m/z 748.46 and 880.70, each repeat unit found m/z 44.

Preparation of TA-PEG2000-OMe (Compound 4)

NH_2-PEG2000-OMe (5.0 g, ~2.5 mmol), 4-(N,N-dimethylamino)pyridine (0.061 g, ~0.5 mmol), N,N'-dicyclo-hexylcarbodiimide (0.53 g, ~2.5 mmol) and CH_2Cl_2 (80 mL) were added into a 250 mL round-bottomed flask equipped with a magnetic stirring bar and an addition funnel. The mixture was cooled at 0 °C in an ice bath. Thioctic acid (0.516 g, ~2.5 mmol) dissolved in 30 mL of CH_2Cl_2 was transferred to the addition funnel. Thioctic acid solution was added dropwisely over 30 min under N_2 while stirring. After the addition was complete, the reaction mixture was allowed to warm up to room temperature gradually, and the mixture was stirred overnight. The mixture was then filtered off through celite and the celite plug was rinsed with $CHCl_3$. The solvent was then evaporated on a rotary evaporator, and the residue was added with saturated $NaHCO_3$, The aqueous mixture was extracted with ether (100 mL x 2). The aqueous layer was transferred to a separate funnel, and extracted with CH_2Cl_2 (100 mL x 2). The combined organic layer was dried over $MgSO_4$, after filtration, the solvent was evaporated to yield the desired product as a yellow solid, weight 2.77 g, yield = 50.3%. TLC analysis ($CHCl_3$: MeOH=5: 1 (vol/vol) as elution) results, $R_{f\ (TA\text{-}PEG2000\text{-}OMe)}$ = ~0.33, whereas $R_{f\ (NH2\text{-}PEG2000\text{-}OMe)}$ = 0.25. ^{1}H NMR (500 MHz, $CDCl_3$), δ_H (ppm): 1.45 (2H, m), 1.60 (m, 4H), 2.10 (t, 2H); 2.50 (m, 2H), 3.08-3.30 (m, 3H), 3.40 (m, 5H, -OC*H*$_3$ + (CO)-NH-C*H*$_2$-), 3.6-3.9 (m, 205H, C*H*$_2$ in repeated PEG unit), 5.3 (s, 2H, CH_2Cl_2 residue solvent).

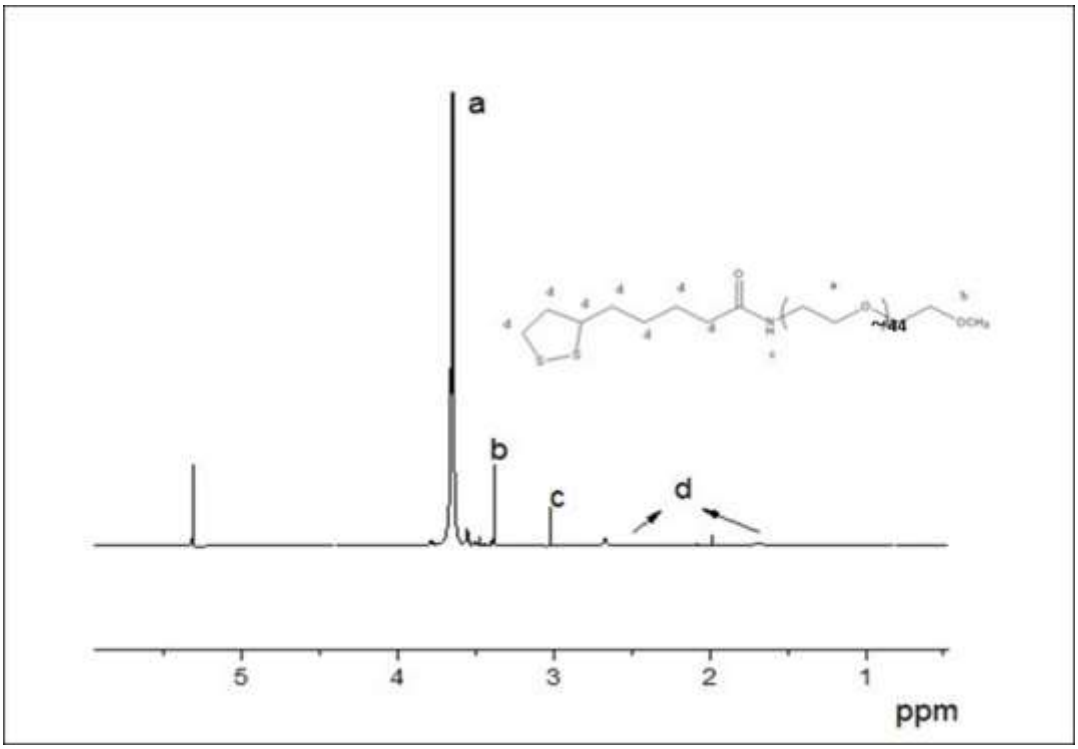

Figure 2-9: ^{1}H NMR spectrum of prepared MeO-PEG2000-TA.

For TA-PEG2000-OMe, its LC-MS analysis revealed a single UV absorption band with a retention time of ~31.8 seconds. The corresponding MS spectrum displayed a series of species with m/z ratios separated by multiple numbers of 44 (the molecular weight of the EG unit): HPLC-MS: found m/z $[M+1H]^{1+:}$ 771.02, each repeat unit found m/z 44.

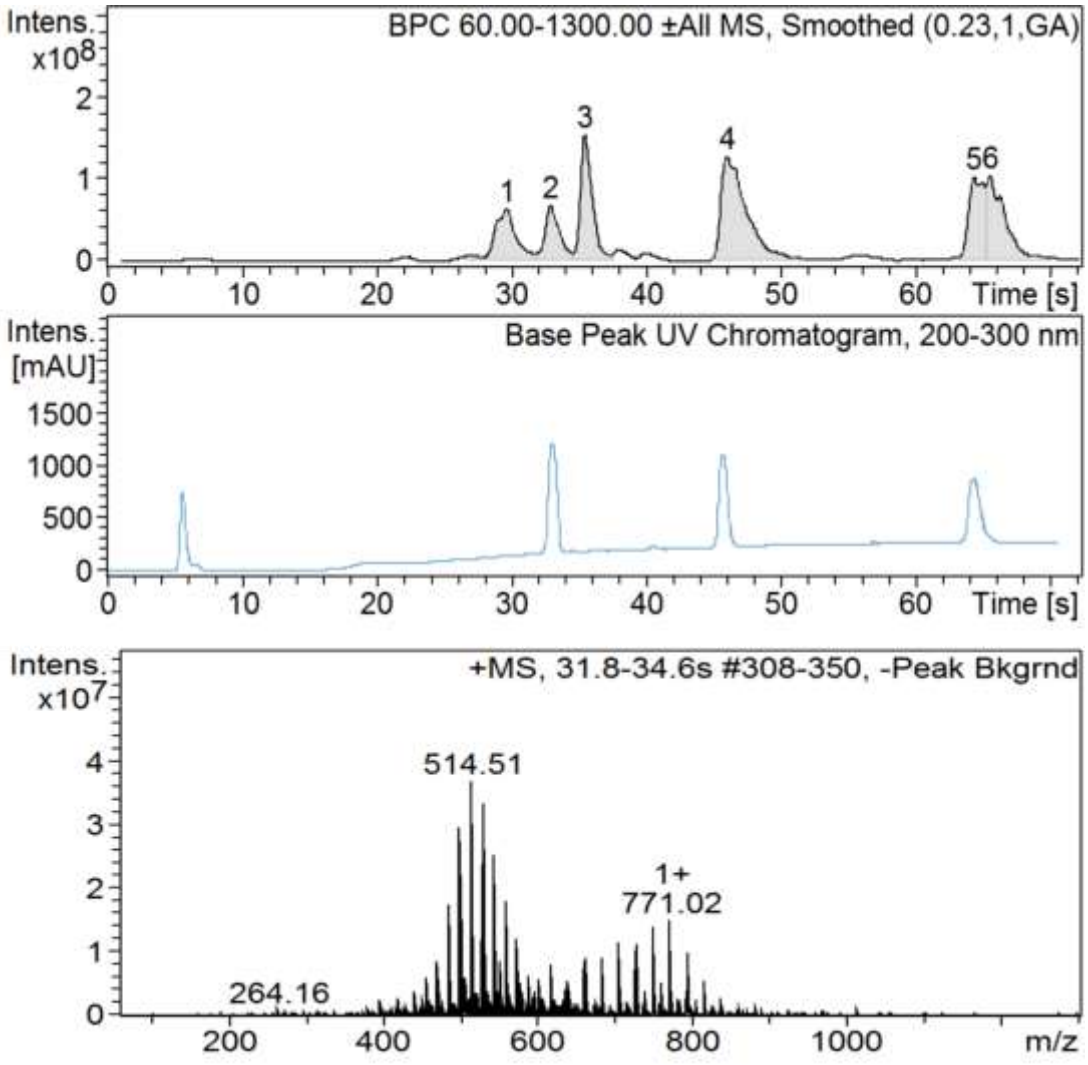

Figure 2-10: HPLC-MS analysis of TA-PEG2000-OMe

2.2.2 The synthetic route to TA-ZW.[2]

The chemical structures and synthetic routes for TA-ZW was shown in **Scheme 2-11**

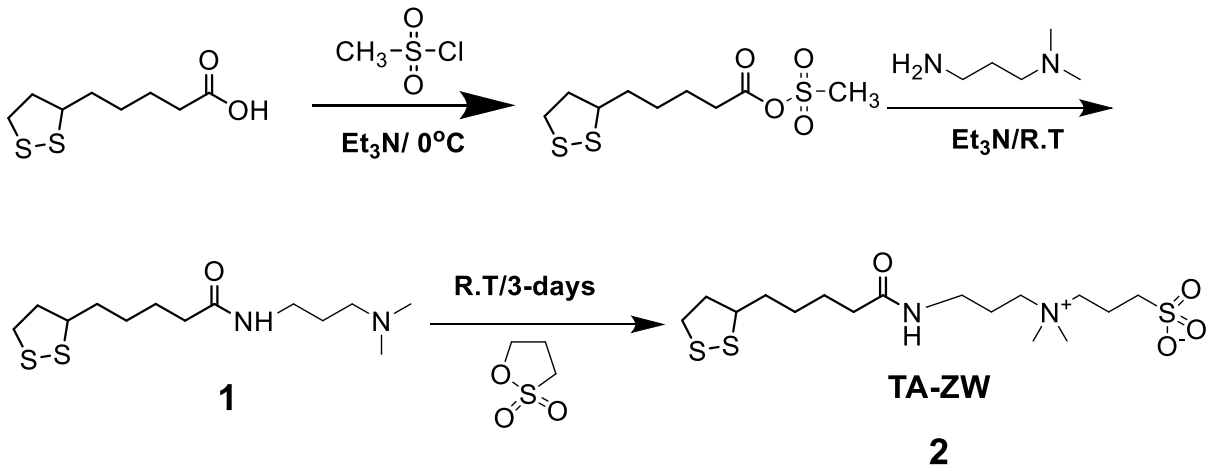

Figure 2-11: Scheme of the synthetic route to TA-ZW. Reaction conditions are: i) TA, Et_3N, CH_2Cl_2, MsCl, N,N-dimethyl-1,3-propanediamine; ii) $CHCl_3$, H_2O, 1,3-propanesultone [5]

Step 1: Synthesis of TA-N, N-Dimethyl-1, 3-propanediamine.

DL-Thioctic acid (3.0 g, ~15 mmol), triethylamine (1.47 g, ~15 mmol) and 30 mL CH_2Cl_2 were placed in three-necked bottom flask (250 mL). The mixture was cooled to 0°C in an ice-bath while being continuously flushed with N_2 gas, the mixture was left stirring for 30 mins. Methanesulfonyl chloride (1.67 g, ~15 mmol) was added dropwisely with a syringe (1mL), and the mixture was slowly warmed up to RT by removing the ice bath and left stirring for 5 hrs. A mixture of N,N-dimethyl-1,3-propanediamine (1.24, ~12 mmol) and triethylamine (0.61 g, ~6 mmol) in 20 mL CH_2Cl_2 was slowly added, followed by overnight stirring at room temperature under N_2 atmosphere. Afterwards, the reaction mixture was then washed with water (30 mL

x 2) using a separating funnel, then with saturated Na_2CO_3 solution (100ml). The organic layer was dried over Na_2SO_4 and filtered. The solvent was evaporated, yielding this compound as yellow oil 1.48 g, yield 34.7%. 1H NMR (500 MHz, $CDCl_3$): δ (ppm): 5.45 (s, 1H), 3.50-3.59 (m,1H), 3.30(m, 2H), 3.05-3.20 (m, 2H), 2.38-2.49 (m, 1H), 2.38 (t, 2H, J = 6Hz), 2.20 (s, 6H), 2.17 (t, 2H, J=6Hz), 1.83-1.94 (m, 1H), 1.57-1.72 (m, 6H), 1.38-1.52 (m, 2H), 5.3 (s, 2H, CH_2Cl_2 residue solvent).

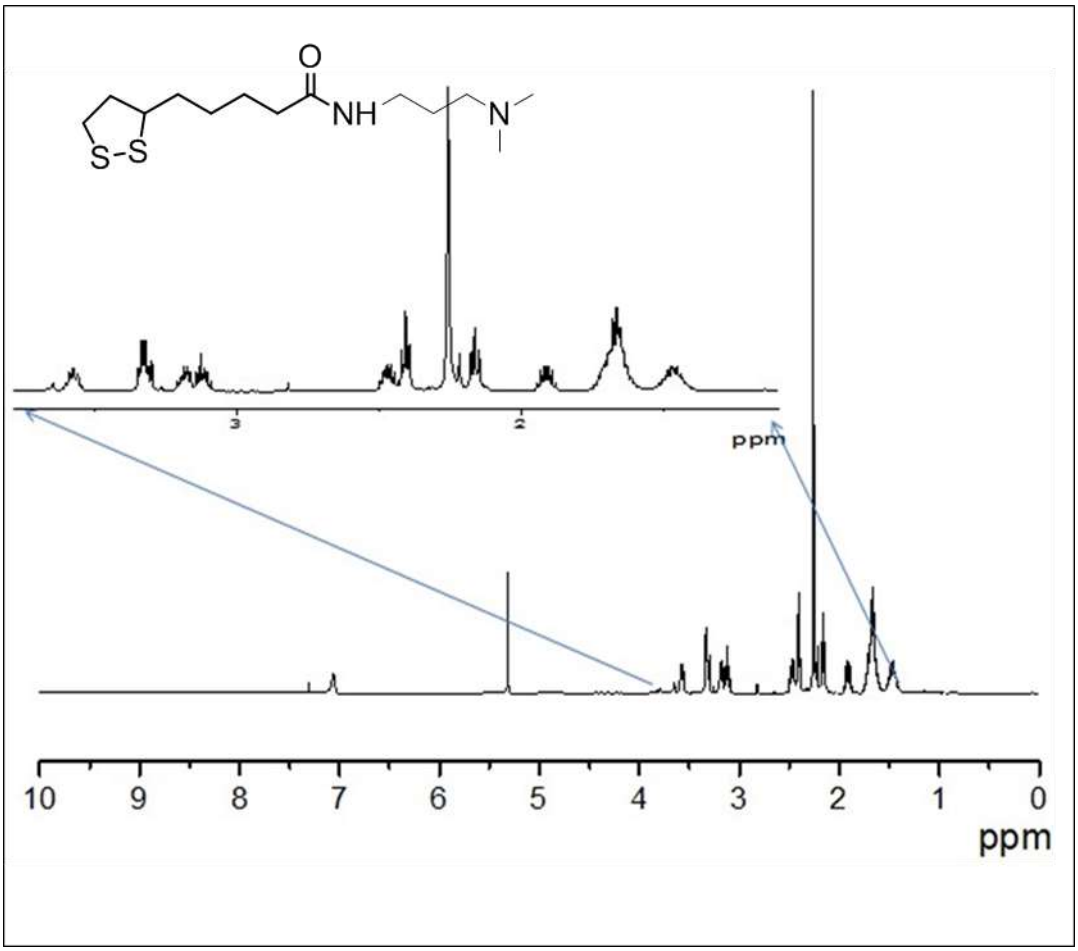

Figure 2-12: ^{1}H NMR spectrum of prepared TA-N, N-Dimethyl-1, 3-propanediamine.

Step 2: Synthesis of TA-ZW.

TA-N, N-Dimethyl-1,3-propanediamine (1.48 g, ~5.2 mmol) was dissolve in 20 mL dried TMF and purged with N_2 for 30 mins, 1,3-propanesultone (1.0 g, ~8 mmol) was dissolve in 4 mL dried TMF was added at room temperature. The reaction mixture was left stirring continuously for 3 days. A turbidity instantly build up once 1,3-propanesultone was injected due to limited solubility of the formed TA-Zwitterion in TMF. After that, the solvent was evaporated, yielding a pale yellow solid. The crude product was washed by chloroform 3 times (to remove any impurities) and the fully dissolved in H_2O. The reaction yield was ~ 23% after purified by HPLC. ^{1}H NMR (300 MHz, CDCl3): δ (ppm) 3.60-3.70 (m,1H), 3.40-3.50 (m, 2H), 3.28-3.35 (m, 2H), 3.20-3.28 (m, 2H), 3.10-3.20 (m, 2H), 3.10 (s, 6H), 2.90 (t, 2H), 2.40-2.50 (m, 1H), 2.20 (t, 2H), 2.15 (m, 2H), 1.93-2.0 (m, 2H), 1.70 (m, 1H), 1.50-1.60 (m, 4H), 1.35-1.40 (m, 2H). HPLC-MS: TA-Zwitterion m/z is 412.15, calculated m/z for $[M + H]^+$ = 413.34. (Shown in Figure 2-14)

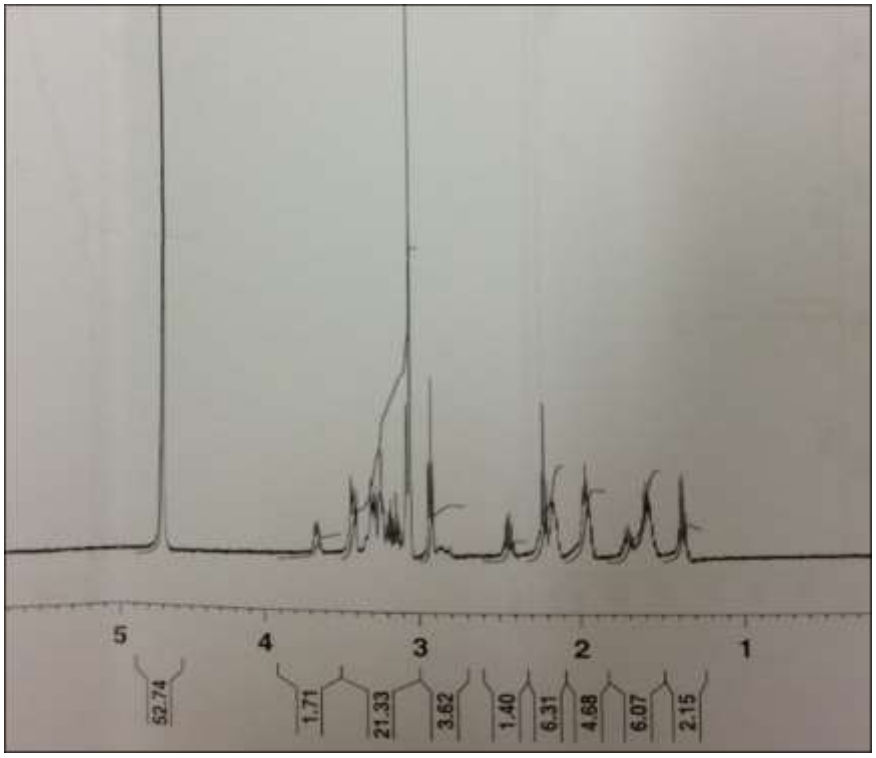

Figure 2-13: ^{1}H NMR spectrum of prepared TA-ZW, 1H NMR (300 MHz, CDCl3): δ (ppm) 3.60-3.70 (m,1H), 3.40-3.50 (m, 2H), 3.28-3.35 (m, 2H), 3.20-3.28 (m, 2H), 3.10-3.20 (m, 2H), 3.10 (s, 6H), 2.90 (t, 2H), 2.40-2.50 (m, 1H), 2.20 (t, 2H), 2.15 (m, 2H), 1.93-2.0 (m, 2H), 1.70 (m, 1H), 1.50-1.60 (m, 4H), 1.35-1.40 (m, 2H).

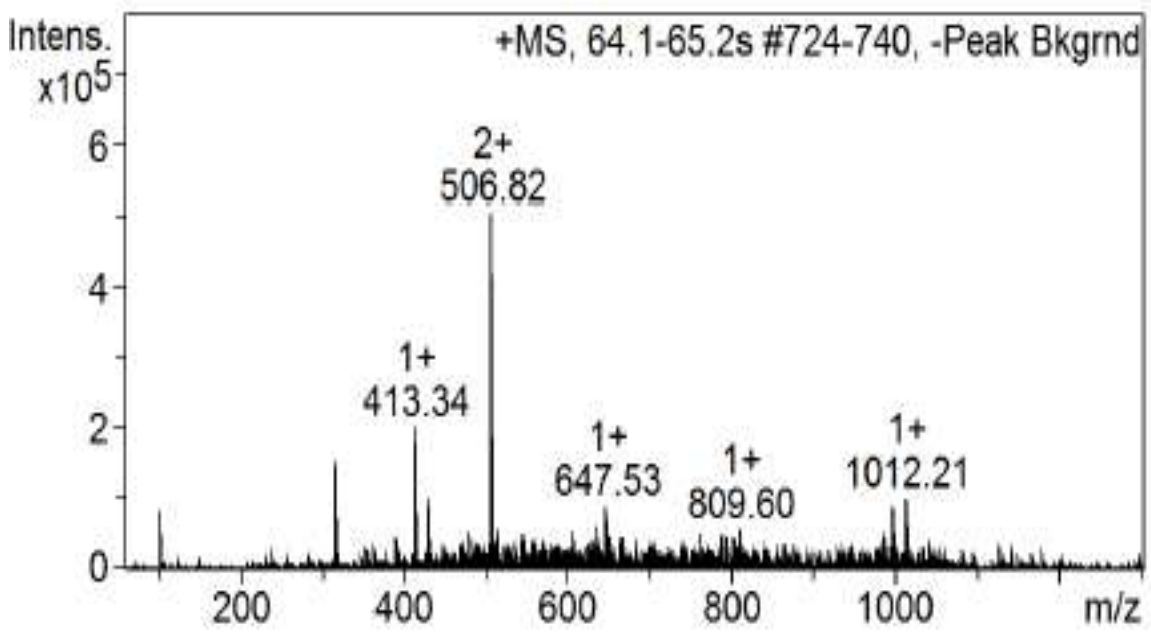

Figure 2-14: HPLC-MS analysis spectra m/z for $[M + H]^+$ = 413.34

2.2.3 Synthesis of TA-PEG600-Biotin

The chemical structures and synthetic routes for TA-PEG600-Biotin was shown in **Figure 2-15**

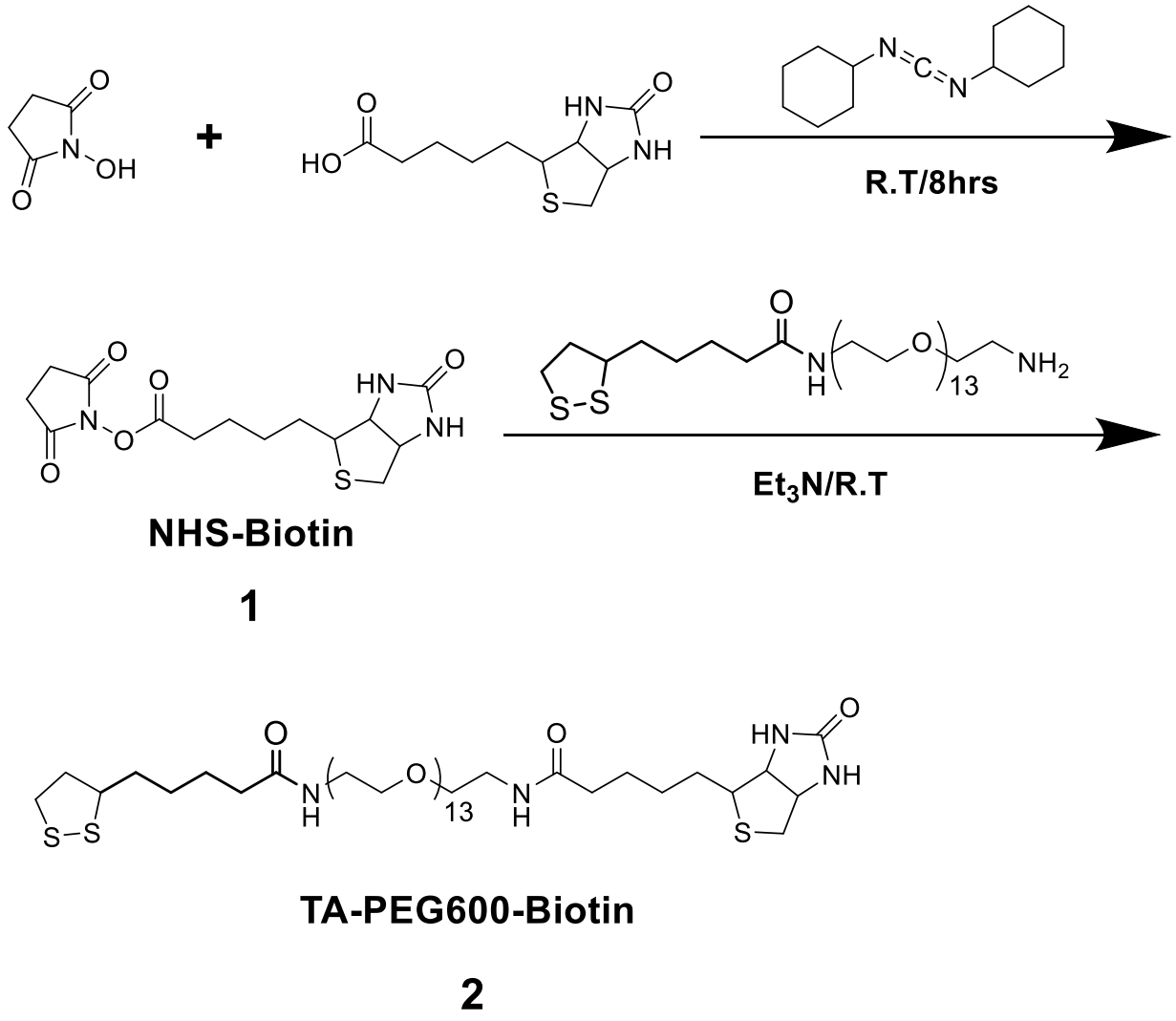

Figure 2-15: The synthetic route to TA-PEG600-biotin. Reaction conditions are: **i**) N,N'-dicyclohexylcarbodiimide, Biotin, NHS, DMF; **ii**) TA-PEG600-NH_2, NHS-biotin, DMF, Et_3N

Step 1 Synthesis of NHS-biotin.

Biotin (2.0 g, ~8.2 mmol), NHS (0.94 g, ~8.2 mmol) and 100 mL DMF were placed in a round-bottomed flask (250 mL). The mixture was flushed with N_2 gas, the mixture was left stirring for 30 mins. N,N'-dicyclohexylcarbodiimide (2.47 g, ~12 mmol) was added slowly to the mixture and left stirring overnight at room temperature under N_2. A white precipitate was filtered out. The solvent was evaporated by using a rotary evaporator and filtered out by wash with ether. The white powder was dried under vacuum, weight 1.22 g, yield = 43.9 %.

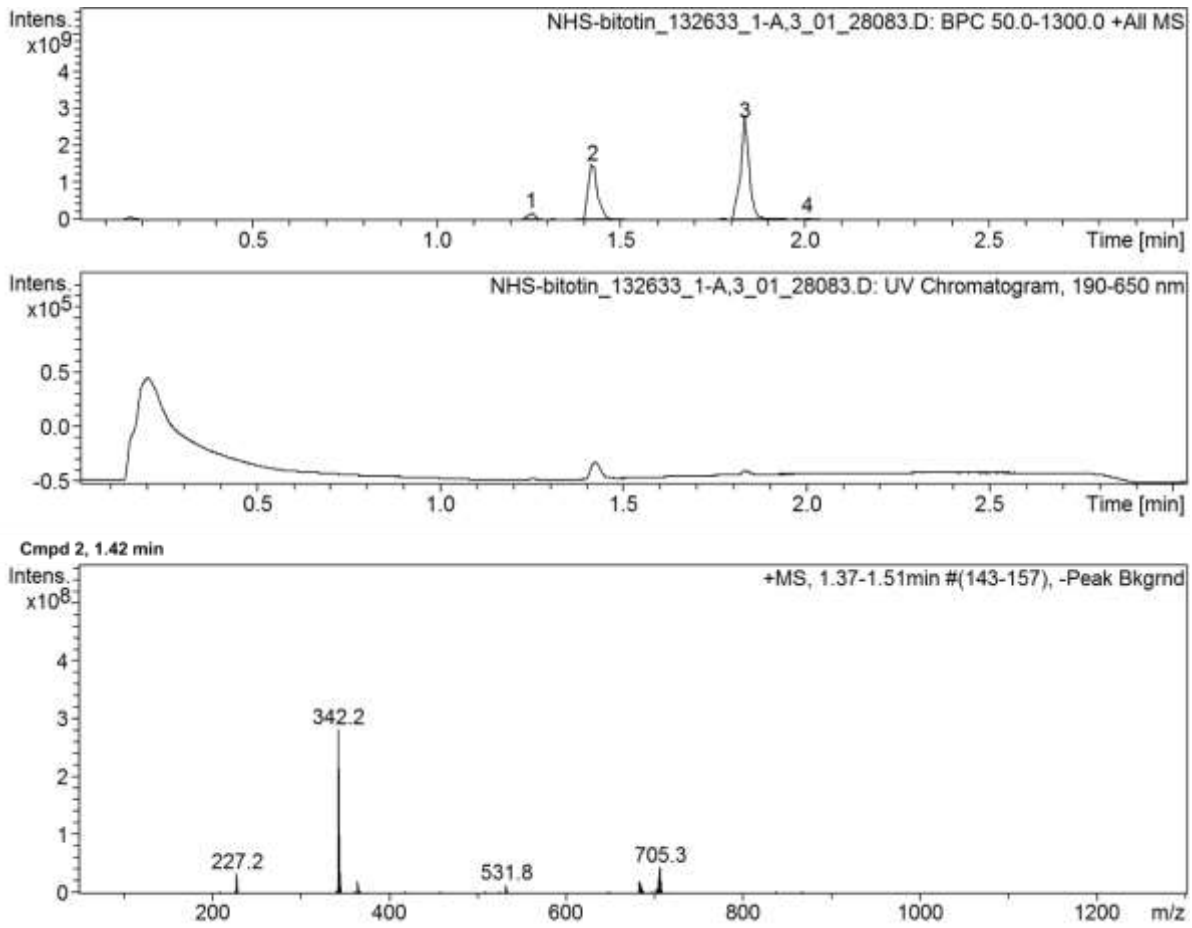

Figure 2-16: HPLC-MS spectrum of NHS-Biotin ($[M+H]^+$, 342.2)

HPLCMS: found m/z 341.2, calculated m/z for $[M + H]^+$ = 342.2. A further LC-MS analysis of the NHS-biotin revealed a single UV absorption band with a retention time of ~1.42 min. The corresponding MS spectrum displayed a peak with m/z value of 342.2, corresponding to the $[M+H]^+$ (Figure 2-16)

Step 2 Synthesis of TA-PEG600-biotin

TA-PEG600-NH_2 (0.29 g ~0.37 mmol), NHS-biotin (0.122 g, ~0.36 mmol) and DMF (8.0 mL) were added into a 20 mL round-bottomed flask equipped with a magnetic stirring bar and a septum. The reaction vessel was purged with N_2 and cooled to 0 °C in an ice-bath while stirring. Then triethylamine (0.50 mmol) was then added dropwisely under N_2. Once the addition was completed, the reaction mixture was stirred overnight under N_2 at room temperature. Once the reaction was complete, the reaction mixture was filtered by a paper filter and evaporated out DMF solvent. The pure TA-PEG600 was collected by HPLC-MS column, weight 0.185 g, yield = 51.3 %. ^{1}H NMR (300 MHz, $CDCl_3$): δ (ppm) 6.79-6.98 (m,1H), 6.43-6.65 (m, 1H), 5.65-5.85 (m, 1H), 4.92-5.12 (m, 1H), 4.47-4.63 (m, 1H), 4.33 (m, 1H), 3.5-3.9 (m), 3.40-3.50 (m, 2H), 3.10-3.20 (m, 3H), 2.80-2.98 (m, 1H), 2.75 (d, 1H), 2.40-2.60 (m, 1H), 2.10-2.30 (m, 4H), 1.80-1.96 (m, 1H), 1.60-1.80 (m, 8H), 1.40-1.60 (m, 4H), HPLC-MS found a series of peaks that were separated by 44 m/z units, corresponding to different PEG chain lengths in the mixed length PEG600 linker, *e.g.* 1048.0, 1004.8, 959.6, 915.7, 871.7. The calculated corresponding $[M+H]^+$ peaks for TA-PEGn-Biotin where n = 13, 12, 11, 10 and 9 were 1048, 1004, 959, 915 and 871, respectively. (Figure 2-18)

An HPLC-MS spectrum of TA-PEG600-NH2 is shown below.

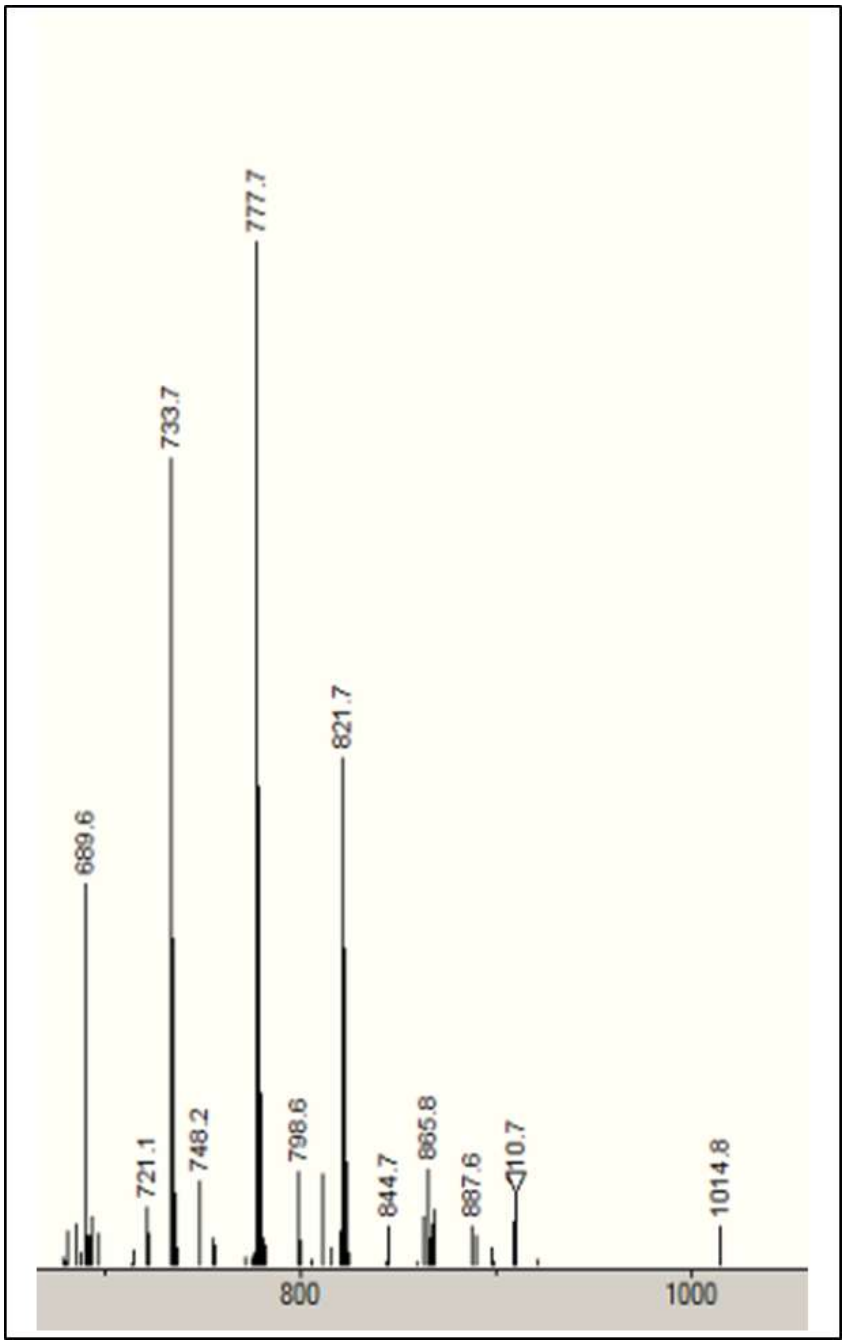

Figure 2-17: HPLC-MS spectrum of TA-PEG600-NH_2. HPLC-MS found a series of peaks that were separated by 44 m/z units, corresponding to different PEG chain lengths in the mixed length PEG600 linker, e.g. 689.6, 733.7, 777.7, 821.7, and 865.8 respectively. The calculated peaks for TA-PEGn-NH_2 where n = 10, 11, 12, 13 and 14.

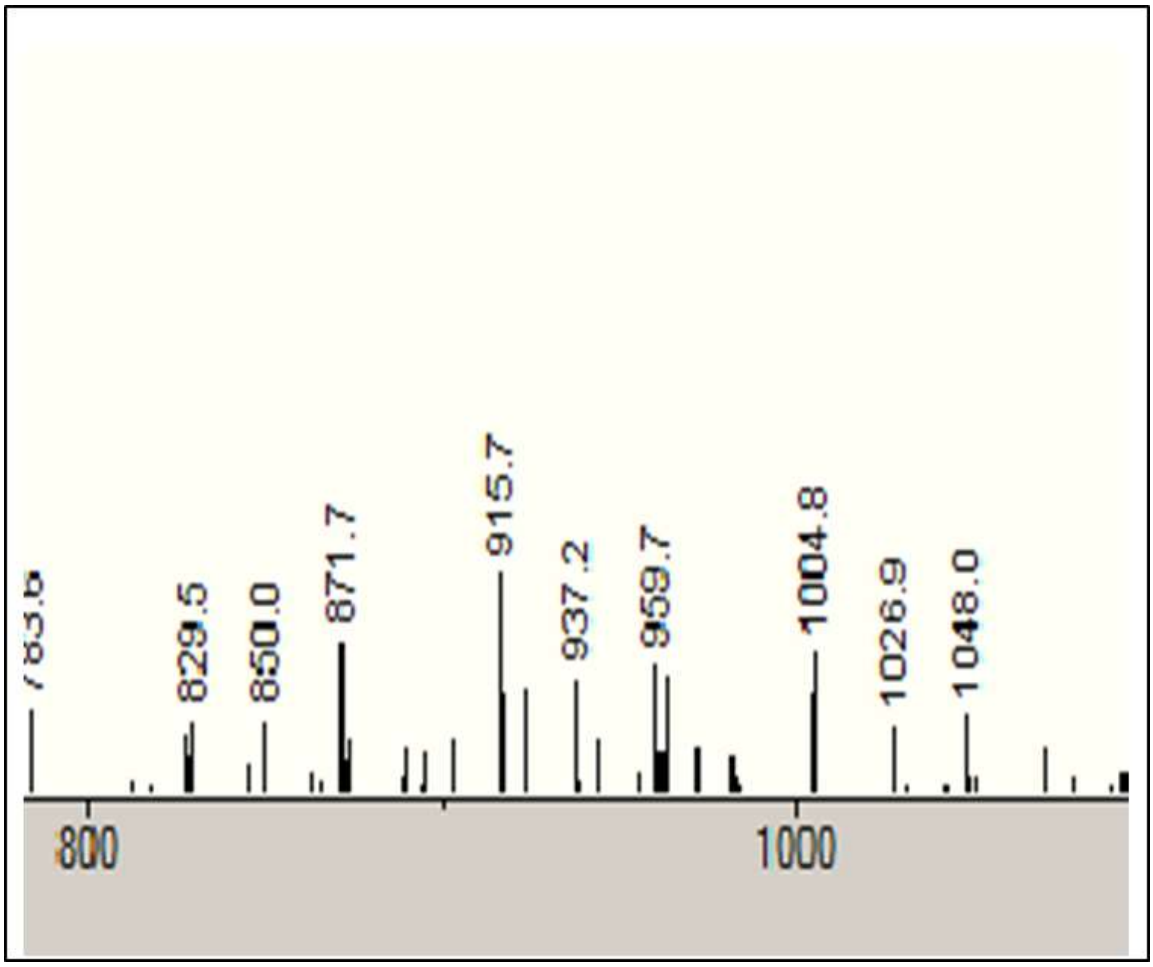

Figure 2-18: HPLC-MS found a series of peaks that were separated by 44 m/z units, corresponding to different PEG chain lengths in the mixed length PEG600 linker, e.g. 1048.0, 1004.8, 959.6, 915.7, 871.7. The calculated corresponding $[M+H]^+$ peaks for TA-PEGn-Biotin where n = 13, 12, 11, 10 and 9 were 1048, 1004, 959, 915 and 871, respectively.

2.3 Summary

In this chapter, the preparation of specific ligands to be used in making QD-biosensors in the following chapters is described. First, I have synthesized a series of TA-based ligands, TA-PEG750-OMe, TA-PEG2000-OMe and TA-ZW to ensure the QD water solubility in further QD-sensor application. A TA-PEG600-Biotin functional ligand not only guarantees the QD water solubility but also provides a functional group for efficient conjugation to biomolecule (*e.g.* Neutravidin) was also synthesized. With the water-soluble functional ligands being prepared, the next step is to prepare QD-DHLA-based probes and investigate their FRET based sensing performances for specific biomolecule targets.

2.4 Reference

1. Susumu, K.; Mei; B. C.; Mattoussi, H. *Nat. Protoc.* **2009**, *4*, 424-436.

2. Zhan, N.; Mattoussi, H. *ACS Appl. Mater. Interf.* **2013**, *5*, 2861-2869.

3. Zhou, D.; Ying, L.; Hong, X.; Hall, E. A.; Abell, C.; Klenerman, D. *Langmuir*, **2008**, *24*, 1659-1664.

4. Grabolle, M., Speieles, M., Lesnyak, V., Gaponik, N., Eychmüller, A. & Resch-Genger, U. *Analytical Chemistry* **2009**, *81*, 6285-6294.

5. Zhou, D., Piper, J. D., Abell, C., Klenerman, D., Kang, D.-J. & Ying, L. *Chemical Communications.* **2005**, *38*, 4807-4809.

6. Zhang, H.; Guo, Y.; Feng, G.; Zhou, D. *Nanoscale* **2013**, *5*, 10307-10315.

7. Tiede, C.; Tang, A. A. S.; Deacon, S. E.; Mandal, U.; Nettleship, J. E.; Owen, R. L.; George, S. E.; Harrison, D. J.; Owens, R. J.; Tomlinson, D. C.; McPherson, M. J. *Protein Engineering Design & Selection* **2014**, *27*, 145.

8. Zhou, D.; Bruckbauer, A.; Ying, L.; Abell, C.; Klenerman, D. *Nano Lett.*, **2003**, *3*, 1517-1520.

Chapter 3. An Ultra-efficient Cap-Exchange to Compact Biofunctional Quantum Dots for Sensitive Ratiometric Biosensing and Cell Imaging

Abstract

In this chapter, an ultra-efficient cap-exchange protocol (UCEP) to render commercial hydrophobic quantum dots (QDs) completely water-soluble using >50-fold less of the air-stable Thioctic acid (TA) based functional ligands following a rapid *in situ* reduction by tris(2-carboxylethyl phosphine, TECP) is developed. The resulting water-soluble QDs are compact (D_h <10 nm), bright (retaining >90% of original fluorescence), resist nonspecific adsorption and display good stability in biological buffers even with high salt content (*e.g.* 2 M NaCl), making them well-suited for cell imaging and ratiometric biosensing. A dihydrolipoic acid (DHLA)-zwitterion capped QD prepared by the UCEP is readily biofunctionalized with octa-histidine-tagged antibody mimetic proteins (also known as Affimers), allowing for rapid, ratiometric detection of its target protein down to 5 pM *via* the QD-sensitized Förster resonance energy transfer (FRET) readout signal. Moreover, compact biotin functionalized QDs were readily prepared by a facile, one-step cap-exchange process for ratiometric quantitation detection of 5 pM neutravidin as well as for fluorescence imaging of target model cancer cells.

3.1 Introduction

Quantum dots (QDs) have been of significant research focus over the past two decades because of their unique, size-dependent, stable and bright fluorescence which makes them powerful tools in broad research areas such as energy, materials, biology, and medicine.[1-7] Their broad absorption and stable, narrow symmetric emission are particularly well-suited for multiplexed sensing, bio-diagnostics, bioimaging, cell tracking and trafficking studies.[3,4,8-18] In this regard, a robust, compact and biocompatible QD structure is paramount. However, since high quality QDs (*e.g.* CdSe/ZnS, CdSe/CdS/ZnS) are widely prepared by an organometallic route, they are naturally capped with hydrophobic ligands and are therefore water-insoluble and bio-incompatible.[1,2,8,9] To make such QDs biocompatible, three main approaches such as encapsulation with PEGylated phospholipids or amphiphilic/block copolymers,[8,9,19] coating with silica,[1] and cap-exchange are widely employed.[2,4] The first two methods often produce stable but relatively bulky QDs (with typical hydrodynamic radius, R_h, >10 nm) which can limit their application in bioimaging particularly in crowded regions such as neuronal synapses,[20] and more critically in Förster resonance energy transfer (FRET) based applications. This is because such R_h values are greater than the R_0 (Förster radius) values of most QD-dye FRET pairs (*e.g.* 4-7 nm) even prior to bio-conjugation. Given the reverse 6th power dependence of FRET efficiency (E) on the donor-acceptor distance (r): $E = 1/[1 + (r/R_0)^6]$, such bulky QDs will lead to diminished E.[21-24] In contrast, cap-exchange often produces compact QDs which are better suited for FRET applications.[11,13,24-33] In this regard, cap-exchange using dihydrolipoic acid (DHLA) based ligands is highly attractive because such ligands chelate strongly to the QD,

providing a compact, robust coating which also resists non-specific adsorption upon appending a poly(ethylene glycol) (PEG) or zwitterion terminal group.[34-39]

Despite significant research, two limitations still remain to be solved for most current cap-exchange methods: 1) the requirement of using a large excess of ligand (with ligand:QD molar ratio, LQMR, of *ca*. 10^4-10^5, Table 3-1) which limits its use with precious or expensive ligands; and 2) the production of significantly quenched florescence over the parent hydrophobic QDs (with typical reduction of *ca.* 30-95%, depending on the QD types and cap-exchange procedures), which undoubtedly compromise their fluorescence applications.[39-41] These limitations are mainly due to non-optimal conditions employed by current cap-exchange methods (*e.g.* reaction in two immiscible phases using non-/partially-deprotonated ligands which do not offer rapid QD-ligand transport, exchange and strong binding). Theoretically, a spherical 4.5 nm red emitting (λ_{EM} ~600 nm) CdSe/ZnS QD (Figure 3-3A) has a total surface area of 63.6 nm^2. Assuming the QD is terminated with a full Zn^{2+} outer layer in stable Wurtzite structure with each Zn^{2+} occupying a surface area of 0.126 nm^2 (Figure 3-1), then the QD would contain 505 surface Zn^{2+} ions. Assuming each thiolate binds to one Zn^{2+} ion, then 505 single thiolate ligands (or 253 DHLA-based ligands, each containing 2 thiol groups and hence a footprint area of 0.252 nm^2) would saturate the QD surface Zn^{2+} ions completely. Note this is the theoretical maximum number of ligands required for a 4.5 nm QD; the actual number could be smaller because the QD surface may not be fully terminated with a Zn^{2+} layer. Consistent with this, the Mattoussi group recently reported a footprint of ~0.5 nm^2 for each TA-PEG1000-benzaldehyde ligand on a CdSe/ZnS QD surface, about twice that of our estimate. This is reasonable considering the possible steric effect of the long PEG chain as well as the non-pure zinc layer nature of the QD surface.[42] This simple calculation

reveals that only a tiny fraction (*ca.* ≤ 2%) of the DHLA-ligands used in current literature methods can actually bind to the QD, while the vast majority of ligands exist as free ligands. Given its strong Zn^{2+} binding affinity, such free DHLA-ligands may etch the ZnS protecting shell, generating surface defects (*e.g.* Zn^{2+}/S^{2-} vacant sites) that can effectively trap exciton carriers and compromise the QD fluorescence.[30] This is supported by an observations that performing cap-exchange using Zn^{2+}-metalated DHLA better preserved QD fluorescence than free DHLA, presumably as the introduced Zn^{2+} ions minimized the ZnS shell etching.[43]

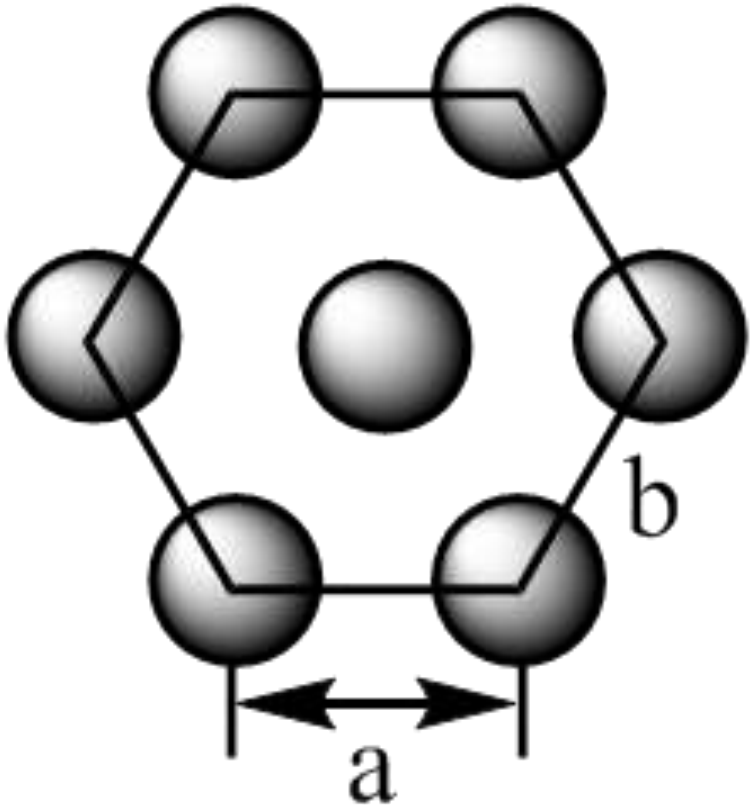

Figure 3-1: Schematic of a hexagonally packed Zn^{2+} outer layer (assuming ZnS being in its most stable Wurtzite structure) where a = b = 382 pm = 0.382 nm.

Within the hexagon area, there are three Zn^{2+} ions (spheres, 1 in the middle + 6 × (1/3) one the corners).

The total area of the hexagon = 6 × (1/2) a^2 × $\sin 60^o$ = 3 × 0.382^2 $\sin 60^o$ = 0.379 nm^2

Therefore the surface area occupied by each Zn^{2+} = 0.379/3 = 0.126 nm^2

Based on this understanding, we hypothesize that reducing the number of the ligands to a level just sufficient for capping the QD surface Zn^{2+} ions should minimize any possible ZnS shell etching, allowing the cap-exchanged QDs to retain high fluorescence. To achieve this goal, it is vital to improve cap-exchange efficiency. We have recently demonstrated that the cap-exchange efficiency can be improved substantially by performing the reaction in homogenous solution using deprotonated DHLA-ligands,[44] presumably due to the greatly improved QD-ligand transport/ exchange rates and enhanced binding affinity. Despite success, it is still a laborious and delicate to handle because the DHLA based ligands need to be freshly prepared as they are air-sensitive and susceptible to oxidization to the thioctic acid (TA) form, which would result in loss of QD binding affinity.[38] By contrast, the photo-ligation method reported by the Mattoussi group can work directly with the air-stable TA form of ligands,[37-39,41] however, the requirement for a large excess of ligands (*ca.* LQMR = 2-4 $\times 10^4$, see Table 3-1) can limit its application with precious or expensive custom ligands. An efficient cap-exchange method that can work with a minimal amount (*ca.* LQMR < 1000) of air-stable ligands without involving any complicated separation/purification steps and without compromising the fluorescence of cap-exchange QDs would be extremely valuable to broaden and enhance QD based biomedical applications.

Herein we report an ultra-efficient cap-exchange protocol (UCEP) that can satisfy such requirements. It is based on a rapid reduction of TA-based ligands to their DHLA form by tris(2-carboxylethyl)phosphine (TCEP). After deprotonation of the thiol groups, the resulting *in situ* reduced DHLA-ligands are directly used to initiate cap-

exchange with hydrophobic CdSe/ZnS or CdSe/CdS/ZnS QDs in homogenous solution. We show that the UCEP can provide complete QD water-solubilization at a LQMR of as low as 200:1, ~50-500 folds lower than most literature protocols (Table 3-1). Moreover, the resulting QDs are compact (with typical hydrodynamic radius, R_h <5 nm), retaining >90% of their original fluorescence and resist non-specific adsorption, making them powerful probes for FRET based ratiometric sensing and cancer cell imaging.

3.2 Experiment details

3.2.1 Chemicals and Reagents

CdSe/ZnS core/shell QD with λ_{EM} of 600 nm was purchased commercially from PlasmaChem GmbH (Berlin, Germany). The QD was supplied as dry powders capped with mixed ligands of trioctylphosphione oxide (TOPO), hexadecylamine and oleic acid. Three different colored CdSe/CdS/ZnS core/shell/shell QDs in toluene (CANdots, λ_{EM}s = ~610, 575 and 525 nm, quantum yield > 40%) were purchased from Strem Chemicals (Cambridge, UK). tris(2-carboxyethyl)phosphine hydrochloride (TCEP.HCl, >98%), chloroform (> 99.8%), methanol (>99.9%), sodium bicarbonate (>99.5%), Dulbecco's modified Eagle's medium (DMEM), fetal bovine serum (FBS), penicillin, typsin-EDTA, Dulbecco's phosphate buffered saline (D-PBS) and other chemicals were all purchased from Sigma-Aldrich (Dorset, UK) and used as received without further purification unless stated otherwise. Solvents were obtained from Fisher Scientific (Loughborough, UK) and used as received. Ultra-pure water (resistance >18.2 MΩ.cm) purified by an ELGA Purelab classic UVF system, was used for all experiments and making buffers. The target protein, yeast SUMO

(SUMO) protein and the anti-SUMO Affimers (nABP) were expressed in BL21 (DE3) cells using isopropyl ß-D-1-thiogalactopyranoside (IPTG) induction and purified by Ni-NTA resin (Qiagen) affinity chromatography according to the manufacturer's instructions. And all the target protein and anti-SUMO Affimers were provide by Darren Tomlinson's group in School of Chemistry and Astbury Structure for Molecular Biology, University of Leeds. The detailed experimental procedures were described in our recent publication.[50]

3.2.2 Instrument and methods

The QD purification was performed by Amicon ultra-centrifugal filter tubes with a cut-off MW of 30,000. All fluorescence spectra were measured on a Spex Fluoro Max-3 Spectrofluorometer (fluorescence linear response up to 5000000 cps) using a 0.70 mL quartz cuvette under a fixed excitation wavelength (λ_{EX}) of 450 nm. This wavelength corresponds to the absorption minimum of the acceptor dye, minimizing the direct excitation of the dye acceptor.[1] An excitation and emission bandwidths of 5 nm and a scan rate of 120 nm/min over 480-800 nm range were used. Confocal fluorescence imaging was recorded on Zeiss LSM-510 inverted laser scanning confocal microscope was done by Rongjun Chen's group in Department of Chemical Engineering, Imperial College London. They using at 488 nm excitation and collecting emission at above 570 nm. Flow cytometry was recorded on a BD LSRFortessa cytometer. The samples were excited at 488 nm and the emission was collected in the 570-585/42 nm band and the results were analysed using the FlowJov10 software.

3.2.3 Experimental Procedures[36]

3.2.3.1 Preparation of water-soluble QDs by ligand exchange

Preparation of DHLA-Zwitterion ligand capped QDs (QD-ZW)

Typical ligand exchange procedures for preparing QD-ZW is as follows: commercial hydrophobic CdSe/ZnS or CdSe/CdS/ZnS QD (1 nmole, 20 µL in hexane) was precipiated by adding 500 µl EtOH followed by centrifugation to remove any free TOPO ligands. The QD pellet was then dissolved in 50 µl $CHCl_3$ and then added with 20 µl EtOH to make solution **A**. TA-ZW (0.10 M, 2 µL in H_2O) was reduced to DHLA-ZW by mixing with TCEP.HCl (0.10 M, 2 µL in H_2O) for 10 mins. After which NaOH (0.10 M in EtOH, 12 µL) was added to fully deprottonate the DHLA thiol-groups and to neutralise acid groups in TCEP.HCl (each containing 4 acid groups) to make solution **B**. After that, the above solutions **A** and **B** were mixed in a new Eppendorf tube for 1-3 mins with occasional shaking by hand, after which H_2O (50 µL) was further added to the reaction mixture. The QD was found to rise to the top aqueous phase, leaving the bottom $CHCl_3$ layer effectively colourless, indicating full QD water-solubilization. The top aqueous layer was then carefully separated from the bottom $CHCl_3$ layer and transfered to an Amicon ultra-centrifugal tube equipped with a 30,000 MW cut-off filter membrane and centrifuged for 1 min at 3000 rpm. The residue was then washed with H_2O (200 µL) and followed by a brief centrifugation. The process was repeated three times with to remove any unbound free ligands, yielding a stable, and water soluble QD stock solution. The stock QD concentration was determined by UV-vis absorption spectra using their first exciton peak and the

respective extinction coefficient using our previously established procedures before.[31, 33]

The ligand exchange procedure for QD-PEG750-OMe

QD (1 nmol, 20 µL in hexane) was first precipitated by adding 500 µl EtOH followed by centrifugation to remove unbound free TOPO ligands. The QD precipitate was then dissolved in 30 µL hexane and then added with 10 µL EtOH to make solution **A**. TA-PEG750-OMe (0.189 M in EtOH, 1.06 µL) was reduced by 1 molar equivalent of TCEP (0.10 M, 2 µL in H_2O) for ~10 mins, and then NaOH (0.10 M in EtOH, 12 µL) was added to make solution **B**. After that, solutions **A** and **B** were mixed for 1-3 mins under agitation, then H_2O (20 µL) was further added and the QD will move to lower aqueous layer, leaving the top organic layer colourless. The aqueous layer was transfered to an Amicon ultra-centrifugal tube equipped with a 30,000 MW cut-off filter membrane. After centrifugation and washing with H_2O three times as above to eliminate the free ligand, a stable, biocompatible QD-PEG750 was obtained.

Preparation of DHLA-PEG750-OMe and DHLA-PEG600-Biotin mixed ligand capped QDs (QD-biotin$_{70/100/150}$)

Commercial hydrophobic CdSe/ZnSe/ZnS core/shell/shell QD (1 nmole, 20 µL in hexane) was precipitated by adding 500 µL EtOH followed by centrifugation to remove any free TOPO ligands. The QD pellet was then dissolved in 100 µL $CHCl_3$ and then added with 50 µL EtOH to make solution **A**. TA-PEG600-Biotin (0.10 M in EtOH, 0.7 µL, 1 µL, 1.5 µL) was reduced to DHLA-PEG600-Biotin by mixing with 1 molar equivalent of TCEP.HCl (0.10 M, 0.7 µL, 1 µL, 1.5 µL in H_2O) for 10 mins. After which NaOH (0.10 M in EtOH, 4.2 µL, 6 µL, 9 µL) was added to fully

deprottonate the DHLA thiol-groups and to neutralise acid groups in TCEP.HCl (each containing 4 acid groups) to make solution **B**. TA-PEG750-OMe (0.10 M in EtOH, 10 µL) was reduced to DHLA-PEG750-OMe by mixing with TCEP.HCl (0.10 M, 10 µL in H_2O) for 15 mins. After which NaOH (0.10 M in EtOH, 60 µL) was added to fully deprotonate the DHLA thiol-groups and to neutralise acid groups in TCEP.HCl (each containing 4 acid groups) to make solution **C**. After that, the above solutions **A** and **B** were mixed in a new Eppendorf tube for 10 mins with occasional shaking by hand, after which solution **C** was further added to the reaction mixture for 15 mins more. After which H_2O (50 µL) was further added to the reaction mixture. The QD was found to rise to the top aqueous phase, leaving the bottom $CHCl_3$ layer effectively colourless, indicating full QD water-solubilization. The top aqueous layer was then carefully separated from the bottom $CHCl_3$ layer and transferred to an Amicon ultra-centrifugal tube equipped with a 30,000 MW cut-off filter membrane and centrifugated for 1 min at 3000 rpm. The residue was then washed with H_2O (200 µL) and followed by a brief centrifugation. The process was repeated three times with to remove any unbound free ligands, yielding a stable, and water soluble QD stock solution.

3.2.3.2 Protein preparation, purification and labelling

The anti-SUMO Affimer (5 mg/ml, 12.5 µL in PBS, MW = 13,267) in a microcentrifuge tube was first mixed with Alexa 647 NHS-ester (50 µg in 2 µL DMSO) and then 5 µL $NaHCO_3$ (0.5 M, pH = 8.3) and 7.5 µl PBS (10 mM phosphate, 150 mM NaCl, pH 7.4) were added and thoroughly mixed at room temperature for 2 h (dye: protein molar ratio ≈ 8:1). After that the reaction mixture was loaded on a small

G25 gel filtration column using PBS as eluting solution on natural flow. The first eluted blue band (corresponding to the labelled anti-SUMO Affimer) was collected and its absorption spectrum was recorded. Using the extinction coefficients of the Alexa-647 dye (ε_{650nm} = 239,000 $M^{-1}cm^{-1}$) and Affimer (ε_{280nm} =7904 $M^{-1}cm^{-1}$) and the CF_{280nm} of 0.03 for Alexa-647 dye, the average dye labelling ratio on per Affimer was calculated as 1.08. The stock protein concentration was 86 µM.[55]

Similarly, the SUMO protein was labelled with Alexa-647 NHS ester using the same procedures under a dye: protein molar ratio of 6.4. After purification by using a G25 column as above, the average number of dyes labelled on each protein was determined as 0.80. The labelled protein stock concentration was 32.7 µM.

Neutravidin was also labelled with Alexa-647 NHS ester using the same procedures under a dye: protein molar ratio of 7. After purification by using a G25 column as above, the average Alexa-647 dye label per protein was determined as 1.67.

3.2.3.3 Cell culture and cell based studies (done by Rongjun Chen's group)

The following works were done by Rongjun Chen's group in Department of Chemical Engineering, Imperial College London. HeLa adherent epithelial cells derived from human cervical carcinoma were grown in Dulbecco's modified Eagle's medium (DMEM) supplemented with 10% (v/v) fetal bovine serum (FBS) and 100 U mL^{-1} penicillin. The HeLa cells were trypsinized using trypsin-EDTA and maintained in a humidified incubator with 5% CO_2 at 37 ^oC.

Laser scanning confocal microscopy

2 mL of HeLa cells (1.5×10^5 cells mL^{-1}) were cultured for 24 h followed by the treatment with 1 mL of the serum free DMEM with or without of the QD samples (50 nM). After incubation for 4 h, the cells were washed three times with Dulbecco's phosphate buffered saline (D-PBS). Hoechst 33342 was added to a final concentration of 5 µg mL^{-1} for nuclei staining. The cells were then imaged by laser scanning confocal microscopy (Zeiss LSM-510 inverted laser scanning confocal microscope, Germany). The QD was excited at 488 nm and the emission above 570 nm was collected.

3.2.3.4 Flow cytometry and free biotin competition (done by Rongjun Chen's group)

1 mL of HeLa cells (3×10^5 cells/mL) were cultured in 6 well plates for 24 h followed by treatment with 1 mL of serum-free DMEM with or without QD (50 nm). After 4h incubation, the cells were washed three times with Dulbecco's Phosphate Buffered Saline (D-PBS). After cell detachment using 0.5 mL of Trypsin-EDTA, 0.5 mL of serum-free DMEM was added to each well and the samples were centrifuged in 2 mL microcentrifuge tubes for 5 minutes at 1000 rpm. The supernatant was discarded and replaced with 0.5 mL of serum-free DMEM. The samples were filtered using Flowmi™ cell strainers (40 µm) and analysed in 5 mL Falcon plastic tubes using BD LSRFortessa cytometer. The samples were excited at 488 nm and the emission was collected in the 570 - 585/42 nm band. The results were analysed using FlowJo v10 software. 1 mL of HeLa cells (3×10^5 cells/mL) were cultured in 6 well plates for 24 h, followed by 1 h treatment of one set of triplicates with 10 mM free biotin in serum-free DMEM. 1 mL of serum-free DMEM with QD (50 nM) with or without free biotin (10 mM) were then added to the wells which had been pre-treated with free biotin or incubated normally, respectively. After a 4 h incubation, the cells were washed three

times with PBS. After cell detachment using 0.5 mL of Trypsin-EDTA, 0.5 mL of serum-free DMEM was added to each well and the samples were centrifuged in 2 mL microcentrifuge tubes for 5 minutes at 1000 rpm. The supernatant was discarded and replaced with 0.5 mL of serum-free DMEM. The samples were filtered using Flowmi™ cell strainers (40 µm) and analysed in 5 mL Falcon plastic tubes using BD LSRFortessa cytometer. The samples were excited at 488 nm and the emission was collected in the 586/16 nm band. The results were analysed using FlowJo v10 software.

3.2.3.5 Gel electrophoresis

2 or 5 µL of a DHLA-ZW capped CdSe/ZnS core/shell QD (QD-ZW, λ_{EM} ~600 nm) prepared at a LQMR of 200, 500 and 1000, respectively was mixed with 18 or 15 µL of 60% glycerol in H_2O. A QD-Affirmer assembly was also prepared by mixing the QD-ZW prepared at a LQMR of 500 with 10 molar equivalent of the His_8-tagged Affirmer. The resulting QD-Affimer conjugate was treated the same way as the above QD-ZW samples. Then 20 uL of each sample was loaded onto a 0.75% agarose gel in TAE buffer pH8.3. Gel was run at 100 mV for ~30 min and QD was visualized under a UV illumination (λ = 365 nm).

3.3 Results and discussion

3.3.1 Ultra-efficient cap-exchange protocol with CdSe/ZnS core/shell QD

Chart 1: Chemical structures of the Thioctic acid (TA)-based ligands used in this study.

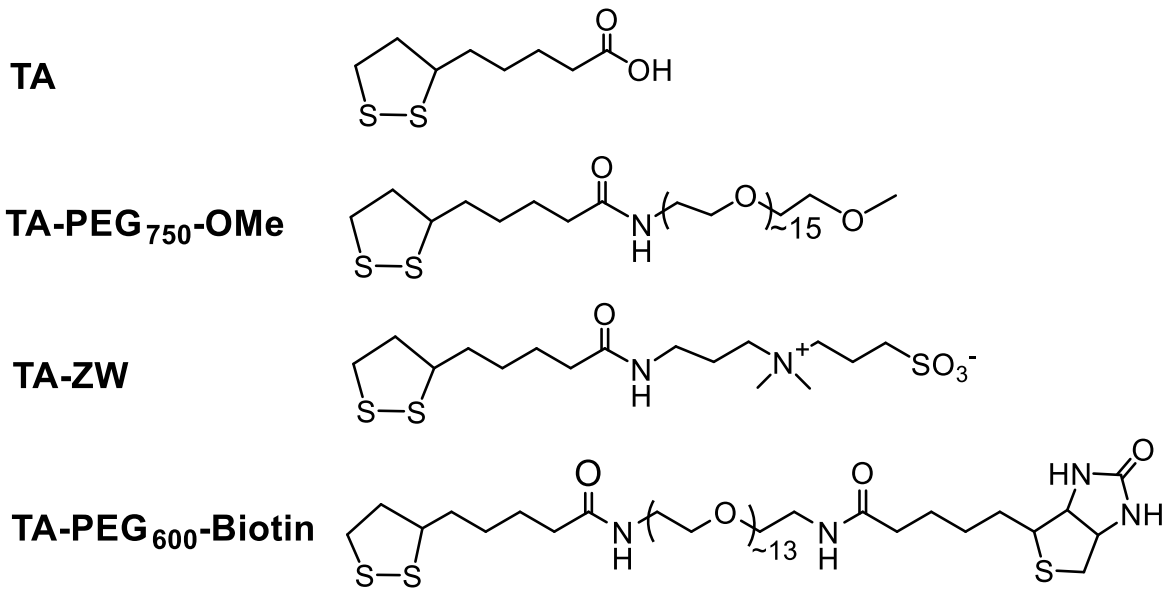

Our UCEP procedure is shown schematically in Figure 3-2(A). First, TA-based ligands with different terminal functional groups (*e.g.* PEG750, zwitterion, PEG600-biotin) were synthesized (see Chapter 2 for details).[34,36,41] Next, the TA-ligand (*e.g.* TA-ZW) was reduced quantitatively to its DHLA form by 1 mole equivalent of TCEP.HCl in a mixed solvent of ethanol/water (1:1 v/v). The reduction happened rapidly (*ca.* ~5 mins) and could be directly visualized by eye (*via* the disappearance

of yellow color that originates from the dithiolane ring), yielding a clear colorless solution. Then six DHLA-ligand molar equivalents of NaOH (in ethanol) was added to fully deprotonate the DHLA di-thiol groups to enhance their QD binding affinity.[43] Six molar equivalents of NaOH were used because each DHLA-based ligand contains two thiol groups and each TCEP.HCl molecule contains 4 acid groups. The *in situ* reduced ligand solution was then added directly into a QD solution (in $CHCl_3$), forming a homogenous solution. After brief shaking, the QDs were found to rapidly rise (< 1 min) to the top aqueous layer (note, the mixed $CHCl_3$/EtOH/H_2O solution itself did not phase separate in the absence of the QD and/or ligands), indicating the formation of hydrophilic QDs. It became clearer after adding more water followed by a brief centrifugation (60 s, 20000×g), where all QDs were found in the top aqueous layer, leaving the bottom $CHCl_3$ layer colorless (Figure 3-2(B)), indicating full QD water-solubilization. The aqueous layer was then transferred to a centrifugal filtration tube with a 30,000 MW cutoff membrane. After three rounds of centrifugation and washing with H_2O to remove unbound free ligands, a stable well-dispersed QD stock aqueous solution was obtained.

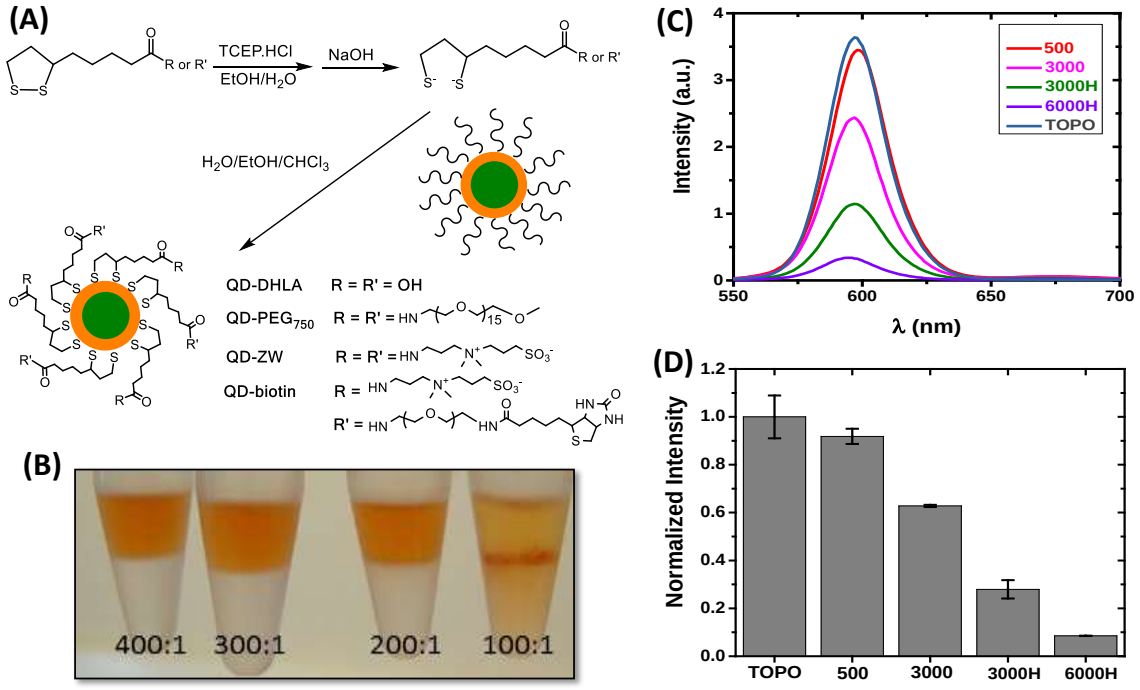

Figure 3-2: (**A**) Schematic procedures of our UCEP to compact, biocompatible DHLA-based ligand capped QDs. (**B**) Photograph of a CdSe/ZnS QD (λ_{EM} ~ 600 nm) after cap-exchange with DHLA-ZW under different ligand:QD molar ratio, top layer: water, bottom layer: $CHCl_3$. (**C**) Fluorescence spectra of a CdSe/ZnS QD prior to (10 nM in $CHCl_3$, TOPO) and after cap-exchange with DHLA-ZW (10 nM in H_2O) under different LQMRs without and with heating (LQMR is indicated for each sample; **H** stands for heating). (**D**) Comparison of the relative fluorescence intensity of the above QDs (data shown as mean ± standard deviation, n = 3).

First, we investigated how LQMR affected the cap-exchange process using the most widely used hydrophobic CdSe/ZnS QD capped with mixed trioctylphoshine/ trioctylphoshine oxide ligands (TOP/TOPO) (λ_{EM} ~600 nm, ~4.5 nm core diameter, Figure 3-3) and the DHLA-zwitterion (ZW) ligand (Chart 1).

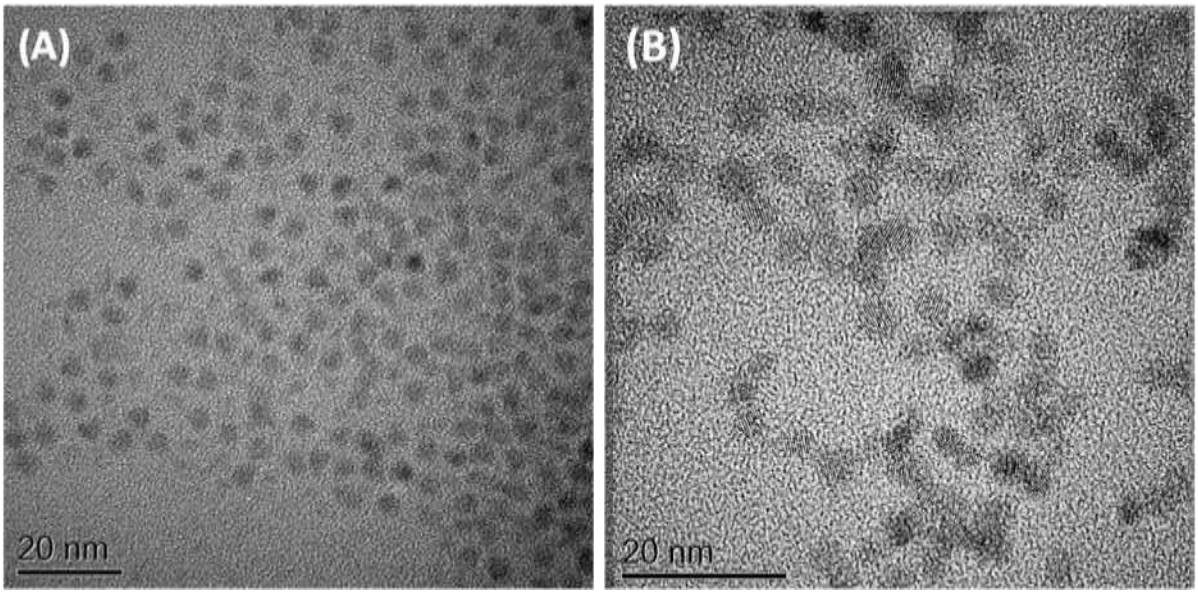

Figure 3-3: (**A**) TEM image of the TOP-TOPO capped CdSe/ZnS core/shell QD (λ_{EM} ~ 600 nm) used in this study prior to ligand exchange. It has an average crystal diameter of ~4.5 nm. (**B**) TEM image of the CdSe/ZnS core/shell QD after ligand exchange with the DHLA-ZW at a ligand: QD molar ratio of 500:1. It has an average crystal diameter of ~4.6 nm.

When cap-exchange was performed at a LQMR of ≥ 200, all of the CdSe/ZnS QDs were fully transferred to the aqueous phase (shown as a brownish colour in the top aqueous layer), leaving the bottom $CHCl_3$ layer colorless. In contrast, the $CHCl_3$ layer still contained some un-transferred QDs at a LQMR of 100, indicating that 200 is the minimum ratio required for complete QD water-solubilization (Figure 3-2(B)). This LQMR is ~2 orders of magnitude lower than most literature protocols (Table 3-1), demonstrating its ultra-efficiency.[32,34-36,40,41,43,45] Moreover, this LQMR number

actually matched well to our estimation that a maximum of 253 DHLA-ligands would be sufficient to cap all the Zn^{2+} sites on the QD surface. Deprotonation of the DHLA thiol groups was essential for a successful cap-exchange. The use of TCEP reduced DHLA-ZW ligand directly without thiol group deprotonation produced no observable QD phase transfer at LQMR = 200, all the QDs were found to remain in the organic phase. This result agrees well with the report that thiolates bind much more strongly to Zn^{2+} ions than free thiols.[43] The use of NaOH deprotonated TCEP only in the absence of DHLA-ZW ligand also produced no observable QD phase transfer, confirming that it was the DHLA-ZW ligand, but not TCEP, that was responsible for the rapid and efficient QD phase transfer observed here.

We subsequently investigated how fluorescence of the cap-exchanged CdSe/ZnS QD was affected by the LQMR. At a LQMR of 200, the cap-exchanged QD effectively retained the native fluorescence of the parent hydrophobic QD in $CHCl_3$ (~96%, Figure 3-5). This relative fluorescence intensity retained was reduced to ~92% at 500 and further to ~63% at 3000 (Figure 3-2(C)). The observation that the higher the LQMR the lower the retained QD fluorescence agreed well with our hypothesis, suggesting that excess free ligands were indeed responsible for the quenched fluorescence of cap-exchanged QD. Besides, heating was also found to impact the retained QD fluorescence. For example, at a LQMR of 3000, heating at ~70 ^{o}C for 1h produced a water-soluble QD displaying half the intensity of its non-heating counterpart (Figure 3-2(D)). Further increasing the LQMR to 6000 with 1 h heating yielded an even more severely quenched QD, retaining just ~10% of the original fluorescence. These results indicated that heating could accelerate the ZnS shell etching by free DHLA-ZW ligands. This effect was exacerbated under high LQMRs

with large excesses of free ligands, leading to efficient etching of the ZnS shell and hence severe quenching of the QD fluorescence.

Table 3-1: A comparison of cap-exchange conditions and retained fluorescence for some DHLA-based ligand capped QDs. hν: photo-irradiation; DHLA-F: DHLA modified with functional group.

LQMR (in 10^3)	Time	QD type	Ligand	Retained original QD fluorescence (%)	Ref
~42	~2h	CdSe/$Zn_xCd_{1-x}S$	DHLA-PEG-NH_2	46-62	[35]
~40	2.5h	CdSe/CdS	DHLA-PEG	~8	[45]
~40	2.5h	CdSe/CdS/ZnS	DHLA-PEG	~26	[45]
~41	2h	CdSe/ZnS	DHLA-Zn^{2+}	28-57	[43]
~10	~2h	CdSe/ZnS	DHLA	3.4-53*	[46]
~40	60 min (hν)	CdSe/ZnS	Bis(LA)-ZW	50-70	[40]
~22-50	~20 min (hν)	CdSe/ZnS	LA-PEG/NH_2/F	50-70	[39]
40-60	~30 min (hν)	CdSe/ZnS	LA-PEG/F	50-70	[37]
10-100	2h	InP/ZnS	DHLA	11	[47]
98	~over night	CdSe/ZnS	DHLA-F	40-57%	[48]
0.2-0.5	~1 min	CdSe/ZnS	DHLA-PEG/ZW	95	This work
0.6	~1 min	CdSe/ZnSe/ZnS	DHLA-ZW	96	This work

* The retained QD fluorescence varied significantly for different colored QDs.

Importantly, the DHLA-ZW capped CdSe/ZnS QD prepared here (abbreviated as QD-ZW) was highly stable in phosphate buffer saline (PBS, 10 mM phosphate, 150 mM NaCl, pH 7.4) and over a broad pH range (*e.g.* 6-10) and even with high salt conditions (*e.g.* 2 M NaCl, Figure 3-4). This figure confirmed that the QD-DHLA-ZW prepared at LQMR of 200:1 is stable for at least 4 weeks in PBS over pH 4-10 and even under high salt conditions of 2 M (NaCl). Such stability is comparable to the QD-DHLA-ZW prepared by photoligation and other literature methods. The stability of the QD-ZW prepared at a LQMR of 200 is comparable to those reported in literature, despite being prepared using 50-500 fold less ligands.[39,41] This result agreed well with our estimation that ~200 DHLA-ZW ligands were sufficient to saturate all of the QD surface Zn^{2+} ions, producing stable biocompatible QDs. Performing cap-exchange in homogenous solution ($CHCl_3$/EtOH/H_2O) also greatly accelerated the process: complete transfer of the QD into the aqueous phase was observed in < 1 min, which was much faster (*ca.* 20-500 fold) than most literature methods using two immiscible phases (Table 3-1). The greatly improved cap-exchange efficiency was attributed to the greatly enhanced QD-ligand exchange and transfer rates in homogeneous solution as well as greatly enhanced affinity between the QD and DHLA-ZW ligands after thiol deprotonation.

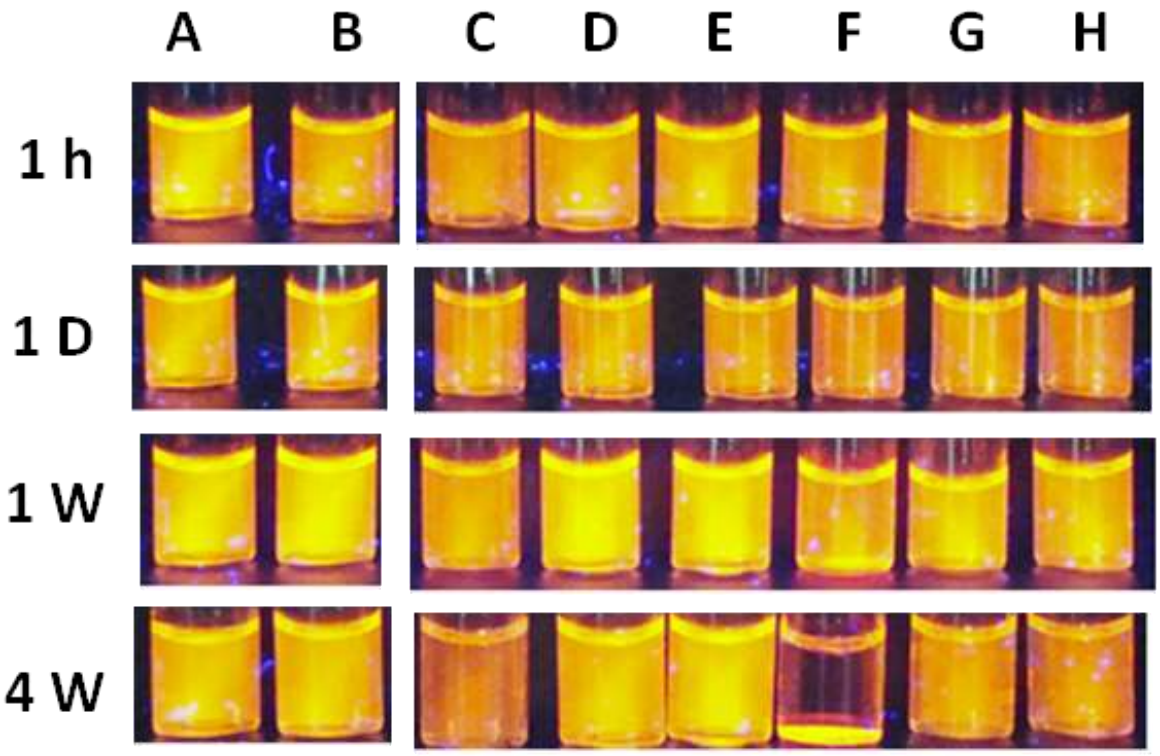

Figure 3-4: Photographs of the 100 nM CdSe/ZnS core/shell QD-DHLA-ZW (maximum λ_{EM} = ~606 nm) upon exposure to a UV lamp (λ = 350 nm) prepared by the UCEP at a Ligand:QD molar ratio (LQMR) of 200 at different post-preparation intervals (1 h, 1 day, 1 week and 4 weeks from top to bottom panels). The solution conditions are H_2O (**A**), PBS (pH 7.4, **B**), PBS with pH adjusted to 4 (**C**), 7 (**D**), 10 (**E**), 13 (**F**), and with NaCl concentration of 1M (**G**) and 2M (**H**), respectively.

Besides DHLA-ZW, the UCEP can be readily applied to other DHLA based ligands such as DHLA and DHLA-PEG750, where a LQMR of 200 was also found to be sufficient to water-solubilize the CdSe/ZnS QD completely (Figure 3-5).

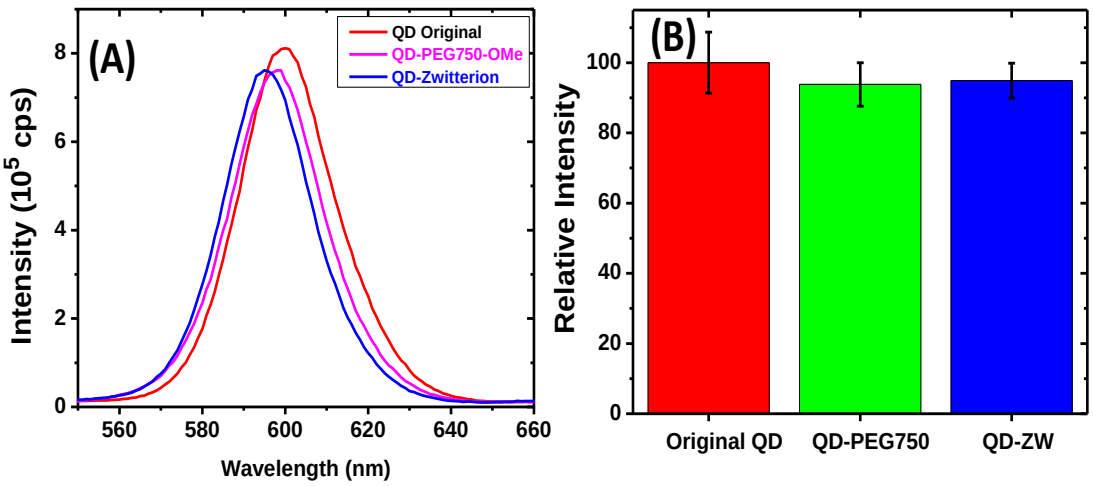

Figure 3-5: **(A)** Fluorescence spectra of the CdSe/ZnS core/shell QD before (red) and after ligand exchange with DHLA-ZW (blue) and DHLA-PEG750 (pink) at a LQ-MR of 200:1 (**B**) Comparison of the relative fluorescence intensity for the above QDs.

Moreover, all cap-exchanged QDs retained > 95% of their original fluorescence. This is attributed to the ultra-efficient and gentle cap-exchange conditions (short exposure to homogenous solution at room temperature) with minimal free ligands that can etch the ZnS protective shell. As a result, the ZnS shell may be effectively intact after cap-exchange, allowing the QD to retain native fluorescence. Such a gentle yet robust approach is particularly well-suited for core/shell QDs with relatively thin ZnS shells (which is the case for most commercial CdSe/ZnS QDs) whose fluorescence is known to be highly sensitive to environmental conditions (*e.g.* oxidation, precipitation *etc*.) and can be especially badly affected after cap-exchange with strongly

coordination ligands.[30,49] A further dynamic light scattering analysis[44] of the CdSe/ZnS QD after cap-exchange with the DHLA-ZW under different LQMRs revealed that compact (*ca.* D_h < 9 nm) water-soluble QDs with uniform narrow size distribution were obtained at LQMR of ≥500. Those prepared under lower LQMRs showed some minor aggregation or clustering (Figure 3-6, Table 3-2). The different QD sizes were further verified by a gel electrophoresis analysis:[44] the QD prepared at 200 LQMR apparently showed evidences of aggregation and exhibited lower gel mobility (larger sizes) than those prepared at 500 or 1000, while the latter two QDs displayed identical gel mobility (Figure 3-6). Thus the gel mobility results were fully consistent and in perfect agreement with those expected from their different R_{hs} measured by DLS. Together, these results indicate that not all of the added DHLA-ligands may have bound to the QD or the dithiolates in each DHLA may simply chelate to one Zn^{2+} ion rather than bind to two separate Zn^{2+} ions on the QD surface. Therefore a DHLA-ligand: QD surface Zn^{2+} molar ratio of ~1:1 (rather than the original estimate of 1:2) is required to produce compact, aggregation-free QDs suitable for practical biomedical applications.

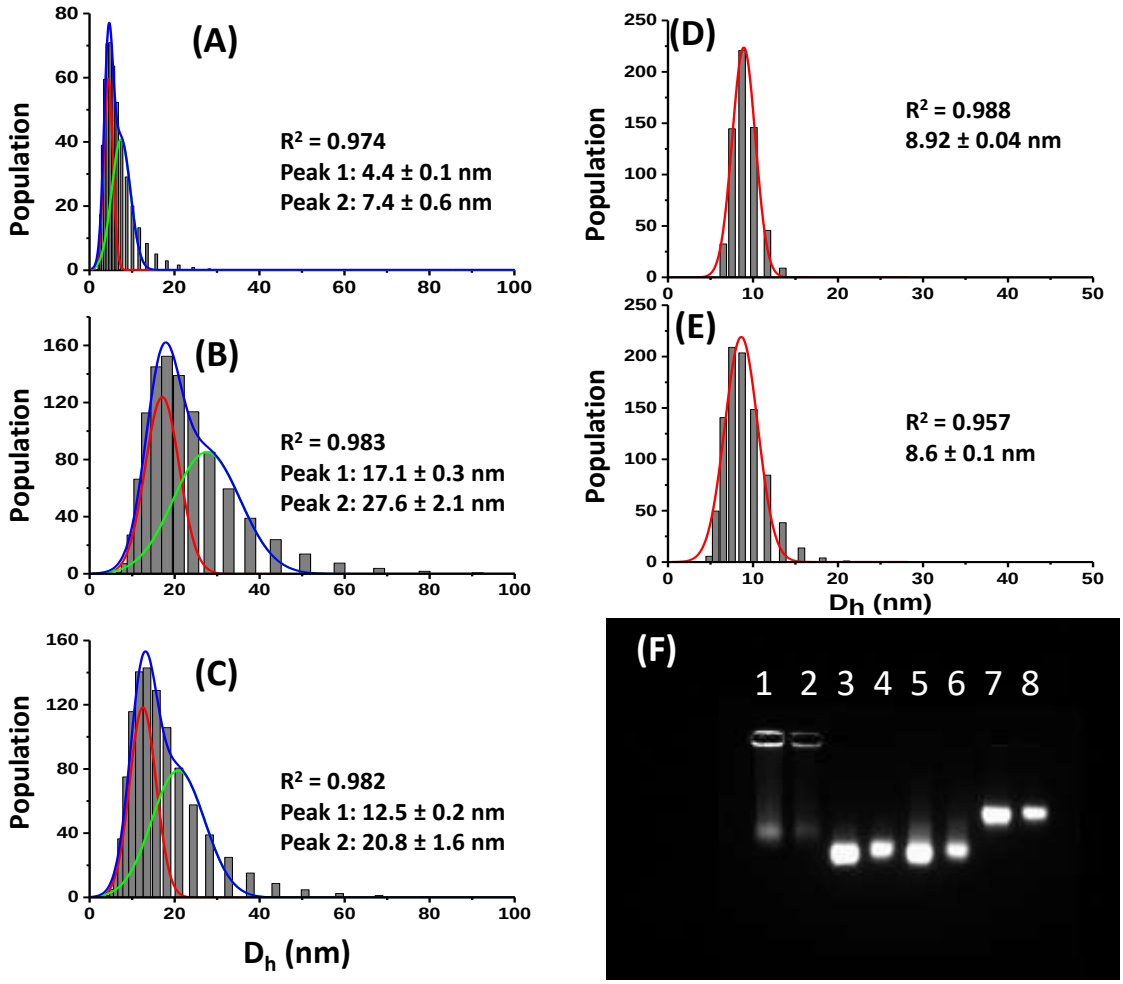

Figure 3-6: Hydrodynamic diameter (volume, $D_h = 2R_h$) distribution histograms of a CdSe/ZnS core/shell QD (λ_{EM} ~ 600 nm) before (**A**, in hexane) and after cap-exchange with DHLA-ZW under different LQMRs: 200 (**B**); 300 (**C**); 500 (**D**); 1000 (**E**). Data were fitted by the Gaussian function: (**A-C)** appeared to contain two different sizes while **D** and **E** contained just one species. (**F**) A typical gel electrophoresis diagram of this QD after cap-exchange with DHLA-ZW at a LQMR of 200 (lane 1 and 2); 500 (lane 3 and 4), 1000 (lane 5 and 6) and 500 after assembly with a His_8-tagged Affimer at a protein:QD molar ratio of 10:1 (lane 7 and 8). The sample volumes were for 5 μL for lane 1, 3, 5 and 7 and 2 μL for lane 2, 4, 6 and 8.The histograms were fitted by double Gaussian (normal) distribution.

Table 3-2. Hydrodynamic diameters (volume, D_h) of the CdSe/ZnS QD before and after cap-exchange with DHLA-ZW under different LQMRs. The polydispersity index, PDI, is obtained by PDI = FWHM/D_h.

QD samples	Average D_h (nm)	D_h (nm, %)	FWHM (nm)	PDI
QD-TOPO	6.2	4.4±0.1 (41%)	2.1±0.3	0.48
		7.4±0.6 (59%)	4.4±0.8	0.59
QD-ZW (200)	23.2	17.1±0.3 (42%)	8.0±0.9	0.47
		27.5±2.1 (58%)	15.9±2.8	0.58
QD-ZW (300)	17.2	12.5±0.2 (43%)	6.2±0.6	0.50
		20.8±1.6 (57%)	12.5±2.2	0.60
QD-ZW (500)	8.9	8.9±0.1 (100%)	2.7±0.1	0.30
QD-ZW (1000)	8.6	8.6±0.1 (100%)	3.87±0.2	0.45

The original QD and the cap-exchanged QDs at low LQMRs (<500) appear to have bimodal size distributions (*e.g*. containing two species). In this case, the average D_h was calculated by: $D_h = D_h1 \times A1\% + D_h2 \times A2\%$.

Where D_h1 and D_h2 are the D_h values, and A1% and A2% are the percentage areas (abundance %) of the two species obtained from the bimodal Gaussian fit. The resulting data are summarised in Table 3-2.

Assuming 8.6 nm corresponds to the D_h of an isolated individual QD-ZW particle, then its hydrodynamic volume:

$V_h = (4/3)\ \pi\ (D_h/2)^3 = (4/3)\ \pi\ (8.6/2)^3 = 333\ nm^3$.

Using the D_h values obtained from the Gaussian fits given in Table 3-2, the average particle hydrodynamic volume V_h for the QD cap-exchanged with the DHLA-ZW ligand at a LQMR of 200 and 300 is calculated as:

V_h (200) = (4/3) π $(23.2/2)^3$ = 6535 nm^3.

V_h (300) = (4/3) π $(17.2/2)^3$ = 2663 nm^3.

Therefore the V_h (200) and V_h (300) values are ~20 and ~8 times that of an isolated QD-ZW particle, respectively, suggesting that the QD forms small clusters or assemblies each containing a few to ~20 QDs after cap-exchange with the DHLA-ZW ligands under these low LQMRs of <500.

3.3.2 Ultra-efficient cap-exchange protocol with CdSe/CdS/ZnS QD

Besides the CdSe/ZnS core/shell QD, the UCEP was readily extended to different colored CdSe/CdS/ZnS core/shell/shell QDs with λ_{EM}s = 525, 575 and 606 nm, respectively. These QDs have more robust fluorescence because their fluorescent cores were protected by two layers of inorganic shells. Cap-exchange carried out at a LQMR of 200 with the DHLA-ZW ligand was be able to completely water-solubilize all these three different colored CdSe/CdS/ZnS QDs. Moreover, all three water-soluble CdSe/CdS/ZnS QDs also retained >95% of their respective original fluorescence (Figure 3-7), demonstrating the excellent robustness of the UCEP approach. It was noticed that although a LQMR of 200 was able to water-solubilize the CdSe/CdS/ZnS QDs, their long term stability was limited, and the QDs eventually precipitated from the aqueous solution in a week. Increasing the LQMR to 600 produced highly stable, biocompatible QDs that remained visibly clear without any noticeable changes of physical appearance or fluorescence for several months. This is likely due to the larger sizes of the CdSe/CdS/ZnS (*e.g.* λ_{EM} = 606 nm) over the

CdSe/ZnS QD (Figure 3-7 and 3-8), and hence more ligands are required to cap all its surface Zn^{2+} ions to ensure high stability.

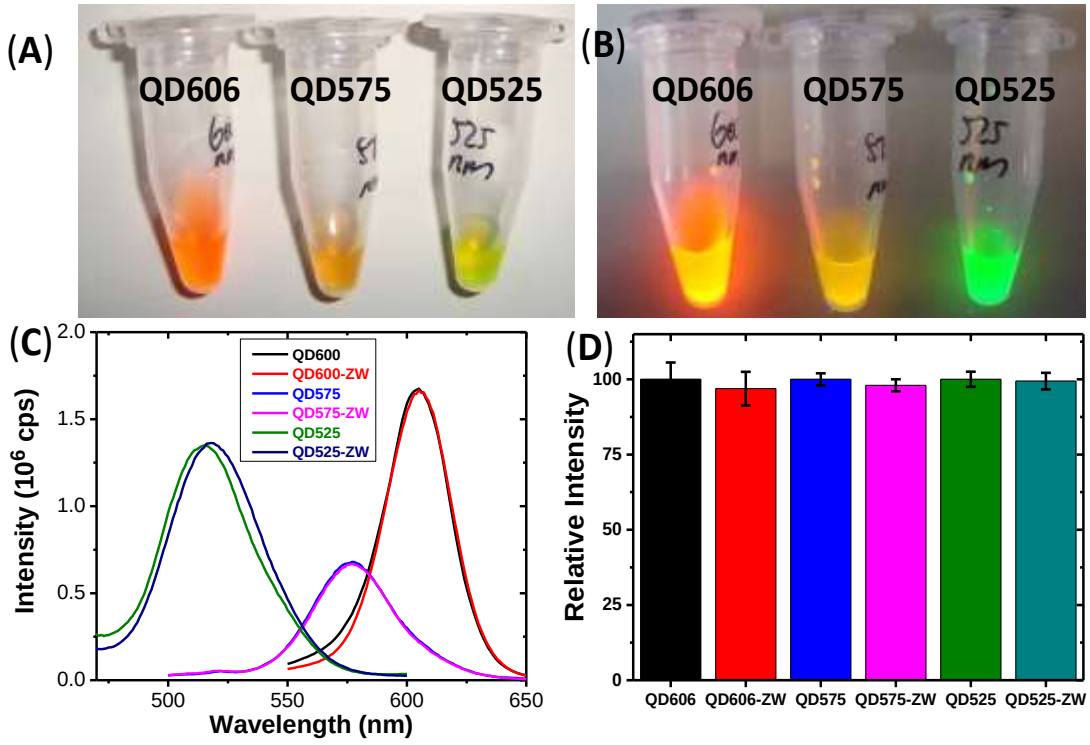

Figure 3-7: (**A, B**) Photographs of aqueous solutions of three different coloured CdSe/CdS/ZnS core/shell/shell QDs with λ_{EMs} of 606, 575 and 525 nm respectively after cap-exchange with DHLA-ZW at a LQMR of 200 under day light (**A**) and a hand-held UV-lamp (365 nm, **B**) illuminations. (**C**) Fluorescence spectra of the three QDs (10 nM) before (in $CHCl_3$) and after cap-exchange with DHLA-ZW (in H_2O) at a LQMR of 200. The intensity of the 606 nm emitting QD was reduced by 3 fold in order to display in the same graph. (**D**) Comparison of the normalised fluorescence intensity for each QD before and after cap-exchange with DHLA-ZW (the QD intensity in $CHCl_3$ prior to cap-exchange was set to 100).

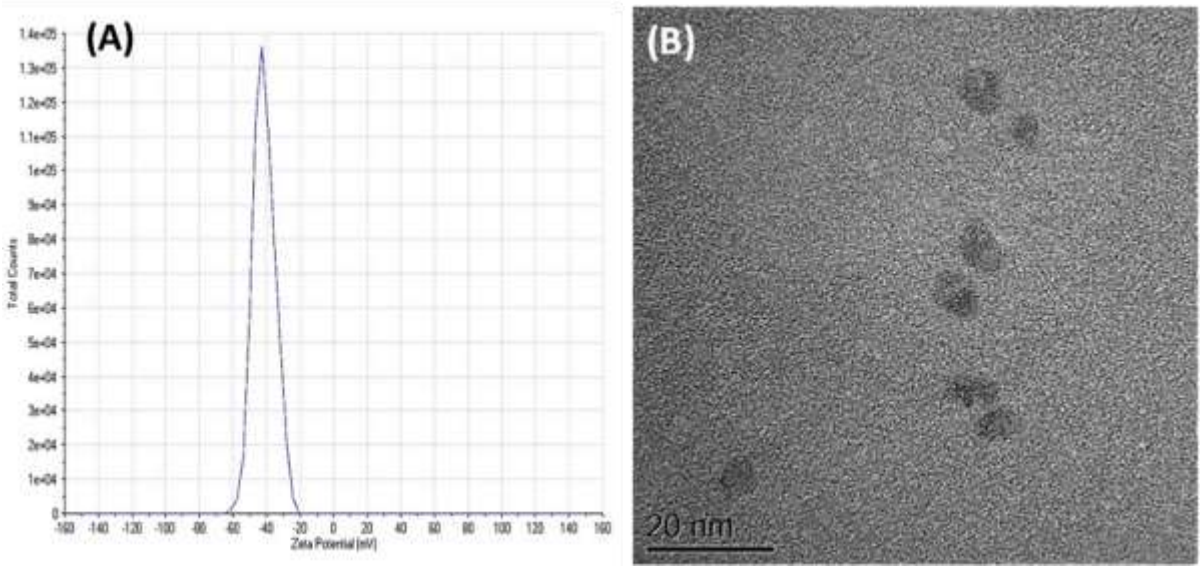

Figure 3-8: (**A**) Zeta potential test of the CdSe/CdS/ZnS core/shell/shell QD after ligand exchange with the DHLA-ZW at a ligand: QD molar ratio of 600:1. The Zeta potential value is -41.4 mV. (**B**) TEM image of the CdSe/CdS/ZnS core/shell/shell QD after ligand exchange with the DHLA-ZW at a ligand: QD molar ratio of 600:1. This QD appears somewhat eclipse, with long and short axis of ~8.2 and ~6.0 nm respectively.

Despite the increase of LQMR, this ratio is still 20-150 folds lower than most other methods reported in literature (Table 3-1). More importantly, all these water-soluble QDs prepared by the UCEP retained >95% of their respective original fluorescence. In contrast, most literature methods often reported *ca.* >50% fluorescence reduction even for such photo-chemically robust CdSe/CdS/ZnS or CdSe/Zn*x*Cd1-*x*S alloyed shell QDs after cap-exchange with DHLA-based ligands (Table 3-1). This is presumably because the large excesses of metal-free DHLA-ligands existing in these literature methods (due to high LQMRs) effectively etched the protective shells

during the relatively long cap-exchange process, significantly compromising the shell quality and hence fluorescence of post-exchange QDs.

3.3.3 QD-Affimer for ratiometric biosensing

The excellent fluorescence, compact structure and robust stability in biologically relevant buffer of the UCEP prepared QDs make them extremely attractive for FRET-based applications. This is because a compact QD structure gives a small *r* value while the high QD fluorescence yields a large R_0 value, both factors are strongly beneficial to improve *E* and hence FRET based sensitivity as $E = 1/[1 + (r/R_0)^6]$. Since *r* is not only determined by the QD but also the associated bio-recognition molecule (binder) size, the use of small binders is also critical to improve FRET sensitivity. Here, small antibody mimetic proteins (also known as Affimers, first reported as Adhirons)[47] were employed as binders for target proteins. Compared to the widely used antibodies, Affimers have the advantages of high thermal stability (typically T_m ≥80 ^oC), excellent binding affinity (nM-pM) and specificity, animal-free production (*via* bacterial expression) and ease of incorporating site-specific functional tags (*e.g.* His_8, cysteine) for controlled bioconjugation with maximal binding site accessibility.[50-52] More importantly, their small sizes (MW ~12 kDa, <10% that of a whole antibody) is especially attractive for FRET based applications, allowing for significantly reduced *r* value and thereby improving sensitivity. To demonstrate this potential, an Affimer that specifically recognizes the yeast small ubiquitin-like modifier (SUMO) protein was employed as a proof of concept for detecting its target SUMO protein. The SUMO proteins play an important role in a number of cellular process which include nuclear-cytosolic transport, transcriptional

regulation, apoptosis, protein stability and response to stress, making them useful diagnostic markers for genotoxic stress, cancer development and proliferation.[50]

First, we studied the QD-Affimer conjugation *via* a convenient, highly efficient His_8-tag-metal affinity based self-assembly.[3] The C-terminal His_8-tagged Affimer was reacted with an Alexa-647-NHS ester dye, yielding an average labeling of 1.06 Alexa-647 dyes per Affimer (see experiment section above). The labeled Affimers were then mixed with a DHLA-ZW capped CdSe/CdS/ZnS QD (λ_{EM} ~606 nm) at different molar ratios (but with a constant total Affimer:QD molar ratio of 12 by adjusting the label/unlabel Affimers to minimize the possible change of QD fluorescence quantum yield upon protein conjugation).[3] The resulting fluorescence spectra (λ_{EM} = 450 nm, corresponding to the absorption minimum of the Alexa-647 dye to minimize dye direct excitation) revealed a progressively quenched QD fluorescence and simultaneously enhanced Alexa-647 FRET signal (at ~667 nm) with the increasing dye/QD ratio, consistent with the QD-sensitized Alex-647 dye FRET mechanism[3] (Figure 3-9 & 3-10). This result confirmed the successful QD-Affimer conjugation. The QD-Alexa-647 FRET pair has good spectral overlap with a relatively large R_0 value of ~6.4 nm (Figure 3-9). By using E obtained from QD fluorescence quenching ($E = 1 - I_{DA}/I_D$, where I_D and I_{DA} are the QD intensity in the absence and presence of the acceptor) and a single QD in FRET interaction with N identical acceptors model ($E = 1/[1 + r^6/N*R_0^6)]$,[25] the average QD-dye distance r was found to be ~6.5 nm (Figure 3-10), matching well to the sum of the Affimer size (~3 nm)[50] and radius of the CdSe/CdS/ZnS QD core ~3.5 nm (Figure 3-8), confirming the formation of compact QD-Affimer conjugate.

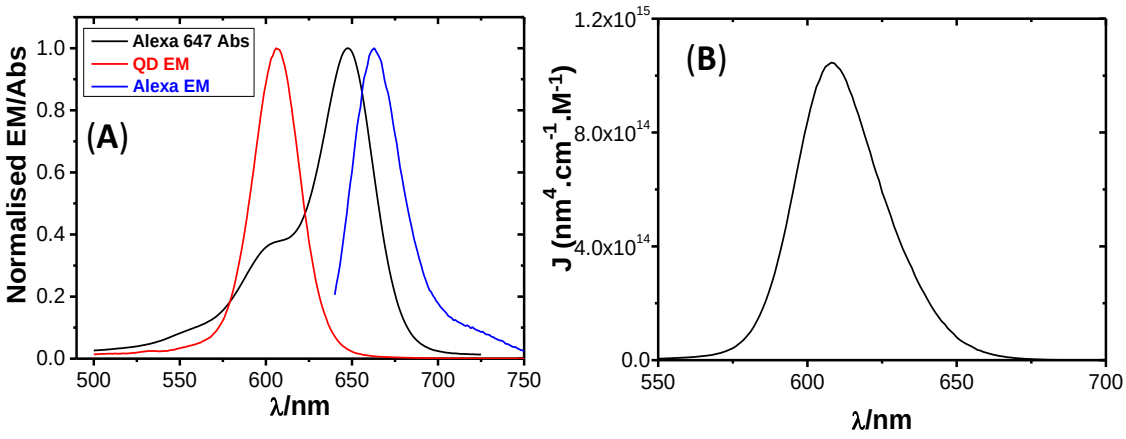

Figure 3-9: Photophysical properties of the QD donor and the Alexa 647 acceptor. **(A)** Normalized fluorescence emission spectrum of the QD_{606} (**red**), and the normalized absorption spectrum (**Black**) of the Alexa 647 labeled Adhiron. **(B)** Spectral overlap function of the Alexa 647 and QD_{600} FRET pair.

$$J_{(\lambda)} = \frac{\int PL_{D(\lambda)}\, \varepsilon_{A(\lambda)}\, \lambda^4\, d\lambda}{\int PL_{D(\lambda)} d\lambda}$$

Where $PL_{D(\lambda)}$ is the normalised QD fluorescence intensity at λ; $\varepsilon_{A(\lambda)}$ is the acceptor absorption coefficient at λ.

The integral of the spectral overlap: $I = 1.32 \times 10^{16}$ ($nm^4.cm^{-1}.M^{-1}$)

Assuming a media refractive index of 1.45, and random orientation of the dipoles of the FRET pair (where $K^2 = 2/3$). The quantum yield of the CdSe/ZnSe/ZnS core/shell/shell QD, Q_{QY}, was determined as ~40%, then the Förster radius ($R_{0,}$ in the unit of Å) of the above QD-dye FRET pair (at 1:1 molar ratio) can be calculated *via* the following equation:[56]

$R_0 = (8.79 \times 10^{-5}\ n_r^{-4} \times Q_{QY} \times K^2 \times I)^{1/6}$

$= (8.79 \times 10^{-5} \times 1.45^{-4} \times 0.40 \times (2/3) \times 1.32 \times 10^{16})^{1/6}$

$= 64$ Å

$= 6.4$ nm

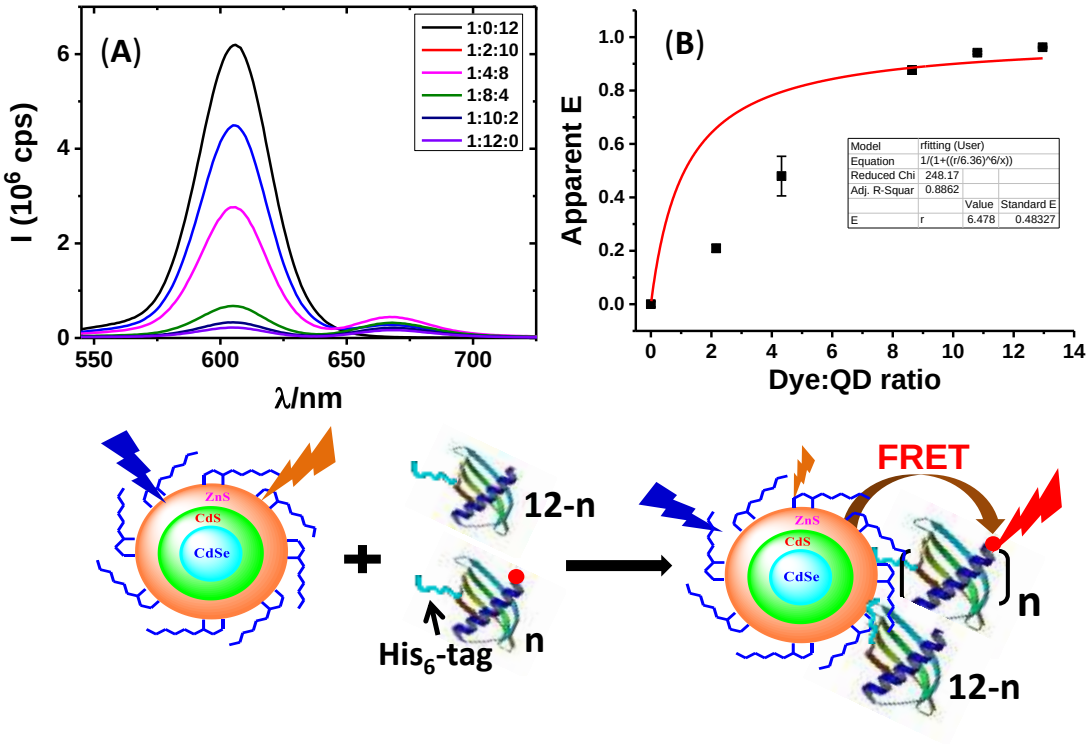

Figure 3-10: (**A**) Fluorescence spectra of a DHLA-ZW capped CdSe/CdS/ZnS core/shell/shell QD (λ_{EM} = 605 nm) after self-assembly with different molar ratios of Alexa-647 labelled Affimer (with total Affimer: QD molar ratio fixed at 12). (**B**) The apparent FRET efficiency *E* (obtained by QD fluorescence quenching) as a function of labelled Affimer: QD molar ratio. The scheme beneath showing the FRET process

Next we exploited their use in target protein detection. Here DHLA-ZW ligand capped CdSe/ZnSe/ZnS QD each conjugated with 12 copies of unlabeled anti-SUMO Affimer (His_8-tagged) was mixed with different amount of the target SUMO protein (Alexa-647 labeled).[50] The resulting fluorescence spectra (Figure 3-11) clearly showed that, with the increasing SUMO concentration, the QD fluorescence was greatly quenched while the Alexa 647 FRET signal was enhanced simultaneously. This result was fully consistent with a mechanism of QD-sensitized Alexa-647 FRET induced by the specific Affimer-SUMO binding. A plot of the integrated fluorescence intensity ratio between the Alexa-647 FRET (from 650-750 nm) and the QD (560-650 nm), I_{Dye}/I_{QD}, *versus* the SUMO concentration yielded a positive linear relationship over 0-500 pM (R^2 = 0.957), suggesting the QD-Affimer conjugate is suitable for ratiometric quantitation of pM levels target proteins. The positive linear increase of the I_{667}/I_{606} ratio with the increasing SUMO concentration matched exactly what was expected for the multiple acceptors FRET to a single QD donor model,[25,32] suggesting that all SUMO proteins were bound in the same orientation on the QD surface (with the same QD-dye distance).

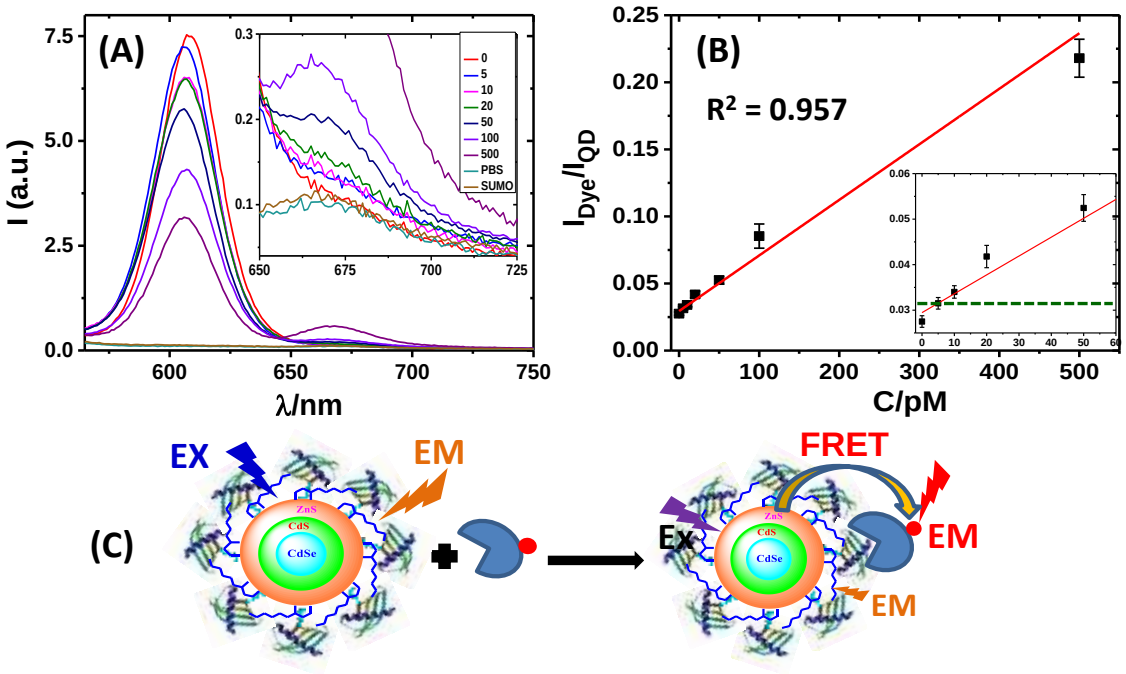

Figure 3-11: **(A)** Fluorescence spectra of the QD-Affimer (final C_{QD} = 0.50 nM) after incubation with different concentration of the target SUMO protein (Alexa-647 labeled) in PBS containing 1 mg/ml of bovine serum albumin. Inset shows the amplified FRET signals over 650-725 nm and the PBS and PBS+10 nM labeled SUMO protein backgrounds. (B) A plot of the integrated fluorescence intensity ratio (I_{Dye}/I_{QD}) between the dye (over 650-750 nm) and QD (over 560-650 nm) *versus* the SUMO protein concentration fitted to a linear function. Inset shows the response over 0-50 pM and green line indicates the limit of detection (background +3σ). (C) A schematic presentation of the QD-Affimer for detection of labeled target SUMO *via* QD-sensitized Alexa-647 FRET readout strategy.

A significant advantage of FRET-based sensing over others is ratiometric readout signal with internal self-calibration function and is therefore insensitive to instrumental noise and/or signal fluctuations, allowing for highly reliable, accurate quantitation.[21,24] Moreover, the signal of 10 pM SUMO protein was well-separated from the background (by >3 × standard deviation, 3σ, as indicated by a broken line in

Figure 3-11 B inset), suggesting this sensor is capable of detecting 5 pM target SUMO protein. Such sensitivity places it among the very best for QD-FRET sensors for direct protein detection (Table 3-3).

Table 3-3. Comparison of the sensing performance of some QD-FRET sensors for direct target detection using fluorescence spectroscopy without target amplification.

Sensing Mechanism	Target	LOD (nM) limit	Dynamic range (nM)	**Reference**
QD-FRET	Thrombin	10	10-1000	[57]
QD-MB FRET	Thrombin	1	1-500	[58]
ET quenching	Thrombin	10	10-210	[59]
QD-FRET	Mucin-1	250	250-2000	[60]
Electrochemical	Thrombin	~ 1	1-1000	[61]
Tb-complex QD FRET	PSA	0.05-0.27	0.05-21	[62]*
QD-FRET	SUMO protein	0.5	0.10-150	This work
QD-FRET	SUMO protein (labeled)	0.005	0.005-1	This work
QD-FRET	Neutravidin (labeled)	0.005	0.005-50	This work

***** The sensitivity (LOD) is dependent on the sizes of the antibody or antibody fragment used as target binder.

The reasons for the excellent sensitivity here are two folds: 1) our UCEP allows for the water-soluble QD to retain native high fluorescence (hence large R_0 value); 2) the small size of the Affimer binder (hence compact QD-Affimer conjugate) leads to short QD-dye distance *r*. Both factors are strongly beneficial for improving *E* and hence sensitivity. Importantly, the QD-Affimer sensor was highly robust; it gave an excellent positive linear detection of target SUMO protein in the presence of large excesses of

a non-target protein, bovine serum albumin (BSA, 1 mg/mL, see Figure 3-12). It also specifically detected the target SUMO protein even in 50% of human serum (Figure 3-13), demonstrating an excellent sensing robustness. It should be noted that, despite a number of different QD-FRET sensors being reported in literature, most sensing tests were carried out in "clean" buffers, few have demonstrated robust sensing in clinically relevant media, *e.g.* 50% human serum,[16,32] especially for QDs capped with small-molecule ligands. The fact that the QD-Affimer sensor can work robustly in 50% human serum demonstrates an excellent potential for possible clinical applications.

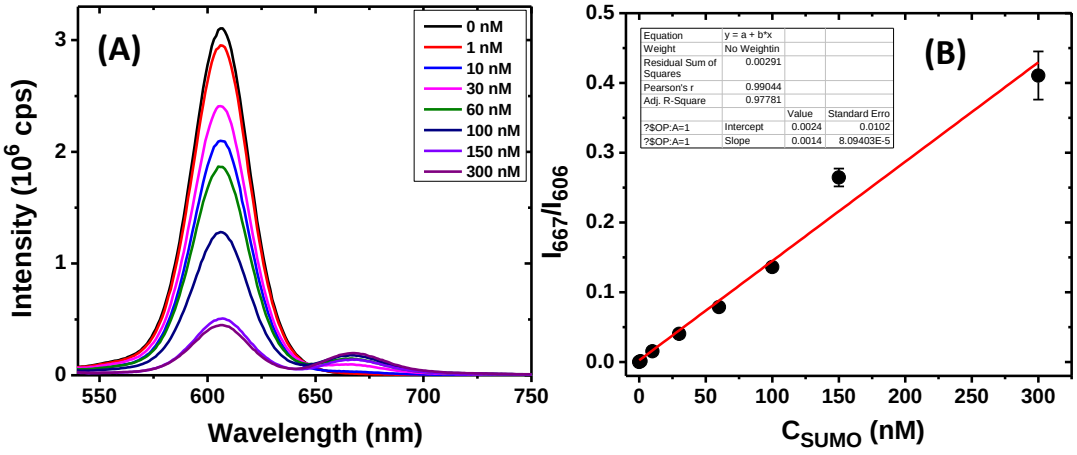

Figure 3-12: (**A**) Fluorescence spectra of the self-assembled QD-Affimer (unlabelled, specific for SUMO protein, 10 nM) conjugate after incubation with different amounts of Alexa 647 labelled SUMO protein target in the presence of 1 mg/mL bovine serum albumin. (**B**) A plot of the I_{667}/I_{606} as a function of SUMO protein concentration, data was fitted to a linear function: $y = 0.0024 + 0.0014x$, $R^2 = 0.9778$.

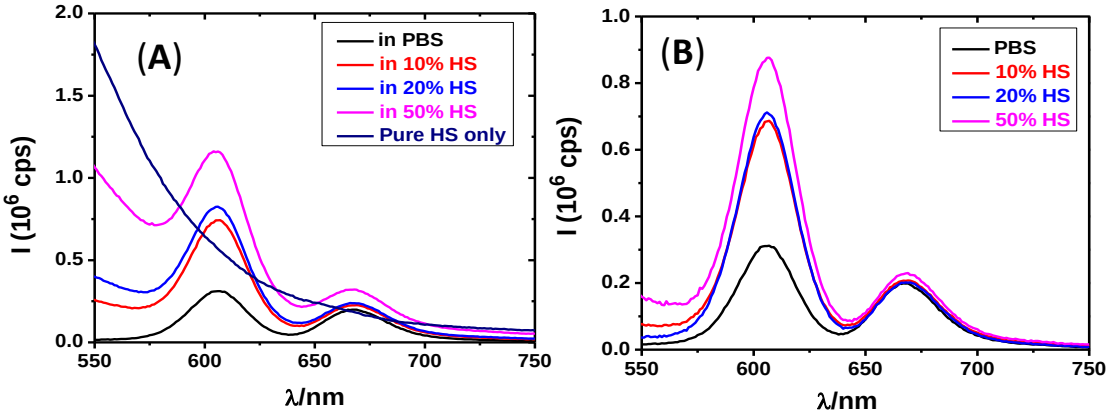

Figure 3-13: Fluorescence spectra of the self-assembled QD-Affimer (unlabelled, specific for SUMO protein, 10 nM) conjugate after incubation with Alexa 647 labelled SUMO protein targets (300 nM) under different conditions: (**A**) prior to and (**B**) after human serum background correction. The figure clearly shows that the self-assembled QD-Affimer sensor prepared here is highly robust; it can specifically detect its target protein even under complex conditions such as 50% human serum.

The ability of detecting unlabeled protein target is more useful for biodiagnostics because target labeling may not be feasible for naturally occurring proteins in biological samples. To investigate this potential, we first conjugated each CdSe/CdS/ZnS QD with 1 copy of the anti-SUMO Affimer (*via* His_8-tag self-assembly) and then blocked the QD with 20 copies of a control Affimer (His_8-tagged) that showing no binding affinity to the SUMO protein.[50] An Alexa-647 labeled SUMO protein was used as FRET reporter. The final assay concentration of the QD and labeled SUMO reporter was fixed at 0.5 nM each. Introducing the unlabeled SUMO protein would compete with the labeled SUMO protein reporter binding to the QD-Affimer conjugate, reducing the number of labeled proteins binding to the QD and resulting in the QD fluorescence recovery (Figure 3-14). A plot of the resulting I_{606}/I_{667}

versus the unlabeled SUMO concentration revealed a good positive linear relationship over 0-10 nM range (R^2 = 0.977) with 500 pM being clearly detectable (Figure 3-14). The label-free sensitivity is lower than that of label detection (*ca.* 5 pM), presumably because each QD is conjugated with only 1 copy of the Affimer binder *versus* 12 copies in labeled detection which may enhance the Affimer-SUMO binding affinity *via* multivalency effect. Moreover, not all target Affimers on the QD surface may have bound to the labelled protein reporters due to their natural binding-dissociation equilibrium, thus some of the introduced unlabeled SUMO proteins may simply bind to the unbound free Affimers on the QD surface without displacing the reporter proteins. Nevertheless, the label-free sensitivity reported herein is comparable or better than most other QD-FRET based protein sensors (Table 3-3).

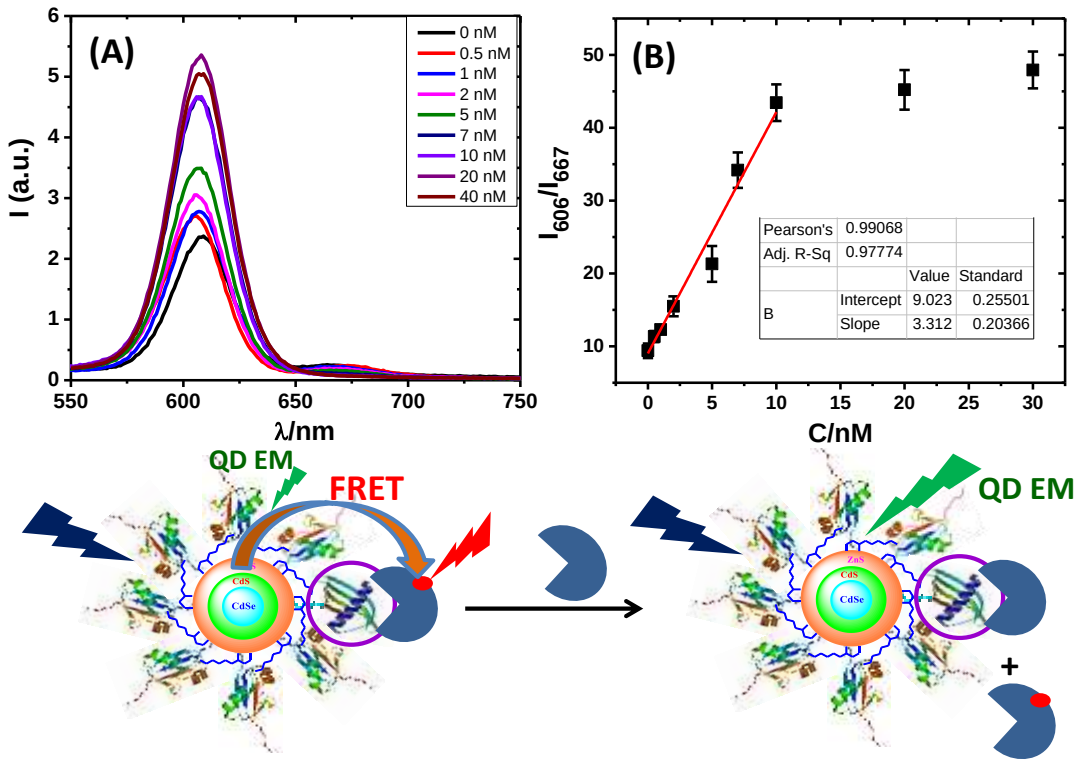

Figure 3-14: **(A)** Fluorescence spectra of the QD-Affimer conjugate (0.5 nM) mixed with Alexa-647 labeled SUMO protein reporter (0.5 nM) in the presence of different amounts of unlabeled SUMO protein. (**B**) A plot of I_{606}/I_{667} as a function of the unlabeled SUMO concentration: data over 0-10 nM were fitted by a linear function. The scheme below shows the assay principle (the protein circled being the anti-SUMO Affimer while all others are non-SUMO binding Affimers).

3.3.4 Preparation of QD-biotin for biosensing and cancer cell imaging

Besides making stable QDs using non-directly bioactive DHLA-ligands, biotin-functionalized QDs were readily prepared by in one step using mixed DHLA-PEG600-biotin/DHLA-ZW or DHLA-PEG750 ligands. Tuning the ratio of the DHLA-PEG600-biotin ligand to DHLA-ZW or DHLA-PEG750 spacer ligand ratio allowed for control of the QD surface biotin valency. The resulting CdSe/CdS/ZnS QD-biotin (each having ~100 DHLA-PEG600-biotins with the rest being DHLA-ZW ligands, denoted as QD-biotin$_{100}$) was employed for detection of neutravidin (NAV, each labelled with 1.7 Alexa-647 dyes) by exploiting the extremely strong bio-specific interaction between biotin and NeutrAvidin (NAV) (dissociation constant: K_d ~10^{-15} M). With the increasing amount of NAV being added to the QD-biotin$_{100}$ (0.5 nM QD), the QD fluorescence was progressively quenched while the Alexa-647 FRET signal was enhanced concurrently before reaching saturation at ~50 nM (Figure 3-15). This result conform the specific biotin-NAV binding brought the Alexa-647 label to the close proximity with the QD, producing efficient QD-sensitized Alex-647 FRET. This was validated by a control experiment where the QD capped with DHLA-ZW ligands only without DHLA-PEG600-biotin displayed no detectable FRET signal under identical conditions (Figure 3-16). A plot of the I_{667}/I_{607} ratio *versus* NAV concentration gave a good positive linear calibration over 0-50 nM range (R^2 = 0.982, Figure 3-15B). Moreover, 5pM NAV was clearly distinguished from the background, suggesting a detecting limit of 5 pM and confirming it is among the most sensitive QD-FRET protein sensors (Table 3-3). The signal saturation at ≥50 nM NAV suggests that all of the QD surface biotins have bound to NAV, matching well to the total biotin content expected for 0.5 nM QD-biotin$_{100}$.

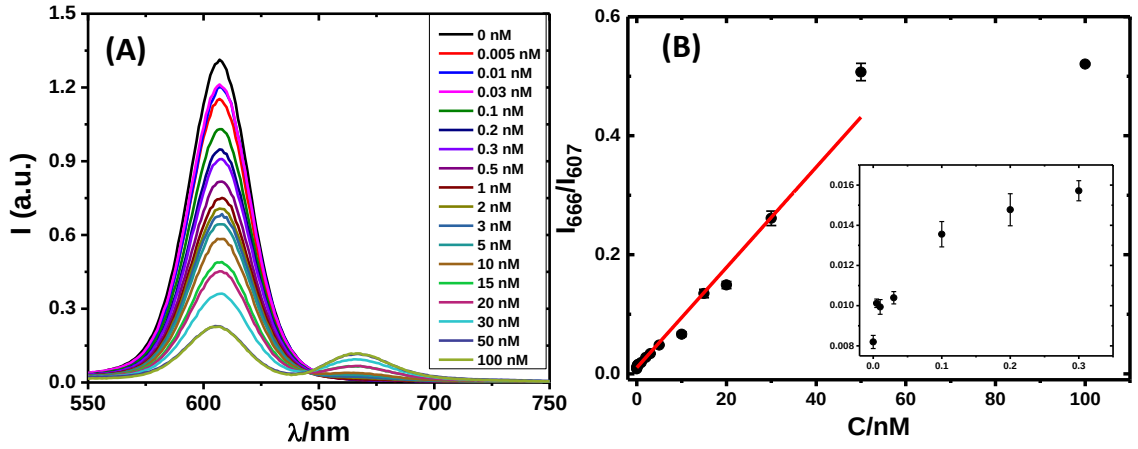

Figure 3-15: (**A**) Fluorescence spectra of QD-biotin$_{100}$ (0.5 nM) mixed with different amounts of Alexa-647 labeled neutravidin (NAV). (**B**) Relationship between the I_{667}/I_{607} ratio and NAV concentration. Data over 0-50 nM were fitted by the linear function: Y = 0.01037 + 0.0084X, R^2 = 0.982 (inset showing the data over 0-0.3 nM)

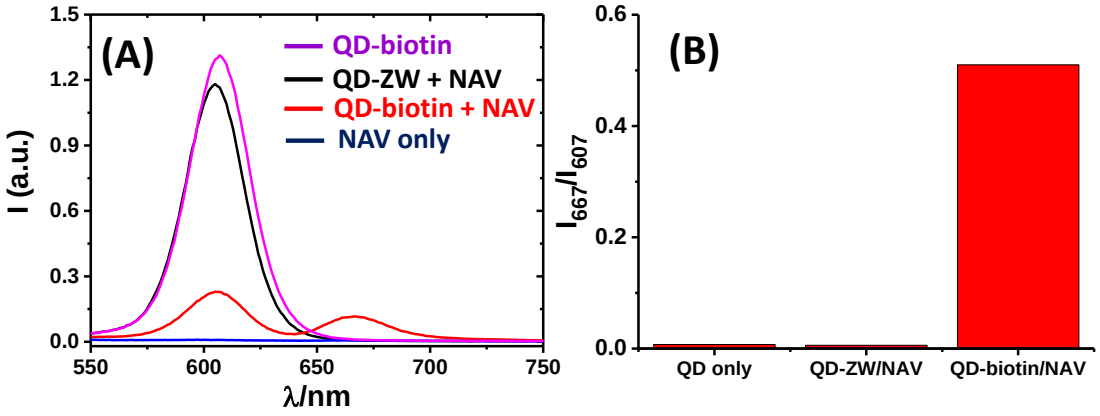

Figure 3-16: (**A**) Fluorescence spectra of 0.5 nM QD-biotin$_{100}$ (**purple**); 0.5 nM QD-ZW + 50 nM Alexa-647 labelled neutravidin (abbreviated as NAV, **black**); 0.5 nM QD-biotin$_{100}$ + 50 nM NAV (**red**) and 50 nM NAV only (**blue**). (**B**) Comparison of the I_{667}/I_{607} intensity ratio of the QD-Biotin$_{100}$ only (QD only), QD-ZW+NAV and QD-biotin+NAV obtained from the spectra shown in (**A**).

Using the labeled NAV as FRET reporter, the QD-biotin/NAV was further exploited for label-free detection of biotin. This was based on the fact that free biotin can effectively compete with the QD-biotin$_{100}$ for binding to NAV, reducing the amounts of NAV binding to the QD and hence the QD to Alexa-647 FRET efficiency. Indeed significant QD fluorescence recovery together with concurrently reduced Alex-647 FRET signal was observed with the increasing free biotin concentration. Moreover, 10 nM biotin was positively detected (Figure 3-17), suggesting the QD-biotin sensor can detect low nM level of unlabeled biotin, a small molecule target.

Besides a high affinity binding to NAV, biotin is an important vitamin (known as vitamin H) necessary for cell growth, the production of fatty acids, and the metabolism of fats and amino acids. A number of cancer cells over-express biotin receptors on their surfaces, making biotin an attractive ligand for cancer cell targeting.[51-53] Thus we further investigated the potential of using the QD-biotin in cancer cell imaging. Here two QD-biotin samples with valencies of ~70 and ~150 per QD respectively (the rest being the DHLA-PEG750 ligand) were prepared and incubated with the human cervical cancer (HeLa) cells which are known to over-express biotin receptors.[51,53] The resulting confocal fluorescence images revealed that cells incubated with the QD-biotin displayed the higher fluorescence than the DHLA-PEG750 capped control QD (red channel, Figure 3-18). This result showed that biotin modification on the QD enhanced the uptake by HeLa cells, presumably *via* biotin receptor mediate endocytosis. Interestingly, most intracellular QDs appeared to be located close to the cell nuclei (stained by Hoechst and displayed in blue) without enter the nuclei. A flow cytometry analysis further revealed that the strongest QD fluorescence was observed for cells incubated with the QD-biotin$_{150}$, followed by QD-biotin$_{70}$, and then the control QD (Figure 3-19). This result is fully

consistent with the confocal fluorescence imaging, demonstrating the good potential of the biotinylated QD in targeted cancer cell imaging.

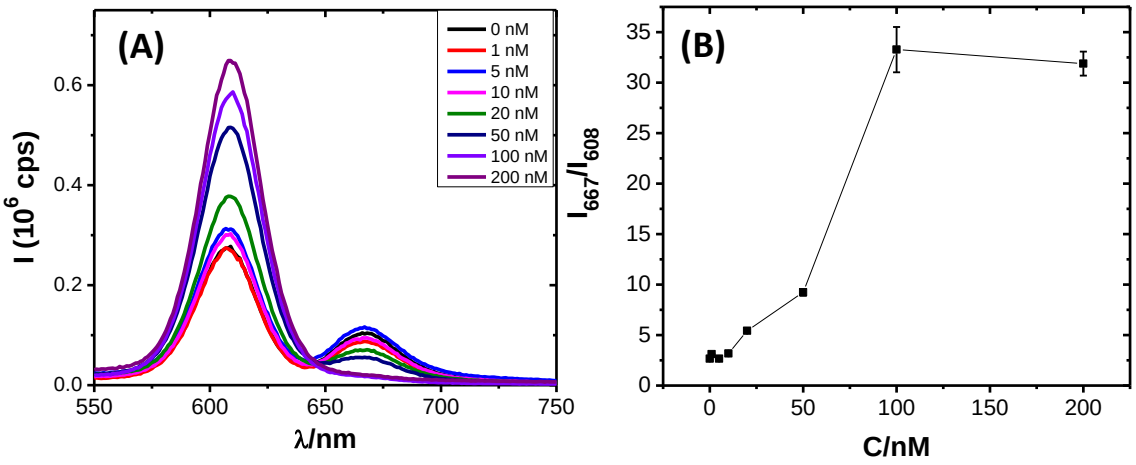

Figure 3-17: (**A**) Fluorescence spectra of QD-biotin100 (0.5 nM) + Alexa-647 labelled NAV (50 nM) in the presence of different concentrations of free biotin. (**B**) A plot of the corresponding I_{608}/I_{667} ratio *versus* free biotin concentration. The 10 nM free biotin produced a clearly distinguishable signal from the background, suggesting that the QD-biotin/NAV system is suitable for label-free detection of low nM level of free biotin.

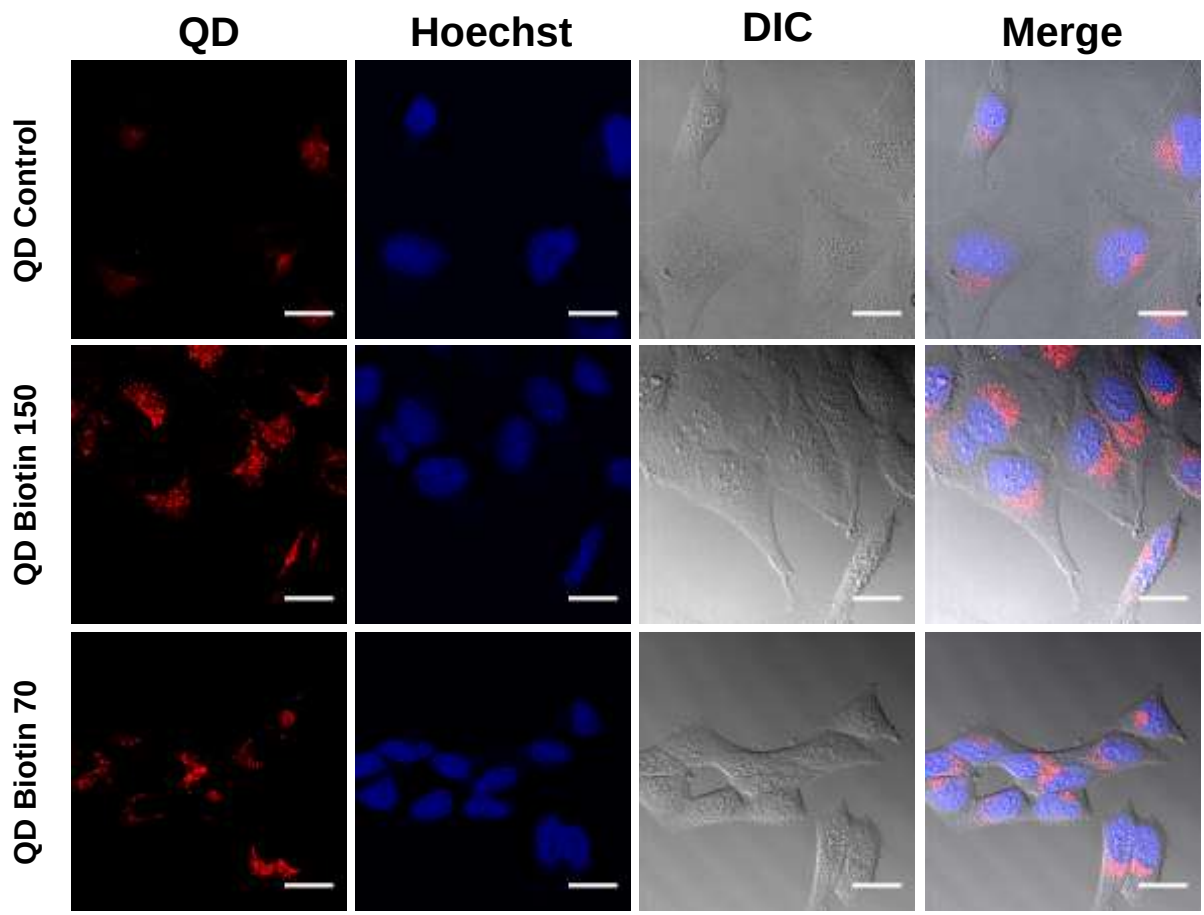

Figure 3-18: Confocal fluorescence images of HeLa cells after 4 h treatment with 50 nM of the DHLA-PEG750 ligand capped control QD (top panel) and two QD-biotin samples containing ~150 (middle panel) or ~70 (bottom panel) biotins per QD. From left to right, the images are displayed as QD fluorescence image (red), DAPI fluorescence (staining the nuclei, blue), optical image DIC and the merged fluorescence and optical images. (This work is done by Rongjun's group in imperial)

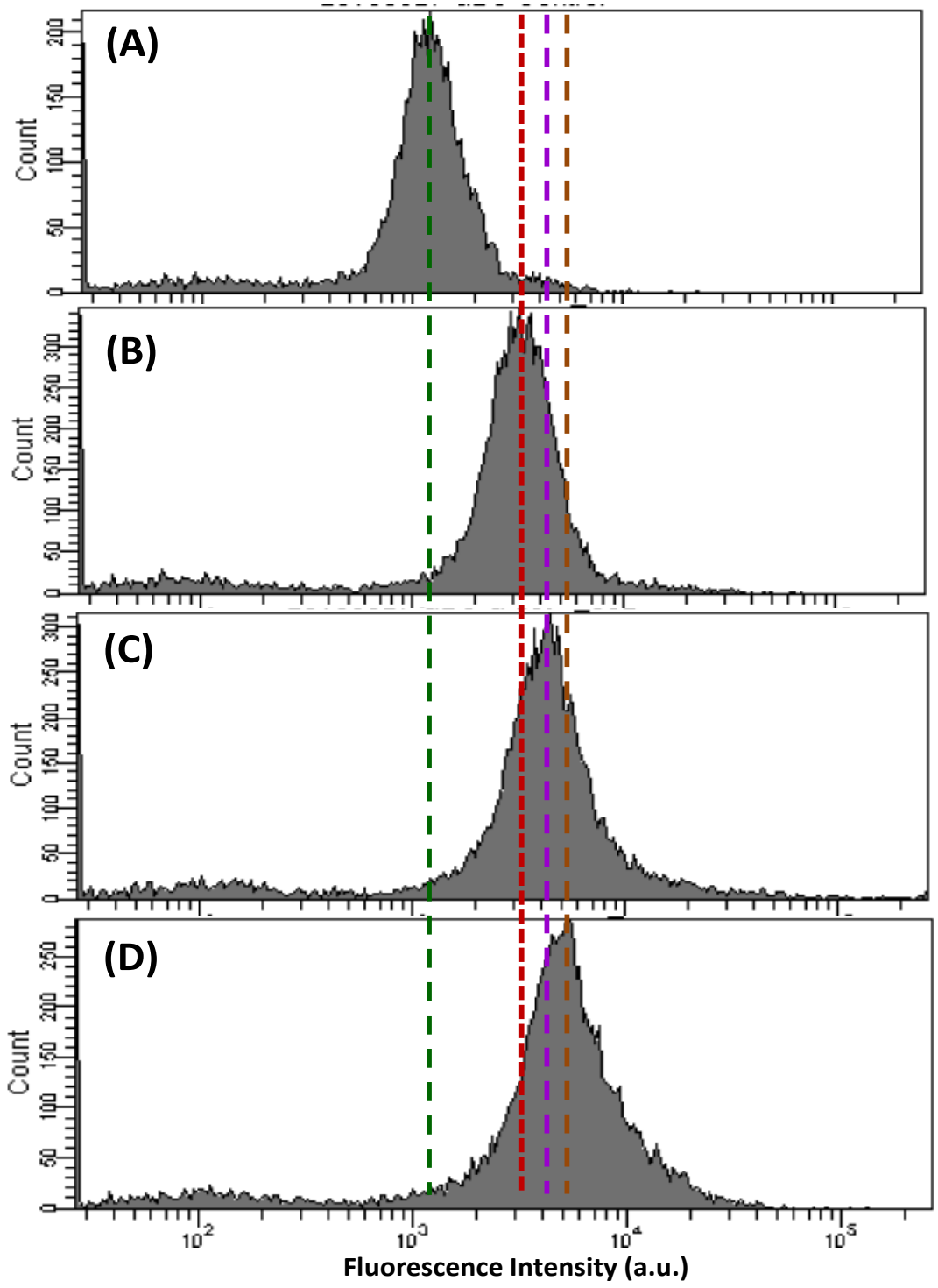

Figure 3-19: (**left**): Typical cell fluorescence distribution histograms of HeLa cells measured by flow cytometry after 4 h incubation with the DMEM medium only **(A)** and DMEM medium supplemented with 50 nM of the control QD **(B)**, QD-biotin$_{70}$ **(C)** or QD-biotin$_{150}$ **(D)**. The media cell fluorescence intensities (a.u.) were 1218, 3255,

4194, and 5071, for A, B, C and D respectively. A significant increase (by *ca*. 56%) of cell median fluorescence (marked by broken lines for each treatment) was observed for HeLa cells after treatment with the QD-biotin$_{150}$ over the control QD (capped with DHLA-PEG750 only, note the logarithmic scale of the intensity). This result was consistent with the higher fluorescence intensities observed from the confocal fluorescence image shown in Figure 3-18 (This work is done by Rongjun's group in imperial)

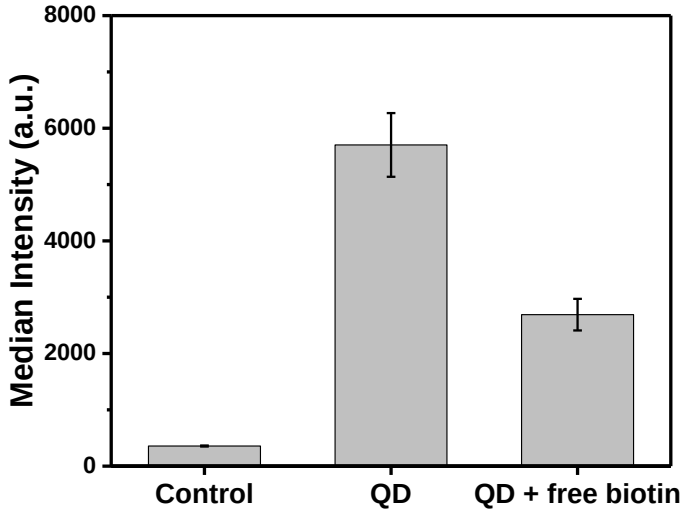

Figure 3-20: Comparison of the median fluorescence intensity of HeLa cells after incubation with the DMEM medium only **(Control)**; 1 h incubation with EMEM medium followed by 4 h incubation with EMEM medium contianing 50 nM of QD-Biotin$_{150}$ **(QD)**; and 1h incubation with DMEM medium suplemented with 10 mM free biotin followed by 4 h incubation with DMEM medium containing 50 nM of QD-Biotin150 and 10 mM free biotin **(QD + free biotin)**. A signficant decrease of ca. 53% of cell median fluorescnece intensity (from 5700±560 to 2690±280) was obtainted by the presence of free biotin.

3.4 Conclusion

In summary, an UCEP that allows for rapid, complete water-solubilization of the widely used hydrophobic CdSe/ZnS and CdSe/CdS/ZnS QDs using 50-1000 folds less amounts of the DHLA-based ligands over most literature methods has been developed. It readily produces compact, biocompatible QDs with excellent stability in biological buffers and effectively retaining the native parent QD fluorescence (>90%). The resulting QD is readily bioconjugated with His_8-tagged Affimers for robust, sensitive detection of 5 pM of a specific target protein and works robustly in clinical relevant media (50% human serum). The UCEP also allows for readily one-step preparation of biotinylated QDs for sensitive biosensing and cancer cell imaging. Compared to other QD cap-exchange methods reported in literature, the UCEP has four notable advantages: 1) using far fewer ligands (by 50-1000 fold) which is extremely valuable for precious, expensive or difficult to access ligands; 2) it is a rapid procedure; 3) it is easy to operate (using air-stable compounds and rapid *in situ* reduction at ambient condition); and 4) it shows no compromise of the post cap-exchange QD fluorescence. Therefore, we believe this UCEP will impact significantly in broad QD-based biomedical research field, including biosensing, bioimaging, drug delivery, clinical diagnostics and therapeutics, and most importantly in areas involving the use of QD-FRET based readout strategies.

3.5 REFERENCES

1 Bruchez, M.; Moronne, M.; Gin, P.; Weiss, S.; Alivisatos, A. P. *Science* **1998**, *281*, 2013.

2 Chan, W. C. W.; Nie, S. M. *Science* **1998**, *281*, 2016.

3 Medintz, I. L.; Clapp, A. R.; Mattoussi, H.; Goldman, E. R.; Fisher, B.; Mauro, J. M. *Nature Materials* **2003**, *2*, 630.

4 Michalet, X.; Pinaud, F. F.; Bentolila, L. A.; Tsay, J. M.; Doose, S.; Li, J. J.; Sundaresan, G.; Wu, A. M.; Gambhir, S. S.; Weiss, S. *Science* **2005**, *307*, 538.

5 Erathodiyil, N.; Ying, J. Y. *Accounts of Chemical Research* **2011**, *44*, 925.

6 Sapsford, K. E.; Algar, W. R.; Berti, L.; Gemmill, K. B.; Casey, B. J.; Oh, E.; Stewart, M. H.; Medintz, I. L. *Chemical Reviews* **2013**, *113*, 1904.

7 Wegner, K. D.; Hildebrandt, N. *Chemical Society Reviews* **2015**, *44*, 4792.

8 Dubertret, B.; Skourides, P.; Norris, D. J.; Noireaux, V.; Brivanlou, A. H.; Libchaber, A. *Science* **2002**, *298*, 1759.

9 Larson, D. R.; Zipfel, W. R.; Williams, R. M.; Clark, S. W.; Bruchez, M. P.; Wise, F. W.; Webb, W. W. *Science* **2003**, *300*, 1434.

10 Gao, X. H.; Cui, Y. Y.; Levenson, R. M.; Chung, L. W. K.; Nie, S. M. *Nature Biotechnology* **2004**, *22*, 969.

11 Medintz, I. L.; Konnert, J. H.; Clapp, A. R.; Stanish, I.; Twigg, M. E.; Mattoussi, H.; Mauro, J. M.; Deschamps, J. R. *Proceedings of the National Academy of Sciences of the United States of America* **2004**, *101*, 9612.

12 Goldman, E. R.; Medintz, I. L.; Whitley, J. L.; Hayhurst, A.; Clapp, A. R.; Uyeda, H. T.; Deschamps, J. R.; Lassman, M. E.; Mattoussi, H. *Journal of the American Chemical Society* **2005**, *127*, 6744.

13 Zhang, C. Y.; Yeh, H. C.; Kuroki, M. T.; Wang, T. H. *Nature Materials* **2005**, *4*, 826.

14 Giepmans, B. N. G.; Adams, S. R.; Ellisman, M. H.; Tsien, R. Y. *Science* **2006**, *312*, 217.

15 Biju, V. *Chemical Society Reviews* **2014**, *43*, 744.

16 Wegner, K. D.; Jin, Z.; Linden, S.; Jennings, T. L.; Hildebrandt, N. *Acs Nano* **2013**, *7*, 7411.

17 Samanta, A.; Zhou, Y.; Zou, S.; Yan, H.; Liu, Y. *Nano Letters* **2014**, *14*, 5052.

18 Zamaleeva, A. I.; Collot, M.; Bahembera, E.; Tisseyre, C.; Rostaing, P.; Yakovlev, A. V.; Oheim, M.; de Waard, M.; Mallet, J. M.; Feltz, A. *Nano Letters* **2014**, *14*, 2994.

19 Yu, W. W.; Chang, E.; Falkner, J. C.; Zhang, J.; Al-Somali, A. M.; Sayes, C. M.; Johns, J.; Drezek, R.; Colvin, V. L. *Journal of the American Chemical Society* **2007**, *129*, 2871.

20 Howarth, M.; Liu, W.; Puthenveetil, S.; Zheng, Y.; Marshall, L. F.; Schmidt, M. M.; Wittrup, K. D.; Bawendi, M. G.; Ting, A. Y. *Nature Methods* **2008**, *5*, 397.

21 Medintz, I. L.; Mattoussi, H. *Physical Chemistry Chemical Physics* **2009**, *11*, 17.

22 Mattoussi, H.; Palui, G.; Na, H. B. *Advanced Drug Delivery Reviews* **2012**, *64*, 138.

23 Algar, W. R.; Kim, H.; Medintz, I. L.; Hildebrandt, N. *Coordination Chemistry Reviews* **2014**, *263*, 65.

24 Zhou, D. *Biochemical Society Transactions* **2012**, *40*, 635.

25 Clapp, A. R.; Medintz, I. L.; Mauro, J. M.; Fisher, B. R.; Bawendi, M. G.; Mattoussi, H. *Journal of the American Chemical Society* **2004**, *126*, 301.

26 Chang, E.; Miller, J. S.; Sun, J. T.; Yu, W. W.; Colvin, V. L.; Drezek, R.; West, J. L. *Biochemical and Biophysical Research Communications* **2005**, *334*, 1317.

27 Zhou, D. J.; Piper, J. D.; Abell, C.; Klenerman, D.; Kang, D. J.; Ying, L. M. *Chemical Communications* **2005**, 4807.

28 Clapp, A. R.; Medintz, I. L.; Mattoussi, H. *ChemPhySchem* **2006**, *7*, 47.

29 Pons, T.; Medintz, I. L.; Wang, X.; English, D. S.; Mattoussi, H. *Journal of the American Chemical Society* **2006**, *128*, 15324.

30 Zhou, D.; Li, Y.; Hall, E. A. H.; Abell, C.; Klenerman, D. *Nanoscale* **2011**, *3*, 201.

31 Zhang, H.; Zhou, D. *Chemical Communications* **2012**, *48*, 5097.

32 Zhang, H.; Feng, G.; Guo, Y.; Zhou, D. *Nanoscale* **2013**, *5*, 10307.

33 Zhou, D.; Ying, L.; Hong, X.; Hall, E. A.; Abell, C.; Klenerman, D. *Langmuir* **2008**, *24*, 1659.

34 Susumu, K.; Uyeda, H. T.; Medintz, I. L.; Pons, T.; Delehanty, J. B.; Mattoussi, H. *Journal of the American Chemical Society* **2007**, *129*, 13987.

35 Liu, W.; Howarth, M.; Greytak, A. B.; Zheng, Y.; Nocera, D. G.; Ting, A. Y.; Bawendi, M. G. *Journal of the American Chemical Society* **2008**, *130*, 1274.

36 Susumu, K.; Mei, B. C.; Mattoussi, H. *Nature Protocols* **2009**, *4*, 424.

37 Zhan, N.; Palui, G.; Mattoussi, H. *Nature Protocols* **2015**, *10*, 859.

38 Aldeek, F.; Hawkins, D.; Palomo, V.; Safi, M.; Palui, G.; Dawson, P. E.; Alabugin, I.; Mattoussi, H. *Journal of the American Chemical Society* **2015**, *137*, 2704.

39 Palui, G.; Avellini, T.; Zhan, N. Q.; Pan, F.; Gray, D.; Alabugin, I.; Mattoussi, H. *Journal of the American Chemical Society* **2012**, *134*, 16370.

40 Zhan, N.; Palui, G.; Safi, M.; Ji, X.; Mattoussi, H. *Journal of the American Chemical Society* **2013**, *135*, 13786.

41 Zhan, N. Q.; Palui, G.; Grise, H.; Tang, H. L.; Alabugin, I.; Mattoussi, H. *Acs Applied Materials & Interfaces* **2013**, *5*, 2861.

42 Zhan, N.; Palui, G.; Merkl, J.-P.; Mattoussi, H. *Journal of the American Chemical Society* **2016**, *138*, 3190.

43 Liu, D.; Snee, P. T. *Acs Nano* **2011**, *5*, 546.

44 Guo, Y.; Sakonsinsiri, C.; Nehlmeier, I.; Fascione, M. A.; Zhang, H.; Wang, W.; Poehlmann, S.; Turnbull, W. B.; Zhou, D. *Angewandte Chemie-International Edition* **2016**, *55*, 4738.

45 Greytak, A. B.; Allen, P. M.; Liu, W. H.; Zhao, J.; Young, E. R.; Popovic, Z.; Walker, B. J.; Nocera, D. G.; Bawendi, M. G. *Chemical Science* **2012**, *3*, 2028.

46 Dai, M. Q.; Yung, L. Y. L. *Chemistry of Materials* **2013**, *25*, 2193.

47 Tamang, S.; Beaune, G.; Texier, I.; Reiss, P. *Acs Nano* **2011**, *5*, 9392.

48 Susumu, K.; Oh, E.; Delehanty, J. B.; Blanco-Canosa, J. B.; Johnson, B. J.; Jain, V.; Hervey, W. J.; Algar, W. R.; Boeneman, K.; Dawson, P. E.; Medintz, I. L. *Journal of the American Chemical Society* **2011**, *133*, 9480.

49 Chen, Y.; Vela, J.; Htoon, H.; Casson, J. L.; Werder, D. J.; Bussian, D. A.; Klimov, V. I.; Hollingsworth, J. A. *Journal of the American Chemical Society* **2008**, *130*, 5026.

50 Tiede, C.; Tang, A. A. S.; Deacon, S. E.; Mandal, U.; Nettleship, J. E.; Owen, R. L.; George, S. E.; Harrison, D. J.; Owens, R. J.; Tomlinson, D. C.; McPherson, M. J. *Protein Engineering Design & Selection* **2014**, *27*, 145.

51 Park, S.; Kim, E.; Kim, W. Y.; Kang, C.; Kim, J. S. *Chemical Communications* **2015**, *51*, 9343.

52 Wang, J.; Wang, F.; Li, F.; Zhang, W.; Shen, Y.; Zhou, D.; Guo, S. *Journal of Materials Chemistry B* **2016**, *4*, 2954.

53 Lv, L.; Guo, Y.; Shen, Y.; Liu, J.; Zhang, W.; Zhou, D.; Guo, S. *Advanced Healthcare Materials* **2015**, *4*, 1496.

54 Zhang, W.; Wang, F.; Wang, Y.; Wang, J.; Yu, Y.; Guo, S.; Chen, R.; Zhou, D. *Journal of Controlled Release* **2016**, *232*, 9.

55 Zhou, D.; Bruckbauer, A.; Ying, L.; Abell, C.; Klenerman, D. *Nano Lett.*, **2003**, *3*, 1517-1520.

56 Medintz, I. L., et al., *J. Phys. Chem. C.* **2009***, 113*, 18552-18561.

57 Zhang, H.Y.; Stockley, P.G.; Zhou, D.J. *Faraday Discuss.* **2011**, *149*, 319-332.

58 Chi, C. W.; Lao, Y. H.; Li, Y. S.; Chen, L. C. *Biosens. Bioelectron*. 2011, *26*, 3346-3352.

59 Raichlin, S.; Sharon, E.; Freeman, R.; Tzfati, Y.; Willner, I. *Biosens. Bioelectron*. **2011**, *26*, 4681-4689.

60 Cheng, A. K. H.; Su, H.; Wang, Y. A.; Yu, H.-Z. *Anal. Chem.* 2009, **81**, 6130-6139.

61 Polsky, R.; Gill, R.; Kaganovsky, L.; Willner, I. *Anal. Chem*. 2006, **78**, 2268.

62 Wegner, K. D.; Jin, Z.; Linden, S.; Jennings, T. L.; Hildebrandt, N. *ACS Nano* 2013, **7**, 7411-7419.

Chapter 4. Photon induced fluorescence recovery of cap-exchanged quantum rod for ultra-sensitive ratiometric biosensing

Abstract

In this chapter, a stable, water-soluble rod-shaped fluorescence semiconductor nanocrystal (CdSe/CdS core/shell quantum rod, QR) was made by an efficient cap exchange protocol. However, in most cases the fluorescence of the cap-exchanged QR was almost quenched, hindering their biomedical applications. Herein I have solved this problem by discovering a simple method that allows for efficient recovery of the QR quantum yield, making them suitable for biological applications. The resulting water-soluble QRs are compact (D_h < 20 nm), bright (recovering to >67% of original fluorescence), resisting nonspecific adsorption and displaying good stabilities in biological buffers, making them well-suited for ratiometric biosensing. After tris(2-carboxylethyl phosphine, (TECP) reduction, a dihydrolipoic acid-zwitterion ligand (DHLA-ZW) capped QR was self-assembled with (His_8)-tagged anti-yeast SUMO non-antibody binding proteins (Affimers), allowing for ratiometric detection of its target protein down to 5 pM via the QR-sensitized Förster resonance energy transfer (FRET) readout signal. Furthermore, compact biotin functionalized QRs are prepared by a facile, one-step cap-exchange process for ratiometric quantitation of labelled neutravidin down to 5 pM. Such sensitivity is among the very best for QR-FRET based biosensors. These stable, bright QR-based probes have many potential

applications where they can be advantageous over the more widely sued quantum dots as biological labels. These include larger absorption cross section, higher extinction coefficient and individual particle brightness, higher quantum yield and a bigger stokes shift and a bigger particle size that can be functionalized with more functional/binding moieties.

4.1 Introduction

Fluorescent semiconductor nanocrystals, also known as “quantum dots, rods, and wires”, have been intensely investigated over the past twenty years because of their unique, size-dependent, stable and bright fluorescence properties which have board applications in energy, materials, biology, and medicine[1-12].

Despite significant recent progress, high quality QRs are typically synthesised by the organometallic route based on reactions performed in coordinating organic solvents[13]. Approaches capable of preparing high quality QRs with accurate control of size and aspect ratios have also been reported. However such nanocrystals are capped with hydrophobic surface ligands, making them only soluble in organic solvents such as hexane, toluene or chloroform, and hence biologically incompatible. For applications like biosensing and bio-imaging, the QRs need to be soluble in aqueous solutions and compatible with clinic diagnostic biological media. Encapsulation of QRs with amphiphilic ligands[1] is one of the methods that is often used to make the QR soluble in aqueous solution and retain its photo-physical properties. Although the resulting QRs can be suitable for bioimaging, but they have limited use in biosensing and Förster resonance energy transfer (FRET) applications because of the significantly increased hydrodynamic diameters arising from the QR

encapsulation (Dh > 20 nm) [14-21]. As discussed in the previous chapters, for sensitive biosensing and FRET based applications, the QR-bioconjugate should have short separation distance between the QR and the functional label on the target and binder molecules (*e.g.* the non-antibody binding protein (Affimer), Yeast SUMO 10, and its specific target protein (Yeast SUMO 28b)) used in this chapter. Whereas, ligand exchange (LE), a frequently used methodology to replace the native hydrophobic ligands with hydrophilic ones to promote the QR water-solubility and biocompatibility,[22, 23] is better suitable for FRET applications because of the resulting smaller D_hs.

As in the previous QD chapter, we also use the small dithiol-containing ligands such as dihydrolipoic acid (DHLA) and DHLA based compounds (DHLA-PEG600-Biotin) to perform the QR ligand-exchange, owing to their ability to form a stable and thin coating (small hydrodynamic diameters) on the QR surface. DHLA is made from TA (lipoic acid) by reducing its S-S bond of 1,2-dithiolane ring using tris(2-carboxylethyl)phosphine (TCEP). The reduced DHLA-ligands are directly used to initiate cap-exchange with hydrophobic CdSe/CdS QRs in homogenous solution similar to the previous QD chapter. This method allows for complete water-solubilisation of commercial hydrophobic QRs (CdSe/CdS) at a ligand: QR molar ratio of as low as 1000:1. Despite success in making the QR water-soluble, a major problem we found here is that the post cap-exchange Quasi-Type II QRs have almost totally lost their fluorescence property. To address this problem, we have discovered a new simple method that allows the QR to recover its fluorescence up to 90% of its original value. Moreover, the water-solubilized QRs retain compact sizes, resist nonspecific adsorption of proteins and display good stabilities in biological buffers. Furthermore, such QRs can be readily conjugated with a His_8-tagged Affimer

(Yeast SUMO10) for specific detection of 5 pM of its protein target (Yeast SUMO28b) *via* the QR-sensitized dye FRET signal in the presence of large excess of a non-target protein (*ca.* 0.1 mg/ml BSA (bovine serum albumin)). Additionally, biotinylated QRs are prepared by a facile, one-step cap-exchange process that can be used for ratiometric quantitation of labelled NeutrAvidin down to 5 pM.

4.2 Experiment details

4.2.1 Chemicals and Regents

CdSe/CdS core/shell QR (λ_{EM} max ~556 nm, CANdots, quantum yield >60%) was supplied as a hexane solution. The QR was coated with hydrophobic organic molecules. CdSe/CdS/ZnS core/shell/shell QDs in toluene (CANdots, λ_{EM} = ~610 nm, quantum yield > 40%) were purchased from Strem Chemicals (Cambridge, UK). lipoic acid (LA, > 99%), tris(2-carboxyethyl)phosphine hydrochloride (TCEP.HCl, >98%), chloroform (> 99.8%), ethanol (>99.9%), methanol (>99.9%), sodium bicarbonate (>99.5%), Dulbecco's phosphate buffered saline (D-PBS) and other chemicals were all purchased from Sigma-Aldrich (Dorset, UK) and used as received without further purification unless stated otherwise. Solvents were obtained from Fisher Scientific (Loughborough, UK) and used as received. Ultra-pure water (resistance >18.2 MΩ.cm) purified by an ELGA Purelab classic UVF system, was used for all experiments and making buffers. All moisture-sensitive reactions are performed under nitrogen atmosphere using oven-dried glassware. All solvents are dried by innovative technology prior to use, or are taken from sealed-bottles under nitrogen atmosphere. Evaporations are performed under reduced pressure on a rotary evaporator.

4.2.2 Experimental Procedures

4.2.2.1 Preparation of water-soluble DHLA-Zwitterion ligand capped QRs (QR-ZW) by ligand exchange

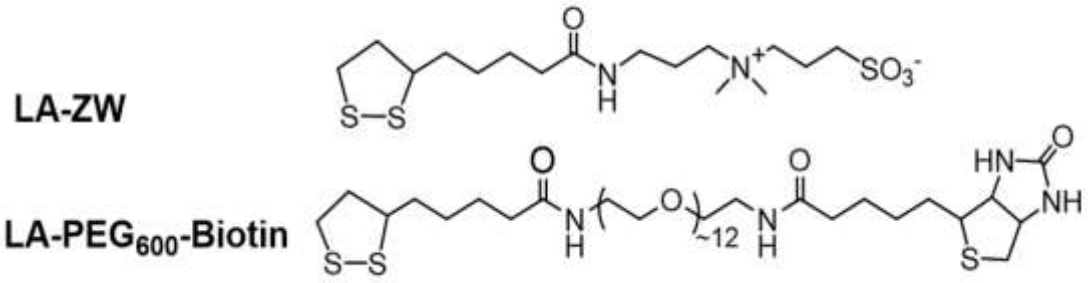

Chart 1: Chemical structures of the lipoic acid (LA)-based ligands used in this study.

Our ligand exchange procedure is shown in Figure 4-2. The synthesis, purification and characterization of the LA-Zwitterion and LA-PEG600-Biotin ligands were described in Chapter 2[18-20]. A typical ligand exchange procedure for preparing of DHLA-ZW ligand capped QR (abbreviated as QR-ZW) is as follows: the hydrophobic CdSe/CdS QR (0.2 nmole, 10 µl in hexane) was precipitated by adding 500 µl EtOH (or MeOH) followed by centrifugation to remove any free TOPO ligands. The QR pellet was then dissolved in 200 µl $CHCl_3$ and then added with 100 µl EtOH to make solution **A**. The LA-ZW ligand (0.10 M, 2 µl in H_2O) was reduced to DHLA-ZW by mixing with TCEP.HCl (0.10 M, 2 µl in H_2O) for 15 mins. After which NaOH (0.10 M in EtOH, 12 µl) was added to fully deprotonate the DHLA thiol-groups and to neutralise acid groups in TCEP.HCl (each containing 4 acid groups) to make solution **B**. The above solutions **A** and **B** were then mixed in a new Eppendorf tube for 1-5 mins with occasional shaking by hand. After that, the reaction mixture was centrifuged (1000 rpm for 10 seconds) and all the QR was precipitated at the bottom

of the Eppendorf tube as a pellet, leaving the supernatant ($CHCl_3$, EtOH and H_2O homogeneous solution) effective colourless. The supernatant was then carefully removed and the QR pellet was sonicated in a mixed $CHCl_3$ (500µl) and EtOH (200µl) solution to break up the QR-ZW pellet. After that, the tube was centrifuged for 1 min at 3000 rpm to collect the QR pellet and the clear supernatant was discarded. The process was repeated twice to remove any unbound free ligands, the QR pellet was finally added with H_2O (100 µl), yielding a stable, and water soluble QR stock solution. The stock QR concentration was determined by UV-vis absorption spectra using their first exciton peak at 550 nm and the respective extinction coefficient (2.56 x 10^5 L mol^{-1} cm^{-1}) using our previously established procedures before[24, 25].

4.2.2.2 The ligand exchange procedure to make water soluble QR-ZW,-PEG600-biotin (1:1000 ratio for DHLA-ZW, 1:200 ratio for DHLA-biotin)

A typical ligand exchange procedure is as follows: QR (0.2 nmol, 10 µl in toluene or hexane) was first precipitated by adding 500 µl EtOH or MeOH and centrifuged to remove any free TOPO ligands. The QR precipitate was then dissolved in a 100 µl $CHCl_3$ followed by addition of 60 µl EtOH to make solution **A**. LA-ZW (0.10 M, 2 µl in H_2O) and LA-PEG600-Biotin (0.01 M, 4 µl in EtOH) were mixed with TCEP (0.10 M, 2.4 µl in H_2O) for 15-20 mins to reduce the LA-ZW and LA-PEG600-Biotin into DHLA-ZW and DHLA-PEG600-Biotin, after that NaOH (0.10 M in EtOH, 14.4 µl) was added to fully deprotonate the DHLA thiol-groups and to neutralise acid groups in TCEP to make solution **B**. After that, the above solutions **A** and **B** were mixed in a new Eppendorf tube for around 1 min with occasional shaking by hand. The QR was found precipitated to the bottom of the tube. After removal of clear supernatant, washing and centrifugation steps to remove any free DHLA based ligands as above,

the QR pellet was dissolved in pure H_2O (50 µl), yielding a stable QR stock aqueous solution.

4.2.2.3 Yeast SUMO protein preparation, purification and labelling

The target protein, yeast SUMO (SUMO) protein and the anti-Yeast SUMO Affirmer were expressed in BL21 (DE3) cells using isopropyl b-D-1-thiogalactopyranoside (IPTG) induction and purified by Ni-NTA resin (Qiagen) affinity chromatography according to the manufacturer's instructions. All the target protein and anti-SUMO Affimers were provide by the Tomlinson group at Faculty of Biological Sciences, University of Leeds. The detailed experimental procedures were described in our recent publication[26]. The anti-SUMO Affimer (5 mg/ml, 12.5 µl in PBS, MW = 13,267) in an Eppendorf tube was first mixed with Atto 594 NHS-ester (30 µg in 2 µl DMSO) and then 5 µl $NaHCO_3$ (0.5 M, pH = 8.3) and 7.5 µl PBS (10 mM phosphate, 150 mM NaCl, pH 7.4) were added and thoroughly mixed at room temperature overnight (dye: protein molar ratio $\approx$ 5:1). After that the reaction mixture was loaded on a small G25 gel filtration column using PBS as eluting solution on natural flow. The first eluted blue band (corresponding to the labelled anti-SUMO Affimer) was collected and its absorption spectrum was recorded. (Figure 1) Using the extinction coefficients of the Atto-594 dye (ε_{594nm} = 120,000 $M^{-1}cm^{-1}$) and Affimer (ε_{280nm}=7904 $M^{-1}cm^{-1}$) and the CF280nm of 0.51 for Atto-594, the average dye labelling ratio on per Affimer was calculated as 0.35. The stock protein concentration was determined as 8.4 µM[27].

Similarity, the SUMO protein was labelled with Atto-594 NHS ester using the same procedures under a dye: protein molar ratio of 5. After purification by using a G25 column as above, the average number of dyes labelled on each protein was determined as 0.25. The labelled protein stock concentration was 10 µM.

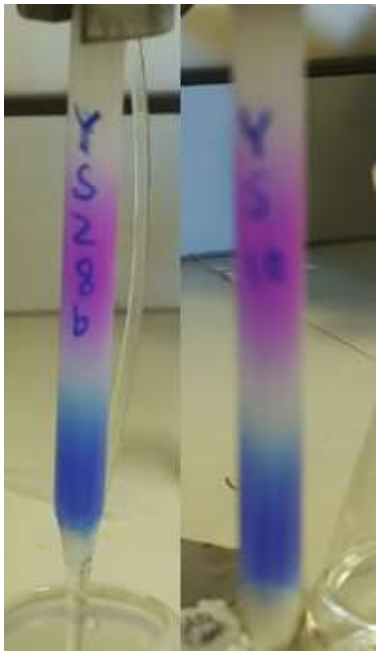

Figure 4-1: Picture of Yeast SUMO10 Affimer and Yeast SUMO28b target protein labelled by Atto-594 go through G25 column.

4.2.2.4 NeutrAvidin Protein labelling

Neutravidin (28.8 µl, MW = 60000 g/mol, ε = 1.66 at 1mg/mL, c = 10 mg/mL) in an Eppendorf sample tube was added Atto 694 NHS-ester 50 µg (Mw ≈ 1358 g/mol, ε_{594nm} = 120,000 $M^{-1}cm^{-1}$) dissolved in 2 µl DMSO, and the CF280nm of 0.51 for Atto-594 and 7.5 µl PBS (10 mM phosphate, 150 mM NaCl, pH 7.4) were added and mixed together at room temperature for 8 h (reaction ratio of protein : dye ≈ 1: 8). After that, the mixture was separated on a small G25 gel filtration column using PBS as eluting solution on natural flow. The first eluted blue band (the labelled Neutravidin) was collected the dye labelling ratio was calculated by following our earlier established procedures, yielding a dye: neutravidin ratio of 0.67. The stock protein concentration was 4.6 µM.

4.3 Results and discussion

4.3.1 Preparation and investigation of water soluble QR-ZW

First we studied how ligand: QR molar ratio (LQMR) affected the cap-exchange process using the hydrophobic CdSe/CdS QR capped with mixed trioctylphoshine/trioctylphoshine oxide ligands and the DHLA-zwitterion (ZW) ligand (Chart 1). When cap-exchange was performed at a LQMR of ≥ 1000, all of the CdSe/CdS QRs were fully transferred to the aqueous phase (shown as a yellow colour in the top aqueous layer), leaving the bottom $CHCl_3$ layer colourless (Figure 4-2). Those prepared under lower LQMRs showed some minor aggregation or clustering (Figure 4-2, 3). Thus a LQMR of 1000:1 was determined as the minimum ratio to allow full CdSe/CdS QR water-solubilization. A further dynamic light scattering (DLS) analysis of the CdSe/CdS QR after cap-exchange with the DHLA-ZW revealed that compact (ca. D_h =13.5 ± 2.6 nm, mean ± ½ FWHM) water-soluble QRs with uniform narrow size distribution was obtained at LQMR of 1000 (Figure 4-3). Then we investigated the crystal size of QR (λ_{EM} ~550 nm) before and after LE procedure by Transmission electron microscopy (TEM) (Figure 4-4). The QR appeared as uniform rod shaped nanocrystals of ~3.6 nm wide and ~23 nm in length. No observable change of the shape or size of the QRs were observed after the cap-exchange.

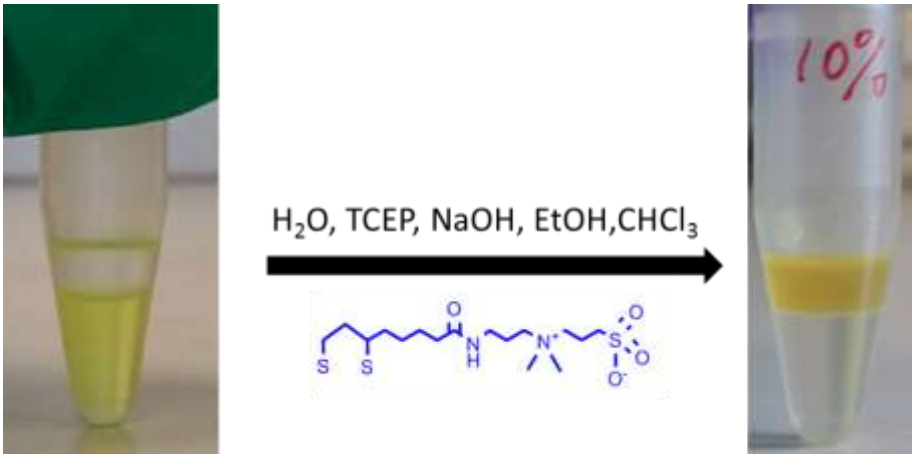

Figure 4-2: A picture of our approach to transfer of the hydrophobic CdSe/CdS QRs (λ_{EM} ~ 550 nm) into aqueous media by ligand exchange with DHLA-ZW ligands at LQMR =1000:1. The LA-ZW ligands, after TCEP reduction and NaOH deprotonation, are used directly to initiate ligand exchange with hydrophobic QRs in a homogenous solution of $CHCl_3$/EtOH/H_2O.

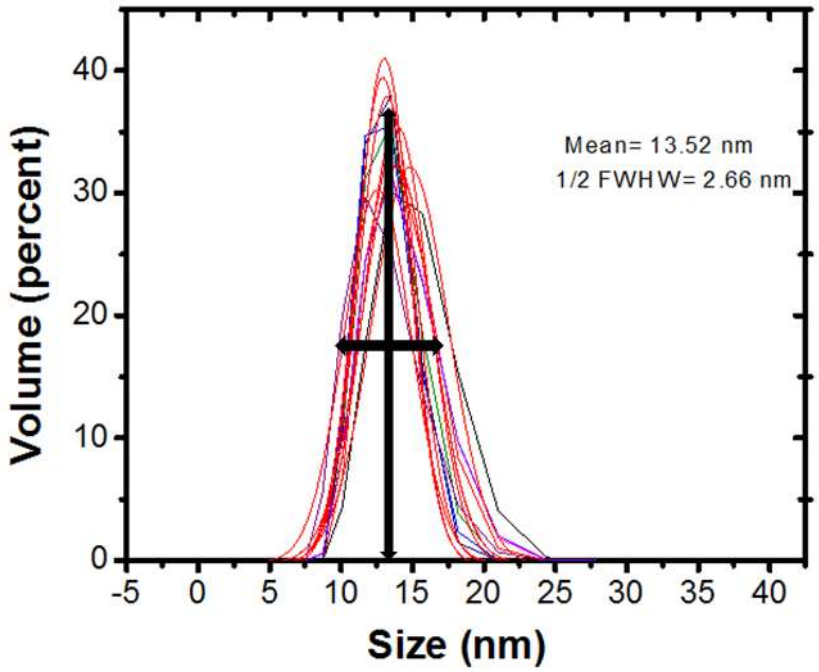

Figure 4-3: Size distribution diagrams measured by dynamic light scattering (DLS) for the CdSe/CdS core/shell QR (λ_{EM} ~ 550 nm) after cap-exchange with DHLA-ZW under LQMR: 1000. Mean size is 13.5 nm, and ½ FWHW is 2.7 nm.

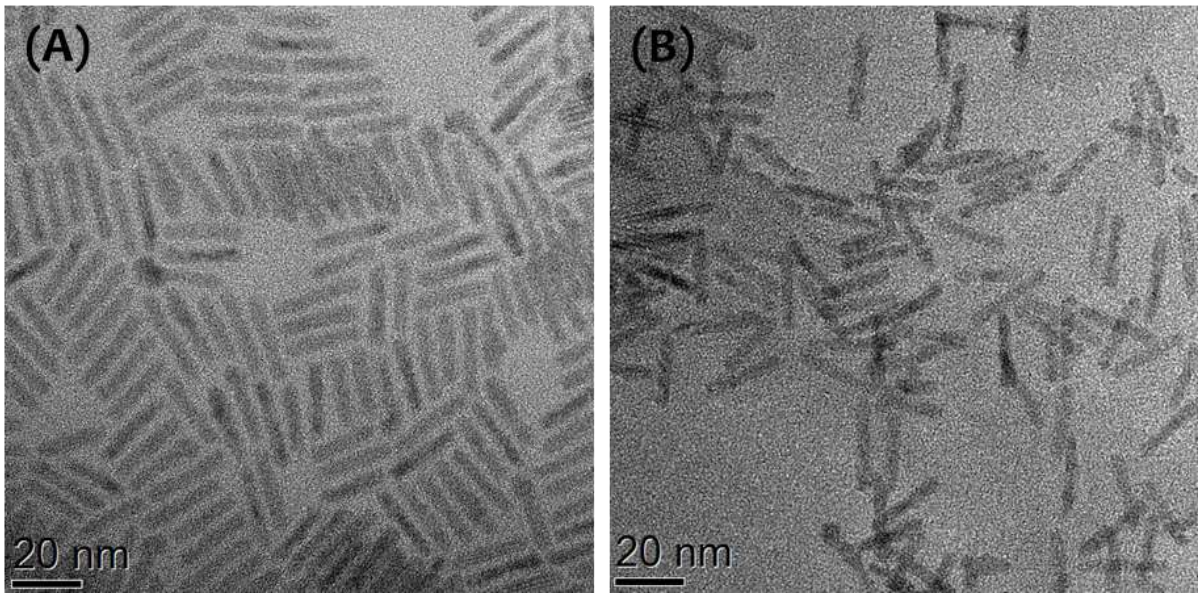

Figure 4-4: (**A**) TEM image of the TOP-TOPO capped CdSe/CdS core/shell QR (λ_{EM} ~ 550 nm) used in this study prior to ligand exchange. It has an average wide of ~3.6 nm and length of ~23 nm. (**B**) TEM image of the CdSe/CdS core/shell QR after ligand exchange with the DHLA-ZW at a ligand: QR molar ratio of 1000:1.

Theoretically, a cylinder 3.6 nm wide and 23 nm length green emitting (λ_{EM} ~550 nm) CdSe/CdS QR (Figure 4-4) has a total surface area of 300.6 nm^2 (Figure 4-5). Assuming the QR is terminated with a full Cd^{2+} outer layer in stable Wurtzite structure with each Cd^{2+} occupying a surface area of 0.15 nm^2 (Figure 4-6), then the QR would contain a maximum of 2004 surface Cd^{2+} ions. Assuming each thiolate binds to one Cd^{2+} ion, then 2004 single thiolate ligands (or 1002 DHLA-based ligands, each containing 2 thiol groups and hence a footprint area of 0.30 nm^2) would saturate the QR surface Cd^{2+} ions completely. This result may indicate that all of the added DHLA-ligands have bound to the QR and each DHLA may have chelatd to two Cd^{2+} ions. Thus a QR surface Cd^{2+}:DHLA-ligand ratio of ~2:1 is needed to produce compact, isolated individual biocompatible QRs. The observation that a

LQMR of 1000:1 can promote a complete phase transfer and formation of stable water-soluble QRs may indicate that all of the added DHLA-ligands have bound to the QR.

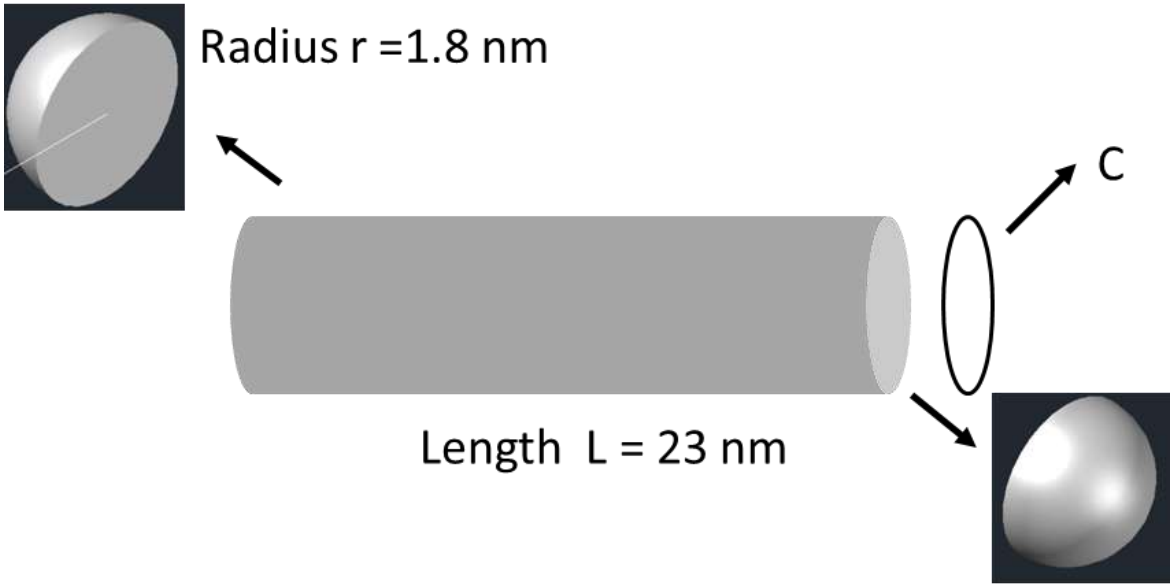

Sphere surface area $A = 4\pi r^2$ = 40.69 nm^2

Circumference of a circle C = $2\pi r = 11.30\ nm$

Rectangle area Q = LC = 259.99 nm^2

QR total surface area = 300.68 nm^2

Figure 4-5: the calculation of QR total surface area.

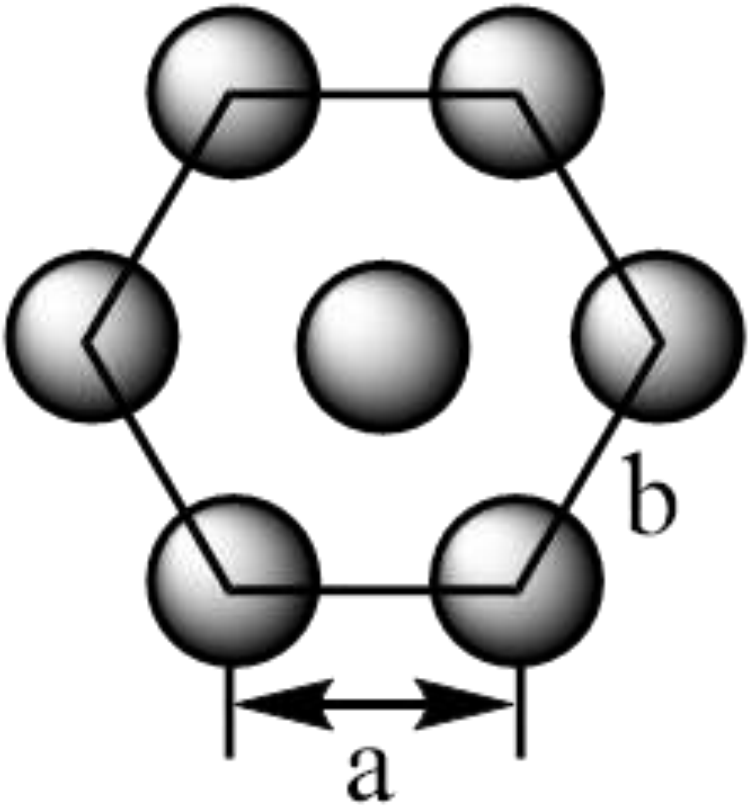

Figure 4-6: Schematic of a hexagonally packed Cd^{2+} outer layer (assuming CdS being in its most stable Wurtzite structure) where $a = b$ = 416 pm = 0.416 nm.

Within the hexagon area, there are three Cd^{2+} ions (spheres, 1 in the middle + 6 × (1/3) one the corners).

The total area of the hexagon = $6 \times (1/2)\, a^2 \times \sin 60^o = 3 \times 0.416^2 \sin 60^o = 0.449\ nm^2$

Therefore the surface area occupied by each $Cd^{2+} = 0.449/3 = 0.150\ nm^2$

Despite the success in the phase transfer and formation of stable water-soluble QR, a major problem here was that the post ligand-exchange QR displayed a significantly reduced fluorescence quantum yield (QY) compared to the parent QR in organic phase, typically retaining <5% of original fluorescence even the same LE method as the QD described in chapter 3 was used. In contrast, the CdSe/ZnS or

CdSe/CdS/ZnS QDs typically retained >96% of their original quantum yields as described in chapter 3 (Figures 4-7, 8)

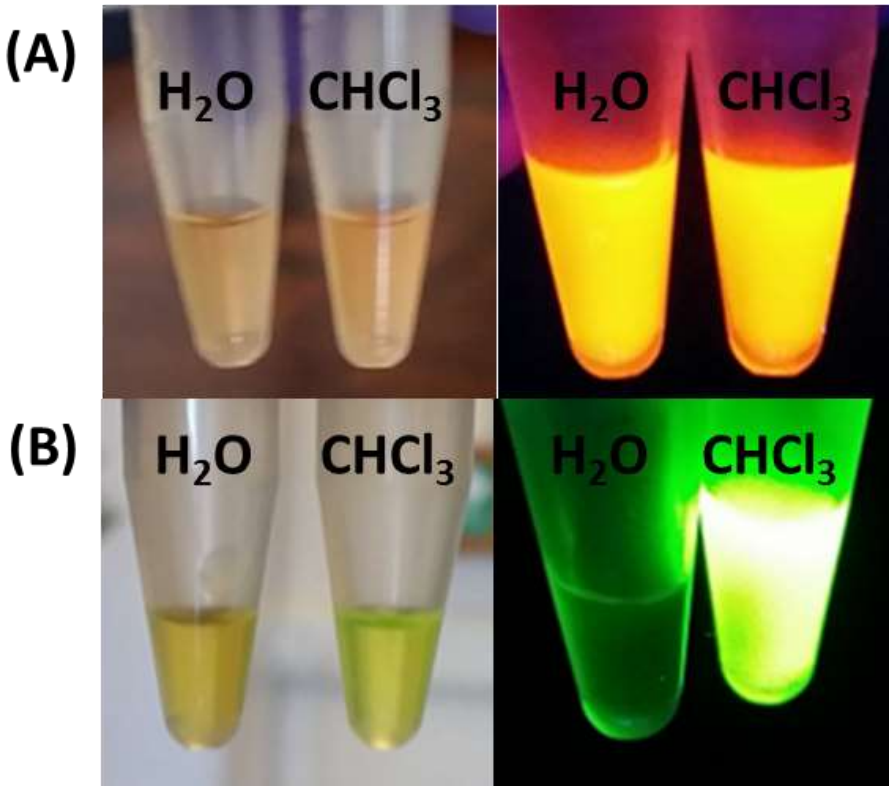

Figure 4-7: Pictures of 1 nmol Type I QDs and 0.2 nmol Quasi-Type II QRs in H_2O and $CHCl_3$ under sunlight ambient and UV light. **(A)** Picture of 1 nmol core/shell/shell Type I QD600 in H_2O after LE method and 1 nmol original QD600 in $CHCl_3$, **(B)** Picture of 0.2 nmol core/shell Quasi-Type II QR550 in H_2O after LE method and 0.2 nmol original QR550 in $CHCl_3$ [28].

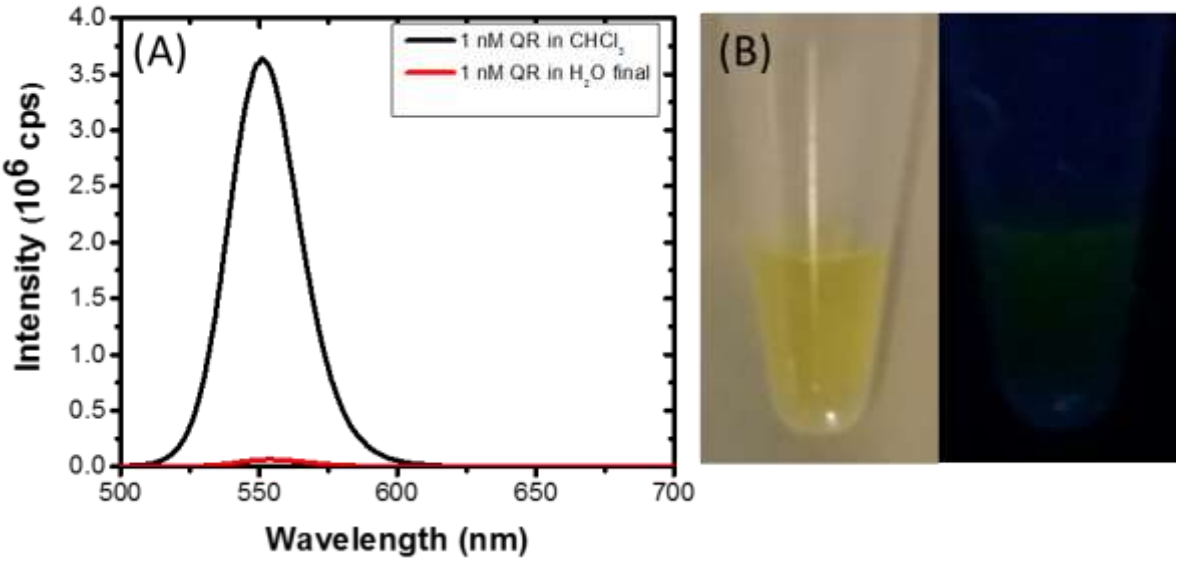

Figure 4-8: (A) Emission spectra of 1 nmol CdSe/CdS core/shell QRs organic ligand capped in $CHCl_3$ (black) and DHLA-ZW capped in H_2O (red). After LE, the QR was almost totally quenched compared to original QR before LE (original QR fluorescence intensity at 556 nm $I_{556} \approx 3.5*10^6$ cps, DHLA-ZW capped QR $I_{556} \approx 0.1*10^6$ cps). (B) The picture of 0.2 nmol DHLA-ZW capped QR dissolved in H_2O under ambient and UV light.

The reason behind this problem is likely due to the different band structures of the QR and QD used here. The CdSe/ZnS or CdSe/CdS/ZnS QDs used in chapter 3 are both type I QDs whose exciton carriers are fully confined within the core of the core/shell structure, so any changes to the shell as a result of the ligand exchange do not affect its fluorescence significantly. (Figure 4-7, 4-9) However, the CdSe/CdS QR used here has a Quasi-type II band structure, whose excited electron can spread across the whole core and shell structures[29]. Ligand exchange with the strongly chelating DHLA-based ligands may produce cation/anion vacant sites on the shell

which can trap the exciton carriers to prevent their emissive recombination[30], leading to greatly quenched fluorescence. Particularly, the excited electron can spread throughout of the whole core/shell structure in the CdSe/CdS QR, making its fluorescence be strongly dependent on surface properties and hence highly sensitive to cap-exchange[28].(Figure 4-9) This represents a major challenge/problem for realising the full potential for QR based biomedical applications which are all relied on its fluorescence property. Here we have developed a simple but effective approach to solve this problem.

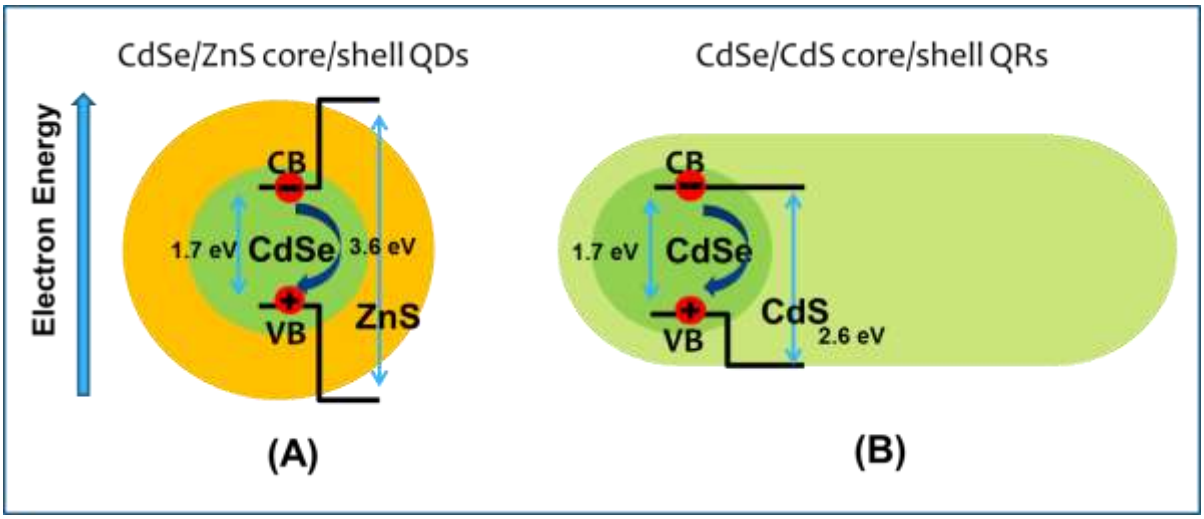

Figure 4-9: Schematic representation of energy – level alignment by selection core and shell materials. (**A**) A CdSe/ZnS core/shell type I QD with both electron and hole are confined within the core; (**B**) A CdSe/CdS quasi-Type II QR with the electron being spread in both core and shell structure[28].

4.3.2 Photon-induced fluorescence recovery of the QR-ZW

In order to make the QR reach its full potential in biomedical applications, we discovered a simple method to recover the QR fluorescence after LE. The schematics of our process for transferring the hydrophobic ligand (TOPO) capped QRs (soluble in $CHCl_3$) into water-soluble ones capped with DHLA-ZW ligand is shown in Figure 4-10.

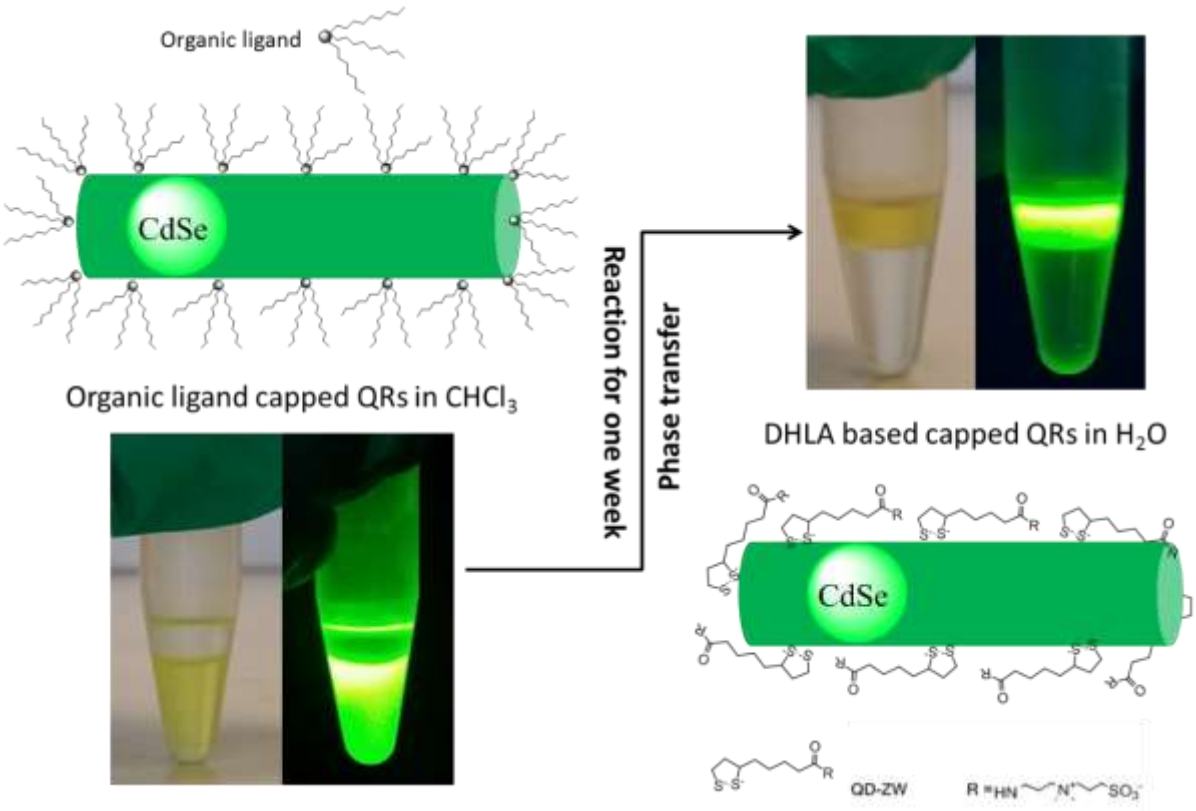

Figure 4-10: A schematic of our approach to transfer of the hydrophobic QRs into aqueous media by ligand exchange with DHLA-ZW ligands. The LA-ligands, after TCEP reduction and NaOH deprotonation, are used directly to initiate ligand exchange with hydrophobic QRs in a homogenous solution of $CHCl_3$/EtOH/H_2O. Photograph of a CdSe/CdS QR (λ_{EM} ~ 550 nm) under ambient and UV light before

(left) after ligand exchange with DHLA-ZW (right, top layer: H_2O; bottom layer: $CHCl_3$).

Because the QRs were practically non-emissive immediately after the ligand exchange when the ligand: QR molar ratios (LQMRs) used were higher than 1000:1. (1000:1 was minimum LQMR required for the complete transfer of the oil-soluble QRs into the aqueous phase) (Figure 4-2, 4-4, 4-11) As shown in Figure 4-8, the original QR fluorescence intensity was reduced by >97% after LE (reduced from ca. 3.5 $x10^6$ to ≈ 0.1 $x10^6$ cps). The dramatic decrease of QR fluorescence was observed immediately after ligand exchange with DHLA-ZW. This effect cannot be eliminated even when minimum ligands (LQMR of 1000: 1) were used in the cap-exchange to minimum the shell etching using the same principle as described in Chapter 3. Interestingly, we found that the fluorescence of the QR-ZW can recover automatically when being stored under ambient conditions. To the best of our knowledge, this fluorescence automatically recovery for post cap-exchanged QDs or QRs has not been reported previously in literature.

In order to investigate what is the main cause of fluorescence recovery, we made a batch of three identical QR-ZW samples fully dispersed in H_2O and exposed them under different light conditions: sunlight, UV light (a UV lamp typically used for imaging the TLC plate) or total darkness wrapped with aluminium foil. (Figure 4-11) The QRs exposed to UV light was found to recover its fluorescence very rapidly, gaining ~86% of its original fluorescence in 5 hours, whereas the fluorescence of the QR stored under ambient light conditions recovered more slowly, gaining ~60% of its original fluorescence in 1 week (Figure 4-12). Presumably because the UV light has higher energy than normal sunlight. In contrast, the QR-ZW sample stored in total darkness (in a fridge) has the lowest fluorescence recovery rate. Since the sample

was occasionally taken out from fridge for fluorescence checking, during which it was also exposed to the ambient sunlight in a very short time which may have led to the slow fluorescence recovery. (Figure 4-11) Nevertheless, it remained very dim even after 1 month. Based on these results, we concluded that the ambient room light and more effectively the UV light can provide enough energy to the QR for fluorescence recovery.

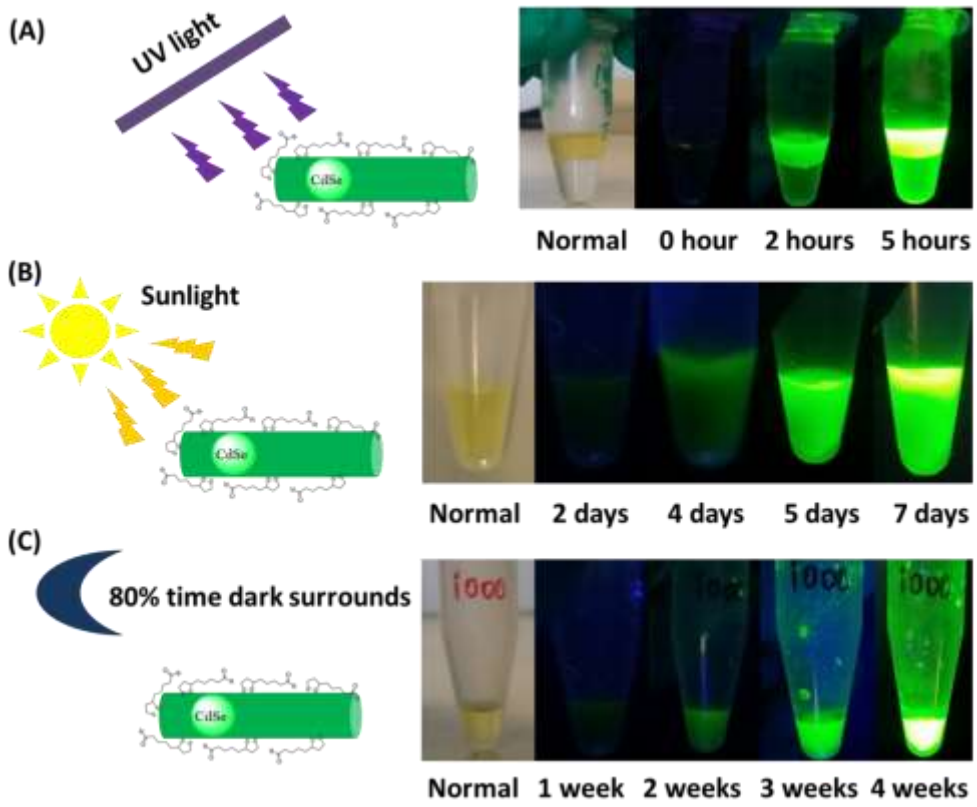

Figure 4-11: **(A)** Photographs showing a rapid fluorescence recovery of CdSe/CdS core/shell QR-ZW (maximum λ_{EM} = ~550 nm, 2 μM) prepared immediately by ligand exchange at a ligand: QR molar ratio of 1000:1 after upon exposure to a laboratory TLC UV lamp (λ = 350 nm) at different time intervals. The top layer is H_2O and bottom layer is $CHCl_3$. **(B)** Fluorescence auto-recovery of a QR-ZW sample (1 μM in H_2O) upon exposure to the ambient sunlight over a course of 7 days. **(C)** A QR-ZW (2 μM in H_2O) stored in a fridge in darkness with occasional exposure to the sunlight

(due to taken out for inspection) shows very slow fluorescence recovery over 4 weeks. All the QR samples were prepared at a LQMR of 1000:1.

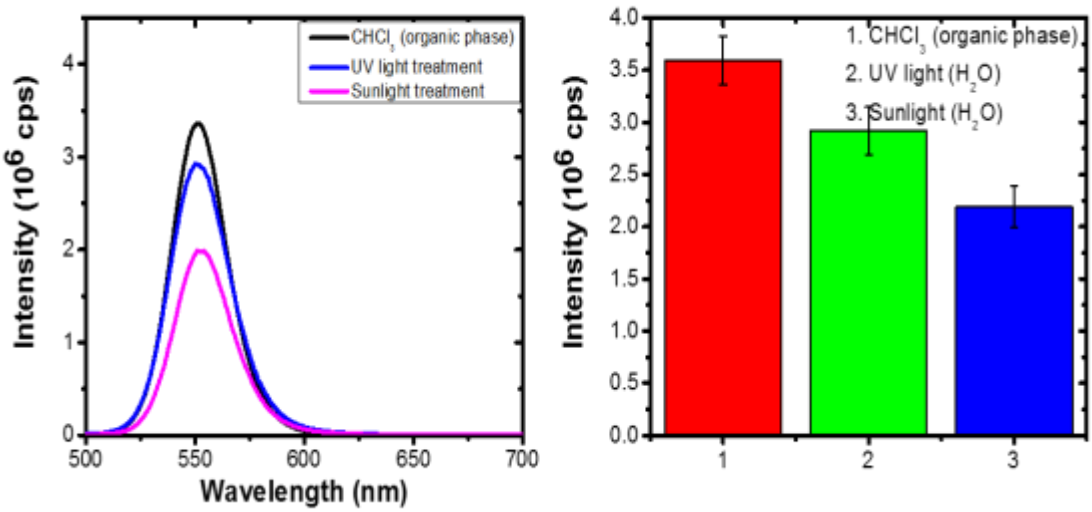

Figure 4-12: **(A)** Fluorescence spectra of the CdSe/CdS core/shell QR before LE in $CHCl_3$ (black) and after LE with DHLA-ZW at a LQ-MR of 1000:1 in H_2O after treatment by UV light (blue) and sunlight (pink). (**B**) Comparison of the relative fluorescence intensity for the above QRs.

In order to confirm that the QR fluorescence recovery is induced by the light energy, another experiment has been done. As shown in Figure 4-13 (A), no fluorescence recovery was observed for a water soluble QR-ZW sample that was wrapped in an aluminium foil and kept in total darkness for two weeks. Upon exposure this sample to the ambient light for 5 days, significant fluorescence recovery was observed. After fluorescence recovery, the two samples (parent QR in $CHCl_3$ and QR-ZW in H_2O) cannot be easily distinguished when being exposed to UV light (λ = 350 nm) as

shown in Figure 4-13 (B). Moreover, the water-soluble QR in H_2O can recover to ~86% of its original fluorescence intensity in $CHCl_3$ (Figure 4-12). In addition, two parallel water soluble QR-ZW samples before and after the light treatment can also be easily distinguished by the naked eye from the photograph shown in Figure 4-13 (C): the light treated QR (right) looks much brighter than the non-treated one (left). Overall, all of the cap-exchanged QRs can recover to > 60% of their original fluorescence after 'light activation' (Figure 4-12).

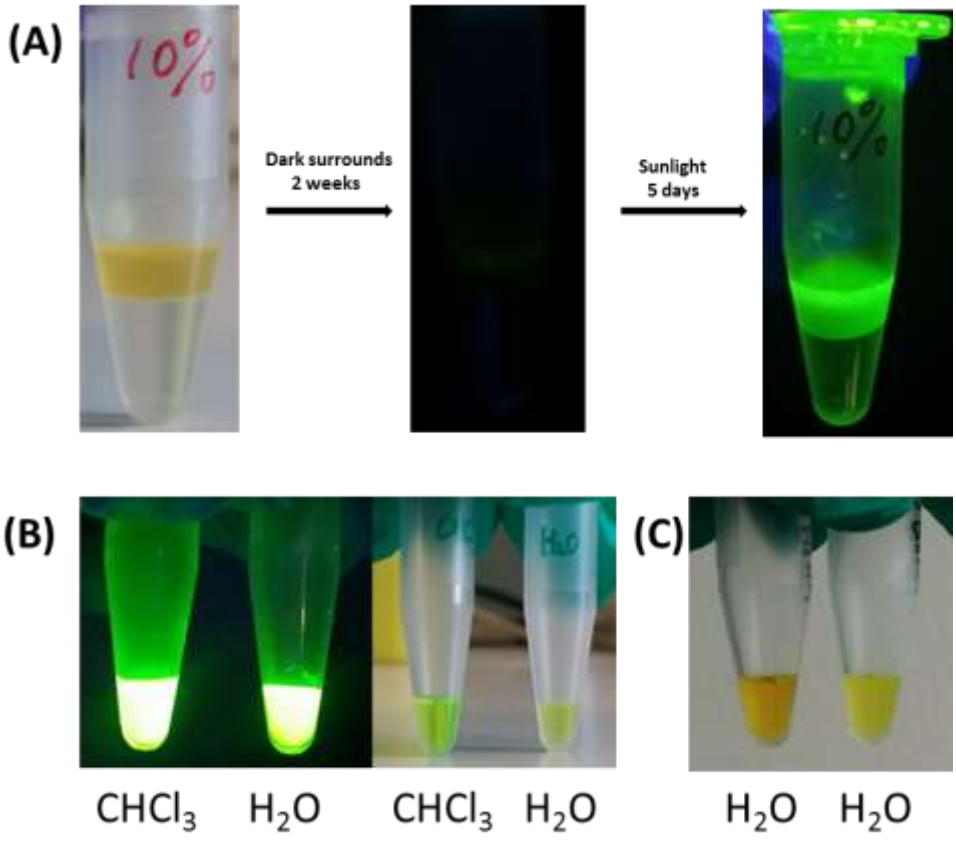

Figure 4-13: **(A)** After LE, the QR-ZW (2 μM) was fully transferred to the upper H_2O phase, leaving the bottom $CHCl_3$ layer colorless in an Eppendorf tube. Photograph of the tube sample exited by a hand-held UV lamp after being wrapped in aluminium foil and stored in total darkness for two weeks showed no fluorescence. After this, the sample was exposed to the ambient sunlight for 5 days, and then excited by the UK lamp where the QY was recovered. **(B)** Comparison of the same concentration

(both 1.5 μM) original QR in $CHCl_3$ and light treated QR-ZW in H_2O under UV light (λ = 350 nm, left panel) radiation and normal ambient sunlight situation (right panel). **(C)** Two parallel water soluble QR-ZW samples (both at 2 μM) before and after light treatment can be easily distinguished by eye under ambient conditions, the light treated QR (**right**) looks much lighter and brighter than other one (**left**).

Another interesting finding is that dilution of the QR-ZW sample can also increase the fluorescence recovery speed. A 10-fold dilution of the QR-ZW sample (*e.g.* from a stock concentration of 2 μM to 0.2 μM) by adding H_2O to the sample tube greatly increased the rate of the fluorescence recovery, where 4 hour exposure of the sample to the sunlight produced a fluorescence recovery comparable to the more concentrated stock sample for at least 3 days (Figure 4-14). This is presumably because the volume of the diluted QR sample is much bigger than the concentrated one, hence it is able to absorb a greater number of photons to initiate fluorescence recovery (i.e. the number of excitation photon is the limiting factor for the QR fluorescence recovery) (Figure 4-14). Therefore, dilution of the post LE QR sample appears to be an efficient way to make stable, bright and water-soluble QRs with light treatment. This result further confirmed that light can help the quenched QR to recover its fluorescence.

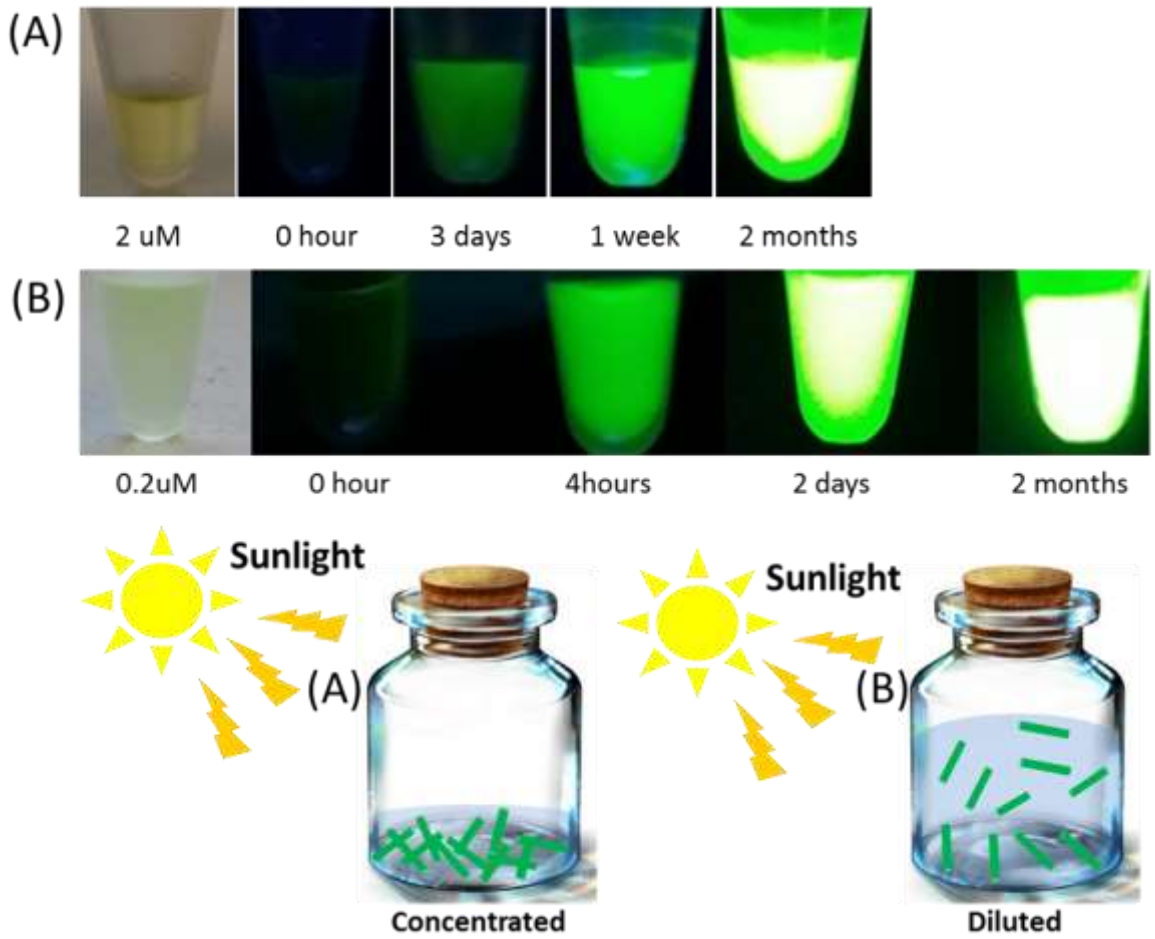

Figure 4-14: (A) Photos of a 2 μM QR-ZW stock in H_2O (100 μl) recorded under a UV lamp (λ = 350 nm) after exposure to ambient light for 0 hour, 3 days, 1 week and 2 months. (**B**) Photos of a 10-fold diluted QR-ZW (0.2 μM, 500 μl) in H_2O recorded under a UV light (λ = 350 nm) after exposure to ambient light for 0 hour, 4 hours, 2 days and 2 months respectively. Schematic procedures of the QR QY recovery by light treatment for the concentrated sample (A) and diluted sample (B).

After the QR has already recovered its fluorescence for 2 weeks, the quantum yield (QY) test has been done. The method for QY determined used here is a comparative method, which involves the use of a standard sample of known QY value. In this regard, Rhodamine 6G which dissolved in EtOH, under 480nm excitation was used as the reference standard (QY = 0.95)[31]. The QR QY was calculated by the equation:

$$Yu = \mathrm{Ys} * \left(\frac{\mathrm{Fu}}{\mathrm{Fs}}\right) * \left(\frac{\mathrm{As}}{\mathrm{Au}}\right)$$

Yu: quantum yield for QRs, **Ys**: quantum yield for Rhodamine 6G (0.95), **Fu**: integrated fluorescence intensity (I = 18794950) for QRs at 480nm, **Fs**: integrated fluorescence intensity (I = 57441080) for Rhodamine 6G at 480nm, **As**: Absorbance (A = 0.010) of Rhodamine 6G at 480nm, **Au**: Absorbance (A = 0.013) of QRs at 480nm.

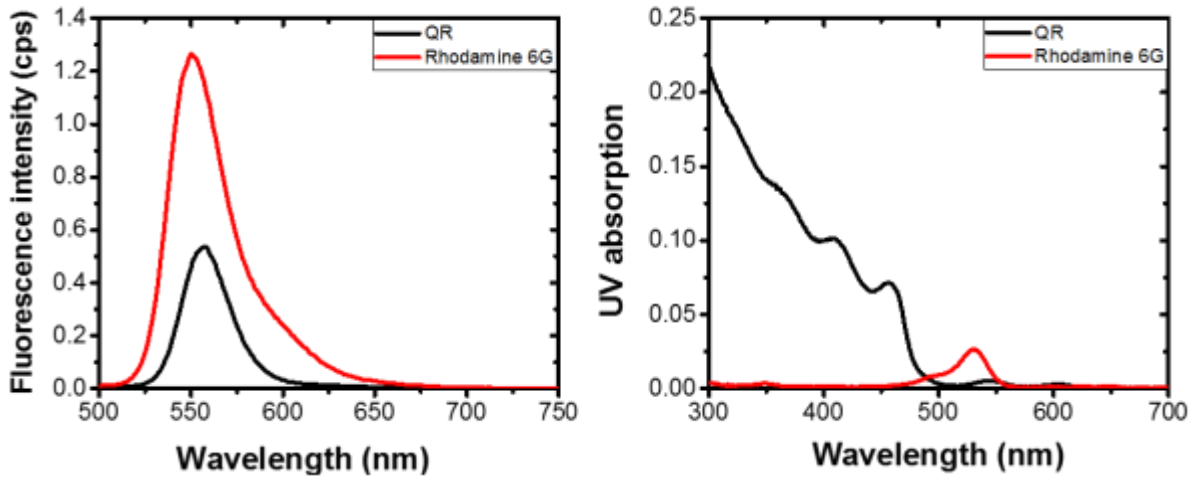

Figure 4-15: (Left) the Plot of fluorescence intensity test of QR (integrate =18794950) and Rhodamine 6G (integrate =57441080). (Right) the plot of UV absorption test after eliminates H_2O and EtOH background. The concentration of QR and Rhodamine 6G in UV-absorption test and fluorescence test are same.

Using the above data, the QY of QR-ZW sample after treatment with the ambient sunlight is thus determined as 24.6% (Figure 4-15), and this result is recorded instantly without further exciting the QR sample which have found to further brighter the QRs until the fluorescence intensity keep stable. After excited sample for more than 30 mins in fluorimeter, the fluorescence intensity will further increase. (See Figure 4-16) This light activated QR is suitable for further FRET biosensing application.

4.3.3 QR-Affimer for ratiometric biosensing

After light activation, the stability of QR-ZW sample was also investigated. The fluorescence spectra of two QR-ZW samples in H_2O and phosphate buffer saline (PBS, 10 mM phosphate, 150 mM NaCl, pH 7.4) were recorded. Interestingly, as shown in Figure 4-16, the florescence intensity of the QR-ZW sample was found to increase after each fluorescence recording and finally plateaued in ~60 mins. As shown in Figure 4-16 (A, B), the intensity of 1 nM QR-ZW in H_2O increased from 4000000 cps to 8500000 cps in 60 mins, after which it showed little change. Similar behaviour was also obverted for the 0.1 nM QR-ZW sample in PBS buffer, where its intensity increased from 1250000 cps to 2000000 cps in 30 mins and then plateaued out afterwards. This result may indicate that the QR-ZW sample used here has yet to reach full fluorescence recovery; hence it can further absorb the excitation light to trigger further fluorescence recovery till maximum is reached. The 1 nM QR gave too high a florescence intensity (>8 x 10^6 cps) which is beyond the linear response of the fluorimeter. Whereas the 0.1 nM QR gave a highly respectable florescence intensity of ~ 2 x 10^6 cps, making it suitable for sensitive biosensor detection. To minimise the

signal change due to different excitation scans, all sensing samples were scanned for ~5 runs till its florescence intensity became stable.

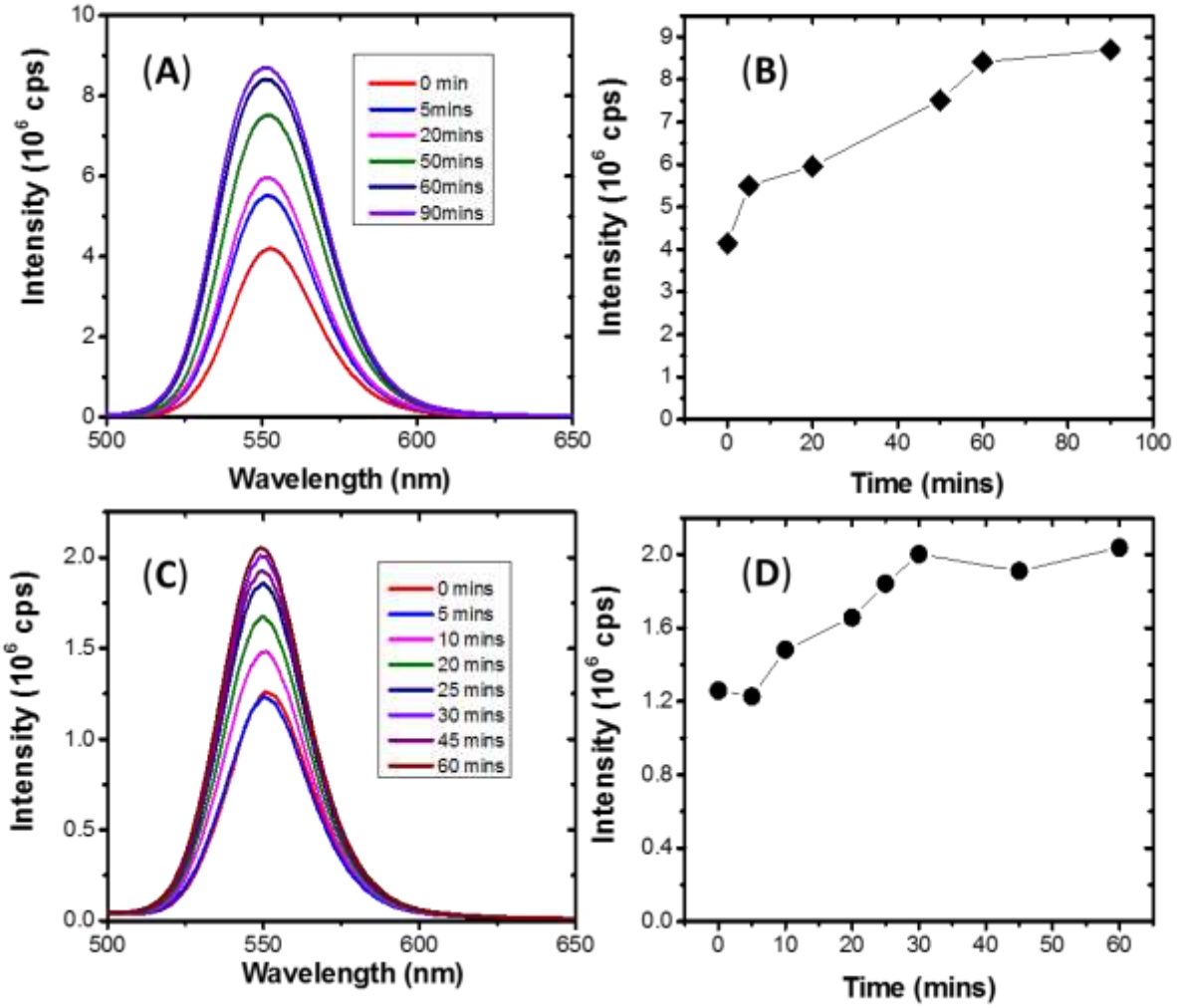

Figure 4-16: (A) Fluorescence spectra of 1 nM QR_{550}-DHLA-ZW in H_2O stability test in 90 mins. **(B)** A plot of 1 nM QR_{550}-DHLA-ZW Fluorescence intensity in H_2O time dependent. **(C)** Fluorescence spectra of 0.1 nM QR_{550}-DHLA-ZW in PBS buffer stability test in 60 mins. **(D)** A plot of 0.1 nM QR_{550}-DHLA-ZW fluorescence intensity in PBS buffer time dependent.

The high fluorescence and compact structure in biologically relevant buffer of the LE prepared QRs make them extremely attractive for FRET-based applications. The fact that the QRs have recovered to retain > 60% of their native fluorescence (Figure 4-12) after exposure to ambient for 2 months make them especially attractive for ultra-sensitive biosensing and biomedical applications. Herein, the QR was combined with the non-antibody binding protein (Affimer) to develop protein biosensors using same principles as the QD-biosensor described in chapter 3. The same Affimer and its target small ubiquitin-like modifier (SUMO) protein playing an important role in a number of cellular processes, such as nuclear-cytosolic transport and transcriptional regulation were used. The Affimer against Yeast SUMO protein were selected and prepared the Tomlinson group at the Faculty of Biological Sciences, University of Leeds[26]. The nABP was modified by His_8-tag at N-terminal, allowing it to self-assemble on the QR surface Cd^{2+} ions[32]. As mentioned in Chapter 3, the Affimers are especially well-suited for FRET based biosensing because of their small molecular sizes, allowing significantly reduced donor-acceptor distance and hence achieving high FRET efficiency and sensitivity.

First we studied the QR-Affimer self-assembly by mixing the Atto-594 labelled Affimer with the QD-ZW (λ_{EM} ~550 nm) at different molar ratios. The resulting fluorescence spectra (**λ_{EX}** = 450 nm, corresponding to the absorption minimum of the Atto-594 dye to minimize dye direct excitation) revealed a progressively quenched QR fluorescence and simultaneously enhanced Atto-594 FRET signal (at ~625 nm) with the increasing dye/QR ratio, consistent to the QR-sensitized Atto-594 dye FRET mechanism[32] (Figure 4-17). This result confirmed the successful QR-Affimer

conjugation. Because the average dye labelling ratio on per Affimer was low (at 0.35), the observed the FRET signal was also weak.

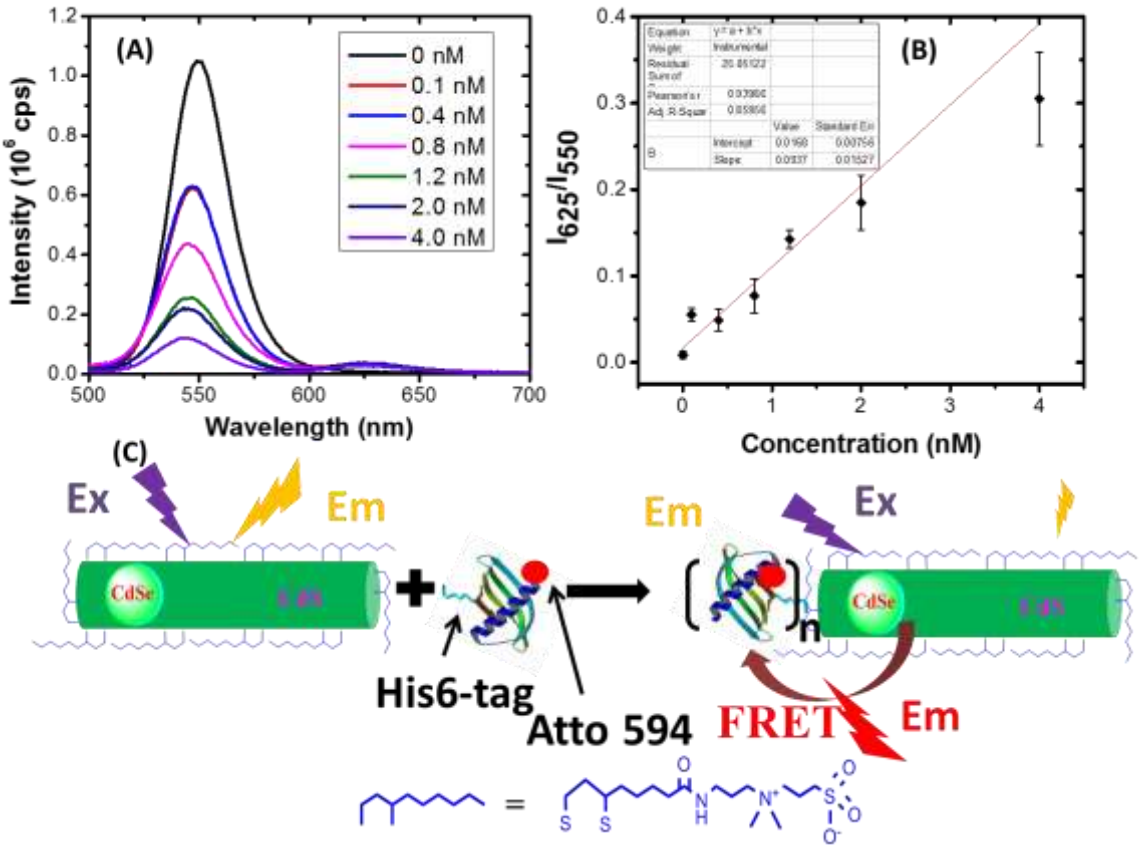

Figure 4-17: (A) Fluorescence spectra of the QR550-ZW (100 pM QR) after incubation with different concentration of Atto-594 labelled Yeast SUMO Affimers in PBS (B) A plot of the I_{625}/I_{550} ratio versus the Yeast SUMO nABP concentration fitted to a linear function: R^2 = 0.8596. (C) Schematic show of the QR self-assembled by labelled Affimer via the FRET readout strategy.

After that, the QR-Affimer bio-conjugate was further tested for biosensing function by binding to its specific target protein (Yeast SUMO 28b). Here the QR-ZW each

conjugated with 40 copies of unlabelled anti-SUMO Affimer (His8-tagged) was mixed with different amount of the target Yeast SUMO28b protein (Atto-594 labelled)[26]. The resulting fluorescence spectra (Figure 4-18) clearly showed that, with the increasing target binding Yeast SUMO28b concentration, the QR fluorescence was greatly quenched while the Atto 594 FRET signal was enhanced simultaneously, in agreement with the expectation that the specific Affimer-SUMO binding would bring the Atto-594 label close to the QR, producing QR-sensitized Atto 647 FRET signal. A plot of the peak intensity ratio (direct excitation background corrected) of the Atto-594 FRET (at 625 nm) to that of the QR (at 549 nm), I_{625}/I_{549}, versus the Yeast SUMO28b concentration gave a good positive linear relationship over 0-2000 pM (R^2 = 0.904) with a detect limit of as low as 5 pM, suggesting the QR-Affimer conjugate is suitable for ratiometric quantitation of pM level target proteins. The positive linear increase of the I_{625}/I_{549} ratio with the increasing SUMO concentration matched exactly what was expected for the multiple acceptors FRET to a single QR donor model.[24, 33]

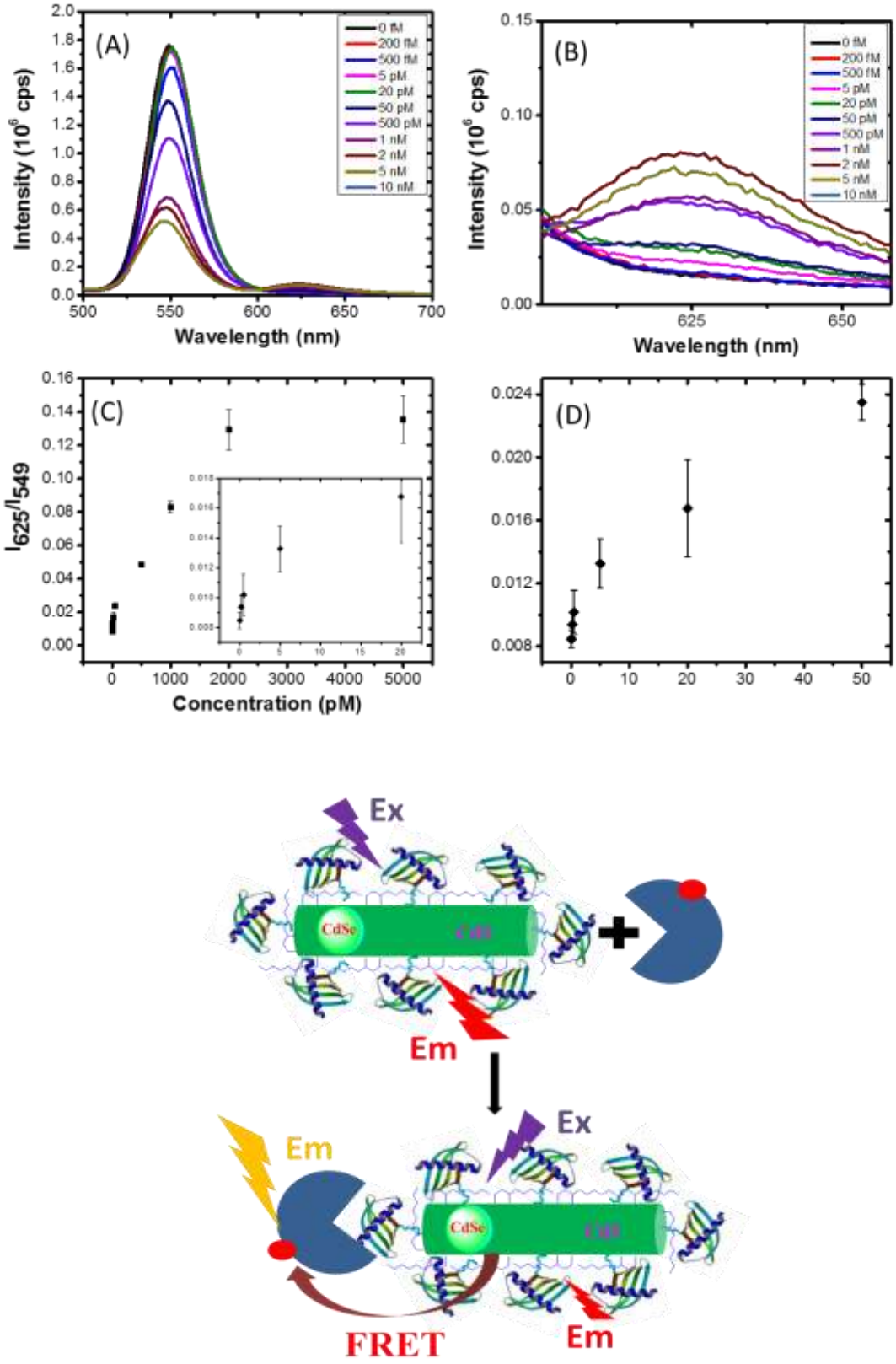

Figure 4-18: **(A)** Fluorescence spectra of the QR-ZW-Affimer (0.1 nM QR and 4 nM nABP) after incubation with different concentration of Atto-594 labelled Yeast SUMO

in PBS. **(B)** Fluorescence spectra amplify wavelength from 600nm to 650nm **(C)** A plot of the I_{625}/I_{549} ratio versus the SUMO concentration from 0 to 5000 pM and 0 to 20 pM. **(D)** A plot of the I_{625}/I_{549} ratio versus the SUMO concentration from 0 to 50 pM. And the schematic show of the QR-Affimer for detection of labelled target SUMO via QR-sensitized Atto-594 FRET readout strategy.

After confirming that the QR-Affimer can detect the labelled target SUMO protein, label free test was also done. The ability of detecting unlabelled protein target is more useful for bio diagnostics because target labelling may not be feasible for real situations. To investigate this potential, we first conjugated each CdSe/CdS QR with 1 copy of the anti-SUMO Affimer (via His8-tag self-assembly) and then blocked the QR with 40 copies of a control Affimer (His8-tagged) that showed no binding affinity to the Yeast SUMO28b protein[26]. An Atto-594 labelled Yeast SUMO28b protein was used as FRET reporter (with C_{QR} = C_{SUMO} = 0.1 nM) similar to that described in Chapter 3. Adding different concentration of unlabelled Yeast SUMO28b protein should compete with the labelled Yeast SUMO28b protein binding to the QR-Affimer, reducing the number of labelled Yeast SUMO28b binding to the QR and resulting in the QR fluorescence recovery (Figure 4-19). A plot of the resulting fluorescence intensity ratio I_{549}/I_{625} versus the unlabelled Yeast SUMO28b concentration showed that, with the increasing unlabelled target Yeast SUMO28b concentration (particularly at > 50 pM), the QR fluorescence was greatly enhanced while the Atto 594 FRET signal was decreased simultaneously, in agreement with the expectation that the unlabelled SUMO protein would compete and displace the Atto-594 labelled SUMO protein from binding to the QR. The label-free sensitivity (ca. 50 pM) is lower than that of the label detection (ca. 5 pM), presumably because each QR here is

conjugated with only 1 copy of the Affimer binder versus 40 copies in labelled detection which may enhance the Affimer-SUMO binding affinity via multivalency effect. Moreover, not all labelled Yeast SUMO protein reporters may have bound to the QR-Affimer conjugates due to their natural binding-dissociation equilibrium, thus some of the introduced unlabelled SUMO proteins may simply bind to the unbound free Affimers on the QR surface without displacing the reporter proteins. Nevertheless, the label-free sensitivity achieved here is comparable or even better than most other QD-FRET based protein sensors (see Chapter 3).

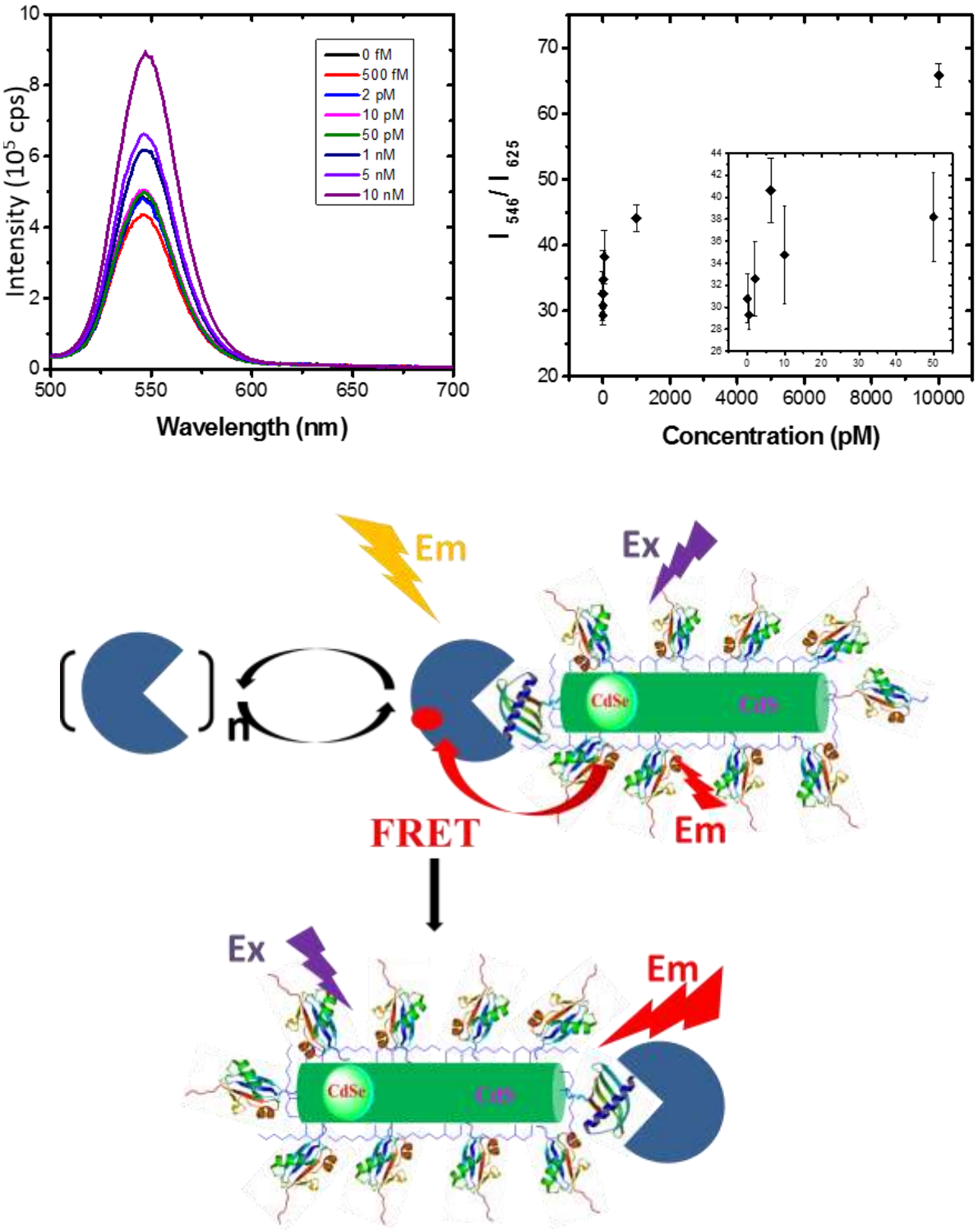

Figure 4-19: (A) Fluorescence spectra of the QR-Affimer conjugate (0.1 nM) mixed with Atto-594 labelled SUMO protein reporter (0.1 nM) in the presence of different amounts of unlabelled Yeast SUMO28b protein. (B) A plot of I_{549}/I_{625} as a function of the unlabelled SUMO concentration: data over 0-10 nM range and 0-50 pM. The

scheme below shows the assay principle (the protein circled being the anti-SUMO Affimer while all others are non-SUMO binding Affimer).

4.3.4 Preparation of QR-biotin for biosensing

After demonstration the ability of making stable and fluorescence recovered QR-ZW samples, biotin-functionalized QRs were further prepared in one step using mixed DHLA-PEG600-biotin/DHLA-ZW. Tuning the ratio of the DHLA-PEG600-biotin ligand to DHLA-ZW spacer ligand ratio allowed for control of the QR surface biotin valency. The preparation procedures of the mixed ligand cap-exchanged QRs were described in experiment section. After that, the QRs prepared at a LQMR of 1000:1 with DHLA-ZW and 200:1 with DHLA-PEG600-biotin were exposed to ambient light conditions to allow fluorescence recovery over 1 week, gaining ~60% of its original fluorescence. Such QR-biotin sample was found to be stable and suitable for detection of neutravidin via the strong biotin-neutrAvidin interaction. (Figure 4-20)

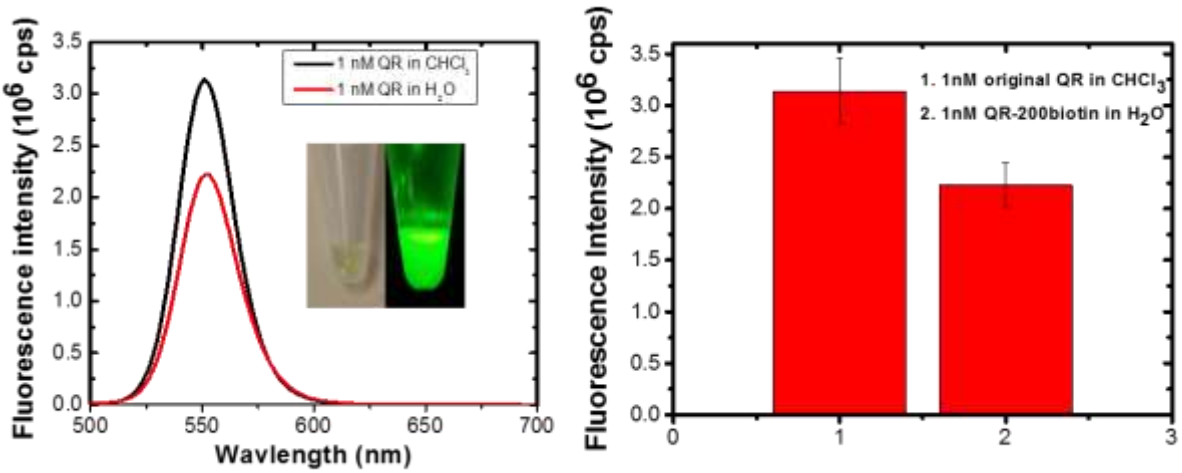

Figure 4-20: **(A)** Fluorescence spectra of the CdSe/CdS core/shell QR before LE (black) and after LE at a LQ-MR of 1000:1 with DHLA-ZW and 200:1 with biotin after

ambient light treatment for 1 week (red). (**B**) Comparison of the relative fluorescence intensity for the above QRs.

Similar to the QR-ZW sample, the QR-biotin sample prepared at a LQMR = 1000:1 with DHLA-ZW and 200:1 with DHLA-PEG600-Biotin was also found to be sufficient to completely water-solubilize the CdSe/CdS QR to form a stable, water-soluble QR-biotin sample.

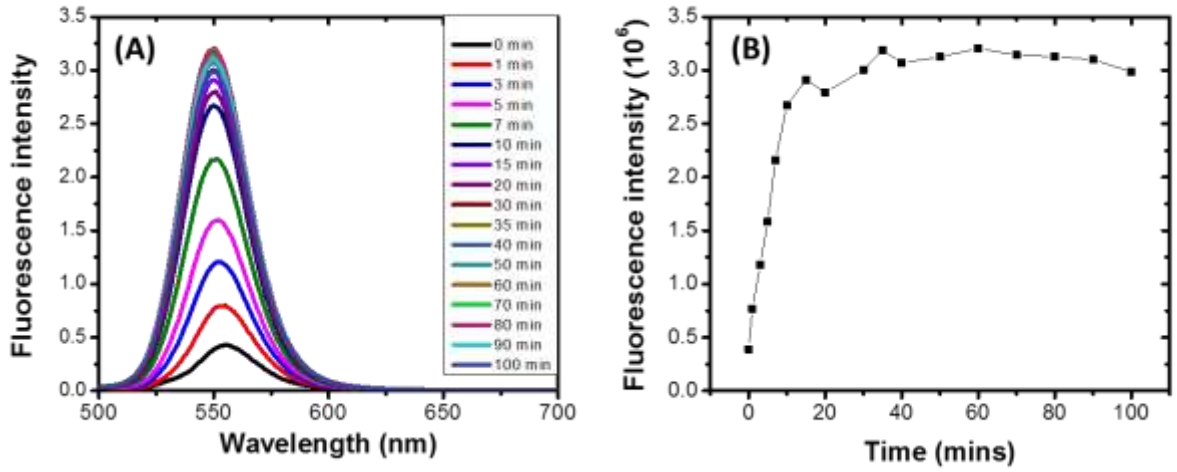

Figure 4-21: (**A**) Fluorescence spectra of 1 nM QR-biotin in PBS containing 0.1 mg/ml of BSA tested over a 90 min period. **(B)** A plot of the QR-biotin fluorescence intensity versus time: a ~7 fold fluorescence enhancement was observed over a course of 30 mins and then plateaued out afterwards.

The stability of the CdSe/CdS QR (λ_{EM} = 550) capped with mixed ligands of DHLA-ZW and DHLA-PEG600-Biotin was first investigated. Similar to the QR-ZW above, its fluorescence was also found to be time dependent in PBS buffer containing 0.1 mg/mL of BSA. As shown in Figure 4-21, its florescence also increased after each

scan over the first 30 mins and then plateaued out, where a very significant 6.7 fold increase of intensity was observed (increasing from ca. 4.5 $x10^5$ to 3 $x10^6$ cps). Based on this result, further sensing experiment was carried out by performing repeated scans of QR-biotin sample for 30 min till its florescence no longer showed significant changes, the same way as the QR-Affimer sensing above. A further TEM imaging reveals that the prepared QR-biotin sample retained the same crystal size and shape as the parent QR (Figure 4-22), similar to that observed with the QR-ZW sample above.

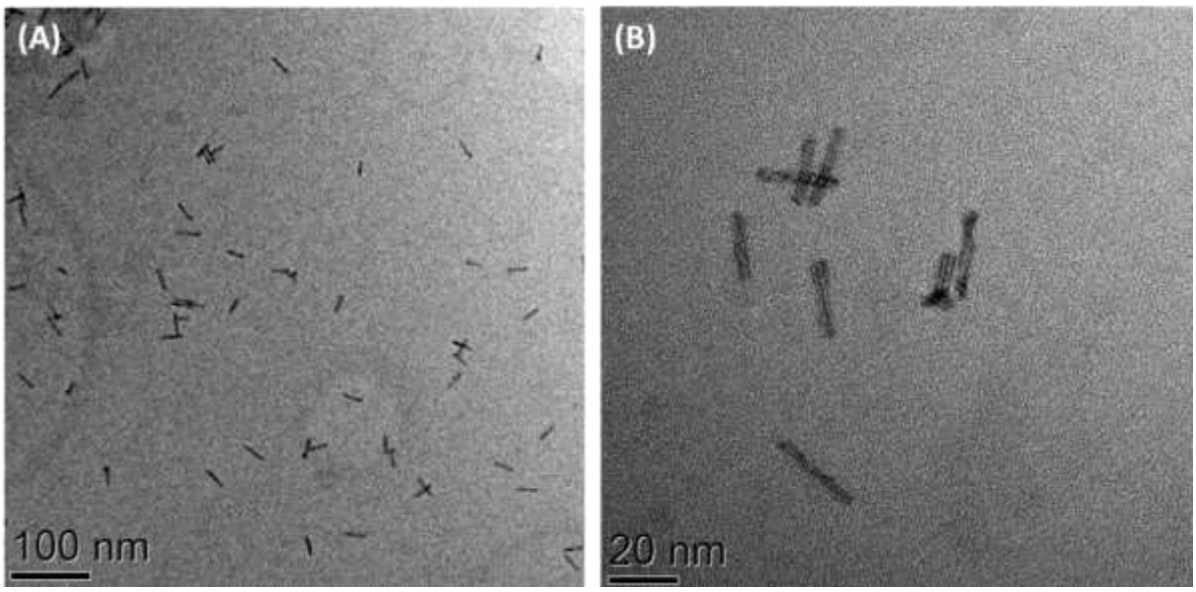

Figure 4-22: (**A**) TEM image of the CdSe/CdS core/shell QR after LE with the DHLA-ZW at a ligand: QR molar ratio of 1000:1 and DHLA-PEG600-biotin at a ligand: QR molar ratio of 200:1 (**B**) of the same TEM image under higher magnification. The QR has an average width of ~3.6 nm and length of ~23 nm.

After that, the QR-ZW/PEG600-biotin probe (abbreviated as QR-biotin200) was further tested for its biosensing application of its specific target protein (NeutrAvidin) by exploiting the extremely strong bio-specific interaction between biotin and Neutravidin (Kd ~10^{-15} M). Here the QR-biotin200 was mixed with different concentration of the Atto 594 labelled NeutrAvidin and the resulting fluorescence spectra were shown in (Figures 4-23). With the increasing NeutrAvidin concentration, the QR fluorescence was greatly quenched while the Atto 594 FRET signal was enhanced simultaneously, in agreement with the expectation that the specific biotin-NeutrAvidin binding would bring the Atto-594 dye close to the QR, producing QR-sensitized Atto-594 FRET signal. A plot of the peak intensity ratio of the Atto-594 FRET (at 623 nm) to that of the QR (at 543 nm), I_{623}/I_{543}, versus the NeutrAvidin concentration revealed a detect limit of as low as 5 pM, suggesting the QR-biotin conjugate is suitable for quantitation of low pM levels of the target NeutrAvidin. The sensing specificity was supported by a control experiment where mixing the Atto-594 labelled neutravidin (100 nM) with the QR capped with DHLA-ZW ligand only but without DHLA-PEG600-biotin ligand displayed almost no quenching of the QR fluorescence. The resulting direct excitation corrected I_{623}/I_{543} ratio was only 0.0042, < 10% of the ratio observed for the QR-biotin200 with 1 nM neutravidin, despite the former neutravidin concentration was 100 fold higher than the later. This result clearly demonstrates that the observed FRET signal here is due to the specific biotin-neutravidin binding, and not due to non-specific adsorption (Figure 4-23 (**D**)).

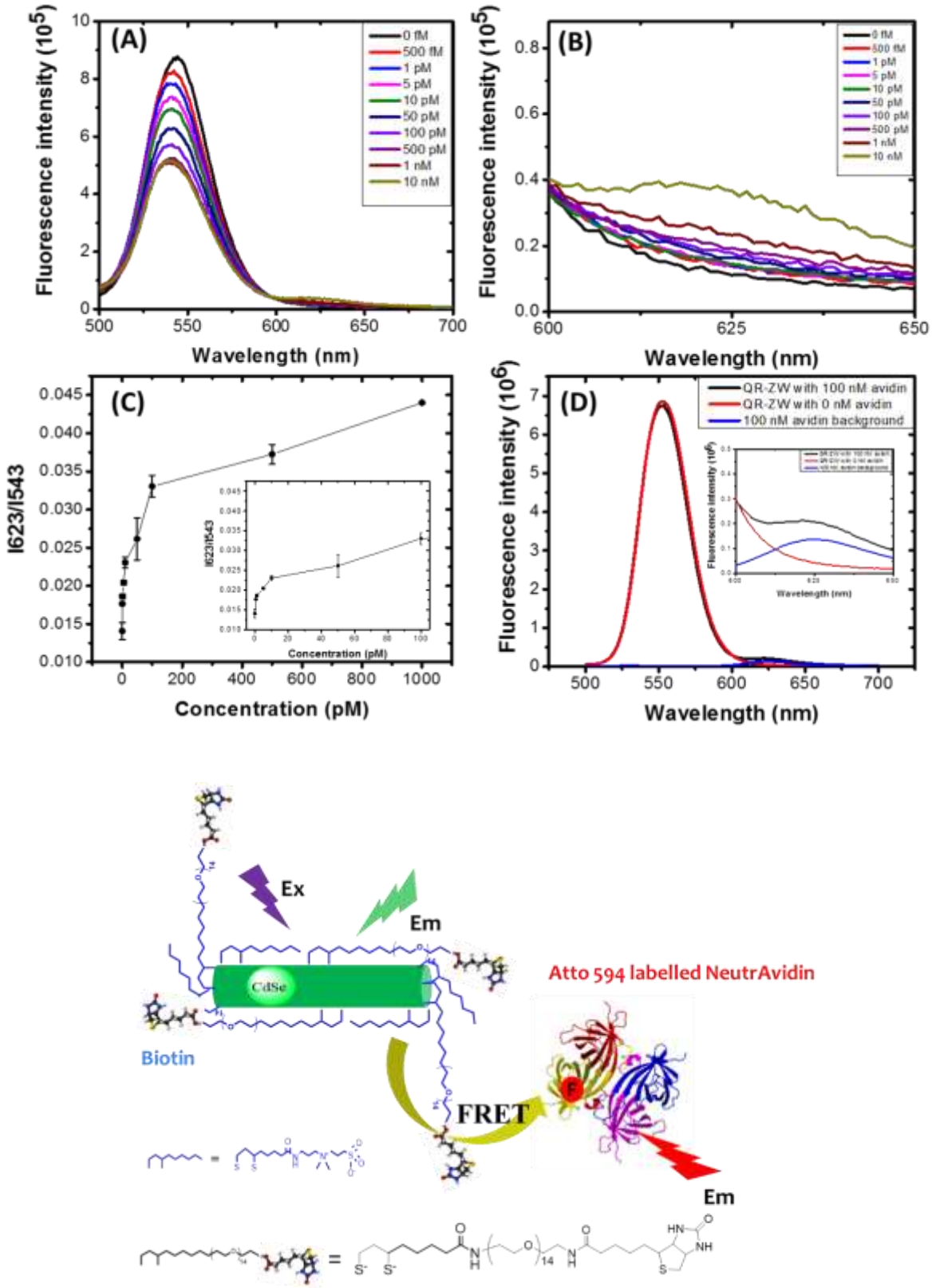

Figure 4-23: (A) Fluorescence spectra of the QR -biotin200 (0.5 nM QR) after incubation with different concentration of Atto-594 labelled NeutrAvidin in PBS

containing 0.1 Mg/mL of BSA. (B) Amplified fluorescence spectra from 600 to 650 nm. (C) A plot of the I_{625}/I_{543} ratio versus the NeutrAvidin concentration from 0 to 1000 pM and 0-100 pM. (D) Fluorescence spectra of the 1 nM QR-ZW (without biotin) after mixing with 100 nM labelled Avidin (black): no QR-fluorescence quenching was observed. Moreover, the resulting I_{625}/I_{543} ratio was only 0.0042 after correction of direct excitation background. Schematic show of the QR-Biotin for detection of labeled target Neutravidin via QR-sensitized Atto-594 FRET readout strategy.

4.4 Conclusion

A rapid and highly efficient LE method that allows for complete water-solubilisation of the hydrophobic CdSe/CdS QR similar to that reported in Chapter 3 has been developed. It readily produces compact, biocompatible QRs with excellent stability in PBS buffers. Moreover, a novel method for effective recovery of the QR fluorescence to >60% of its original value using a light activated method has been discovered. The resulting fluorescence recovered QR can be readily conjugated with His_8-tagged Affimers for sensitive detection of 5 pM of a specific target Yeast SUMO28b protein. The highly efficient LE method has been successfully employed for one-step preparation of biotinylated QRs which can be for sensitive detection of neutravidin down to low pM level. Compared to other QR biosensors reported in literature, our method has three notable advantages: 1) it is a rapid procedure to make stable, biocompatible QRs with a minimum LQMR as low as 1000:1; 2) it is easy to operate (using air-stable compounds and rapid *in situ* reduction at ambient condition); 3) a novel light activation strategy can make the almost totally quenched (<3% original

fluorescence intensity) QR recover to retain > 60% of its original fluorescence, making such QRs attractive for broad biomedical applications. Therefore this novel light activation method discovered herein will impact significantly in broad QR-based biomedical research field, including biosensing, bioimaging, clinical diagnostics, and most importantly in areas involving the use of QR-FRET based readout strategies.

4.5 Reference

1. A. E. Albers, E. M. Chan, P. M. McBride, C. M. Ajo-Franklin, B. E. Cohen and B. A. Helms, *Journal of the American Chemical Society*, 2012, **134**, 9565-9568.
2. W. C. Chan and S. Nie, *Science*, 1998, **281**, 2016-2018.
3. A. Fu, W. Gu, B. Boussert, K. Koski, D. Gerion, L. Manna, M. Le Gros, C. A. Larabell and A. P. Alivisatos, *Nano Letters*, 2007, **7**, 179-182.
4. B. N. Giepmans, S. R. Adams, M. H. Ellisman and R. Y. Tsien, *Science*, 2006, **312**, 217-224.
5. D. R. Larson, W. R. Zipfel, R. M. Williams, S. W. Clark, M. P. Bruchez, F. W. Wise and W. W. Webb, *Science*, 2003, **300**, 1434-1436.
6. L.-s. Li, J. Hu, W. Yang and A. P. Alivisatos, *Nano Letters*, 2001, **1**, 349-351.
7. I. L. Medintz, A. R. Clapp, F. M. Brunel, T. Tiefenbrunn, H. T. Uyeda, E. L. Chang, J. R. Deschamps, P. E. Dawson and H. Mattoussi, *Nature Materials*, 2006, **5**, 581-589.
8. I. L. Medintz, M. H. Stewart, S. A. Trammell, K. Susumu, J. B. Delehanty, B. C. Mei, J. S. Melinger, J. B. Blanco-Canosa, P. E. Dawson and H. Mattoussi, *Nature Materials*, 2010, **9**, 676-684.
9. X. Michalet, F. Pinaud, L. Bentolila, J. Tsay, S. Doose, J. Li, G. Sundaresan, A. Wu, S. Gambhir and S. Weiss, *Science*, 2005, **307**, 538-544.
10. K. E. Sapsford, W. R. Algar, L. Berti, K. B. Gemmill, B. J. Casey, E. Oh, M. H. Stewart and I. L. Medintz, *Chemical reviews*, 2013, **113**, 1904-2074.
11. E. R. Smith, J. M. Luther and J. C. Johnson, *Nano Letters*, 2011, **11**, 4923-4931.

12. F. Wang, R. Tang and W. E. Buhro, *Nano Letters*, 2008, **8**, 3521-3524.

13. L. Manna, E. C. Scher, L.-S. Li and A. P. Alivisatos, *Journal of the American Chemical Society*, 2002, **124**, 7136-7145.

14. W. R. Algar, H. Kim, I. L. Medintz and N. Hildebrandt, *Coordination Chemistry Reviews*, 2014, **263**, 65-85.

15. E. R. Goldman, I. L. Medintz, J. L. Whitley, A. Hayhurst, A. R. Clapp, H. T. Uyeda, J. R. Deschamps, M. E. Lassman and H. Mattoussi, *Journal of the American Chemical Society*, 2005, **127**, 6744-6751.

16. I. L. Medintz, J. Konnert, A. Clapp, I. Stanish, M. Twigg, H. Mattoussi, J. M. Mauro and J. Deschamps, *Proceedings of the National Academy of Sciences of the United States of America*, 2004, **101**, 9612-9617.

17. I. L. Medintz and H. Mattoussi, *Physical Chemistry Chemical Physics*, 2009, **11**, 17-45.

18. K. Susumu, B. C. Mei and H. Mattoussi, *Nature Protocols*, 2009, **4**, 424-436.

19. K. Susumu, H. T. Uyeda, I. L. Medintz, T. Pons, J. B. Delehanty and H. Mattoussi, *Journal of the American Chemical Society*, 2007, **129**, 13987-13996.

20. N. Zhan, G. Palui, H. Grise, H. Tang, I. Alabugin and H. Mattoussi, *ACS Applied Materials & Interfaces*, 2013, **5**, 2861-2869.

21. D. Zhou, *Biochemical Society Transactions*, 2012, **40**, 635-639.

22. A. M. Dennis and G. Bao, *Nano Letters*, 2008, **8**, 1439-1445.

23. Y. Zhang, H. Zhang, J. Hollins, M. E. Webb and D. Zhou, *Physical Chemistry Chemical Physics*, 2011, **13**, 19427-19436.

24. H. Zhang, G. Feng, Y. Guo and D. Zhou, *Nanoscale*, 2013, **5**, 10307-10315.

25. D. Zhou, L. Ying, X. Hong, E. A. Hall, C. Abell and D. Klenerman, *Langmuir*,

2008, **24**, 1659-1664.

26. C. Tiede, A. A. Tang, S. E. Deacon, U. Mandal, J. E. Nettleship, R. L. Owen, S. E. George, D. J. Harrison, R. J. Owens and D. C. Tomlinson, *Protein Engineering Design and Selection*, 2014, **27**, 145-155.
27. D. Zhou, A. Bruckbauer, L. Ying, C. Abell and D. Klenerman, *Nano Letters*, 2003, **3**, 1517-1520.
28. E. Petryayeva, W. R. Algar and I. L. Medintz, *Applied Spectroscopy*, 2013, **67**, 215-252.
29. B. O. Dabbousi, J. Rodriguez-Viejo, F. V. Mikulec, J. R. Heine, H. Mattoussi, R. Ober, K. F. Jensen and M. G. Bawendi, *The Journal of Physical Chemistry B*, 1997, **101**, 9463-9475.
30. A. B. Greytak, P. M. Allen, W. Liu, J. Zhao, E. R. Young, Z. Popović, B. J. Walker, D. G. Nocera and M. G. Bawendi, *Chemical Science*, 2012, **3**, 2028-2034.
31. Z. Deng, A. Samanta, J. Nangreave, H. Yan and Y. Liu, *Journal of the American Chemical Society*, 2012, **134**, 17424-17427.
32. I. L. Medintz, A. R. Clapp, H. Mattoussi, E. R. Goldman, B. Fisher and J. M. Mauro, *Nature Materials*, 2003, **2**, 630-638.
33. A. R. Clapp, I. L. Medintz, J. M. Mauro, B. R. Fisher, M. G. Bawendi and H. Mattoussi, *Journal of the American Chemical Society*, 2004, **126**, 301-310.

Chapter 5. General conclusions and future work suggestions

5.1 General conclusions

Firstly, In order to prepare of robust, compact, biocompatible QDs/QRs probes, a series of surface capping hydrophilic thiolated TA-based ligands, (such as TA-PEG750-OMe, TA-PEG2000-OMe and TA-Zwitterion and TA-PEG600-Biotin) were successful synthesised and characterized in chapter 2. These ligands are very useful for further QD-DHLA-based bioconjugate application, Especially for DHLA-PEG750-OMe and DHLA-Zwitterion ligands, the PEG units and +/- electron charged zwitterion part not only provide an effective 'shield' to improve the QD stability but also resist biomolecule non-specific absorption which make QD/QR well suitable for further his8-tagged nABPs/target SUMO protein FRET based ratiometric biosensor application. Besides, the biotin functional groups at the end of the PEG600 chain enable to formation of QD-biotin-Neutravidin conjugate also well suitable for cancer cell imaging. By using these TA-based ligands. Several achievements in QD/QR-bioconjugate sensing systems have been successfully developed.

Secondly in chapter 3, a successful development of a simple ultra-efficient cap exchange procedure (UCEP) was developed by a rapid reduction of TA-based

ligands to their DHLA form by tris(2-carboxylethyl)phosphine (TCEP). After deprotonation of the thiol groups, the resulting *in situ* reduced DHLA-ligands are directly used to initiate cap-exchange with hydrophobic type I CdSe/ZnS core/shell and CdSe/CdS/ZnS core/shell/shell QDs in homogenous solution which were prepared by using 50-1000 folds less amounts of the DHLA-based ligands over most literature reported. We show that the UCEP can provide complete QD water-solubilization at a LQMR of as low as 200:1. These biocompatible QDs exhibited an excellent stability in biological buffers (PBS with 0.1 mg/ml BSA), effectively retaining the native parent QD fluorescence (> 90%), and small hydrodynamic diameters (< 10 nm). the resulting QDs are readily bio-conjugated with His_8-tagged Affimers for robust, sensitive detection of 5 pM of a specific target protein, the QD-bio probe can works robustly in clinical relevant media (50% human serum). The UCEP also allows for readily one-step preparation of biotinylated QDs for sensitive biosensing, sensitive detection of 5 pM of NeutrAvidin as well.

Thirdly in Chapter 4, the UCEP method is also suitable for Quasi-Type II CdSe/CdS QRs, and provides complete QR water-solubilization at a LQMR of as low as 1000:1. After UCEP in preparing QR, it was totally quenched, but we found a simple photon-induced method to make QR fluorescence recovery their native parent QR fluorescence (>60%), small hydrodynamic diameters (< 15 nm) and sensitive for further biosensing application. Furthermore, these QRs also have excellent stability in PBS buffers, the resulting QDs are readily bio-conjugated with His_8-tagged Affimers for robust, sensitive detection of 5 pM of a specific target protein. The UCEP also allows for readily one-step preparation of biotinylated QRs for sensitive biosensing, sensitive detection of 5 pM of NeutrAvidin as well.

Finally, a more stable, specific, robust, and sensitive compact QD/QR-bioconjugate probes were prepared by new UCEP. This procedure has several advantages: (a) it is a rapid procedure to make water soluble QR/QD in a few minutes; (b) it is easy to operate (using air-stable compounds and rapid *in situ* reduction at ambient condition); (c) this method can save lots of expensive excess ligands; (d) after ligand exchange QDs retaining the native parent QD fluorescence (>90%); (e) Light activation method can make useless totally quenched QR recover fluorescence properties up to > 60% of original fluorescence intensity. (f) After UCEP method QDs and QRs can keep stable in water phase for at least 3 months. The high stability, specificity together with excellent robustness and sensitivity QD-Affimer, QD-biotin, QR-Affimer and QR-biotin sensor will have good potential for a wide biomedical research field, including biosensing, bioimaging, drug delivery, clinical diagnostics and therapeutics.

5.2 Future research

Although the water-soluble QRs prepared by our ligand exchange method using the DHLA-ZW ligands are stable and resisting the non-specific absorption, making them attractive for biosensing, some further work in the following areas are nonetheless necessary.

Firstly, the mechanisms by which the Quasi-Type II QR's fluorescence is quenched upon ligand exchange and why its fluorescence can be recovered after light activation should be investigated in details. This information can be obtained by performing transient absorption spectra as well as fluorescence lifetime measurement. The mechanism of fluorescence recovery of QR is worth further

investigation. It might find new applications in super-resolution imaging similar to PALM.

Secondly, both the QR-Atto-594 labeled SUMO and QR-Atto-594 labeled NeutrAvidin FRET pairs appear to give extremely low FRET signal despite significant quenching of the QR fluorescence. This result appears to contrast significantly with those of the QD560-Atto-594 FRET pair reported in literature where much higher FRET signals were reported despite the QD560 and the QR used here have very similar emission spectra. The reasons behind this phenomenon are also worthy of investigation.

Thirdly, after confirming the specific binding between the QR-biotin and NeutrAvidin, a label free detection of neutravidin as well as free biotin should also be done. This can be based on the same strategy as those employed in the QD-detection where free biotin can effectively compete with the QR-biotin$_{200}$ for binding to labeled NeutrAvidin, reducing the amounts of labelled NeutrAvidin binding to the QR and will hence the QR to Atto 594 FRET efficiency.

Fourthly, nucleic acid aptamer could be a useful choice, allow for detection of a wide range of different target.

Finally, Multiplex detection of several different targets simultaneously by several different coloured QD/QRs, each encoding a unique target binder, that maybe further improve sensitivity and clinical detection.